CR-152040

SYSTEMS TECHNOLOGY, INC.

13766 SOUTH HAWTHORNE BOULEVARD • HAWTHORNE, CALIFORNIA 90250 • PHONE [213] 679-2281

Technical Report No. 1092-1

DEVELOPMENT OF AUTOMATIC AND MANUAL FLIGHT DIRECTOR LANDING SYSTEMS FOR THE XV-15 TILT ROTOR AIRCRAFT IN HELICOPTER MODE

L. G. Hofmann
Roger H. Hoh
Wayne F. Jewell
Gary L. Teper
Pradip D. Patel

January 1978

Contract No. NAS2-9392

National Aeronautics and Space Administration
Ames Research Center
Moffett Field, CA 94035

TECHNICAL REPORT STANDARD TITLE PAGE

1. Report No.	2. Government Accession No.	3. Recipient's Catalog No.

4. Title and Subtitle	5. Report Date
Development of Automatic and Manual Flight Director Landing Systems for the XV-15 Tilt Rotor Aircraft in Helicopter Mode	January 1978
	6. Performing Organization Code
7. Author(s) L. G. Hofmann, Roger H. Hoh, Wayne F. Jewell, G. L. Teper, and Pradip D. Patel	8. Performing Organization Report No. Technical Report No. 1092-1
9. Performing Organization Name and Address Systems Technology, Inc. Hawthorne, California	10. Work Unit No.
	11. Contract or Grant No. NAS2-9392
	13. Type of Report and Period Covered
12. Sponsoring Agency Name and Address National Aeronautics and Space Administration Ames Research Center Moffett Field, California	14. Sponsoring Agency Code

15. Supplementary Notes

16. Abstract

The objective of this effort is to determine IFR approach path and touchdown dispersions for manual and automatic XV-15 tilt rotor landings, and to develop missed approach criteria. Only helicopter mode XV-15 operation is considered. The results will be used to support the development of certification criteria for the XV-15. The analysis and design sections develop the automatic and flight director guidance equations for decelerating curved and straight-in approaches into a typical VTOL landing site equipped with an MLS navigation aid. These system designs satisfy all known pilot-centered, guidance and control requirements for this flying task. Performance data, obtained from nonstationary covariance propagation dispersion analysis for the system, are used to develop the approach monitoring criteria. The autoland and flight director guidance equations are programmed for the VSTOLAND 1819B digital computer. The system design dispersion data developed through analysis and the 1819B digital computer program are verified and refined using the fixed-base, man-in-the-loop XV-15 VSTOLAND simulation at NASA Ames.

17. Key Words		18. Distribution Statement
Automatic Landing	VTOL	
Flight Director	VSTOLAND	
Touchdown Dispersion	Autoland	
Decelerating Approach		
Missed Approach Criteria		

19. Security Classif. (of this report)	20. Security Classif. (of this page)	21. No. of Pages	22. Price
Unclassified	Unclassified		

Form DOT F 1709.7 (8-69)

TABLE OF CONTENTS

TABLE OF CONTENTS

List of Figures

List of Figures

List of Figures

List of Figures

List of Tables

List of Tables

LIST OF ACRONYMS

ALT	Altitude hold mode
AS	Airspeed hold mode
CTOL	Conventional takeoff and landing
DEC, DECL, DECEL	Constant attitude deceleration mode
DME	Distance measuring equipment
GPIP	Glide path initial point
GS	Glide slope track mode
HH	Heading hold mode
HOV	Longitudinal hover mode
IAS	Indicated airspeed
IMC	Instrument meteorological conditions
LOC A	Bank-to-turn localizer mode
LOC B	Bank-to-translate localizer mode
MLS	Microwave landing system
RCAH	Rate command, attitude hold
SCAS	Stability and control augmentation system
TRC	Translational rate command
VD	Vertical descent mode
VTOL	Vertical takeoff and landing

LIST OF SYMBOLS

ALTH, H, h	Altitude (AGL)
AX, a_x	Longitudinal acceleration of c.g.
AYP, $a_{\dot{y}}$	Lateral body-axis acceleration at pilot's location
AZP, $a_{\dot{z}}$	Normal acceleration at pilot's location
d	Actual glide slope deviation, positive for aircraft above glide path, linear units
DC, δ_c	Longitudinal cyclic stick deflection
DCL, δ_{CL}	Total collective pitch deflection in lever units
DE, d_e	Indicated glide slope deviation in linear units
DEH, $\hat{d}_e$	Input to beam rate command limiter during glide slope tracking, altitude command during vertical descent
DLAT, δ_{LAT}	Total lateral cyclic deflection
DLN, δ_{LN}	Total longitudinal cyclic pitch deflection in stick units
DLNS, δ_{LNS}	Longitudinal cyclic series servo deflection
DLTS, δ_{LTS}	Lateral cyclic series servo deflection
DPDS, δ_{PDS}	Rudder series servo deflection
DS, δ_s	Lateral cylic stick deflection
e	Base of natural logarithm, 2.718 ...
e_x	Switching criterion signal for point hover mode initiation
e_θ	Switching criterion signal (or error signal) for constant attitude deceleration initiation (or control law)
ENU, ν	MLS localizer structure (noise) in angular units
ETA, η	MLS glide slope structure (noise) in angular units
f	Input to flight director shaping network
FDC, FD_C	Flight director longitudinal cyclic command bar deflection
FDCL, FD_{CL}	Flight director collective pitch command bar deflection

FDL, FD_L	Flight director lateral cyclic command bar deflection
FDP, FD_P	Flight director rudder pedal command bar
g	Gravity constant
G_{FFS}	Force feel system transfer function for stick deflection in, parallel servo deflection out
h^*	Total altitude of aircraft center of gravity above GPIP on runway
h_{baro}	Pressure altitude
$\dot{h}_{IVSI}$	Instantaneous vertical speed indication
h_o	Altitude at output of synchronizer
h_{ocg}	Aircraft center of gravity altitude at touchdown
h_{radar}	Radar altitude
H_c	Asymptotic flare altitude
HD, $\dot{h}$	Rate of climb
$I_{(\ )}$	Moment of inertia about ( ) axis
k	Complementary filtering gain
$K_{(\cdot)}$	Control system gain specified by $(\cdot)$
K_{BUG}	Calibration parameter, ideally equal to unity
K(W)	Wind profile shaping gain
$K_{\theta VA}$	Trim pitch attitude gradient with airspeed, $\partial\theta_T/\partial V_A$
ℓ_{x_a}, ℓ_{z_a}	Pilot's location with respect to aircraft center of gravity
L	Rolling moment
$L_{(\ )}$	Dimensional rolling moment derivative, $(1/I_x)[\partial L/\partial(\ )]$
$L_{(\cdot)}$	Turbulence or MLS noise characteristic wave lengths specified by $(\cdot)$
LSW	Longitudinal control system mode indicator
m	Mass
M	Pitching moment
$M_{(\ )}$	Dimensional pitching moment derivative, $(1/I_y)[\partial M/\partial(\ )]$

N	Yawing moment
$N_{(\ )}$	Dimensional yawing moment derivative, $(1/I_z)[\partial N/\partial(\ )]$
$N^{(\cdot)}_{[\cdot]}$	Transfer function numerator between $[\cdot]$ input and $(\cdot)$ output
P, p	Angular rate about x-axis
PG, p_g	Effective rolling gust component
PHDC, φ_{DC}	Input to bank angle command limiter
PHI, φ	Euler roll angle
P_{MA}	Probability of having to execute a missed approach on any given IMC approach because of flight technical error
PSI, ψ	Euler yaw angle with respect to runway heading
Q, q	Angular rate about y-axis
R, r	Angular rate about z-axis
R	Slant range between center of gravity of the approaching aircraft and MLS elevation antenna
R_A	Slant range between aircraft and MLS azimuth transmitting antenna
R_G	Distance between MLS elevation and azimuth transmitting antennas
s	Laplace transform variable
$S_{(\cdot)}$	Control system switch variable specified by $(\cdot)$. Permissible values are 0. and 1.
SA, S_A	Lateral-direction control system mode indicator and switch value
SR	Input to sink rate command limiter
TIME, t	Time
$T_{(\cdot)}$	Control system time constant specified by $(\cdot)$
THCD, θ_{cd}	Input to pitch attitude command limiter
THEE, θ_e	Pitch attitude deviation from commanded value
THET, θ	Euler pitch angle
u	Perturbation x-velocity
u_A	Body-fixed x-axis component of headwind and crosswind

U	Total x-velocity
$\dot{U}$	Longitudinal, body-axis kinematic acceleration, $(a_{x_{cg}}-g \sin\Theta)$
UG, u_g	x-axis gust component (body-fixed reference frame)
UW, u_w	Headwind component with respect to runway direction
v	Perturbation y-velocity
v_A	Body-fixed y-axis component of headwind and crosswind
V	Total y-velocity
VA, V_A	Airspeed
VAE, V_{AE}	Smoothed compensated airspeed error
V_{AX}	Airspeed below which airspeed crossfeed to collective pitch is enabled
V_e	Equivalent airspeed
VG, v_g	y-axis gust component (body-fixed reference frame)
V_{HW_o}	Mean headwind component in runway direction at problem initial altitude
V_{IAS}	Indicated airspeed
VW, v_w	Crosswind component with respect to runway direction, positive for wind blowing from right to left
w	Perturbation z-velocity
w_A	Body-fixed z-axis component of headwind and crosswind
W	Total z-velocity
WG, w_g	z-axis gust component (body-fixed reference frame)
X	Force along x body axis
X	Ground range from intended touchdown point, positive in the down-runway direction
XD, $\dot{X}$	Velocity in down-runway direction
$X_{(\ )}$	Dimensional x-force derivative, $(1/m)[\partial X/\partial(\ )]$
XC, X_c	DME noise

X_f	Ground range for first occurrence of $e_x = 0$
XIND, X_i	Indicated DME ground range
X_o	Ground range for first occurrence of $e_\theta = 0$
X_{PED}	Rudder pedal deflection
$\dot{y}$	Velocity in the cross-runway direction, positive when moving to right of runway
Y	Force along y body-axis
Y, y	Lateral deviation in cross-runway direction, positive for aircraft to right of runway centerline
$Y_{(\ )}$	Dimensional y-force derivative, $(1/m)[\partial Y/\partial(\ )]$
YD, $\dot{y}$	Lateral deviation rate
YE, y_e	Indicated localizer deviation, linear units
$Y_{p(\cdot)}$	Transfer function representing pilot's control action in response to flight director specified by $(\cdot)$
Z	Force along z body-axis
$Z_{(\ )}$	Dimensional z-force derivative, $(1/m)[\partial Z/\partial(\ )]$
α	Angle of attack
β	Sideslip angle
γ	Flight path angle
γ_A	Aerodynamic flight path angle
δ	Control deflection
δ_{PED}	Total rudder deflection in pedal units
Δ	Transfer function denominator
$\Delta\delta_{CL}$	Collective pitch component resulting from airspeed crossfeed
$\Delta\theta_{DECEL}$	Computed pitch attitude reference change for deceleration mode
ϵ_d	Switching criterion signal for glide slope capture initiation
ϵ_y	Switching criterion signal for localizer capture initiation
ζ	Damping ratio

θ_c	Pitch attitude hold reference
θ_D	Computed pitch attitude reference for constant attitude deceleration
θ_H	Trim pitch attitude at hover in zero wind
θ_{INC}	Constant attitude increment controlling rapidity of deceleration
$\theta_{o(\cdot)}$	Attitude at output of synchronizer $(\cdot)$
θ_T	Trim pitch attitude as function of airspeed
Θ	Glide slope alignment angle $(= -\gamma_c)$
ρ	Probability density function, or correlation coefficient if subscripted, also air density at altitude
ρ_o	Standard sea level air density
σ	Denotes one standard deviation in general. May be particularized by subscript
ψ_c	Yaw attitude hold reference
Ψ	Localizer alignment angle
Ψ_{REF}	Reference heading for heading hold control system mode
ω	Angular frequency
$\omega_{(\cdot)}$	Control system break frequency specified by $(\cdot)$

MATRIX AND VECTOR SYMBOLS

A	System matrix
b	Input vector
C	Covariance matrix for x
D	Covariance matrix for y
g	Input vector
H	State-to-output distribution matrix
n	Discrete interval index
Q	Power spectral density matrix for w

w	Process noise vector
x	State vector
y	Alternative state vector
z	Output vector
Γ	Forcing matrix for covariance propagation equation
θ, Θ	Forcing matrix or vector for state transition equation
φ, Φ	State transition matrices

PREFIXES AND SUFFIXES

$S(\cdot)$	Standard deviation of $(\cdot)$
$(\cdot)D$	Derivative with respect of time of $(\cdot)$

SPECIAL NOTATION

$E[\cdot]$	Expected value of $[\cdot]$
$(\cdot)_{TD}$	Touchdown-related value of $(\cdot)$
$(\bar{\cdot})$	Denotes mean or expected value of $(\cdot)$
$(\dot{\cdot})$	Derivative with respect to time of $(\cdot)$
$(\cdot)'$	Transpose of matrix $(\cdot)$
$\lvert(\cdot)\rvert$	Absolute value of scalar quantity $(\cdot)$, or determinant of square matrix $(\cdot)$
$(\cdot)_{max}$	Maximum allowable value for $(\cdot)$
$(\cdot)_{min}$	Minimum allowable value for $(\cdot)$
$(\cdot)_{DP}^{-}$	Value of $(\cdot)$ just prior to decision point
$(\cdot)_{DP}^{+}$	Value of $(\cdot)$ just subsequent to decision point
$(\cdot)_o$	Initial value, or value at trim
$(\cdot)^*$	Value in presence of a steady wind
$(\cdot)_c$	Commanded or reference value

SECTION I

INTRODUCTION

This report summarizes the results of a combined analytical and experimental study to determine IFR approach path dispersions under manual and automatic control. These dispersions, in turn, are the basis for missed approach criteria. The basic motivation for this research stems from recognition that the future of V/STOL aircraft as a viable transportation medium depends upon implementation of appropriate terminal control techniques and safety philosophies. Accordingly, the emphasis is directed at the generation of a dual (automatic and manually controlled) system for the guidance and control of the XV-15 aircraft on approach to evaluate performance in this critical terminal flight regime.

A. SCOPE

The purpose of this program is to generate performance data for the XV-15 Tilt Rotor aircraft and control system operating in the terminal area with a digital avionics system. This data is required to assess effects of the system elements (XV-15, flight paths, navigation aids, guidance and flight director laws, etc.), command inputs and disturbances in terms of the precision of control, pilot workload and available margins of safety. This data, in turn, provides insight for design of appropriate automatic or manual approach monitoring criteria for the XV-15.

This research assumes operation within the practical constraints and operating limits of the XV-15 aircraft. XV-15 performance margins (e.g., thrust/power and rate of sink), vibration, and rotor structural fatigue limits as defined in Refs. 1 and 2 preclude descending on the steep glide slopes [e.g., −6 deg (−0.10 rad), −8 deg (−0.14 rad) and −10 deg (−0.17 rad) while decelerating in airspeed in other than the helicopter mode or configuration [i.e., pylon at 90 deg (1.6 rad)]. Therefore, neither the automatic nor the manual systems require consideration of a configuration management command mode (e.g., modulation of pylon and flaps). Furthermore, only the conventional displays and control associated with the XV-15 aircraft are considered. Thus, the many and varied

considerations associated with abort procedures, safety margins, engine-out conditions which are of concern before and during the transition to the helicopter mode of flight are non-operative. Therefore, the pilot need only concern himself with the final stages of the approach — deceleration to a hover on a descending, perhaps curved, flight path while in the terminal area.

B. APPROACH

The research consists of three major elements. The first of these is the development of a compatible set of guidance, autoland, and flight director laws. The word "compatible" refers specifically to the requirement that manual (using the flight director) and automatic (with the autoland system) control laws be compatible not only with the approach requirements but also with each other. Autoland systems capable of decelerating flight to a hover have been built and flown (Refs. 3 and 4). Flight director configurations with similar capabilities have also been flown (Ref. 4). Designs to date are not without pilot reservations — primarily because the flight director was apparently treated as an adjunct to the autoland system rather than a separate system with its own (pilot-centered) requirements in addition to the fundamental guidance requirements common to both manual and automatic systems.

The second element is the assessment of this system by means of exercise of a digital simulation of its characteristics. A statistical approach to the evaluation of the system performance is used. While the necessary statistical performance data could be developed using a Monte Carlo approach, the more effective and efficient covariance propagation technique is used. This provides statistical descriptions of performance directly in terms of dispersions. Further application of this technique is used to develop approach monitoring criteria.

The third key element is verification of system suitability and performance by means of man-in-the-loop simulation (fixed base) at Ames Research Center.

C. ORGANIZATION OF THE REPORT

The remainder of this report is organized into seven sections and three appendices. The next three sections detail development of the guidance, autoland and flight director control laws. The first of these three sections summarizes the qualitative design requirements in consideration of the tasks, XV-15 characteristics, pilot-centered considerations, operating environment, etc. Quantative development of the longitudinal and lateral-directional designs is contained in Sections III and IV, respectively.

A statistical analysis of the approach and touchdown disperions for these longitudinal and lateral-directional systems is reported in Section V. Section VI recommends missed approach criteria based on the statistical analysis.

Results of the fixed-base, man-in-the-loop simulation are reported in Section VII, while the main conclusions from this research program are summarized in Section VIII.

Two appendices cover basic XV-15 aircraft data, equations of motion and parameter values used in the system performance analysis, and the equations suitable for programming the guidance, autoland and flight director control laws and logic for the VSTOLAND 1819B Research Computer.

SECTION II

SYSTEM REQUIREMENTS

System requirements are established on the basis of mission phase or task definitions; fixed characteristics of aircraft, SCAS and disturbance environment; feasible competing systems capable of meeting mission or task objectives; and assessment of the favorable and unfavorable points for each competing system. Establishing requirements is a qualitative process for narrowing the field of potential system solutions to be analyzed in quantitative detail in Sections III and IV.

A. TASK DEFINITION

The mission phases of concern in this study are limited to terminal area vectoring, initial and final approach, and landing. The XV-15 is assumed to be operating in the helicopter mode over its complete speed range in that mode. Vertical landing, curved initial approach path and variable glide slope capability must be provided. All navigation and guidance measurements required for these tasks are obtained from the VSTOLAND navigation system.

B. FIXED CHARACTERISTICS

1. XV-15 Aircraft

The unaugmented XV-15 aircraft in the helicopter mode has the usual helicopter handling deficiencies plus a unique lateral-directional roll control reversal problem in the 40 kt (21 m/s) regime and significant lack of directional stability below 40 kt (21 m/s). These latter points, in turn, place special requirements on the lateral-directional SCAS. All basic handling deficiencies are summarized in Table 1. (Table 1 is based upon the stability derivative data in Tables A-4 and A-6 and the transfer function data in Table 7.

TABLE 1

BASIC XV-15 HANDLING DEFICIENCIES

LONGITUDINAL

Low heave damping below 40 kt*

Long-term attitude response to stick input is near zero

Unacceptable short-term attitude to stick responses at low speed

LATERAL-DIRECTIONAL

Very low dutch roll frequency at all speeds (low ω_d)

Negative or low dutch roll damping at all speeds (low ζ_d)

Unstable spiral mode

Large shift in instantaneous center of rotation ($-Y_{\delta ped}/N_{\delta ped}$) between 60 and 80 kt

Roll reversal at 40 kt

Poor yaw rate to pedal characteristics

Large adverse yaw at speeds below about 70 kt

*1 kt = 5.144×10^{-1} m/s.

2. Disturbance Environment

The disturbance environment considered includes longitudinal, normal, side and effective rolling gusts, steady winds and wind shears, MLS azimuth, elevation and DME noise. Math models for each of these disturbance effects are given

in Appendix A. Effects of curved path commands and of pilot abuse of system operating procedures are also considered.

3. Stability and Control Augmentation System (SCAS)

The installed SCAS is a rate-command, attitude retention system. Installed series actuators have very limited [±1 in. (±0.025 m)] authority because the augmentation is single-thread. The original intent of this project was to design the guidance, flight director and autoland control laws to work with the SCAS as installed. However, the fact that the electrical inputs to the series servos shown in Fig. 16 of Ref. 5 are not in actuality available, and that the attitude hold (more properly, retention) feature is only introduced when there are no pilot inputs, caused modification of the original ground rules. Modification is necessary for manual flight director operation because the attitude feedbacks are cancelled whenever the control stick is moved from the detent. This deficiency might be corrected by using the attitude SCAS feedback full-time (an available option), but then an attitude command system results. Attitude command systems demand series servo deflections which substantially exceed the installed series servo authority. That this is so is illustrated in Fig. 1. Parts a and b compare the series servo deflection required for attitude command and rate command pitch SCAS systems in order to cope with a reasonably large wind shear. It is evident in part a that much of the series servo deflection is devoted to cancelling the parallel servo output for the attitude command system.

An alternative solution might be to include the required attitude feedback signal on the flight directors, but this is sure to result in an unacceptable level of flight director activity from the pilot's viewpoint.

For the above reasons, the ground rules were modified to permit design of a new, rate-command, attitude-hold SCAS operating within the authority limits for the installed series servos.

Provisions for interfacing the VSTOLAND system with the XV-15 is through the force feel/autopilot actuators in the longitudinal, lateral, and directional control systems. The cockpit control motions are also introduced into the

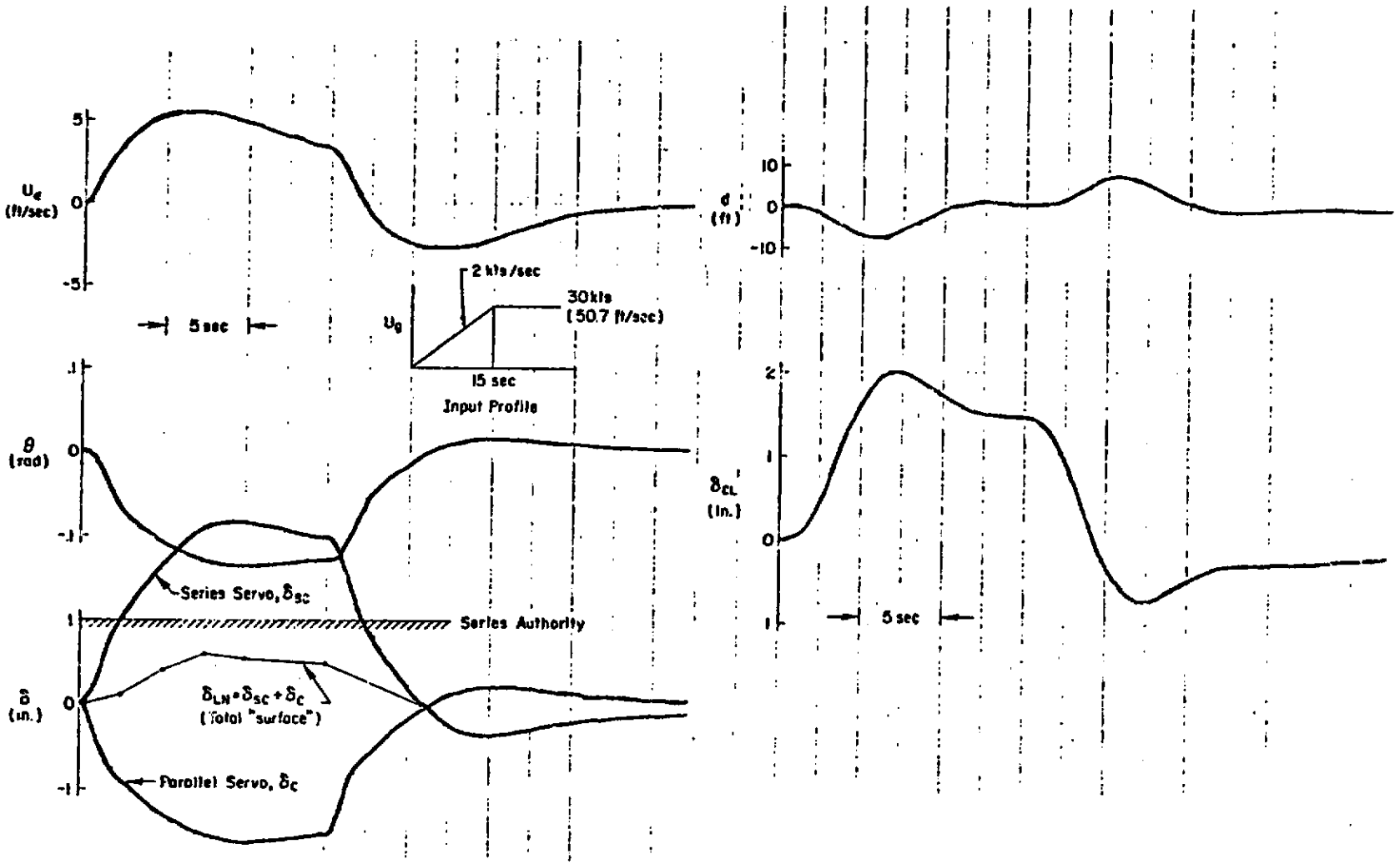

Figure 1a. Response to Large Wind Shear — Attitude Command SCAS; V = 60 kt (31 m/s)

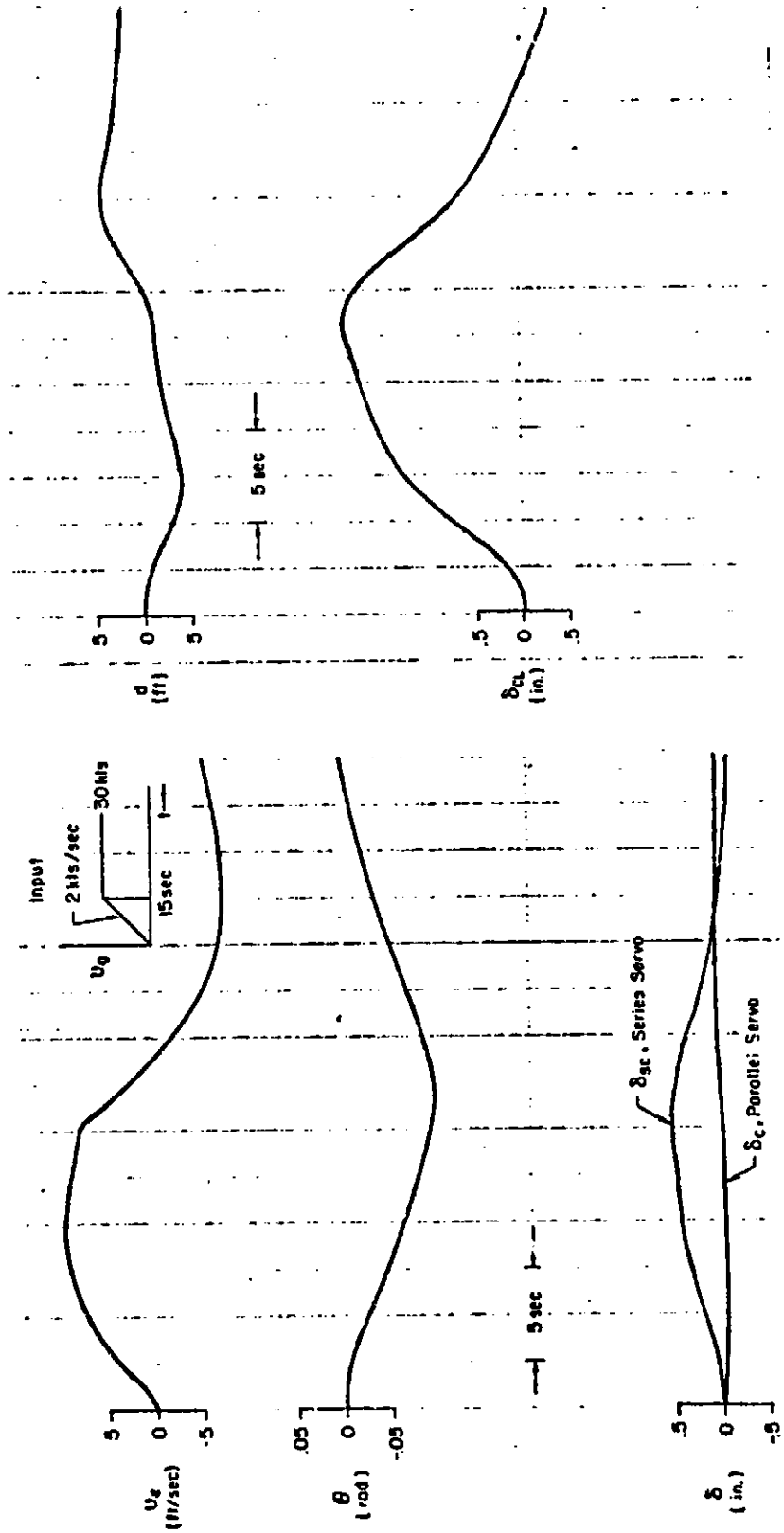

Figure 1b. Response to Large Wind Shear — Rate Command SCAS; V = 60 kt (31 m/s)

aircraft primary controls through the force feel actuators. Input to the power management system is through the power lever actuator.

C. REQUIREMENTS AND COMPETING SYSTEM ALTERNATIVES

Definition of competing candidate systems proceeds directly from formulation of system requirements. Requirements for both the manual (using flight director) and automatic (autoland plus autopilot) landing systems are addressed simultaneously. This is possible because of a NASA stated requirement for similarity in behavior and performance for the two systems. This dictates systems which are functionally similar, that is, have similar loop structures.

However, there are a few significant fundamental differences between the manual and automatic systems which are appropriately identified at the outset, e.g.:

- Control authority and limits — The automatic system has less because the pilot has access to additional controls (the flight director controls pilot inputs, not outputs); and it allows for pilot takeover (e.g., the pilot can override the FFS actuator because of its limited force capability).

- Integration — An automatic system will often have integrators to drive the steady-state errors to zero while the flight director system cannot include such functions because of excessive attentional demands.

- Monitoring criteria — The monitoring and associated takeover criteria for the two systems may differ for a number of reasons. Basically, the pilot has only conventional instruments while the automatic system potentially has access to more variables and may operate on different computed combinations of variables.

With these qualifications we can proceed to establishing requirements and then to definition of the candidate competing systems.

Requirements can be grouped as follows:

- Guidance and control requirements — Fundamental and independent of whether the controller is an automatic or human pilot.

- Pilot-centered requirements — Relate to the fact that the controller is a man (pertains to the flight director design).

A summary of the requirements central to design of these systems is given in Table 2. The satisfaction of these requirements from basic considerations leads to the selection, sensing, shaping, and relative weighting of appropriate feedbacks (and feedforwards) in a way which is best for manual control using the flight director and (with adjustments) to autoland. The pilot-centered

TABLE 2. PILOT/VEHICLE SYSTEM REQUIREMENTS

Guidance and Control

- Command Following
- Disturbance Regulation
- Stability and Damping

Pilot-Centered (Refs. 6 and 7)

- Minimum Pilot Compensation
  - — Feedback paths
  - — Equalization
- Response Quality
- Frequency Separation of Controls (Table 3)
- Non-Interaction of Controls
- Insensitivity to Pilot Response Variations
- Remnant Suppression

requirement for frequency separation of controls is very important for keeping pilot workload within acceptable bounds. This requirement can be met by two alternative choices for axes to be controlled by manual flight director or automatic systems. These two choices are Option A and Option B.

Option A

- All height control is manual.
- FD_{LAT} goes automatic in hover to be consistent with FD_{LN} and to minimize workload.
- Would require series actuator on collective.

Option B

- Lateral and longitudinal cyclic are primarily manual controls for entire approach.
- Heading is fully automatic.
- Display collective trim shifts on FD_{CL}, e.g., step commands for vertical descent

The specific use of manual flight director or automatic control is detailed by control axis and approach mode in Table 3 for both options. The requirements of Table 2 are related to key longitudinal and lateral-directional feedbacks in Table 4.

Once the key alternative longitudinal and lateral-directional feedbacks for meeting the requirements are identified, additional pilot preferences concerning VTOL approach technique are imposed. These preferences are summarized in Table 5.

TABLE 3

MANUAL/AUTOMATIC CONTROL AXIS ALLOCATION OPTIONS FOR THE "FREQUENCY SEPARATION OF CONTROLS" REQUIREMENT

OPTION A				
MLS	FD_{CL}	FD_{LAT} (crab or wing low)	Automatic	Automatic
Deceleration	FD_{CL}	FD_{LAT}	Automatic	Automatic
Hover	FD_{CL}	Automatic	Automatic	Automatic
Vertical Descent	FD_{CL}	Automatic	Automatic	Automatic
OPTION B				
MLS	Automatic + trim	FD_{LAT}	FD_{LN}	Automatic
Deceleration	Automatic + trim	FD_{LAT}	FD_{LN}	Automatic
Hover	Automatic + trim	FD_{LAT}	FD_{LN}	
Vertical Descent	Automatic + trim	FD_{LAT}	FD_{LN}	Automatic

TABLE 4

REQUIREMENTS AND COMPETING SYSTEM ALTERNATIVES

DIRECT REQUIREMENTS	CRITICAL DISTURBANCES AND COMMANDS	IMPLIED REQUIREMENTS	COMPETING SYSTEMS				COMMENTS
			SYSTEM A		SYSTEM B		
			PARALLEL	SERIES	PARALLEL	SERIES	
Altitude hold	w gusts Level off from large vertical rate	Good $\dot{h}/\delta_{LN}$	$h, \dot{h} \rightarrow FD_{LN}$ (IAS hold off) $h, \dot{h} \rightarrow FC_{CL}$ (IAS hold on)	$\theta, \dot{\theta} \rightarrow \delta_{LN}$ SCAS			Pilot option to use on FD_{LN} or automatic system
Airspeed Hold	u gusts Horizontal wind shears Speed changes	Good low-frequency attitude control ($1/T_{\theta_1} \gg 0$)	$IAS \rightarrow FD_{LN}$	$\theta, \dot{\theta} \rightarrow \delta_{LN}$ SCAS			Pilot option — FD or automatic
Vertical Speed Hold	Wind shear w gusts $\dot{h}_c$ changes	Good $\dot{h}/\delta_{LN}$ or $\dot{h}/\delta_{CL}$	$\dot{h} \rightarrow FD_{CL}$	$\theta, \dot{\theta} \rightarrow \delta_{LN}$ SCAS	$\dot{h} \rightarrow FD_{LN}$		Pilot option — FD or automatic FD_{LN} will not work on backside
Pitch Attitude Control	u gusts w gusts δ_{LN} inputs	$\zeta_p', \omega_p', 1/T_{sp}'$ in region of good handling K_{θ_c} optimized Insensitive to gusts without being too abrupt to pitch commands	$\dot{X} > \epsilon$ $\delta_{LN} \underset{FFS}{\Rightarrow} \theta_c$ $\dot{X} < \epsilon$ Same as $IAS > \epsilon$	$\theta, \dot{\theta} \rightarrow \delta_{LN}$ SCAS	$\dot{X} > \epsilon$ $\delta_{LN} \Rightarrow \dot{\theta}_c$ $\dot{X} < \epsilon$ $\delta_{LN} \Rightarrow \theta_c$	$\theta, \dot{\theta} \rightarrow \delta_{LN}$ SCAS $\theta, \theta, X \rightarrow \delta_{LN}$ SCAS	Basic choice is θ_c or $\dot{\theta}_c$. Should be θ_c for hover, e.g., $\dot{X} < \epsilon$ Always on
Bank Angle Control	v gusts δ_{LAT} inputs	$\dot{\varphi}_c$ during approach φ_c in hover and vertical descent Good $\zeta_d, \omega_d, 1/T_R$	$\dot{X} > \epsilon$ $\delta_{LAT} \Rightarrow \dot{\varphi}_c$ $\dot{X} < \epsilon$ $\delta_{LAT} \Rightarrow \varphi_c$	$\dot{\varphi} \rightarrow \delta_{LN}$ SCAS	$\delta_{LAT} \Rightarrow \varphi_c$	$\varphi, \dot{\varphi} \rightarrow X_{LAT}$ SAS	Basic choice is φ_c or $\dot{\varphi}_c$. Should be φ_c in hover but φ_c is very undesirable on approach Always on
Heading Control	δ_{LAT} inputs δ_{PED} inputs Outer loop requirements v gusts	$\mu, I_\delta/N_\delta$ in favorable region when δ_{LAT} is primary ψ control Zero effective coupling between δ_{CL}, δ_{LN} Good RCAH characteristics when ψ is controlled with pedals Must be washed out when used as an inner loop for lateral path damping	Latter stages of approach $\delta_{PED} \underset{FFS}{\Rightarrow} \dot{\psi}_c$ Early in approach $\psi_\epsilon \Rightarrow \varphi_c$	$\psi, \dot{\psi} \rightarrow \delta_{PED}$ SCAS $r - \frac{g\varphi}{V} \rightarrow \delta_{PED}$ SCAS if required			Basic philosophy is to use δ_{LAT} for heading control until some point on localizer During latter stages of approach use δ_{LAT} for lateral corrections with basically constant heading automatically controlled through pedal FFS

TABLE 4 (Continued)

DIRECT REQUIREMENTS	CRITICAL DISTURBANCES AND COMMANDS	IMPLIED REQUIREMENTS	COMPETING SYSTEMS				COMMENTS
			SYSTEM A		SYSTEM B		
			PARALLEL	SERIES	PARALLEL	SERIES	
Localizer Capture	Crosswind from side of capture	Smooth transition from heading hold to localizer track	Switch when $K_y y + K_{\dot{y}}\dot{y} = 0$	$\dot{\phi} \rightarrow \delta_{LAT}$ SCAS	Switch when $y \ll y_o$	$\varphi, \dot{\phi} \rightarrow \delta_{LAT}$ SCAS	
Curved Localizer Capture and Track	Tailwind at capture Tailwind at straight course intercept Low values of R for given approach speed, e.g., $V_{GS}^2/Rg \doteq \varphi_{LIM}$	Switch ΔT sec before before curved course intercept $\varphi_{LIM} = \pm 30^o$ Path damping all with derived and complementary filtered $\dot{y}$	$\varphi_c = V^2/Rg$ feedforward $\varphi, y, \dot{y} \rightarrow FD_{LAT}$	$\dot{\phi} \rightarrow \delta_{LAT}$ SCAS IAS $\rightarrow \theta_c$	Washed-out $\varphi \rightarrow FD_{LAT}$ $y, \dot{y} \rightarrow FD_{LAT}$	$\varphi, \dot{\phi} \rightarrow \delta_{LAT}$ SCAS IAS $\rightarrow \theta_c$	Need high quality beam for B . Washed-out director is less complex to mechanize but will not follow very small radius paths due to initial overshoot Airspeed hold shall be automatic Active controls will be δ_{CL} and δ_{LAT} Cannot have φ_c SAS if System B is selected
Localizer Track (Before Final Deceleration)	Crosswind shear Crosswinds	All inner loops must be washed out to avoid standoffs (except φ) Minimize disturbances due to windshear, e.g., $y_{ss} \doteq \dot{v}_g(K_\varphi/gK_y)$	$y, \dot{y}, \varphi \rightarrow FD_{LAT}$	$\varphi, \varphi \rightarrow \delta_{LAT}$ SCAS (attitude command) or $\dot{\varphi} \rightarrow \delta_{LAT}$ SCAS (rate command) or $\dot{\varphi} \rightarrow \delta_{LAT}$ SCAS $\psi \rightarrow \delta_{YD}$ SCAS $\psi_c \rightarrow \delta_{LOC}$ SCAS (wing low)	Washed-out $\varphi \rightarrow FD_{LAT}$ $y, \dot{y} \rightarrow FD_{LAT}$	$\dot{\varphi} \rightarrow \delta_{LAT}$ SCAS or $\dot{\varphi} \rightarrow \delta_{LAT}$ SCAS $\psi \rightarrow \delta_{PD}$ SCAS $(\psi_c = \psi_{LOC})$	System B is generally higher risk Can track LOC with wing low or conventional. Wing low popular but crosswind limited. Pilots selected wing low at Langley and Calspan.
Localizer Track (During Final Deceleration)	Crosswind shear Crosswinds	All inner loops must be washed out to avoid standoffs Minimize shear offsets Disallow large heading rate excursions when approaching hover in a crosswind (ψ or $\dot{\psi}$ limit)	$y, \dot{y}, \varphi \rightarrow FD_{LAT}$ with φ limits reduced to $\pm 10^o$	$y, \dot{y}, \psi \rightarrow \delta_{PD}$ SCAS $\dot{\psi}_{LIM} = \pm 1.5$ deg/sec $\dot{\phi} \rightarrow \delta_{LAT}$ SCAS (rate command) or $\varphi, \dot{\varphi} \rightarrow \delta_{LAT}$ SCAS (attitude command)	$y, \dot{y}, \varphi \rightarrow FD_{LAT}$ $\varphi_{LIM} = \pm 10^o$	$\dot{\varphi} \rightarrow \delta_{LAT}$ SCAS or $\varphi, \dot{\varphi} \rightarrow \delta_{LAT}$ SCAS	System A – combination wing low plus crab; $\dot{\psi}$ limited to 1.5 deg/sec and slowly transition to wings level & pointed into the wind; tentatively best system. System B is purely wing low Both systems have option for θ_c, ϕ_c Both systems – ψ control automatic with only low frequency trim left to pilot

TABLE 4. (Concluded)

DIRECT REQUIREMENTS	CRITICAL DISTURBANCES AND COMMANDS	IMPLIED REQUIREMENTS	COMPETING SYSTEMS				COMMENTS
			SYSTEM A		SYSTEM B		
			PARALLEL	SERIES	PARALLEL	SERIES	
Glide Slope Capture	Vertical gusts Tailwind	Smooth transition from altitude hold to glide slope track	$K_d d + K_{\dot{d}} \dot{d} = 0$ is switch point Step $\delta_{CL} \rightarrow FD_{CL}$ (set up trim collective)	$\theta, \dot{\theta} \rightarrow \delta_{LN}$ SCAS IAS $\rightarrow \delta_{LN}$ FFS	Switch at fixed distance from glide slope Step $\delta_{CL} \rightarrow FD_{CL}$	$\theta, \dot{\theta} \rightarrow \delta_{LN}$ SCAS IAS $\rightarrow \delta_{LN}$ SCAS	Airspeed control is automatic except for trim changes which exceed SCAS authority System B was used successfully (see Ref. 6) Tentatively use B
Glide Slope Track	Decreasing headwind shear Decreasing tailwind shear	Good $\dot{h}/\delta_{CL}$ bandwidth, e.g., $1/T_{\theta_2}$ large $\left[\frac{\dot{h}}{\delta_{CL}} = \frac{Z_{\delta_{CL}} Z_{\delta_{LN}}^{\dot{h}}}{Z_{\delta_{LN}}^{\theta}} \frac{\theta}{s + 1/T_{\theta_2}}\right]$ Good margins from γ_{max} and γ_{min}. γ_{min} is expected to be limiting factor on FD A due to low deceleration capability No requirement to convert control technique Airspeed command to allow deceleration on glide slope	$d, \dot{d} \rightarrow FD_{CL}$	$\theta, \dot{\theta} \rightarrow \delta_{LN}$ SCAS IAS $\rightarrow \delta_{LN}, \delta_{CL}$ FFS			Use backside control technique at all speeds May need to augment $1/T_{\theta_2}$; problem because δ_{CL} has no SCAS actuator Need γ-V curves to check $\Delta\gamma$ capability and deceleration problems
Deceleration to Hover	Decreasing headwind shear Decreasing tailwind shear	Same as above plus following Account for large trim shift in δ_{CL} Deceleration profile acceptable to pilots	$d, \dot{d} \rightarrow FD_{CL}$ Step $\delta_{CL} \rightarrow FD_{CL}$ for trim shift	$\theta, \dot{\theta} \rightarrow \delta_{LN}$ SCAS $\theta_c \rightarrow \delta_{LN}$ FFS $\dot{X} + KX \rightarrow \delta_{LN}$ FFS at very end			Use constant θ deceleration profile with $\dot{X} + KX = 0$ at the end
Hover	Horizontal winds	Need θ_c and φ_c attitude systems Good $\dot{h}/\delta_{CL}$	$X \rightarrow FD_{LN}$ $y \rightarrow FD_{LAT}$ $b_{TRIM} \rightarrow FD_{CL}$	$\dot{h} \rightarrow \delta_{CL}$ FFS $\dot{X}, \dot{\theta}, \theta \rightarrow \delta_{LN}$ SCAS $\dot{y}, \dot{\varphi}, \varphi \rightarrow \delta_{LAT}$ SCAS	$X, \dot{X}, \theta \rightarrow FD_{LN}$ $y, \dot{y}, \varphi \rightarrow FD_{LAT}$ $b_{TRIM} \rightarrow FD_{CL}$	$\theta, \dot{\theta} \rightarrow \delta_{LN}$ SCAS $\varphi, \dot{\varphi} \rightarrow \delta_{LAT}$ SCAS $\dot{h} \rightarrow \delta_{CL}$ FFS	System A – δ_{LN} and δ_{LAT} are used to command translational rates System B – δ_{LN} and δ_{LAT} are conventional θ_c and φ_c; see Langley, Calspan
Vertical Descent	Horizontal winds	Flare low	$\dot{X}, \dot{\theta}, \theta \rightarrow \delta_{LN}$ $\dot{y}, \dot{\varphi}, \varphi \rightarrow \delta_{LAT}$ $\dot{b}_{TRIM} \rightarrow \delta_{CL}$	$h + (1/T_F)\dot{h} = \dot{h}_{TD_c}$ $\dot{h}_c \rightarrow \delta_{CL}$ FFS			Use exponential flare Altitude automatic with pilot "tweaker" on δ_{CL} Pilot controls X, y

TABLE 5

CONSIDERATIONS AFFECTING CHOICE OF LATERAL PATH CONTROL TECHNIQUE (STRAIGHT LOCALIZER)
(From Refs. 8 and 9)

WING LOW	CRAB
Pro: Flight test showed pilots controlled localizer with greater precision using wing low. Consistently selected wing low shortly after intercepting localizer (pages 11 and 12 of Ref. 8.)	Pro: Crab can handle large crosswinds. Only way to descend vertically and land in significant wind is to point into the wind if Y_v is significant.
Con: Wing low limited to ±5 deg* of bank for pilot acceptance (about 10-15 kt† crosswind). Pilots show some concern for steady lateral acceleration. Concerned about lack of excess control capacity when at 4 or 5 deg bank.	Con: Precise heading control is very difficult at low speed. Small deviations in φ result in large $\dot{\psi}$ excursions since $r = g\varphi/V$.

Conclusion: Best solution is to use crabbed approach for higher speeds wherein precision of heading control is not a problem and wing low at lower speeds. At lower speed Y_v is very small for the XV-15. This permits the wing low technique to be used without requiring large bank angles, and avoids the heading control problems associated with crabbed approaches at low speeds.

*1 deg = 1.745×10^{-2} rad.
†1 kt = 5.144×10^{-1} m/s.

D. SUMMARY

The longitudinal SCAS is a rate-command/attitude-hold system for all phases of the approach. Analysis of each phase of the approach has shown that attitude command is actually closer to optimum in terms of meeting the pilot-centered and guidance and control requirements. In addition, it minimizes system complexity. The decision to use rate-command/attitude-hold is based entirely upon requirements imposed by the limited authority series servo. A 2 kt/sec (1 m/s) wind

shear for 15 sec requires a series actuator displacement of 2 in. (0.05 m) for an attitude command system, which is double the existing authority. The rate command system requires only 1/2 in. (0.013 m) series actuator displacement for the same input. The basic deficiency of the rate command system is that it adds an additional integration to the effective aircraft dynamics, requires more complex equalization, and produces, in some cases, less desirable flight director and aircraft response characteristics. Points favoring the rate command system include the elimination of trim requirements (with a corresponding decrease in pilot workload) and considerable pilot acceptance in recent years in test aircraft.

The lateral SCAS has been configured as a rate-command/attitude-hold system for all flight conditions from cruise to hover, vertical descent and touchdown. It is a well-established fact that attitude command is superior to rate command during hover. However, lateral attitude command at significant forward speed is less desirable than rate command because of the need to hold a constant lateral stick input for the wing-low mode or for the curved path tracking mode. Hence, it would be necessary to use rate command during the approach and phase into attitude command at some point approaching hover. To be successful such blending would require a series of manned simulator experiments to establish its pilot acceptability. These experiments are beyond the scope of this effort.

In the final analysis, the low authority series servos [±1 in. (±0.025 m)] of travel] effectively eliminates all but one manual control system (rate command, attitude hold). It is therefore not possible to exercise the full range of usual considerations of guidance and control and pilot-centered requirements in the competing systems tradeoff analyses. In fact, there is considerable evidence indicating that rate command is among the <u>least</u> desirable SCAS configurations for precision IFR hovering. This results in the difficult position of having to optimize a system within given constraints which are known to lead to a fundamentally deficient manual control system. Based on currently available data Cooper-Harper ratings on the order of 4 to 6 are expected for hovering in turbulence under instrument meteorological conditions (IMC). An advance in the current state of the art would require a tradeoff between an attitude command and a translational rate command (TRC) SCAS for hover. Issues such as consonance

between pitch attitude and stick position with a TRC SCAS in a helicopter would represent the key tradeoffs if actuator authority were not the limiting factor. A good TRC SCAS would be expected to yield pilot ratings on the order of 2 to 3 for hovering in IMC in turbulence.

The system requirements developed in this section lead to the selection of the "best" longitudinal and lateral-directional systems which are analyzed in detail in Sections III and IV, respectively.

SECTION III

LONGITUDINAL SYSTEM DESIGN

A. SYSTEM SUMMARY

A summary of the longitudinal system is given in the block diagram in Fig. 2. The feedback path equalization and switching logic shown in Fig. 2 includes provision for the following modes:

- Altitude hold
- Constant speed approach on MLS flight path
- Deceleration on MLS flight path
- Hover on MLS flight path
- Hover at constant altitude
- Vertical descent to touchdown

A summary of the gains and time constants for the longitudinal system is given in Table 6.

The basic design philosophy is to treat the flight director design as primary. The automatic system design is then obtained by a simple replacement of the pilot block in Fig. 2 with an automatic system gain. The gain values labeled K_c in Table 6 reflect the value to be inserted for the Y_{p_c} block in the automatic mode. The collective axis is fully automatic throughout the approach.

Plots of open-loop flight director frequency response to longitudinal cyclic are shown for each mode throughout this section to illustrate the degree to which the desired K/s frequency response characteristic has been achieved. The airplane plus flight director sensitivity (K) was not optimized at the time these plots were made. Reference 10 has established that the optimum K is 0.4 inches/sec of flight director bar deflection per inch of stick displacement. The values of K_{FD_c} in Table 6 reflect the final adjustment necessary to achieve a 0.4/s flight director. The autopilot gain K_c is simply the pilot gain used for the closures in this section adjusted for the final K_{FD_c}.

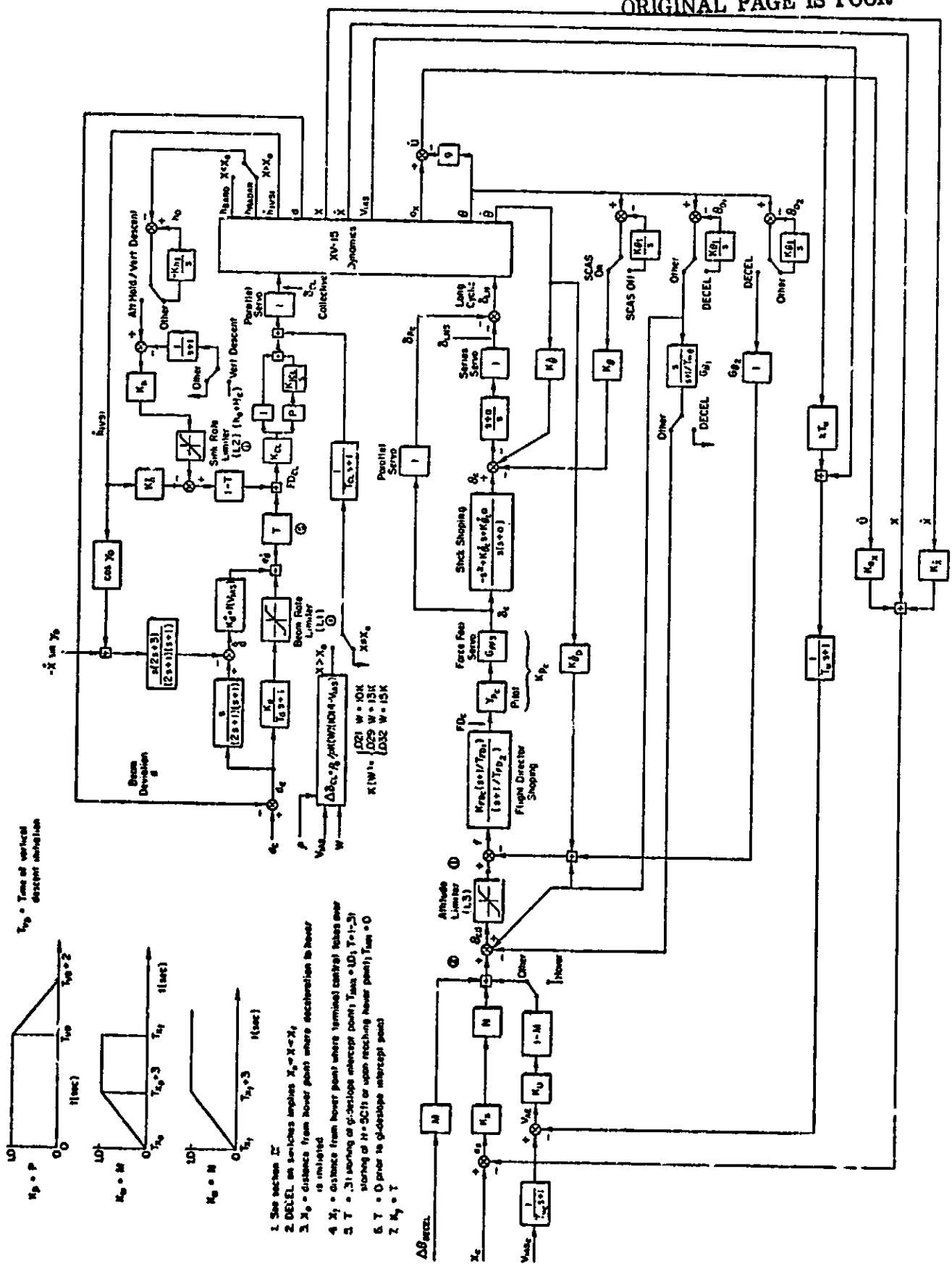

Figure 2. Longitudinal System Block Diagram

TABLE 6. SYSTEM GAINS AND TIME CONSTANTS

1. Rate Command/Attitude Hold SCAS (All Modes)

K_θ = 12 in./rad

$K_{\dot\theta}$ = 8 in./(rad/sec)

a = 1 (1/sec)

$K_{\dot\theta_c}$ = 2.09 1/sec

2. Constant Speed Glide Slope Tracking, $X < X_o$

T_{w_θ} = 5 sec = $1/\omega_{w\theta}$

T_u = 0.67 sec = $1/\omega_u$

T_{u_c} = 10 sec

T_{FD_1} = 0.222 sec = $1/\omega_{FD_1}$

T_{FD_2} = 0.222 sec = $1/\omega_{FD_2}$

k = 7.5

$K_{P_c} = G_{FFS}(0)K_c$ = 3.2

T_d = 0.25 sec = $1/\omega_{11}$

K_d = 0.01 in./ft

$K_{\dot d} = \dfrac{0.01}{0.19 + 0.00296V_{IAS}}$ in./(ft/sec) (V_{IAS} in ft/sec)

$K_{\dot\theta_D}$ = 1.0 sec

K_{FD_c} = 1.43 in./rad

K_{CL} = 5.0

K_{ICL} = 1.0 (1/sec)

K_u = −0.005 rad/(ft/sec)

3. Deceleration to Hover, $X_o < X < X_f$

T_{CL} = 1 sec = $1/\omega_7$

T_{FD_1} = 0.222 sec = $1/\omega_{FD_1}$

T_{FD_2} = 0.222 sec = $1/\omega_{FD_2}$

$K_{\dot\theta_D}$ = 0.5 sec

K_{FD_c} = 2.52 in./rad

K_d, $K_{\dot d}$, K_{CL}, K_{ICL} } Same as for $X < X_o$

T_d = 0.25 sec

4. Hover, $X \geq X_f$

T_{w_θ} = 4.0 sec = $1/\omega_{w\theta}$

T_{FD_1} = 0.5 sec = $1/\omega_{FD_1}$

T_{FD_2} = 0.222 sec = $1/\omega_{FD_2}$

$K_{\dot\theta_D}$ = 1.33 sec

K_{a_x} = 16 sec^2

$K_{\dot x}$ = 8 sec

K_x = −0.005 rad/ft

K_{FD_c} = 1.8 in./rad

$K_{P_c} = G_{FFS}(0)K_c$ = 3.2

$K_d = K_h$ = 0.01 in./ft

$K_{\dot d} = K_{\dot h}$ = 0.053 in./(ft/sec)

K_{CL} = 5.0

K_{ICL} = 1.0 (1/sec)

5. Vertical Descent

T_{w_θ}, T_{FD_1}, T_{FD_2},

$K_{\dot\theta_D}$, K_{a_x}, $K_{\dot x}$, K_H,

$K_{\dot\theta_c}$, K_{FD_c}, and K_c

same as Hover

K_h = 0.032 in./ft

$K_{\dot h}$ = 0.20 in./(ft/sec)

K_{CL} = 1.0

K_{ICL} = 1.0 (1/sec)

H_c = 7 ft (16 ft in performance evaluation)

The remainder of this section contains a description of each of the modes of the longitudinal system, and includes a brief account of the rationale used to select equalization feedbacks and time constants.

A basic design concept for this system has been to limit the number of active flight directors to one in the longitudinal axis (and one in the lateral axis). This design concept follows directly from the pilot-centered requirement for frequency separation of controls (discussed in more detail in Ref. 10). Furthermore, a single control should remain primary throughout the approach. That is, the same control should be primary from glide slope intercept to touchdown. Longitudinal and lateral cyclic have been designated the primary controls for this design. This turns out to be a fortunate choice since the possibility of adding a series servo for the collective axis is currently unlikely. However, a strategy for including the collective control as an inherent part of the manual mode has been included to provide a backup position. In the event that a series actuator should become available for the collective axis, the manual flight director signal for this axis is available directly in the current system design.

B. LONGITUDINAL SCAS

The longitudinal SCAS is a rate-command/attitude-hold system for all phases of the approach.

The stick shaping equalization shown in Fig. 2 was designed to produce a pure rate command in the presence of a mechanical parallel path. The forward loop integrator, $(s + a)/s$, is required to get good mid- and low-frequency attitude responses. The mid- and low-frequency attitude response of the basic XV-15 is poor in the extreme. The feedback gains K_θ and K_q are set to achieve an attitude bandwidth of between 1.5 and 2 rad/sec. This corresponds to a K_θ of 0.2 in. (0.005 m) of series servo travel per degree of attitude. Since the maximum series servo authority is 1 in. (0.025 m), SCAS limiting will occur at 5 deg (0.09 rad) of pitch attitude deviation from trim. This is expected to be marginal but acceptable. Lower values of pitch attitude feedback gain would minimize the limiting problem at the expense of unacceptably low attitude bandwidth. The frequency response characteristics in attitude with and without

the SCAS are shown in Fig. 3 for 60, 40, 20 and 0 kt (31, 21, 10 and 0 m/s). It is not necessary to change the gain as a function of flight condition to achieve these results. The rate command feature of the SCAS is obtained by setting K_{ϑ_c} in Fig. 2 equal to 2.09. This results in 10 deg/sec (0.17 rad/sec) of pitch attitude per inch (0.025 m) of longitudinal cyclic stick deflection. This control sensitivity was found to be optimum in the study done in Ref. 10.

C. CONSTANT SPEED GLIDE SLOPE TRACKING

The feedbacks which are active (switched in) for constant-speed glide slope tracking are listed below:

- Washed-out pitch attitude — Pitch attitude is required for flight director equalization and is washed out to avoid standoffs between the indicated airspeed and trim attitude.

- Pitch attitude rate — This feedback is also required for flight director equalization. Roll stabilized pitch rate must be used (that is, $\dot{\theta}$ in distinction to q) to avoid large pitch-down commands during turns.

- Airspeed feedback — The airspeed feedback has been lagged by $1/T_u$ to keep high-frequency gusts from exciting the system. This in turn results in unacceptably low phase margin in the flight director loop. To overcome this, longitudinal acceleration-independent-of-pitch is pseudo-integrated and complemented with lagged airspeed. For a perfect complementary filter, the constant k is set equal to unity (see Fig. 2 at right-hand side). If k is greater than 1, a lead-lag on the speed feedback results; and if k is less than 1 a lag-lead results. Flight director equalization requirements dictate a lead-lag corresponding to k = 7.5.

The frequency response characteristics of the longitudinal flight director to longitudinal cyclic input are shown for 60 and 40 kt (31 and 21 m/s) in Fig. 4.* This figure indicates that the desired K/s response is achieved up to about 2 rad/sec at 60 kt (31 m/s) and 3 rad/sec at 40 kt (21 m/s). While it would be desirable to have the K/s region extend to a higher frequency, espe-

*Figure 4 has root locus information overplotted on the frequency response, $G(j\omega)$. This root locus information plots the modulus for each closed-loop root (read on the frequency axis) as a function of the inverse of the open loop gain (read on the dB magnitude axis). The interested reader can find a more detailed exposition on pages 139-153 of Ref. 14.

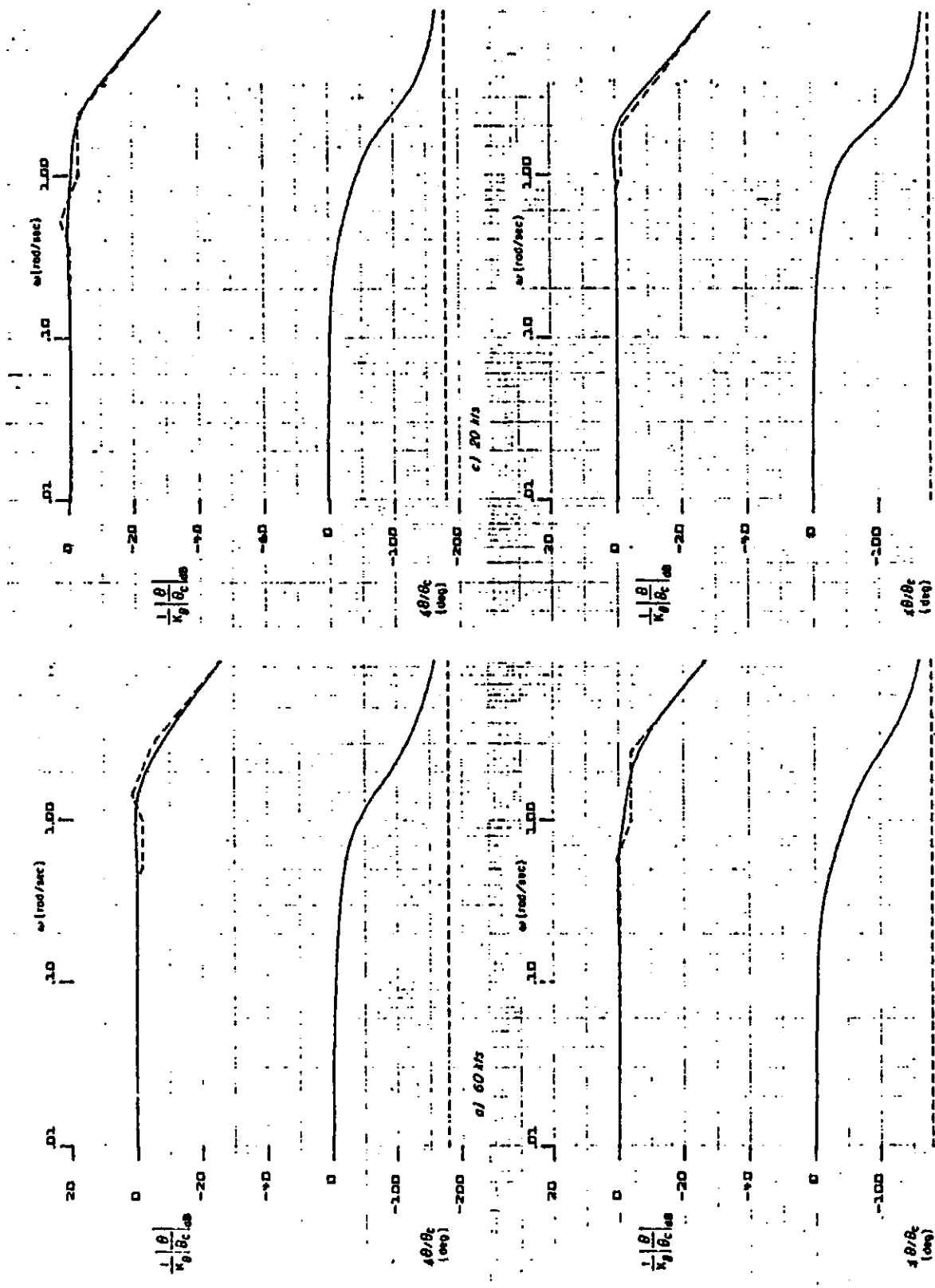

Figure 3. Frequency Response Characteristics of the Attitude Hold Feature of the Rate Command/Attitude Hold SCAS

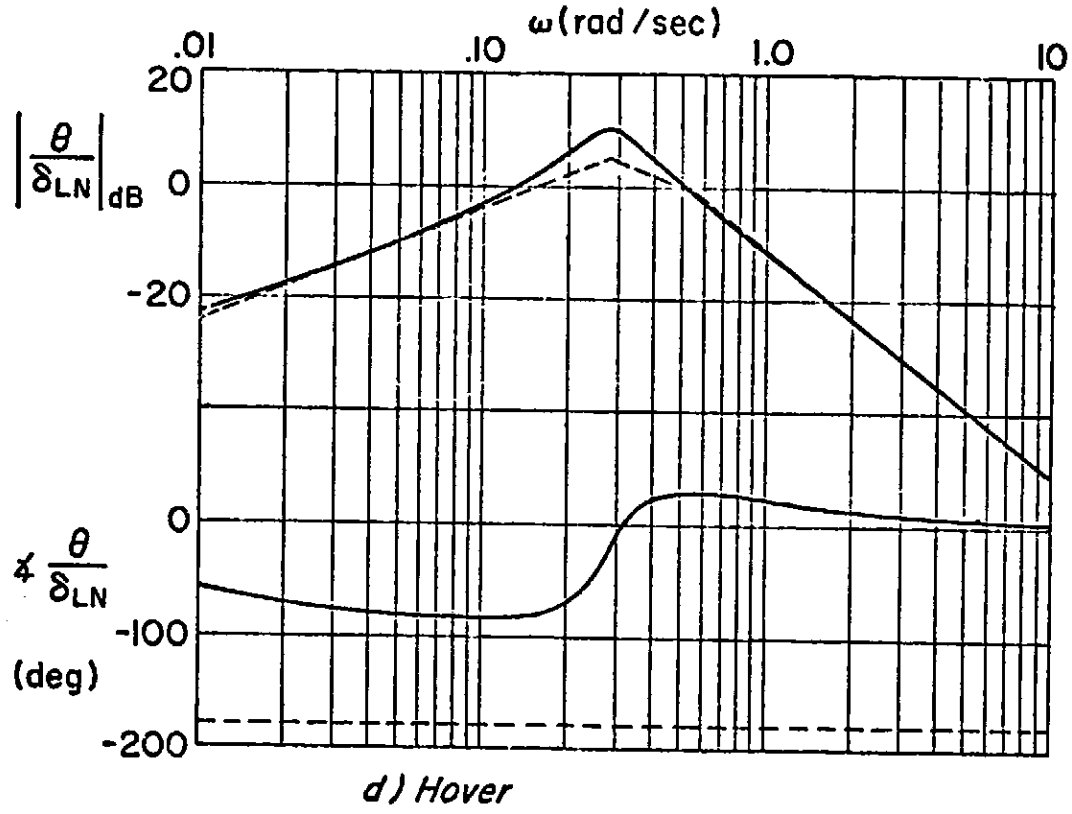

d) Hover

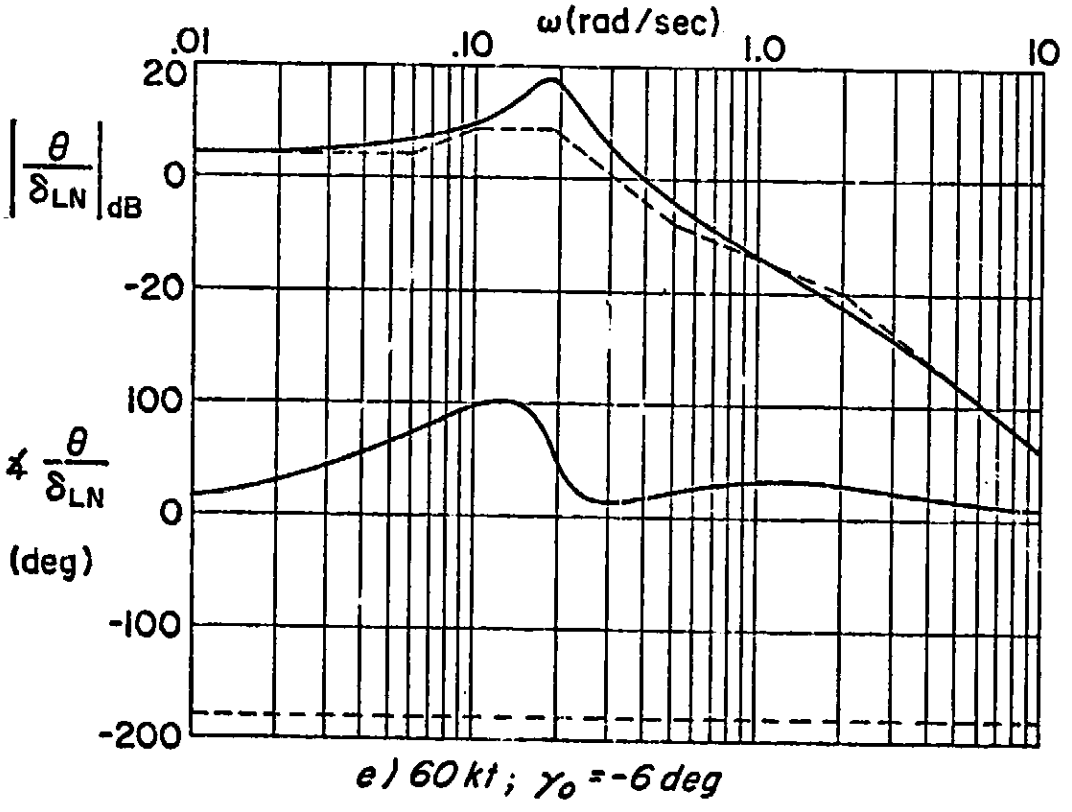

e) 60 kt; $\gamma_o = -6$ deg

Figure 3b. Open-Loop Frequency Response Characteristics for Pitch Attitude in Response to Longitudinal Cyclic Pitch

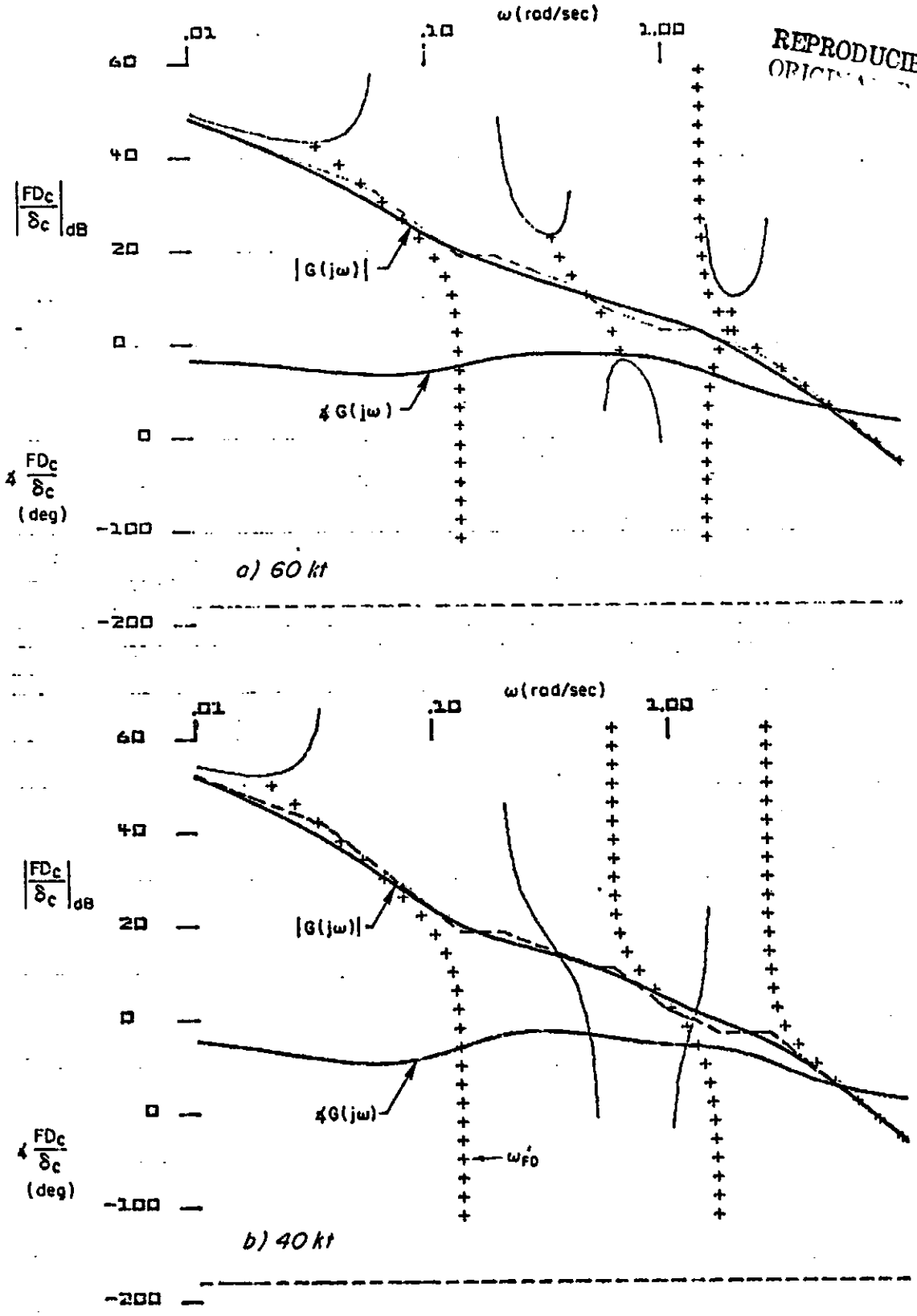

Figure 4. Open-Loop Response Characteristics of Longitudinal Cyclic Flight Director

cially at 60 kt (31 m/s), it is felt that the current system will be adequate. Extending the K/s region to higher frequency would require increased SCAS bandwidth which is currently limited by the series servo authority. Therefore bandwidth extension is not possible with the current system.

The requirements imposed on the longitudinal flight director to achieve regulation of the glide path with collective while pitch attitude is constrained by means of the longitudinal cyclic control are best illustrated by the following equation (from Ref. 7):

$$\left(\frac{\dot{d}}{\delta_{CL}}\right)_{\theta \rightarrow \delta_{LN}} \doteq \frac{N^{\theta}_{\delta_{LN}} N^{\dot{d}}_{\delta_{CL}}}{N^{\theta}_{\delta_{LN}}} = \frac{A_{d\theta}\left(s + \frac{1}{T_{d\theta}}\right)}{\left(s + \frac{1}{T_{\theta_1}}\right)\left(s + \frac{1}{T_{\theta_2}}\right)} \qquad (1)$$

An examination of the transfer functions in Table 7 reveals the following facts concerning the above equation:

- $1/T_{\theta_1}$ cancels $1/T_{d\theta}$ at all flight conditions so that the form of $\dot{d}/\delta_{CL}$ is

$$\frac{\dot{d}}{\delta_{CL}} \doteq \frac{A_{d\theta}}{\left(s + \frac{1}{T_{\theta_2}}\right)} \qquad (2)$$

- The bandwidth of $\dot{d}/\delta_{CL}$ is defined by $1/T_{\theta_2}$ and is unacceptably low at 0 and 20 kt (0 and 10 m/s) and is marginal at 40 and 60 kt (21 and 31 m/s).

- Augmentation of $1/T_{\theta_2}$ will be achieved by feedback of beam rate (approximately vertical velocity) to the collective control. This indicates that the fully automatic collective control will act simultaneously as a SCAS to augment $1/T_{\theta_2}$ and as a path control function to regulate the glide slope errors to zero by virtue of beam deviation feedback to the collective control.

The transfer functions for flight path angles of -6 and -10 deg (-0.10 and -0.17) at 40 and 60 kt (21 and 31 m/s) (see Table 7) are essentially identical, indicating that the effect of flight path angle on vehicle dynamics is small and can be neglected.

TABLE 7. XV-15 TRANSFER FUNCTIONS*
(HELICOPTER MODE ONLY)

F.C.	57-0	58-6	59-6	60-6	61-6	59-10	61-10
V (kt)	0	20	40	60	80	40	80
γ (deg)	0	−6	−6	−6	−6	−10	−10
Δ_{LONG}	(.2)(.57)[−.25,.28]	[−.1,.33][−.03,.33]	[−.11,.19][.61,1.47]	(−.10)(2.1)[.18,.19]	[.09,.29][.89,1.51]	[−.05,.2][.7,1.21]	[−.02,.50][.95,1.14]
$N^{\theta}_{\delta_{LN}}$	−.28(−.006)(.2)	−.31(−.01)(.37)	−.36(.04)(.52)	−.41(.06)(.51)	−.46(.05)(.70)	−.34(.04)(.48)	−.45(.04)(.69)
$N^{\dot{w}}_{\delta_{LN}}$	1.2(.2)[.08,2.71]	1.2(.3)[.31,3.02]	1.06(.46)[.45,3.44]	.95(.60)[.38,3.5]	.79(.76)[−.09,4.12]	1.23(.47)[.43,3.08]	.71(.68)[−.14,4.50]
$N^{\dot{q}}_{\delta_{COL}}$	4.06(.57)[−.25,.28]	4.01(−.07)[.47,1.04]	4.08(−.09)[.54;1.27]	4.5(−.06)(−.55)(2.09)	4.82(1.84)[.31,.35]	4.01(−.08)[.64,1.02]	4.8(1.15)[.27,.55]
$N^{\dot{q}}_{\delta_{LN}}$	.068(2.22)[−.41,1.44]	−.17(−.91)[.09,3.4]	−.48(−.25)[.11,4.63]	−.91(−.06)[.14,4.71]	−1.32(.013)[.17,5.67]	−.47(−.30)[.1,4.21]	−1.36(0)[.13,5.4]
$N^{\theta}_{\delta_{LN}} N^{\dot{q}}_{\delta_{COL}}$	−1.13(−.006)	−1.2(.041)	−1.47(.034)	−1.87(.035)	−2.3(.04)	−1.37(.046)	−2.14(.028)
Δ_{LAT}	(−.10)(.83)[−.13,.41]	(−.19)(.96)[.08,.67]	(.21)(1.14)[−.73,.26]	(.036)(1.42)[.03,.47]	(.05)(1.29)[.17,.60]	(.08)(1.15)[−.45,.23]	(.05)(1.19)[.05,.75]
$N^{v}_{\delta_{LAT}}$	.30[.21,.066]	.29[.14,.51]	.29(.36)(−.48)	.33[.25,.25]	.36[.14,.68]	.29(.27)(−.35)	.37[.21,.60]
$N^{r}_{\delta_{LAT}}$	−.02(−.2.7)[.17,.87]	−.021(−2.6)[.31,1.2]	−.042(1.0)[−.30,.75]	−.026(−.52)[.65,.66]	−.016(−7.4)[.06,.57]	−.02(.89)[−.4,.83]	−.04(−.72)[.65,1.1]
$N^{\dot{v}}_{\delta_{LAT}}$	.0056(.02)[.07,38.]	−.003(.12)(3.7)(−19.7)	−.0007(−.1)(2.6)(−98)	−.0002(.072)(3.1)(−191)	.0004(−.32)(−5.5)(16.8)	−.0007(−.07)(3.3) x (−60.5)	.0005(.15)(4.7)(42.6)
$N^{p}_{\delta_{PED}}$	.21(.62)[−.15, 1.93]	.005(−.32)(1.1)(−27.4)	.0006(−.16)(1.3)(−234)	.001(−.042)(1.55)(−161)	−.002(.006)(1.21)(54.2)	.0007(−.13)(1.36) x (−200)	−.0009(.012)(1.32) x (146)
$N^{r}_{\delta_{PED}}$	.12(.85)[−.24,.43]	.13(.84)[−.16,.38]	.14(1.13)[−.14,.40]	.15(1.35)[−.06,.37]	.13(1.1)[−.13,.38]	.14(1.12)[−.13,.37]	.13(1.11)[−.08,.34]
$N^{\dot{w}_y}_{\delta_{PED}}$	.21(−.21)(.83)[0,.42]	.17(−.28)(1.0)[.04,1.25]	.04(−.14)(1.21)[−.05,.93]	.10(−.04)(1.52) x [−.008,2.8]	−.32(.001)(1.2)(−1.8) x (2.1)	.048(−.12)(1.24) x [−.05,1.23]	−.11(.01)(1.36) x (3.1)(−3.2)
$\dot{\lambda}^{p}_{\delta_{LAT}}$	.25[.16,.065]	.275[.11,.51]	.139(.36)(−.48)	.102[.15,.24]	.085[.17,.67]	.137(.26)(−.34)	.086[.13,.59]
$\dot{\lambda}^{r}_{\delta_{LAT}} N^{r}_{\delta_{PED}}$	.036(0)(.014)	.038(0)(.05)	.039(0)(.0035)	.05(0)(.05)	.046(0)(.064)	.037(0)(.0072)	.042(0)(.071)
$\dot{\lambda}^{r}_{\delta_{LAT}} N^{r}_{\delta_{PED}}$	.0181(0)	.036(0)	.018(0)	.015(0)	.011(0)	.018(0)	.010(0)

*The shorthand transfer function notation used is $s + \frac{1}{\tau} \Rightarrow (\frac{1}{\tau_1})$ and $s^2 + 2\zeta\omega s + \omega^2 \Rightarrow [\zeta,\omega]$.

The above discussion indicates that the beam-rate-to-collective transfer function can be approximated by a first-order lag located at $1/T_{\theta_2}$. The collective flight director response to a collective control input can be approximated as follows:

$$\frac{FD_{CL}}{\delta_{CL}} \doteq -\frac{Z_{\delta_{CL}} K_{\dot{\theta}_c} K_{\dot{d}} T_{L_d} \left[s^2 + \frac{1}{T_d} s + \frac{K_d}{K_{\dot{d}}} \frac{1}{T_d} \right]}{M_{\delta_{LN}} s \left(s + \frac{1}{T_{\theta_2}} \right) \left(s + \frac{1}{T_{L_d}} \right)} \tag{3}$$

From Refs. 6 and 9 a value of K = 0.01 in. (0.00025 m) of flight director per foot (meter) of altitude error appears to give the appropriate sensitivity throughout the approach. The glide slope noise filter time constant T_d was set to 0.25 sec for noise rejection. $K_{\dot{d}}$ was set so that Eq. 3 could be factored as follows:

$$\left[s^2 + \frac{1}{T_{L_d}} s + \frac{K_d}{K_{\dot{d}}} \frac{1}{T_d} \right] = \left(s + \frac{1}{T_{\theta_2}} \right) \left(s + \frac{1}{T_{L_d}} \right) \tag{4}$$

thus providing the required zero at $1/T_{\theta_2}$. The resulting values of $K_d/K_{\dot{d}}$ were plotted versus speed and fitted to obtain the following expression for $K_{\dot{d}}$:

$$K_{\dot{d}} = \frac{K_d}{.19 + .005 V_{IAS}} \quad , \; V_{IAS} \text{ in kt} \tag{5}$$

The above values for K_d, $K_{\dot{d}}$, and T_d result in a K/s open-loop collective flight director response at all frequencies. This is shown in Fig. 5 for 80 and 40 kt (41 and 21 m/s). While the collective axis is fully automatic in the current system, the basic approach of first designing the flight director was used to improve monitoring characteristics for this control axis and to allow for possible future low-frequency manual control of this axis.

Referring to Fig. 2, the block normally allocated to the pilot (just downstream of T) is shown as a constant K_{CL} and a parallel integration K_{ICL}. The parallel integration is included in the forward loop to eliminate the

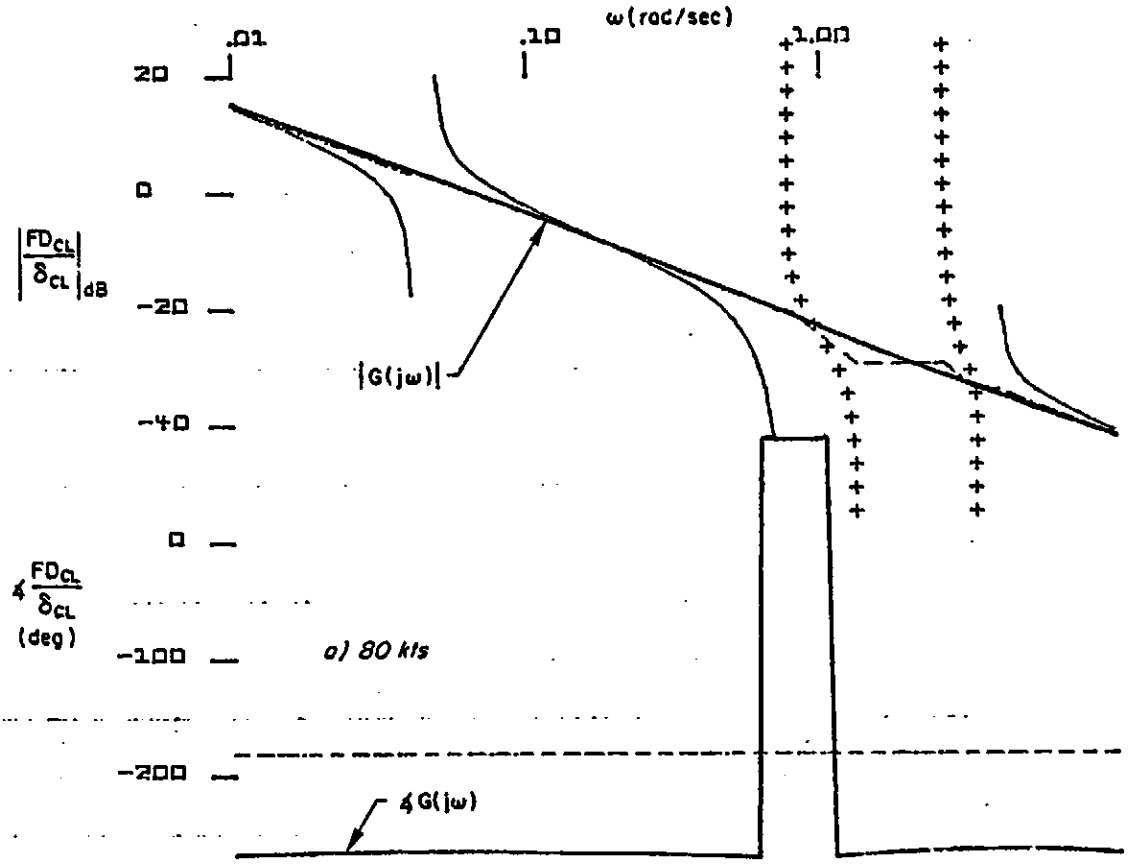

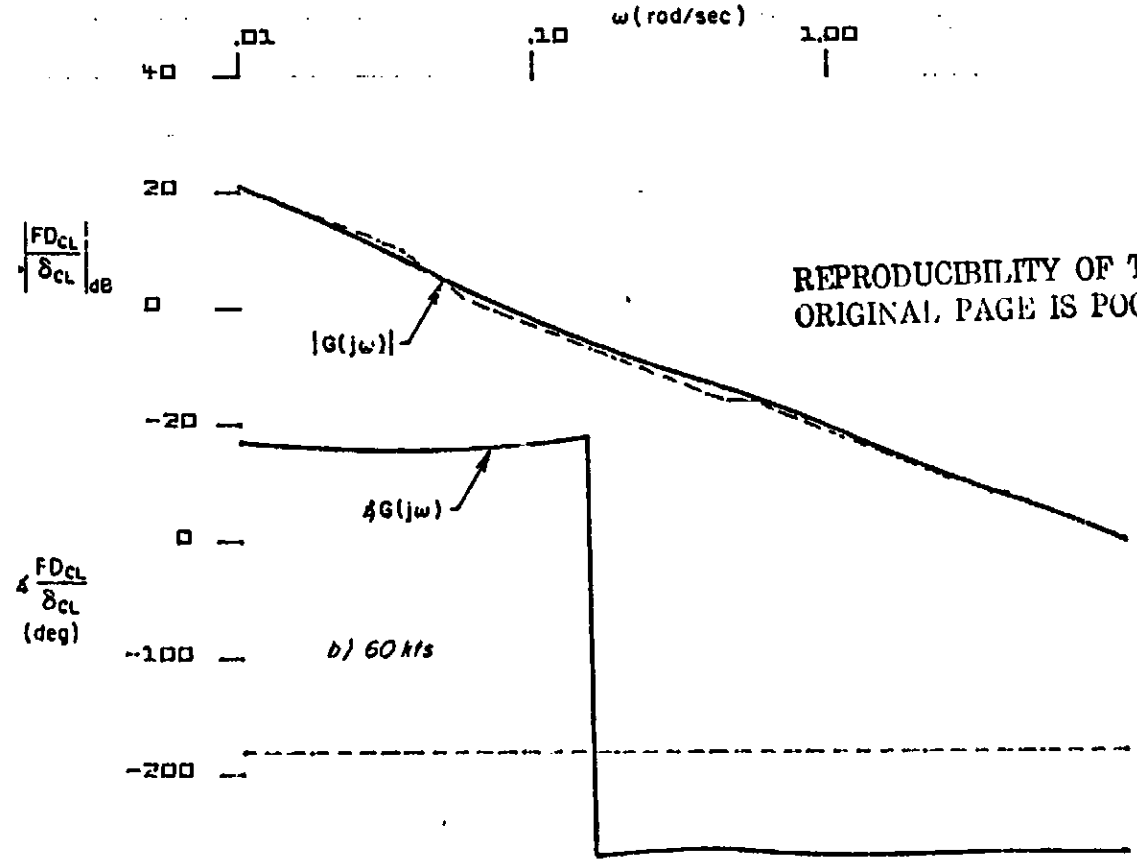

Figure 5. Open-Loop Response Characteristics of Collective Flight Director

possibility of standoffs. These automatic control paths provide control action which is equivalent to human pilot manual control action. That is, a pilot would not allow a constant flight director error to exist.

The speed control characteristics of the closed-loop longitudinal cyclic flight director system are checked by means of the speed-error-to-speed-command and speed-error-to-horizontal-gust frequency responses. A pilot model with a crossover frequency of 1.5 rad/sec and an effective delay of 0.17 sec is assumed for longitudinal cyclic control.

$$G_{FFS}(0)Y_{p_c} = .8e^{-.17j\omega} \qquad (6)$$

The frequency response characteristics are shown in Fig. 6. These responses reveal the following facts:

- Speed responses to horizontal gusts and speed commands exhibit zero steady-state errors. (T_{u_c} was set to zero to check this aspect of closed-loop system performance.)
- A bandwidth of about 0.12 rad/sec is achieved for speed command inputs. This bandwidth results from a tradeoff between conflicting objectives for tight speed control and minimum pitch attitude excursions. Aircraft with an additional control for controlling airspeed generally have higher speed control system bandwidth; however, a bandwidth of 0.12 rad/sec is well within the acceptable range for an aircraft using pitch attitude to control airspeed.
- Maximum gust sensitivity exists between 0.12 and 2.0 rad/sec. This reflects the selection of the airspeed feedback time constant of 0.67 sec at the upper end and the basic airspeed bandwidth of 0.12 rad/sec at the lower end.

The frequency response characteristics of the glide path control system are shown in Fig. 7 and indicate a bandwidth of about 0.85 rad/sec. This is a fairly tight glide slope system.

The final performance metric utilized to evaluate the system design is a critical wind shear disturbance taken from Ref. 11. This wind shear is 2 kt/sec (1 m/s) for 15 sec, followed by a steady 30 kt (15 m/s) wind.

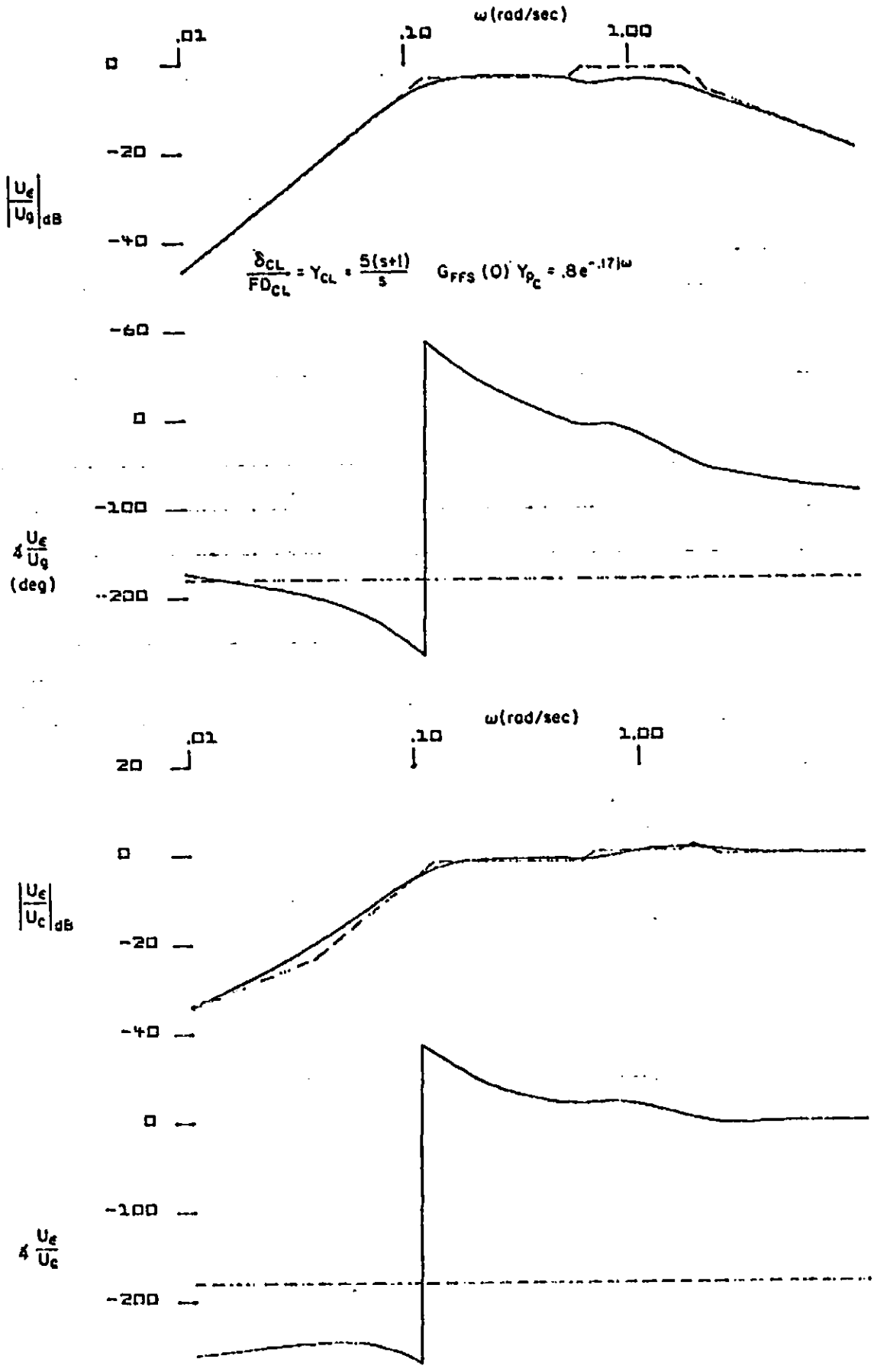

Figure 6. Performance Characteristics of Speed Control at 60 kt (31 m/s)

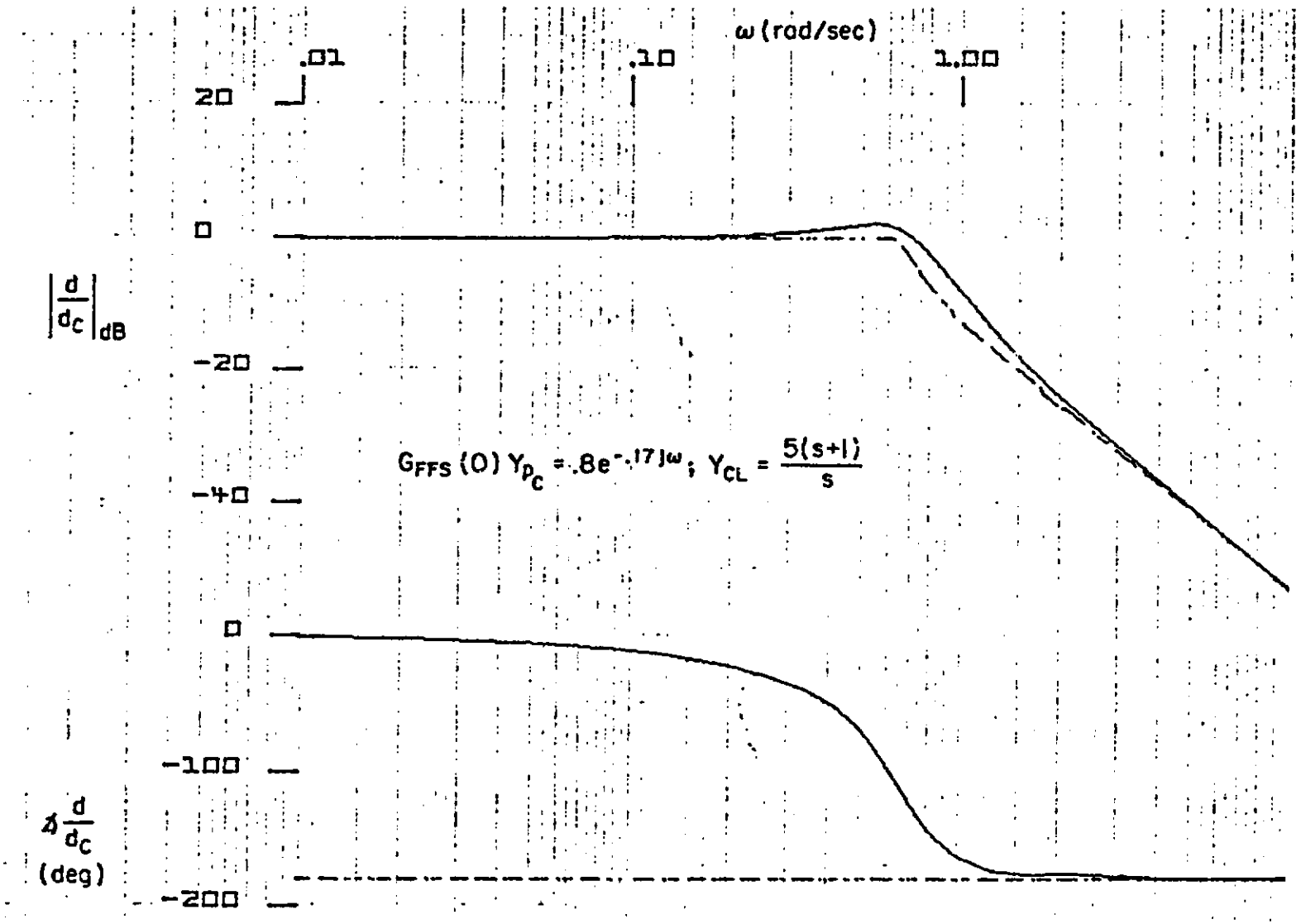

Figure 7. Frequency Response Characteristics of Glide Path Control at 60 kt (31 m/s)

To put this in perspective, Ref. 11 indicates that this shear resulted in marginal glide path control for a DHC-6 Twin Otter Aircraft. The time histories of the system response to this wind shear are shown in Fig. 8 which is subject to the following interpretation:

- The maximum speed error was only 9.5 ft/sec (2.9 m/s) out of a total 51 ft/sec (155 m/s) disturbance.
- The peak pitch attitude excursion was about −0.1 rad or −5.7 deg.
- The maximum series servo excursion was 0.5 in. (0.013 m) (half its total travel).
- The peak glide path excursion was only 4 ft (1.2 m).
- The collective control moved to maximum of 1.9 in. (0.05 m) or less than half its total travel.

D. DECELERATION ON GLIDE SLOPE

Final deceleration to hover is a constant attitude maneuver in order to minimize pilot workload. Inasmuch as the attitude response to a step longitudinal cyclic input is a pitch rate, equalizing the flight director to a K/s response is a simple matter. Attitude and attitude rate feedbacks are used to extend the K/s region as far as possible beyond the closed-loop short-period frequency of the rate-command/attitude-hold SCAS. Open-loop flight director responses to longitudinal cyclic inputs for 20, 40 and 60 kt (10, 21 and 31 m/s) are shown in Fig. 9. The method used to compute the incremental pitch attitude command ($\Delta\theta_{decel}$ in Fig. 2) is discussed later in this section. Inasmuch as the pitch attitude is the state variable being commanded during this phase of the approach, it is inappropriate to wash out the pitch attitude feedback to the flight director. Therefore, it was necessary to include the switching logic shown in Fig. 2 to remove the washout equalization on pitch attitude during the deceleration phase. The rationale for the switching logic shown in Fig. 2 is discussed as follows:

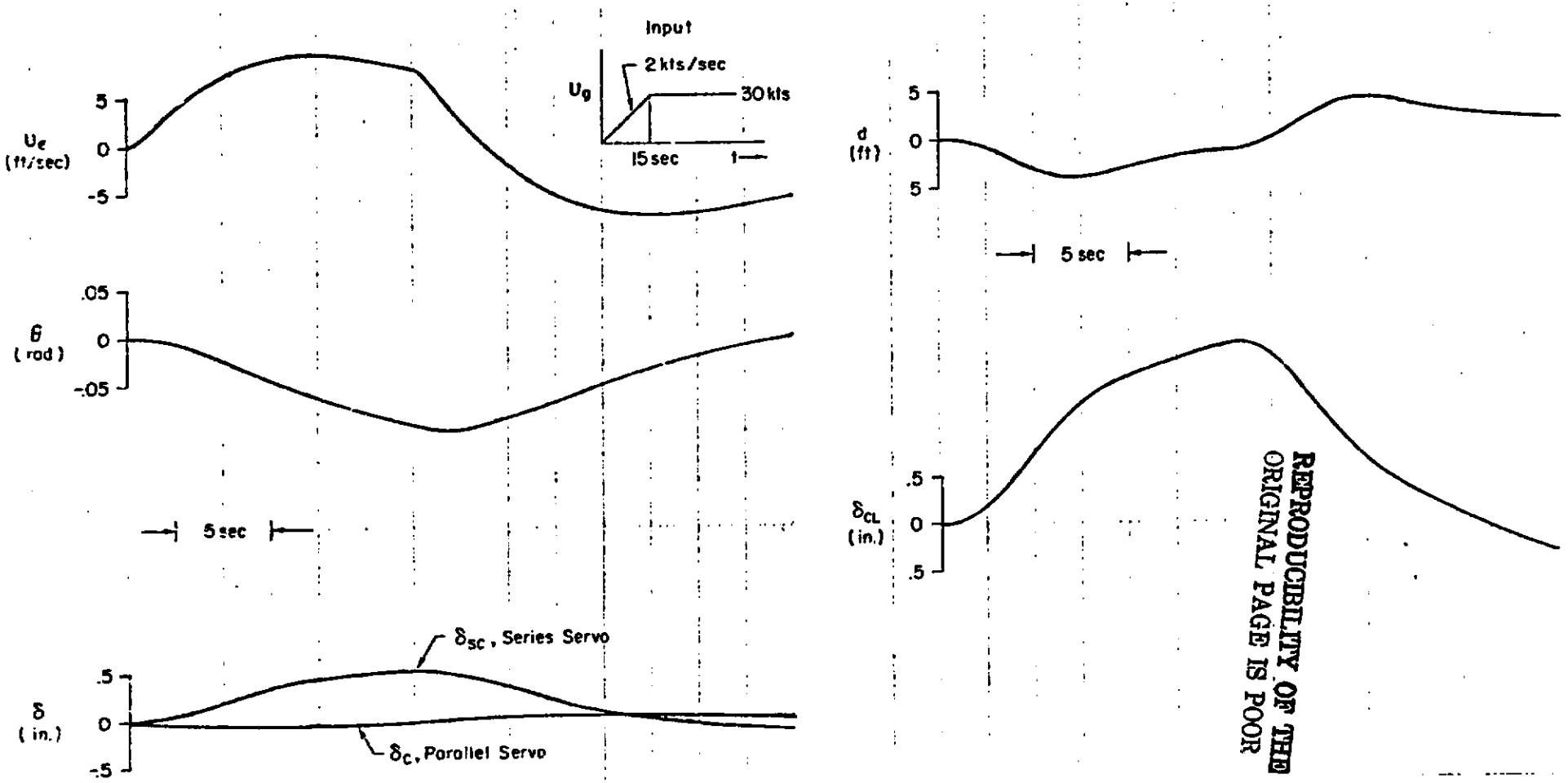

Figure 8. Time Response Characteristics for a Large Wind Shear Input at V = 60 kt (31 m/s)

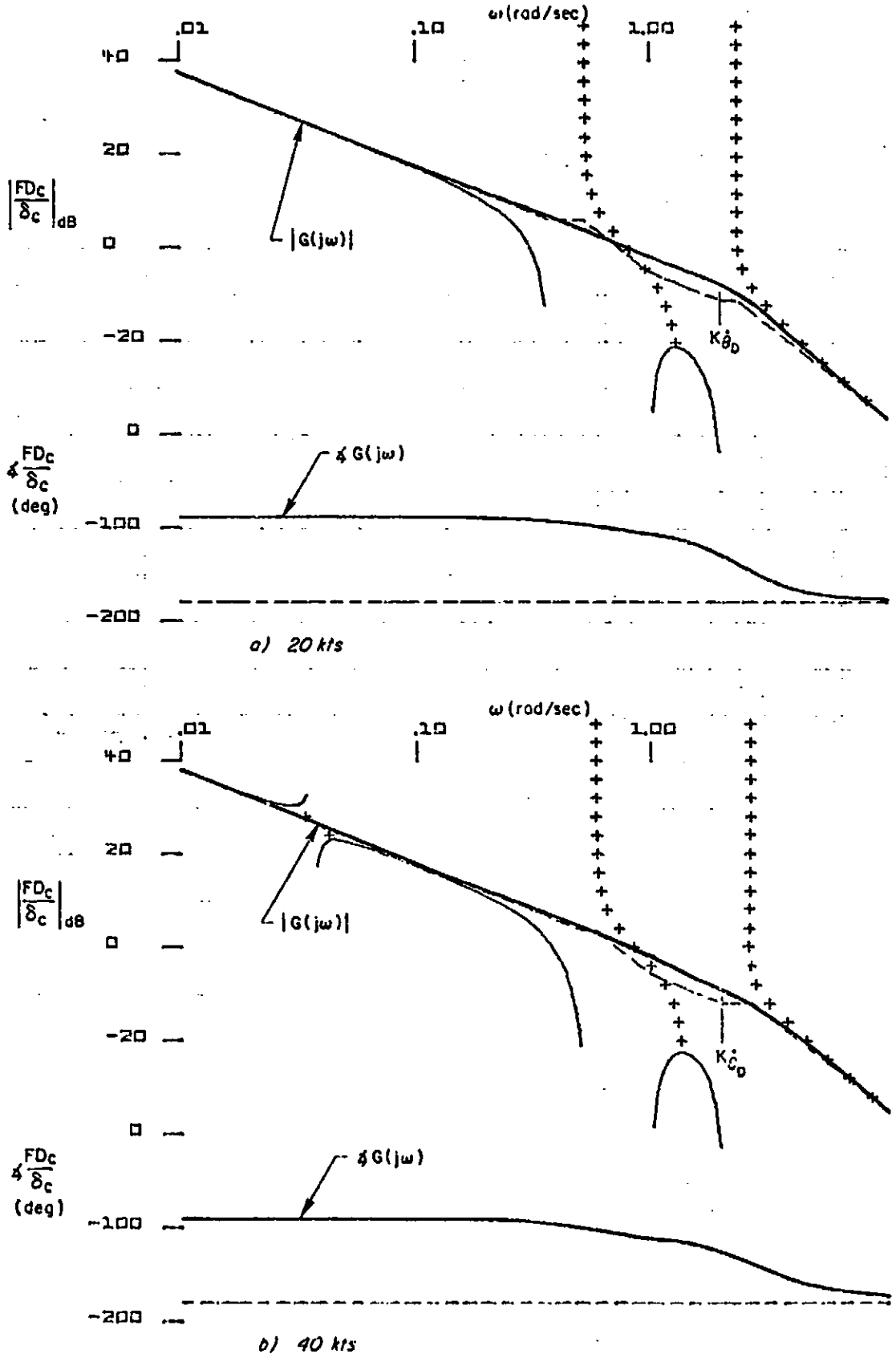

Figure 9. Open-Loop Flight Director Frequency Response, Deceleration to Hover

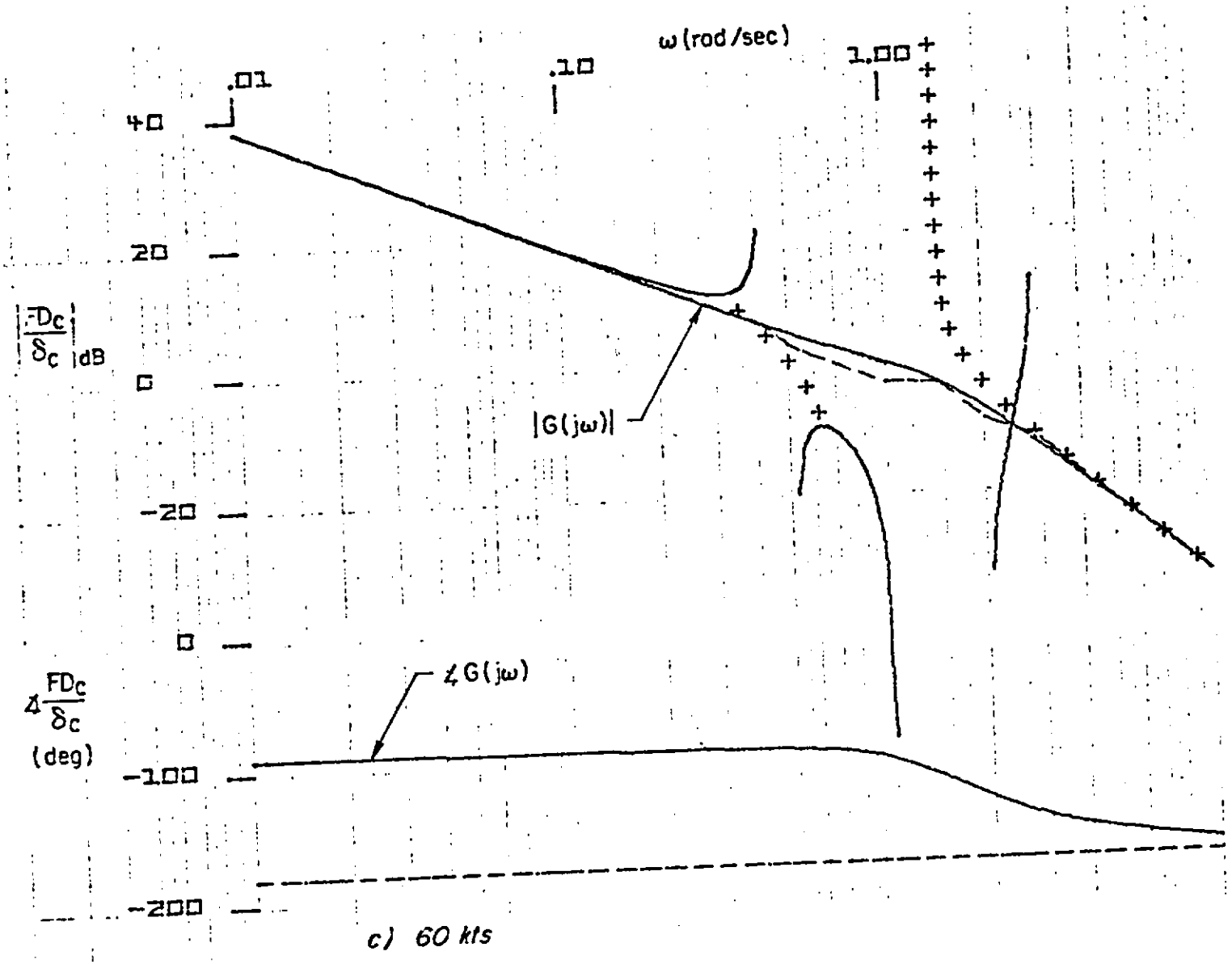

Figure). (Concluded)

1. $X < X_o$ (constant-speed approach phase)
   - Attitude is washed out via G_{θ_1}.
   - Attitude is fed to both sides of the pitch attitude limiter to account for washout in the feedback.

2. $X \geq X_o$ (deceleration phase)
   - The input to G_{θ_1} goes to zero rapidly. This will excite the washout circuit (looks like an input of the opposite sign) resulting in a transient output from G_{θ_1}. Therefore, a switch is included downstream of the washout equalization to avoid this transient.
   - The switch at the input of G_{θ_2} moves to the decel position. The synchronizer at the input of G_{θ_2} eliminates any transient at the switch point.
   - The initial input to G_{θ_2} is zero and becomes $\theta - \theta_{o_2}$ ($\theta_{o_2} = \theta$ at $X = X_o$) for $X > X_o$.
   - The commanded value ($\Delta\theta_{decel}$) must be referenced to the output of the synchronizer θ_{o_2}. Since θ_{o_2} is the last value of pitch attitude before switching from constant speed flight, θ_{o_2} represents the nominal pitch attitude for zero acceleration along the glide path at the trim approach speed. The constant attitude for deceleration ($\Delta\theta_{decel}$) is blended in via the M function shown in Fig. 2. This is done primarily to avoid sudden pitch transients when the system is in the automatic mode. Note that as the M function approaches unity, the speed feedback approaches zero due to the (1 − M) function in that feedback path.

3. $X \geq X_f$ (hover phase)
   - The washout circuit G_{θ_1} is switched back in and the nominal attitude reference is θ_{o_1}. θ_{o_1} is the nominal total pitch attitude used during the deceleration phase and is also defined as θ_f.
   - G_{θ_2}, $\Delta\theta_{decel}$ and K_u are switched out.
   - The longitudinal position feedback for hover control is blended in via the N function.

The switching ranges, X_o and X_f, are specified later in subsection H.2 of this section.

Power required to maintain a constant glide slope increases drastically during the deceleration to hover as the airspeed falls below 60 kt (31 m/s) (see Fig. 10). This fact results in initial excursions below the glide path

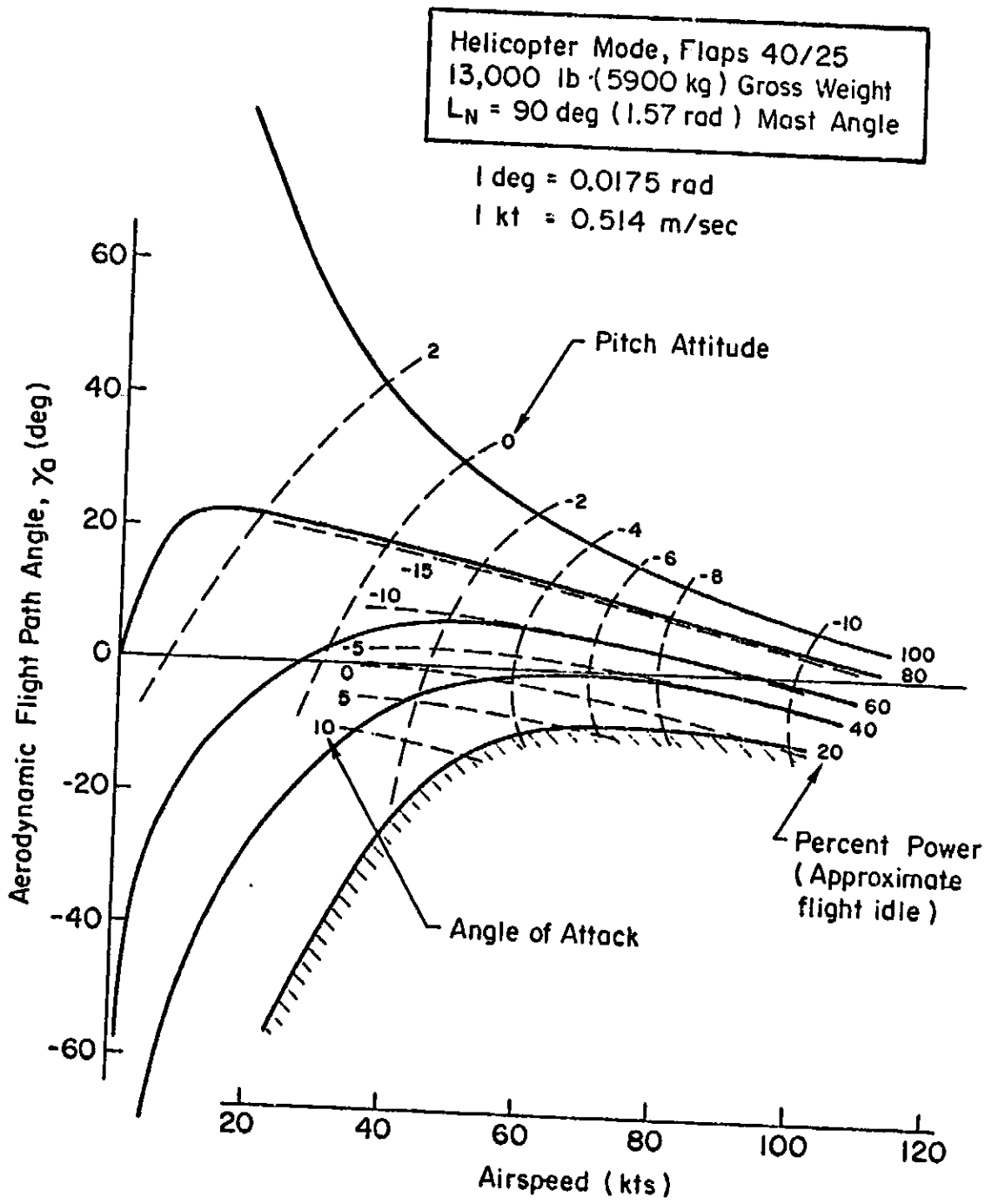

Figure 10. γ-V Plot for XV-15 Aircraft

(in the absence of anticipatory control action) which are ultimately eliminated by the closed-loop action of collective system in Fig. 2. Experience has shown that the initial excursions can be unacceptably large (see Ref. 6). Therefore, an airspeed crossfeed signal ($\Delta\delta_{CL}$ in Fig. 2) has been designed to add collective in accordance with the power-required characteristics of the XV-15. This is akin to the pilot's usual precognitive action to increase collective in a helicopter approaching hover. Review of the XV-15 performance data indicated that the $\Delta\delta_{CL}$ required is essentially the same for glide path angles −6 to −10 deg (−0.10 to −0.17 rad). The power increase required is significantly greater for the heavier weights and varies directly with the density ratio ρ_o/ρ. Straight-line approximations to the power-required curves yield the following:

$$\Delta\delta_{CL} = \frac{\rho_o}{\rho}\,[K(W)](101.4 - V_{IAS}) \tag{7}$$

$$K(W) = 0.021\ \frac{\text{in.}}{\text{ft/sec}}\left(0.18\ \frac{\text{cm}}{\text{m/sec}}\right);\ W = 10{,}000\ \text{lb}\ (4536\ \text{kg})$$

$$= 0.029\ \frac{\text{in.}}{\text{ft/sec}}\left(0.24\ \frac{\text{cm}}{\text{m/sec}}\right);\ W = 13{,}000\ \text{lb}\ (5897\ \text{kg})$$

$$= 0.032\ \frac{\text{in.}}{\text{ft/sec}}\left(0.26\ \frac{\text{cm}}{\text{m/sec}}\right);\ W = 15{,}000\ \text{lb}\ (6804\ \text{kg}) \tag{8}$$

$\Delta\delta_{CL}$ in in. (cm) of collective; V_{IAS} in ft/sec (m/sec) (9)

The straight-line approximation is least accurate at the 10,000 lb (4536 kg) weight where the peak error is about 20 percent at 50 kt (15 m/s). This is of little practical consequence as the closed-loop glide-slope-to-collective system tends to suppress small errors due to improper trim power. Wind and wind shear will also require small trim power increments which must be developed via closed-loop regulation.

E. HOVER

There are numerous references (e.g., Refs. 12 and 13) which illustrate that hover control is best accomplished with an attitude command system. However, as stated earlier, the limited authority XV-15 series actuator characteristics preclude using an attitude command system. The active feedbacks during hover control are washed-out pitch attitude, pitch attitude rate, range rate, range and body-fixed longitudinal acceleration. These feedbacks are weighted to produce a K/s frequency response characteristic for the longitudinal cyclic flight director as shown in Fig. 11. The lead-lag network included at the input to the flight director eliminates phase lag between the region where pitch attitude leaves off and longitudinal acceleration picks up to produce a K/s response. (Neither shaping nor body-fixed longitudinal accelerometer feedback is required to produce an ideal K/s response in the design of the system with the attitude hold SCAS.)

The longitudinal position holding characteristics in hover are shown by the frequency responses of position error to position command and position error to horizontal gusts in Fig. 12. The pilot model used is:

$$G_{FFS}(0)Y_{pc} = 1.0e^{-.17j\omega} \qquad (10)$$

The position control bandwidth is about 0.35 rad/sec. This is well within the acceptable range. The position error response to horizontal gust characteristics indicates effective regulation against horizontal gusts at all frequencies and no tendency toward low-frequency standoff.

An indication of the attitude-to-position harmony characteristics of hover can be obtained from a physical interpretation of the hover position feedback gain K_X (see Fig. 2). This gain is indicative of the attitude commanded per unit position error. The system commands about 0.3 deg (0.005 rad) of pitch attitude per foot (0.30 m) position error. Thinking of it another way, 10 ft (3 m) of position error will result in a 3 deg (0.052 rad) pitch attitude command. Hence, the bandwidth of 0.35 rad/sec shown in Fig. 11 is not obtained at the expense of excessive pitch attitude excursions during hover.

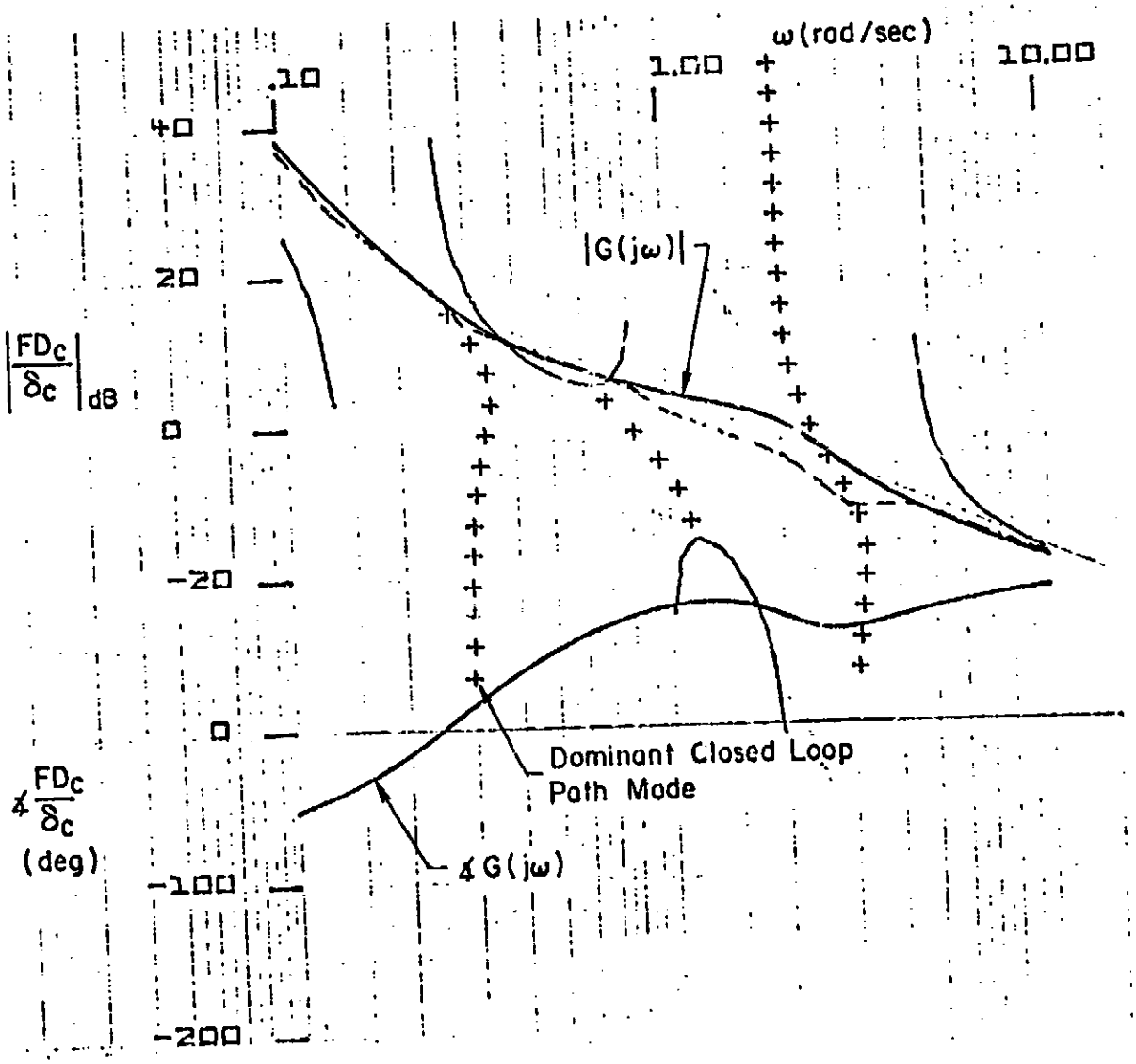

Figure 11. Open-Loop Frequency Response of Longitudinal Cyclic Flight Director for Hover

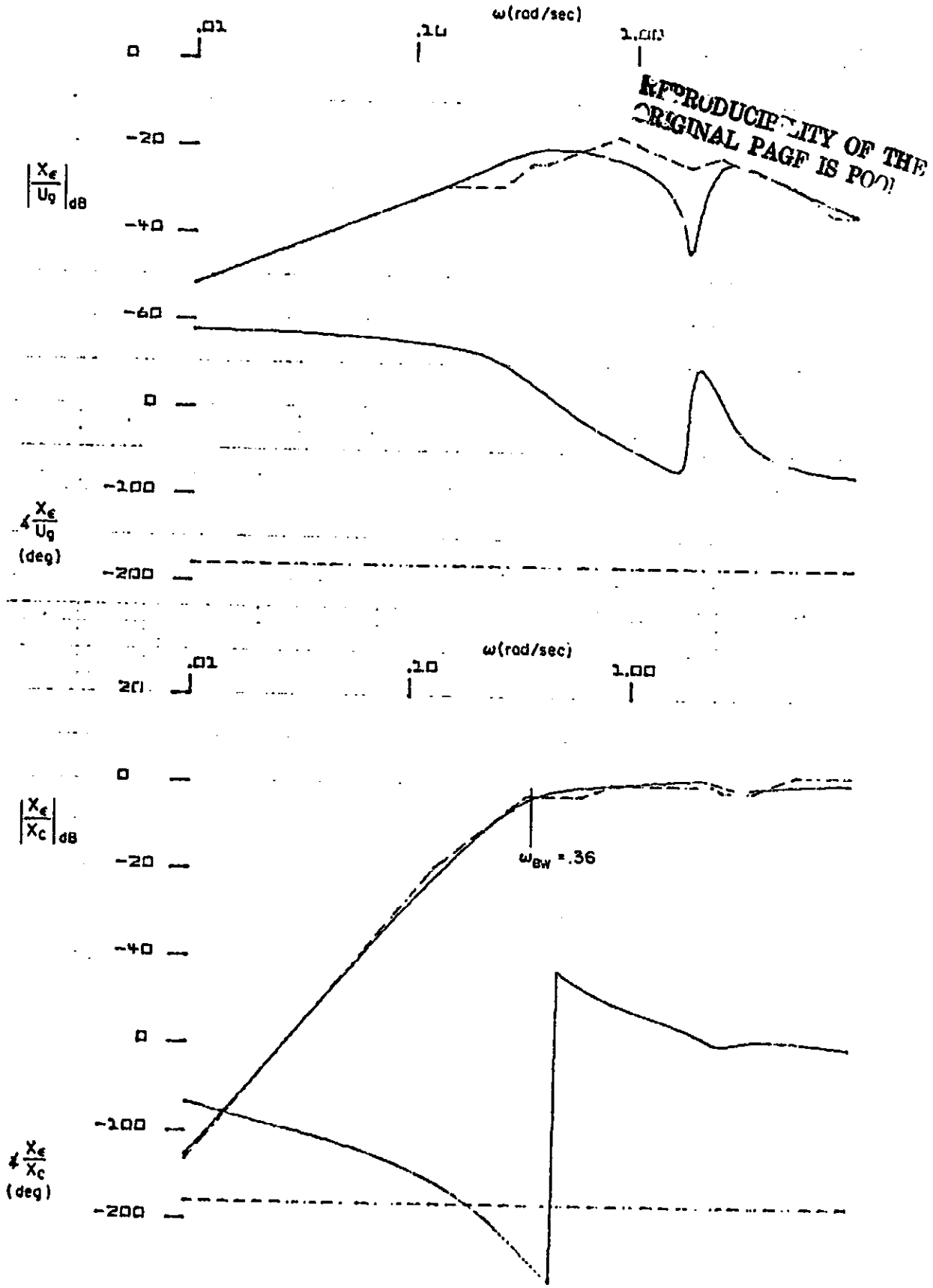

Figure 12. Longitudinal Position Holding Performance Characteristics of Hover System

F. ALTITUDE HOLD IN HOVER

When the radar altimeter reads 50 ft (15 m), the collective system reverts to altitude hold. The beam deviation and deviation rate gains used for glide slope tracking during the terminal phases of the approach are equally appropriate for the altitude hold mode; hence, $K_h = K_d$ and $K_{\dot{h}} = K_{\dot{d}}$ in the altitude hold mode at 50 ft (15 m). The same forward loop gain and parallel integrator time constant are also used [K_{CL} = 5 in./in. (0.13 m/m)] and K_{ICL} = 1.0 (1/sec)].

Precision altitude control in the hover mode is required to maintain pilot confidence in proximity to the ground. The characteristics of the altitude hold system are verified by the frequency response in altitude to vertical gusts and the altitude time response to a 15 ft/sec (4.6 m/s) vertical gust. These are shown in Fig. 13. The time responses in Fig. 13a indicate a peak altitude error of only 2.5 ft (0.76 m) and peak collective displacement of 1.0 in. (0.025 m). Figure 13b shows that the sensitivity to vertical gusts is low with no tendency for low-frequency standoff.

G. VERTICAL DESCENT

Once established in altitude hold over the hover point, the pilot manually initiates vertical descent. Inasmuch as the collective axis is fully automatic, the pilot simply continues to hold his longitudinal and lateral position with cyclic stick and monitors aircraft sink rate. The vertical descent mode is an exponential flare accomplished using collective control. The descent system uses a sink rate command which is proportional to altitude via the gain K_h ($K_{\dot{h}}$ is set to unity). At initiation of vertical descent an altitude command ($h_o + H_c$ in Fig. 2) is introduced through the lag network $1/(s + 1)$. This lag prevents an abrupt down command at initiation of vertical descent which would be disconcerting to the crew. The shape of the descent profile depends on the altitude command H_c and the exponential time constant K_h. H_c is set equal to a few feet below the ground to insure a positive but not hard touchdown ($\dot{h}$ between −1.5 and −3 ft/sec (−0.46 and −0.92 m/s). K_h is set to achieve a reasonable descent profile. A maximum descent rate of 500 ft/min (152 m/min) was set somewhat arbitrarily. Also, a descent time of between 10 and 15 sec was chosen to

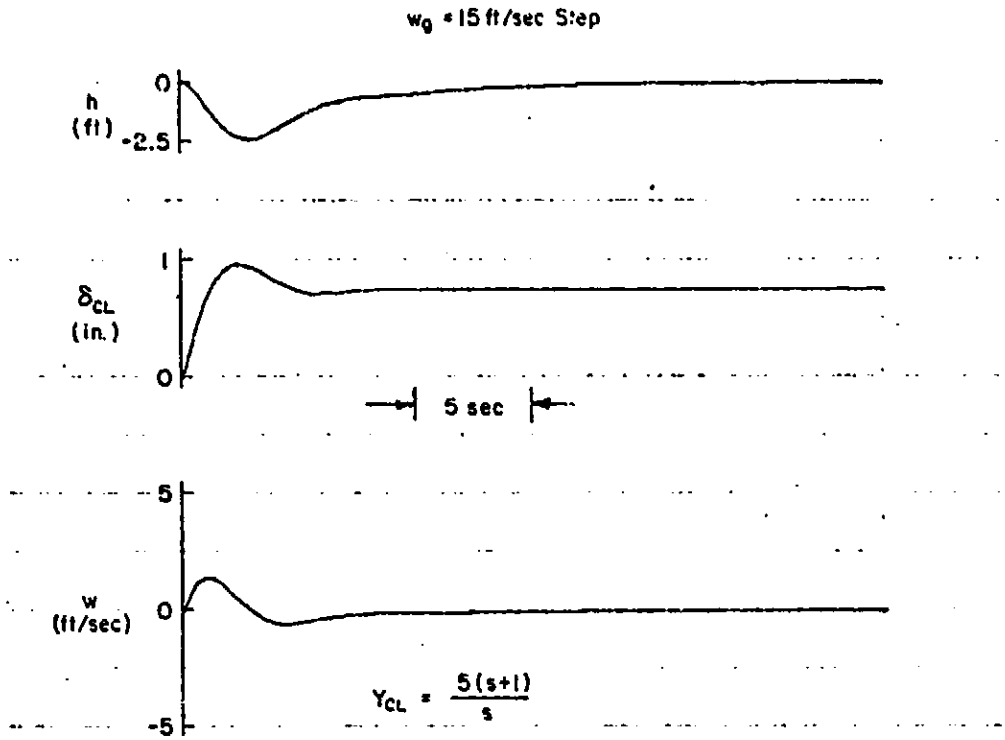

Figure 13a. Altitude Time Response to a 15 ft/sec (4.6 m/s) Vertical Gust, Altitude Hold During Hover

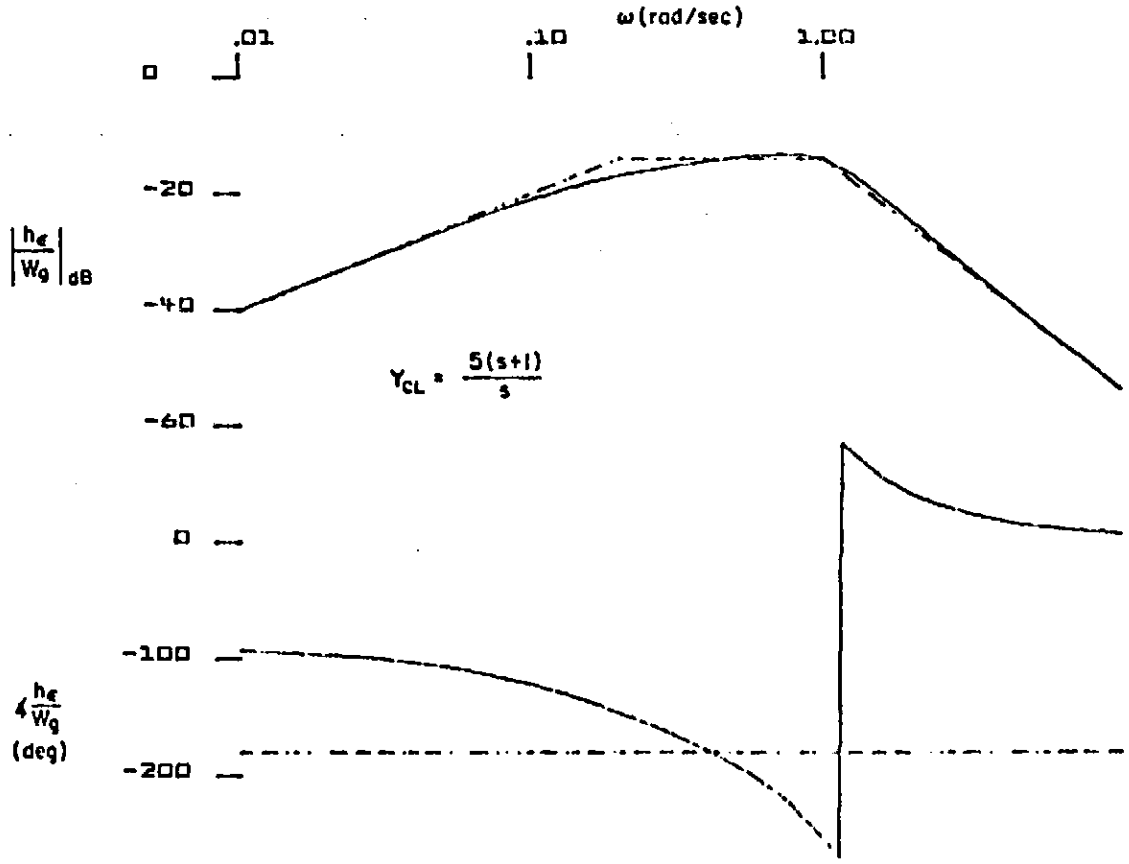

Figure 13b. Altitude Error Frequency Response for Vertical Gust Inputs During Hover

avoid prolonging the maneuver. Because of the relatively short duration of the maneuver, the parallel integrator in the forward loop of the collective system is not required. It is removed to eliminate the phase lag penalties introduced by this integrator. Removal is accomplished by fading P to zero at vertical descent initiation.

Time responses indicating performance of the vertical descent system in the absence of disturbances are given in Fig. 14. This descent profile results in a 14 sec descent time with a peak sink rate of 6 ft/sec (1.8 m/s) [360 ft/min (110 m/min)] and a nominal touchdown sink rate of 1.8 ft/sec (0.55 m/s). Deviations in sink rate ($-\dot{h}_\epsilon$) are eliminated well before touchdown.

H. APPROACH LOGIC

The switching logic in Fig. 2 divides the approach into five basic segments: altitude hold, glide slope track, constant attitude deceleration, hover and vertical descent to touchdown.

1. Glide Slope Tracking

The altitude hold/glide slope track switching occurs when $\epsilon_d \leq 0$* and $|d_\epsilon| \leq 100$ ft (30 m). This logic causes the system to switch from altitude hold to glide slope track without transients. A blending function T insures that undesirable transients do not occur at the switch point. Specifically, the glide slope intercept logic is as follows:

- Altitude hold (AH) when $|d_\epsilon| \geq 100$ ft (30 m) or when $|d_\epsilon| \leq 100$ ft (30 m) and $\epsilon_d > 0$.

- Glide slope track (GS) when $60 \leq V_A \leq 80$ kt (31 to 41 m/s), $|d_\epsilon| \leq 100$ ft (30 m) and $\epsilon_d > 0$. Initiated by start of blender function, T.

The glide slope tracking proceeds at constant airspeed until the point X_o at which time a constant attitude deceleration is commanded.

---

*$\epsilon_d = K_d d + K_{\dot{d}} \dot{d}$.

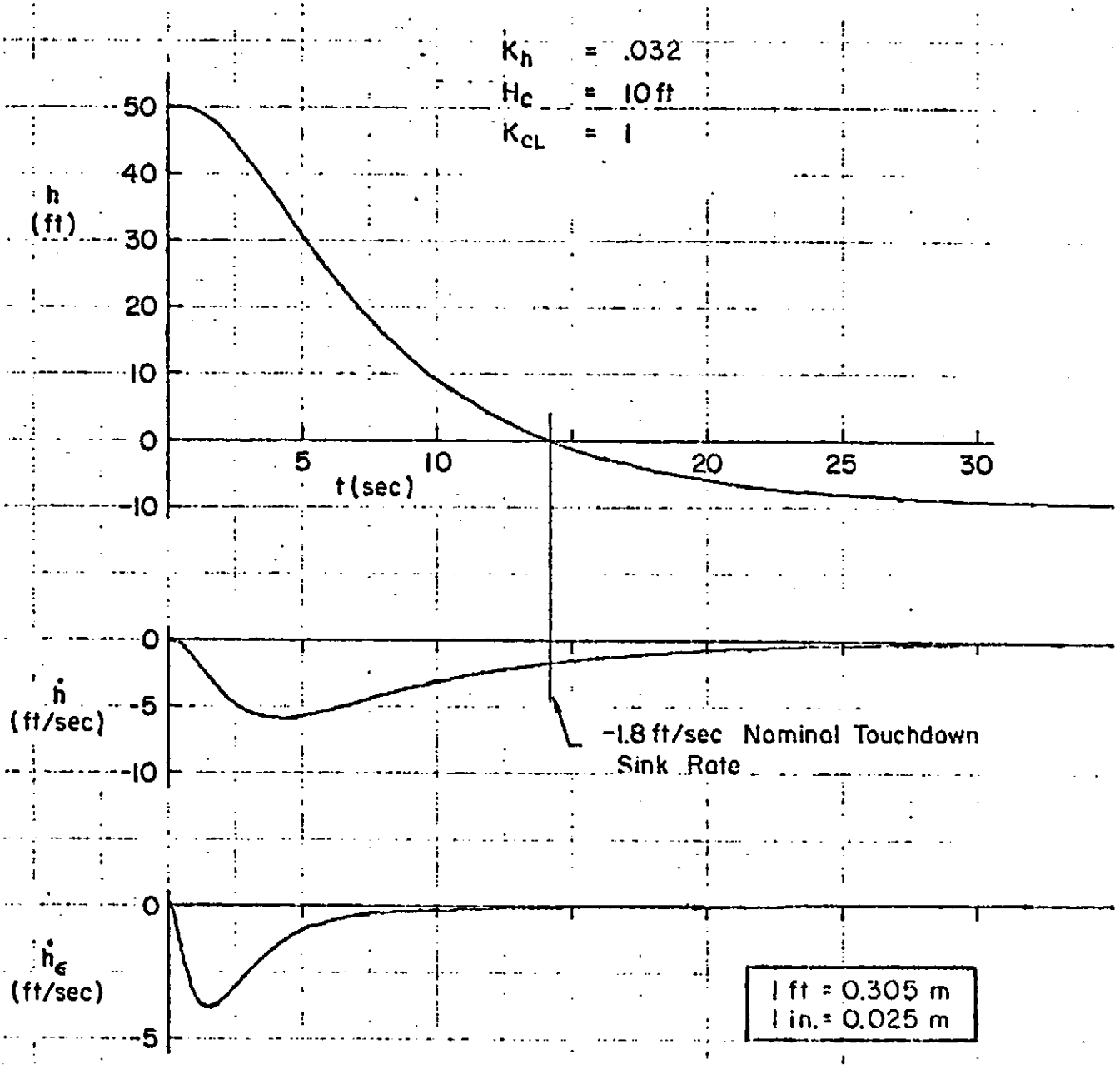

Figure 14. Vertical Descent Profile in Calm Air

2. Constant Attitude Deceleration

The deceleration capability of the XV-15 can be obtained from the γ-V curves in Fig. 10 and the following interpretations. First, note that the specific force acting along the flight path may be written as:

$$a_x = \dot{V}_I + g\gamma \doteq \dot{V}_I + g\gamma_a \tag{11}$$

where $\dot{V}_I$ is inertial acceleration along the inertial flight path, γ is the inertial flight path angle, and γ_a is the aerodynamic flight path angle (angle between airspeed vector and horizon). Physical interpretation of the aircraft specific force capability in the down direction is made easier if a_x is expressed as "minimum achievable trim flight path angle," e.g., $a_{x_{min}} = g\gamma_{a_{min}}$. The available deceleration capability may therefore be read directly from Fig. 10 as $\dot{V}_{I_{min}}/g = \gamma_{a_{min}} - \gamma_a$. For deceleration, the 20 percent power line defines the "minimum achievable trim" flight path angle (in the down direction).

An excellent approximation for deceleration as a function of pitch attitude is:

$$\dot{V}_I \doteq -g(\theta - \theta_T) \tag{12}$$

where θ_T is the trim pitch attitude for the flight path angle and speed being flown. Since the lines of constant attitude are nearly vertical between $\gamma = 0$ deg (0 rad) and $\gamma = -10$ deg (0.17 rad), a unique relationship between <u>trim</u> pitch attitude and airspeed can be derived using Fig. 10. Furthermore, it turns out that this function may be approximated accurately a linear function:

$$\theta_T \doteq \theta_H + \frac{d\theta_T}{dV_a} V_a \tag{13}$$

where θ_H = 3 deg (0.052 rad) is the no-wind hover trim attitude, and

$$K_{\theta VA} = \frac{d\theta_T}{dV_a} = -0.117 \frac{\text{deg}}{\text{kt}} = -0.069 \frac{\text{deg}}{\text{ft/sec}} \left(= -0.0040 \frac{\text{rad}}{\text{m/sec}} \right) \quad (14)$$

The deceleration is therefore approximated as:

$$\dot{V}_I \doteq -g\left(\theta_D - \theta_H - \frac{d\theta_T}{dV_a} V_a\right) \quad (15)$$

where θ_D is the constant attitude used for deceleration. If $\theta_D < \theta_H$, the aircraft will stop decelerating at some positive airspeed. Thereafter, the aircraft will proceed at (trim airspeed for θ_D + wind speed). This slow closure on the hover reference point is undesirable. Therefore, a deceleration attitude of one degree greater than the no-wind hover attitude is selected [θ_D = 4 deg (0.070 rad)] to provide more rapid closure on the hover reference point. This results in the deceleration profile shown in Fig. 15.

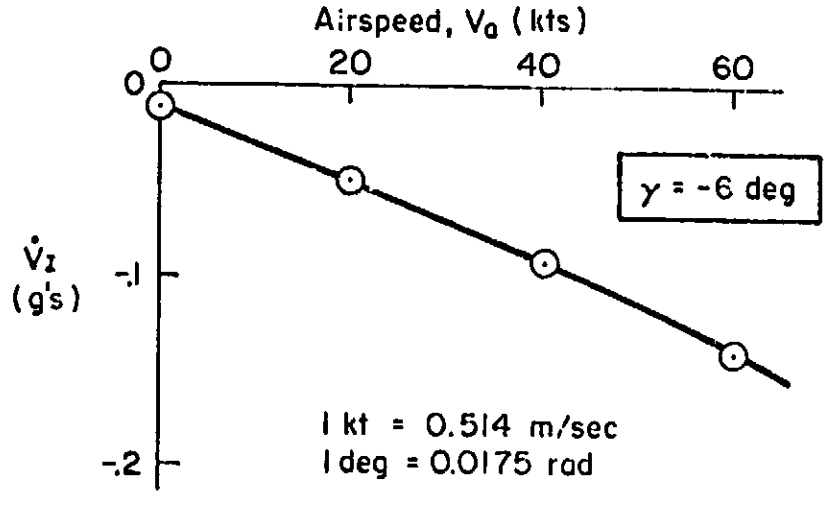

Figure 15. Nominal Deceleration Profile

For a constant wind situation ($\dot{X} = V_a + V_w$) the approach trajectory is defined as:

$$\ddot{X} + K_2\dot{X} = K_1 \tag{16}$$

where

$$K_1 = -g(\theta_D - \theta_H) - g\frac{d\theta_T}{dV_a}V_w$$

$$K_2 = -g\frac{d\theta_T}{dV_a}$$

Solving for $\dot{X} = f(X)$ yields:

$$X = -\frac{1}{K_2}\left[\dot{X} + \frac{K_1}{K_2}\ln\left(1 - \frac{K_2\dot{X}}{K_1}\right)\right] \tag{17}*$$

Hence, the switch from constant speed glide slope tracking to constant attitude deceleration should occur when:

$$\epsilon_\theta = -X + \frac{57.3}{g\frac{d\theta_T}{dV_a}}\left\{\dot{X} + \left[\frac{(\theta_D - \theta_H)}{\frac{d\theta_T}{dV_a}} + V_w\right]\ln\left[1 - \frac{\dot{X}}{\left(\frac{(\theta_D - \theta_H)}{(d\theta_T/dV_a)} + V_w\right)}\right]\right\} \leq 0 \tag{18}$$

The first value of X satisfying Eq. 18 is defined as X_o. Note that the effect of a steady headwind in Eq. 16 or 18 is equivalent to a change in the deceleration attitude [1 deg (0.0175 rad) of θ_D is the same as 8.5 kt (4.4 m/s) of headwind]. The effect of steady winds (or equivalent θ_D value) is shown in Fig. 16. An approximation to the hover control law ($X + 8\dot{X} = 0$) is also plotted in Fig. 16 to indicate where the guidance strategy would switch from the constant attitude deceleration mode to the hover mode ($X \equiv X_f$). For the large headwind cases this occurs at a large closing rate [50 ft/sec (15 m/s) for a 20 kt (10 m/s) headwind]. Since by its definition the hover control law commands deceleration proportional to closing rate ($\dot{X} + 8X = 0$), the commanded

*This solution was developed by W. A. Johnson.

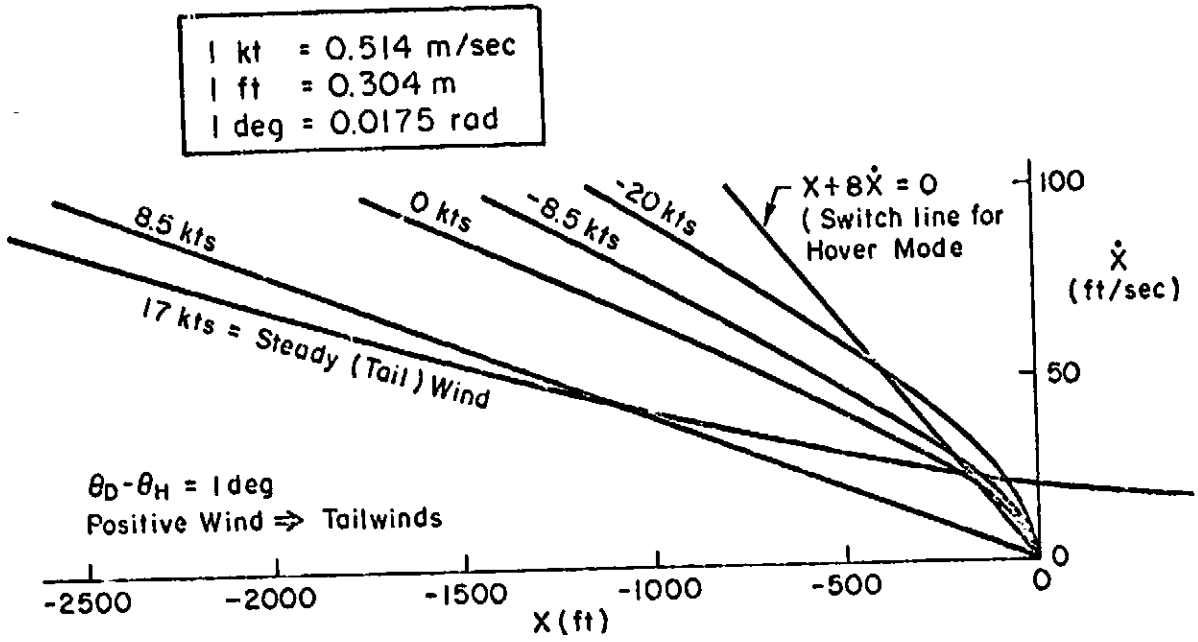

Figure 16. Shape of Constant Attitude Approach Trajectories

pitch attitude at X_f could become excessive. To avoid this, the value of θ_D is adjusted to account for steady winds in order to follow more closely the no-wind trajectory in Fig. 16. This is accomplished by holding K_1 in Eq. 16 constant, e.g.

$$K_1 = -\frac{32.2}{57.3}\,\theta_{INC} = -32.2\,\frac{(\theta_D - \theta_H)}{57.3} - \frac{32.2}{57.3}\,K_{\theta VA}\,V_w \qquad (19)$$

Hence

$$\theta_D = \theta_H + \theta_{INC} - K_{\theta VA}V_w, \quad \left[\theta_{INC} = 1 \text{ deg } (0.0175 \text{ rad}),\right.$$

$$\left.\theta_H = 3 \text{ deg } (0.052 \text{ rad}),\ K_{\theta VA} = -0.069\,\frac{\text{deg}}{\text{ft/sec}}\left(= -0.23\,\frac{\text{deg}}{\text{m/sec}}\right)\right] \qquad (20)$$

where V_w is in ft/sec (m/sec) and θ_D and θ_H are in degrees (radians). The value of V_w can be estimated by computing $(\dot{X} - V_A)$; closure rate minus indicated airspeed.

The effect of wind shear during the constant attitude deceleration will be as follows:

- Decreasing headwind shear. The initial $\dot{X}$ will be low due to the headwind resulting in initiation of deceleration at shorter range. θ_D will be less than 4 deg (0.070 rad). As the headwind shears away, groundspeed will increase, resulting in intercept of the hover mode switch line at larger than normal closure rates. This might result in relatively large attitude requirements at X_f. For example, if $\dot{X}$ = 50 ft/sec (15 m/s) at X_f; the commanded attitude will be 11 deg (0.19 rad) prior to the attitude limiter.
- Decreasing tailwind shear. The initial $\dot{X}$ will be high, resulting in initiation of constant attitude deceleration at increased range. θ_D will be greater than 4 deg (0.070 rad). As the tailwind shears away groundspeed will decrease, resulting in a tendency to come to hover short of the target and the $X + 8\dot{X} = 0$ switch line. The hover control law will be initiated any time the closure rate ($\dot{X}$) decreases below 5.92 [10.0 ft/sec (3.05 m/s)] to avoid this problem.

The switching boundaries which define X_o and X_f are shown in Fig. 17.

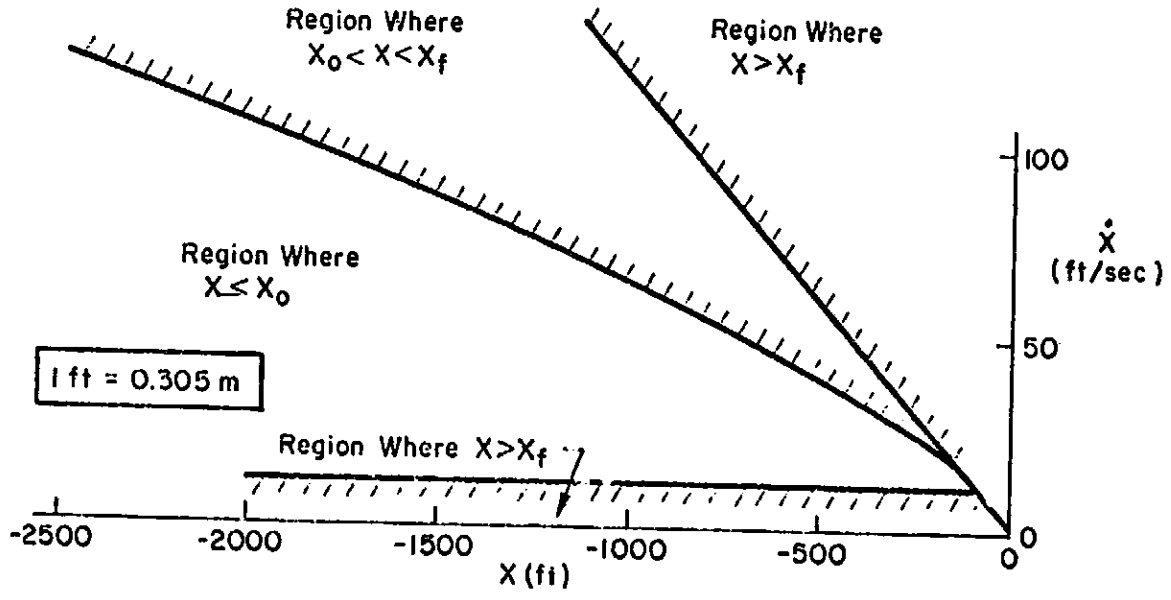

Figure 17. Definitions of X_f and X_o

The equations to be mechanized are summarized as follows:

$\underline{X = X_o}$

when

$$X = \frac{57.3}{32.2\, K_{\theta VA}} \left| \dot{X} + \frac{\theta_{1NC}}{K_{\theta VA}} \ln \left(1 - \frac{K_{\theta VA}\dot{X}}{\theta_{1NC}}\right)\right| \tag{21}$$

$\underline{X = X_f}$

when

$$X + 8\dot{X} + 16\,\dot{U} = 0 \tag{22a}$$

(The $16\dot{U}$ term is added to the switching criterion to eliminate a pitching transient at Hover mode initiation.)

or

$$\dot{X} = 10 \text{ ft/sec } [5.92 \text{ kt } (3.05 \text{ m/s})] \tag{22b}$$

All switching is irreversible so that X_o and X_f can be defined only once during a single approach.

$$\Delta\theta_{decel} = K_{BUG}(\theta_D - (\theta_T)_{X=X_o})$$

$$= K_{BUG}\left\{\theta_H + \theta_{INC} - K_{\theta VA}\,(\dot{X} - Va)_{X=X_o} - [\theta_H + K_{\theta VA}\,(Va)_{X=X_o}]\right\}/57.3$$

$$= K_{BUG}\left\{\theta_{1NC} - K_{\theta VA}\,(\dot{X})_{X=X_o}\right\}/57.3 \tag{23}$$

(K_{BUG} = 1.0 nominal value)

where $\Delta\theta_{decel}$ is in radians and $\dot{X}$ is in ft/sec. K_{BUG} is a parameter introduced to adjust for the fact that θ_T is not a completely linear function of airspeed for the actual aircraft model.

3. Altitude Hold at 50 ft (15 m/s)

The longitudinal hover position is defined as the point where the MLS beam passes through 50 ft (15 m/s) above ground level. Hence the horizontal and vertical velocities will be nominally zero as the XV-15 reaches 50 ft (15 m/s). The vertical descent is made using altimeter data for altitude information. The conversion from MLS to radar altitude vertical guidance is initiated when radar altitude equals 50 ft (15 m/s). This is accomplished via the function T in Fig. 2. Recall that T ramps to unity at glide slope intercept. At 50 ft (15 m/s), $T = [1 - 0.3\ (t - t_{50})]$; where t_{50} is the time at which the aircraft passes through 50 ft (15 m/s) and the minimum value of T is zero. This blends the MLS beam signals out and the altitude and attitude rate signals in over a time of 3.3 sec.

4. Vertical Descent

Vertical descent is initiated manually by the pilot at any time following T = 0 in the altitude hold mode. It is terminated following a positive indication for weight-on-wheels.

I. COMMAND LIMITING

The three limiters shown in Fig. 2 are included in the design to prevent the flight director or automatic flight control system from commanding excessive pitch attitudes, rates of climb, or sink rates which could lead to unfavorable pilot opinion.

The attitude limiter (shown in the upper part of Fig. 2) must account for the output of the synchronizer, which is effectively an attitude command inserted downstream of the limiter. This is accomplished as follows:

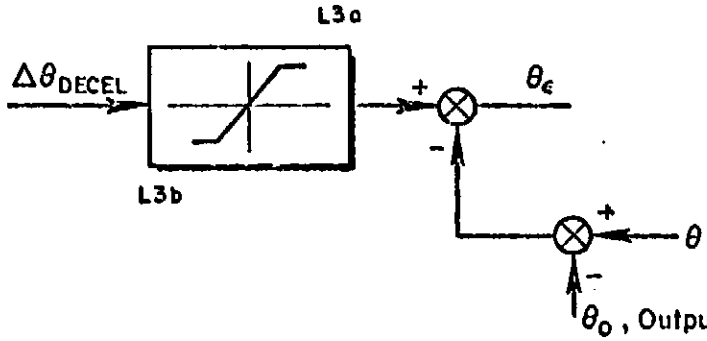

$\theta_D = \Delta\theta_{DECEL} + \theta_o$

θ_D is computed from Equation 20

$$L3a = \theta_{La} - \theta_o$$

$$L3b = \theta_{Lb} - \theta_o \qquad (24)$$

The attitude limits are tentatively set to:

$$\theta_{La} = +10 \text{ deg } (+0.17 \text{ rad})$$

$$\theta_{Lb} = -10 \text{ deg } (-0.17 \text{ rad}) \qquad (25)$$

The beam rate limiter is included to insure that large glide slope errors do not result in excessive rates of sink or climb. The limits are set so the maximum commanded rate of climb is 0 and the maximum commanded rate of descent is 1000 ft/min (305 m/min). This limiter would be removed, of course, if a missed approach mode were added to the design. The upper and lower limit values are defined by the following equations:

$$L1a = K_d \dot{d}_{La}$$

$$L1b = K_d \dot{d}_{Lb} \qquad (26)$$

where

$$\dot{d}_{La} = -\dot{d}_{Lb} = 8.33 \text{ ft/sec } (2.53 \text{ m/s}) \qquad (27)$$

The altitude rate limiter shown in the upper right part of Fig. 2 is set to limit sink rate or rate of climb commands to 500 ft/min (152 m/min). This limiter is in effect in the altitude hold and in the vertical descent modes. Its values are defined by the following equations:

$$L2a = K_h \dot{h}_{max}$$

$$L2b = K_h \dot{h}_{min} \tag{27}$$

$$\dot{h}_{max} = -\dot{h}_{min} = 8.33 \text{ ft/sec } (2.53 \text{ m/s}) \tag{28}$$

SECTION IV

LATERAL-DIRECTIONAL SYSTEM DESIGN

A. SUMMARY

A block diagram which summarizes the feedback selection, shaping and switching for the lateral stability and command augmentation system (SCAS) and the lateral flight director system is shown in Fig. 18. The numerical values of the time constants and gains in Fig. 18 are given in Table 8. The fully automatic approach mode is achieved by simply replacing the pilot in Fig. 18 with a gain element. Since-low frequency standoffs are eliminated by washing out the inner-loop feedbacks to the flight director, it is not necessary to add forward loop integrations upon changing from the flight director mode to the fully automatic approach mode.

The lateral SCAS has been configured as a rate-command/attitude-hold system for all flight conditions from cruise to hover, vertical descent and touchdown.

Referring to Fig. 18, it can be seen that the switching involves three basic modes, e.g., Localizer A (LOC A), Localizer B (LOC B) and heading hold (HH). A brief description of each of these modes is given as follows.

- Heading hold (HH). This is a conventional heading hold mode and is based on coordinated turns to pilot-selected headings (ψ_{ref} in Fig. 18).
- LOC A. Straight or curved localizer tracking via coordinated turns to correct for lateral errors.
- LOC B. Straight localizer tracking using bank angle regulation at constant heading to correct for localizer errors. A constant pilot-selected heading is obtained via pilot input to the pedals.

The XV-15 aerodynamic data indicate that the side force characteristics (Y_v) are very low. This means large magnitude crosswinds can be handled with small bank angles in the LOC B mode; hence, a complex system to cause the

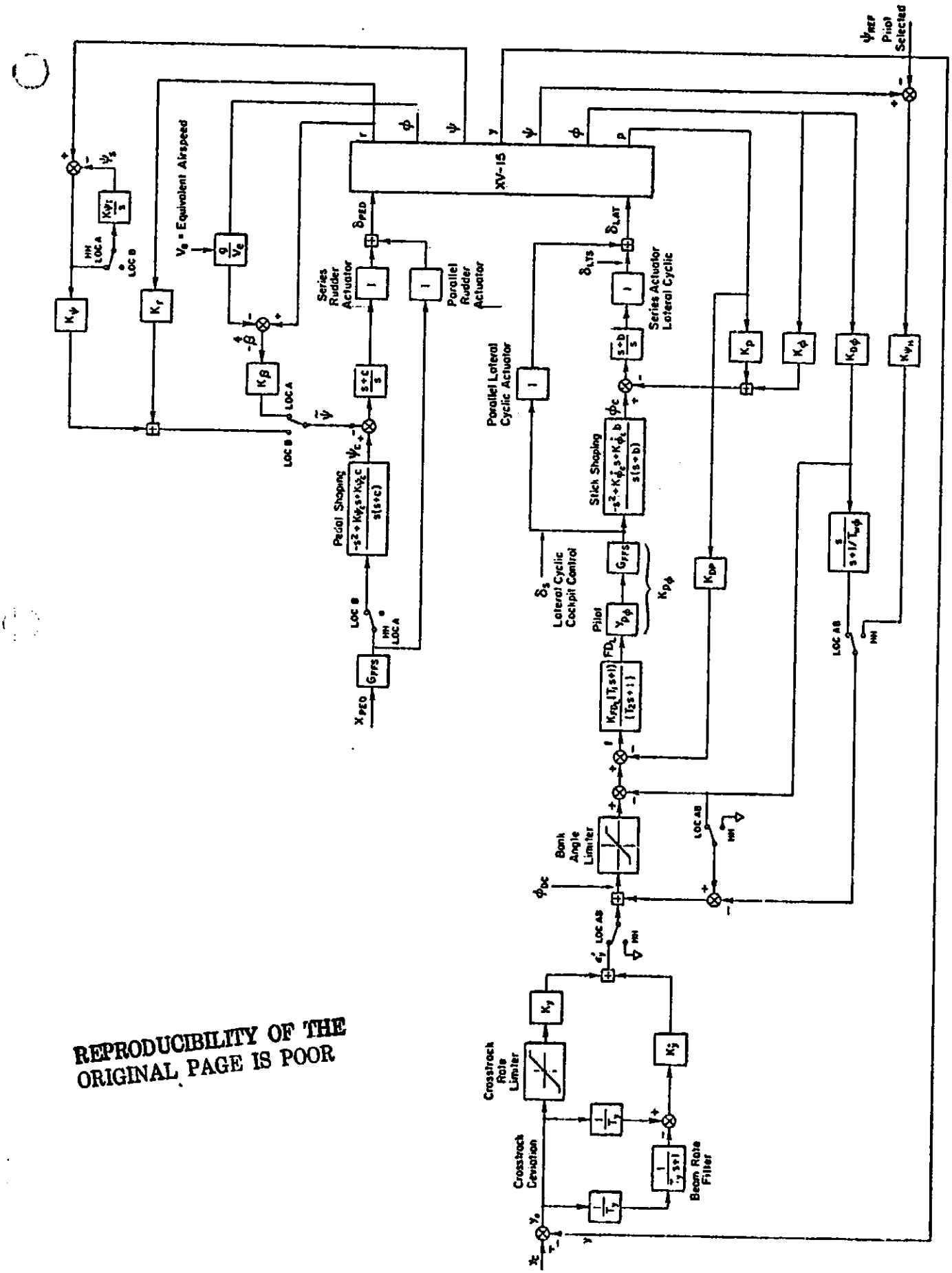

Figure 15. Block Diagram of Lateral System

TABLE 8. SUMMARY OF LATERAL DIRECTIONAL SCAS, FLIGHT DIRECTOR, AND AUTOPILOT GAINS AND TIME CONSTANTS

Turn Following SCAS (used for LOC A and HH)

K_p = 5.6 in*/(rad/sec)

K_φ = 11.2 in./rad

K_β = 10.0 in./(rad/sec)

b = 0 1/sec

c = 0 1/sec

$K_{\dot{\varphi}_c}$ = 2.93 1/sec

K_{ψ_H} = 1.0

Wing Low SCAS (used for LOC B)

K_p = 8 in./(rad/sec)

K_φ = 12 in./rad

K_β = 0

K_ψ = 13 in./rad

K_r = 13 in./(rad/sec)

b = 1 (1/sec)

c = .5 (1/sec)

$K_{\dot{\varphi}_c}$ = 3.14

$K_{\dot{\psi}_c}$ = .087 (rad/sec)/in.

LOC A and LOC B Flight Directors

K_y = .002 rad/ft†

$K_{\dot{y}}$ = .017 rad/(ft/sec)

K_{D_p} = .425 sec

K_{D_φ} = 1.06

T_{w_φ} = 10 sec = $1/\omega_{w_\varphi}$

T_1 = .5 sec = $1/\omega_1$

T_2 = .067 sec = $1/\omega_2$

T_y = .25 sec = $1/\omega_y$

$$K_{FD_L} = \begin{cases} 1.0 \text{ in./rad (LOC A)} \\ 1.6 \text{ in./rad (LOC B)} \end{cases}$$

Autopilot

$K_{p_\varphi} = G_{FFS}(0)Y_{p_\varphi}$ = 5.62 (LOC A)

$K_{p_\varphi} = G_{FFS}(0)Y_{p_\varphi}$ = 2.5 (LOC B)

*1 in. = 2.54×10^{-2} m.
†1 ft = 3.048×10^{-1} m.

vehicle to be pointed into the wind in hover is not warranted. LOC B will be used for localizer tracking at low speeds [below about 60 kt (31 m/s) including hover.

B. STABILITY AND COMMAND AUGMENTATION SYSTEM (SCAS)

A review of the vehicle transfer functions at speeds from 80 kt (41 m/s) down to hover (see Table 7) indicates the following basic airplane deficiencies for lateral-directional control:

- Very low dutch roll frequency at all speeds (low ω_d)
- Negative or low dutch roll damping at all speeds (low ζ_d)
- Unstable spiral mode
- Large shift in instantaneous center of rotation ($-Y_{\delta_{ped}}/N_{\delta_{ped}}$) between 60 and 80 kt (31 and 41 m/s). This characteristic makes it impractical to use a lateral acceleration-to-pedal feedback to improve the low dutch roll damping.
- Roll reversal at 40 kt (21 m/s). The bank angle to lateral cyclic numerator consists of two real zeros, one of which is in the right half plane, indicating that the aircraft will ultimately roll left to a right lateral cyclic input. This unusual characteristic only occurs at speeds near 40 kt (21 m/s) and is attributed to rotor wash characteristics on the horizontal tail at this speed.
- Poor yaw rate-to-pedal response characteristics resulting in marginal improvements in dutch roll damping with a conventional yaw damper feedback.
- Large adverse yaw at speeds below about 70 kt (36 m/s) at $\gamma = -10$ deg (-0.17 rad).

Two separate stability and command augmentation systems have been developed to resolve the above deficiencies. At higher speeds heading changes will be made in the conventional way, that is, utilizing bank angle to develop a turn rate. At low speeds, the heading response to bank angle changes becomes too sensitive for effective closed-loop path control ($\dot{\psi} \doteq g\varphi/V$). Experience has shown that this characteristic becomes unacceptable at speeds below 60 kt (31 m/s); hence, the system is designed to be switched from the turn-following SCAS to the

wing-low SCAS as the aircraft is slowed to speeds below 60 kt (31 m/s). The wing-low SCAS is a constant heading mode where lateral position changes are made by varying the bank angle. It is intended that this mode be used during straight localizer tracking on final approach when speed reductions below 60 kt (31 m/s) will occur. Nominally, the pilot will switch manually from the turn-following SCAS to the wing-low SCAS once he is established on the straight-in localizer approach course. However, if the speed decreases to 50 kt (26 m/s), this switch will be accomplished automatically to avoid getting into a region of unfavorable dynamics with the turn-following SCAS. If the system automatically switches (due to inadvertent low-speed excursions), the pilot must switch back manually to turn-following mode if he so wishes. However, if the aircraft is in the wing-low SCAS mode, and the speed exceeds 70 kt (36 m/s), the system will automatically switch back to the turn-following mode. This is done to avoid getting into a region of unfavorable dynamics with the wing-low SCAS.

The following paragraphs describe the turn-following SCAS and the wing-low SCAS.

1. Turn-Following SCAS [$V \geq 50$ kt (26 m/s)]

Bank angle (φ) and body-fixed roll rate (p) are fed to the lateral cyclic series servo to stabilize the spiral mode and achieve a bank angle command SCAS. The ratio of K_φ/K_p was set to the desired bandwidth of the bank angle command system, or 1.5 rad/sec. The fact that the ratio of K_φ/K_p is approximately equal to the bandwidth of the closed-loop system can be seen from the following approximation:

$$\lim_{K_\varphi \to \infty} \left(\frac{p}{\varphi_c}\right) = \lim_{K_\varphi \to \infty} \frac{K_\varphi N^p_{\delta_s}}{\Delta + K_p\left(s + \frac{K_\varphi}{K_p}\right)N^p_{\delta_s}}$$

$$= \frac{K_\varphi/K_p}{s + K_\varphi/K_p} \qquad (29)$$

Based on the flight test results of Ref. 9, a bandwidth of 1.5 rad/sec achieves acceptable bank angle regulation characteristics. Larger bandwidth tends to result in poor ride qualities due to jerky responses to stick inputs. The effect of feeding bank angle and roll rate to the lateral cyclic series servo on the vehicle lateral characteristic equation is shown in Fig. 19 for the 60 kt (31 m/s) flight condition. Figure 19 indicates that additional augmentation is required to increase the damping and frequency of the closed-loop dutch roll mode. The possible alternatives that were considered to achieve these objectives are listed below. (See Ref. 14.)

- Utilize feedback of yaw rate and lateral acceleration to the pedal series servo. This is a classic combination utilized to increase the dutch roll frequency via the lateral acceleration feedback and to improve the dutch roll damping via the yaw rate to pedal feedback. In order to be effective, the lateral accelerometer must be at or near the instantaneous center of rotation, which is located forward of the center of gravity for aircraft with aft-mounted vertical tails. In the case of the XV-15, the vertical tail effectively moves from a forward location to a rearward location as directional control is shifted from differential cyclic to conventional rudders. This occurs as the speed is increased from 60 to 80 kt (31 to 41 m/s). This large shift is in the instantaneous center of rotation [approximately 0.65 ft (0.2 m) behind the c.g. at 60 kt (31 m/s) to 2.38 ft (0.7 m) forward of the c.g. at 80 kt (41 m/s)] makes the use of a lateral acceleration feedback impractical for this airplane. Additionally, the location of the zeros of the yaw rate-to-pedal-numerator make the feedback of yaw rate to pedals ineffective in terms of increasing the dutch roll damping.

- Another conventional way of increasing the dutch roll damping and frequency is to use lateral acceleration-to-pedal feedback (with a lateral accelerometer located at the instantaneous center of rotation) with a lead/lag network. However, because of the above discussed movement of the instantaneous center of rotation at speeds below 60 and 80 kt (31 and 41 m/s), this scheme is also impractical for the XV-15.

- The feedback of sideslip angle to the pedal series servo with a lead/lag network is very effective for increasing both the damping and frequency of the dutch roll mode. Recognizing that the measurement of sideslip angle in a rotor craft is highly impractical, an attractive alternative is to feed back other signals, which when combined, have the same characteristics as sideslip angle with a lead/lag network.

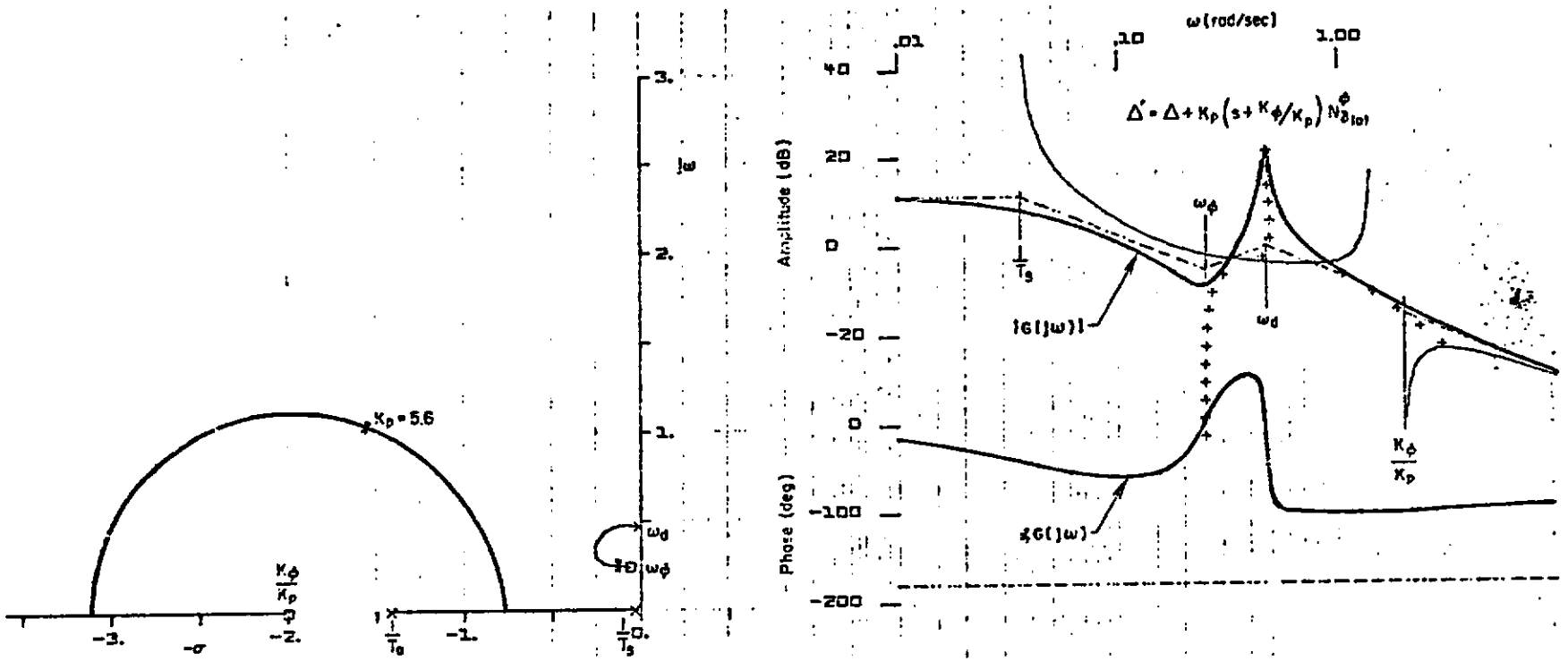

Figure 19. Effect of Roll Loop Closure on Lateral Characteristic Equation; V = 60 kt (31 m/s); Turn-Following SCAS (LOC A)

The turn-following SCAS design for the XV-15 is based on the third of the above alternatives and uses the following approximation for (inertial) side-slip angle rate:

$$\dot{\beta} \doteq -\left(r - \frac{g\varphi}{V}\right) \tag{30}$$

This approximation assumes that Y_β and Y_v are small. A review of the derivatives presented in Table A-6 indicates that this is a very good approximation. Inasmuch as $r - g\varphi/V$ is being fed back to simulate $\dot{\beta}$, the feedback gain was labeled K_β. The effect of K_β on the characteristics equation as modified by the φ and p feedbacks is shown in Fig. 20. The root locus plot in Fig. 20 clearly illustrates that the feedback $r - g\varphi/V$ has very little effect on the ω'_{sr} mode (the combined spiral and roll subsidence mode obtained from the bank angle and roll rate feedback), but does drive the undesirable low-frequency dutch roll mode to the real axis to form two real roots. The highest frequency real root becomes the dominant response to rudder or gust inputs. The dominant response to lateral cyclic inputs is ω''_{sr}. ω''_{sr} is nearly equal to ω'_{sr}, that is, the $(r - g\varphi/V)$ feedback does little to change the bandwidth of the bank angle loop. The feedback gain K_β is set to 10 in. (0.25 m) of series servo motion per rad/sec of $\dot{\beta}$ so that the real dominant dutch roll root would be slightly greater than 1 rad/sec. Consideration of pedal series servo limiting reveals that a value of $K_\beta = 10$ implies that 5.7 deg/sec of yaw rate will result in saturation. This is felt to be marginal but not unreasonable.

Two performance metrics are used to evaluate the turn-following SCAS. The attitude hold feature of the roll rate-command/attitude-hold system was evaluated by consideration of the φ/φ_c frequency response where φ_c is the output of the lateral stick shaping in Fig. 18. The feedback of $r - g\varphi/V$ inherently tends to minimize adverse yaw. The time response of yaw rate to a step φ_c was used to evaluate the adverse yaw characteristics of the turn-following SCAS.

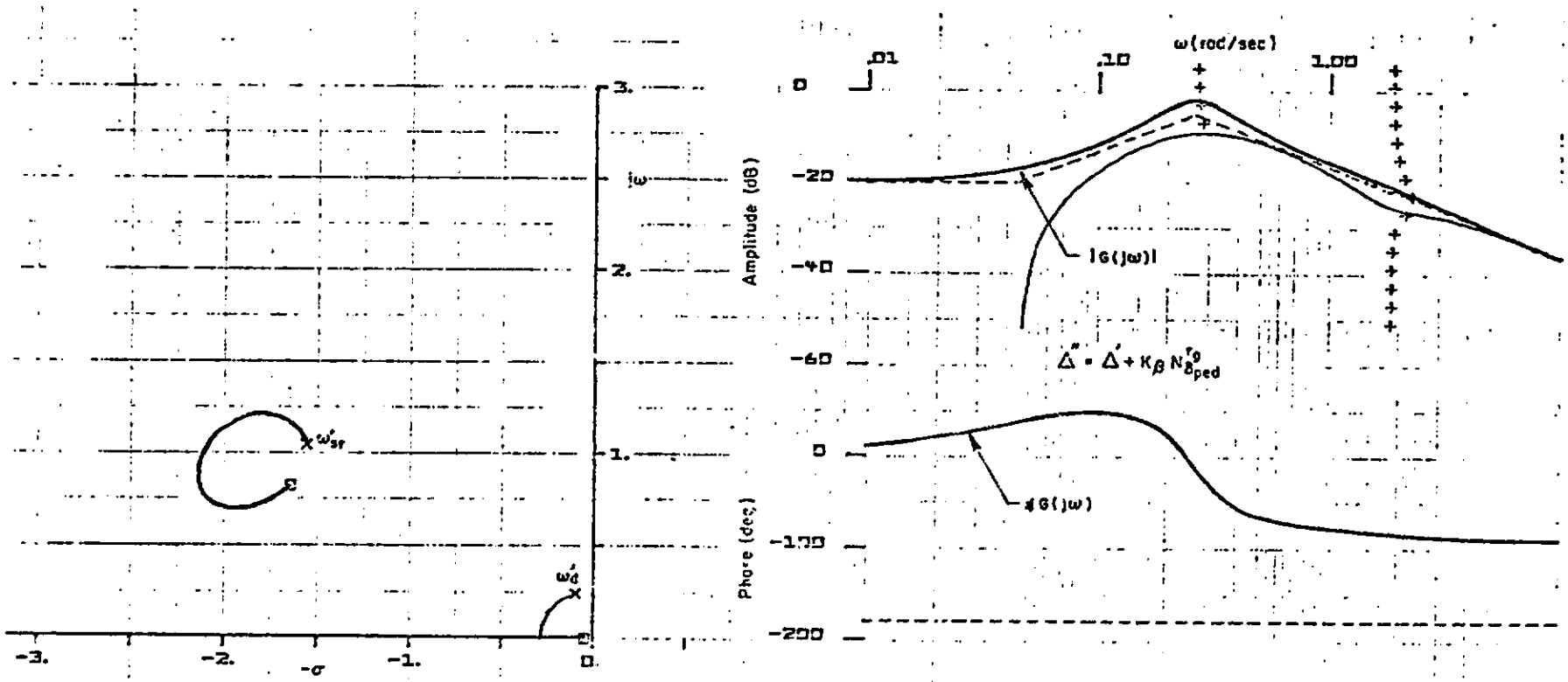

Figure 20. Effect of $(r - g_\varphi/V)$ Feedback to Pedals on Lateral Characteristic Equation; V = 60 kt (31 m/s); Turn-Following SCAS (LOC A)

The frequency response characteristics of φ/φ_c are shown in Fig. 21. It can be seen that the system bandwidth is 1.5 rad/sec at 60 kt (31 m/s) and 1.75 rad/sec at 80 kt (41 m/s). Notice that this is consistent with the Eq. 29 approximation which was the basis for setting $K_\varphi/K_p = 1.5$. The stick shaping network in Fig. 18 when combined with the proportional-plus-integral (1 + b/s) in the series actuator path and the parallel actuator path results in an integration between stick and the effective φ_c. The value of K_{φ_c} was set to achieve a sensitivity of 15 deg/sec of roll rate per inch (0.025 m) of lateral cyclic on the basis of the results achieved in Ref. 6. The time histories of bank angle and yaw rate to a step φ_c input are shown in Fig. 22. Here it is seen that there is essentially no adverse yaw at 80 kt (41 m/s) and a small amount of adverse yaw at 60 kt (31 m/s), that is, there is an effective delay between developing the proper sign of yaw rate to φ_c of about 0.6 sec. This is felt to be negligible. The steady-state turn rate at 60 kt (41 m/s) is slightly less than that at 60 kt (31 m/s), indicating the presence of a small steady sideslip angle during turns at 80 kt (41 m/s). This effect is not felt to be important enough to warrant additional SCAS feedbacks. Because the turns are automatically coordinated, very little pedal usage is expected in IOC A or HH modes. Therefore, no pedal shaping has been included and pedal inputs are transmitted via the parallel servo only (see Fig. 18).

It is felt that the stability and command augmentation system in the turn-following mode will receive reasonably good pilot ratings because of its snappy but not oversensitive roll response and lack of any appreciable aileron/rudder coordination requirements arising from adverse yaw. The primary system limitation is expected to be possible saturation of the pedal and lateral cyclic series servos.

2. Wing-Low Stability and Command Augmentation System [V ≤ 50 kt (26 m/s)]

The nominal wing-low SCAS was designed at the 40 kt (21 m/s) condition. This was done assuming that a SCAS designed to yield acceptable flying qualities with the extremely poor basic vehicle dynamics at 40 kt (21 m/s) should also work well at other flight conditions. This in fact turned out to be the case.

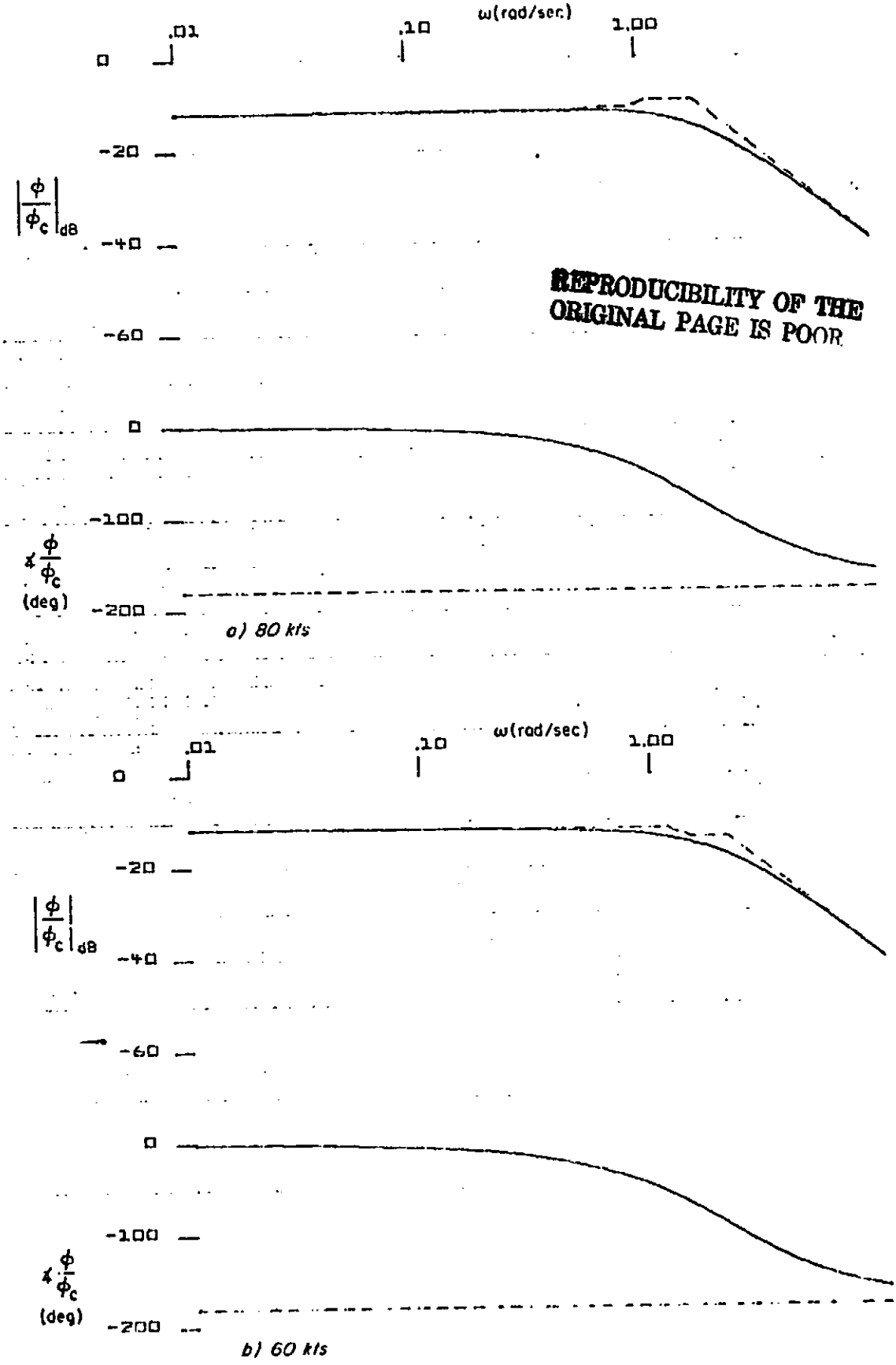

Figure 21. Frequency Response Characteristics of Roll Rate to Lateral Stick; Turn Following SCAS (LOC A)

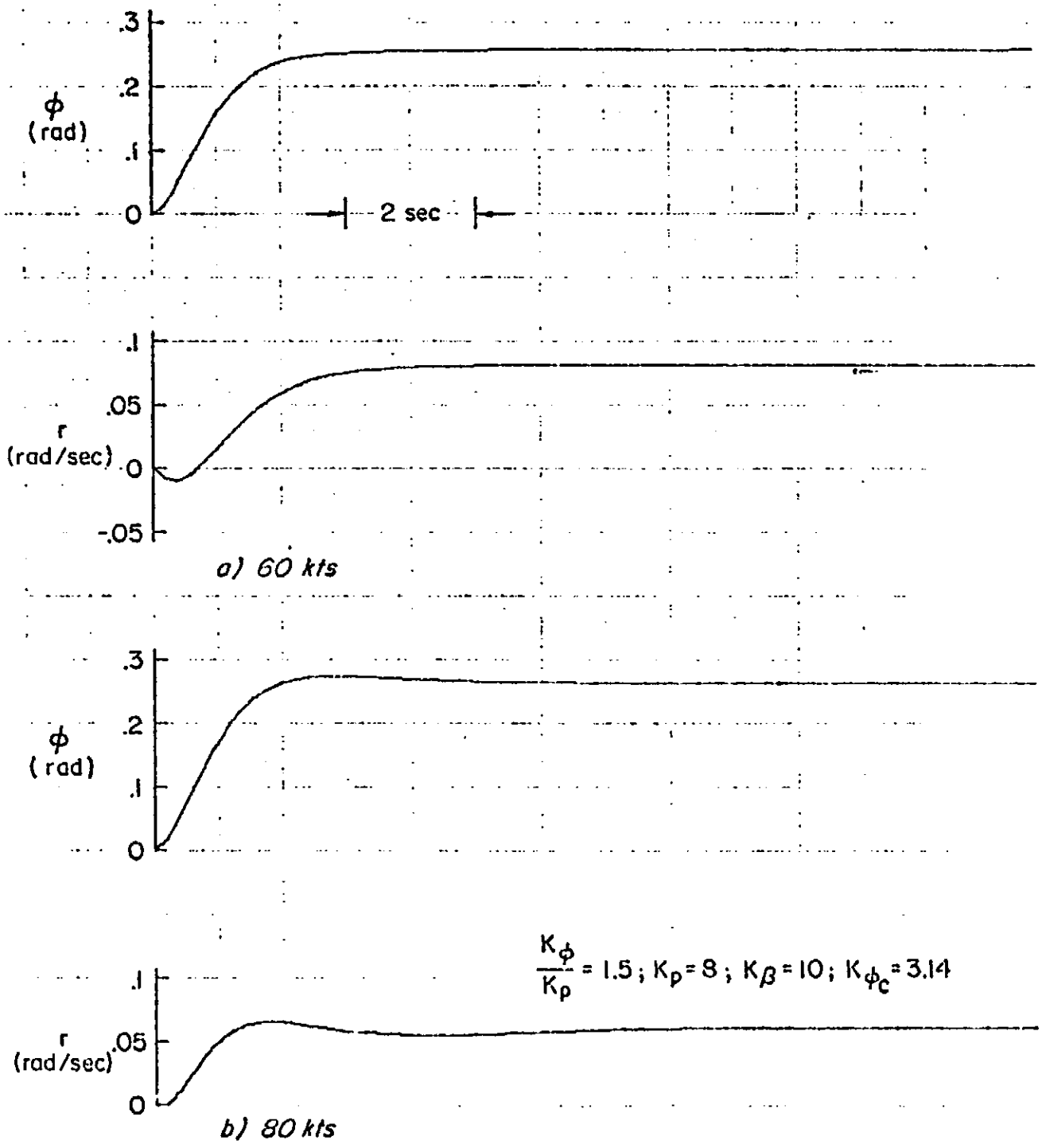

Figure 22. Bank Angle, and Yaw Rate Responses to φ_c = 1 in. (0.25 m) at Output of Stick Shaping Network

Since, by definition, heading is constant in this mode it is possible to use heading feedback to the pedal series servo to provide the necessary increase in the dutch roll frequency. Yaw rate to pedal feedback was also utilized to provide the necessary damping. Proportional-plus-integral (1 + c/s) is required in the forward loop pedal series servo path to insure that heading error is zero at low frequency. Important tradeoff considerations in this loop closure require maximum c for the best heading error suppression and minimum c for stability. The best compromise is reached by decreasing the ratio of K_ψ/K_r to make up for damping lost because of the parallel integrator. The ultimate outcome is a small decrease in the closed-loop dutch roll frequency, ζ_d'. The effect on the lateral characteristic equation of heading and yaw rate feedback to pedals in the presence of this parallel integrator is shown in Fig. 23. Notice that for a given K_r the total damping, $\zeta_d'\omega_d'$, is independent of K_p/K_r but that ζ_d' increases with decreasing K_ψ/K_r. K_ψ and K_r are set equal to 13 ($K_\psi/K_r = 1.0$) as a best compromise between maximizing ζ_d' and minimizing K_ψ to avoid an unacceptable degree of series servo limiting. K_ψ = 13 in. (0.33 m) per radian of heading results in pedal series servo limiting when heading excursions exceed 4.4 deg (0.076 rad). This is felt to be marginal but probably acceptable. Notice also the kinematic roots at the origin are driven into the low frequency zero (ω_{r_g}) (see Fig. 23). This lightly damped, low-frequency closed-loop mode has been labeled ω_{SAS}'.

The pedal shaping network in Fig. 18 when combined with the parallel integrator (1 + c/s) results in an integration between pedals and ψ_c. This results in a rate command attitude hold SCAS in heading. $K_{\dot{\psi}_c}$ was set to 1.13 so that 1 in. (0.025 m) of pedal commands 5 deg/sec (0.087 m/s) of heading rate.

It is shown in Fig. 24 that feedback of bank angle and roll rate to the lateral cyclic series servo results in ω_{SAS}' being driven to the approximate location of ω_d' while ω_d' is driven to higher values of frequency and damping (resulting in ω_d''). A parallel integrator (1 + b/s) was required in the roll loop for good mid- and low-frequency regulation. A value of K_p = 8.0 in./(rad/sec) [0.2 m/(rad/sec)] was picked to maximize the bandwidth of the closed-loop bank angle-to-lateral cyclic system (e.g., to maximize ω_d'' and ζ_d''),

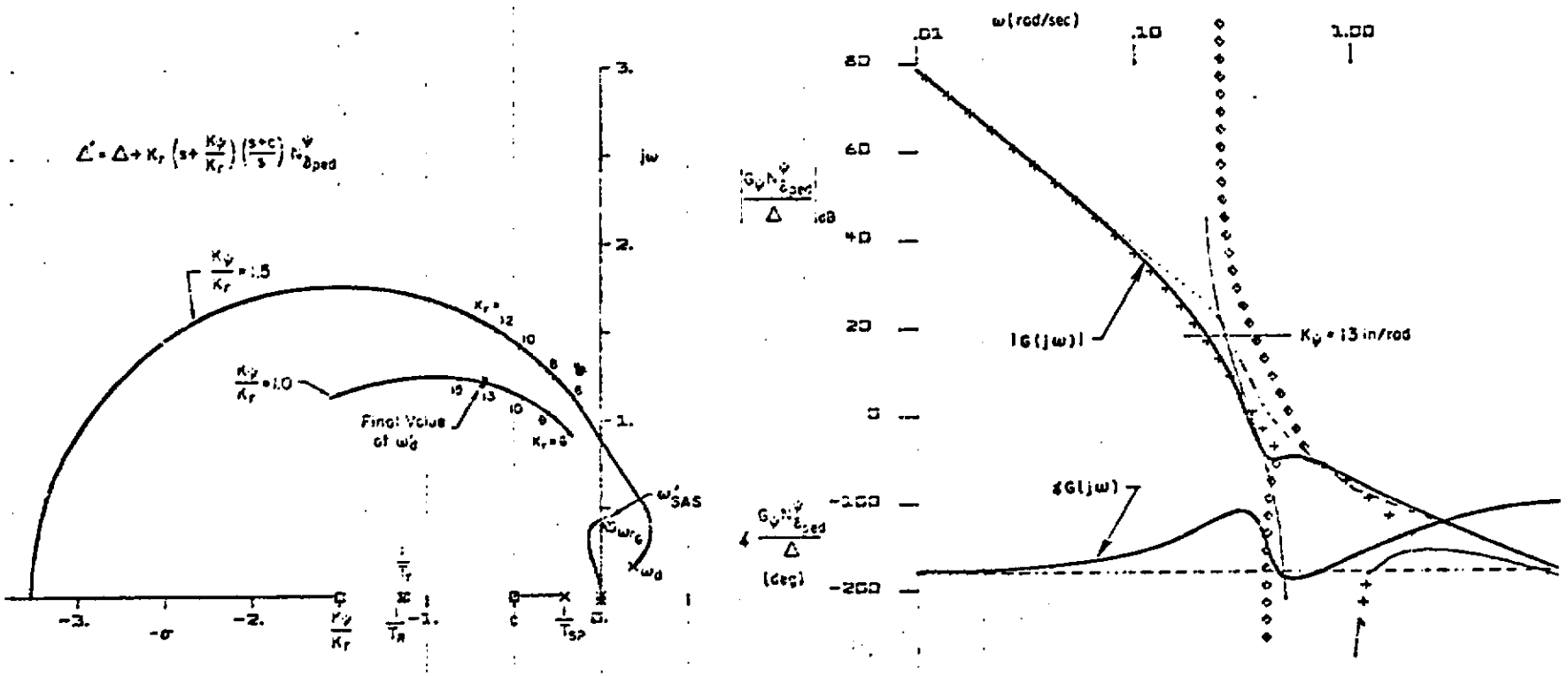

Figure 23. Effect of ψ and r Feedback to Pedals on Lateral Characteristic Equation; V - 40 kt (21 m/s); Wing Low SCAS (LOC B)

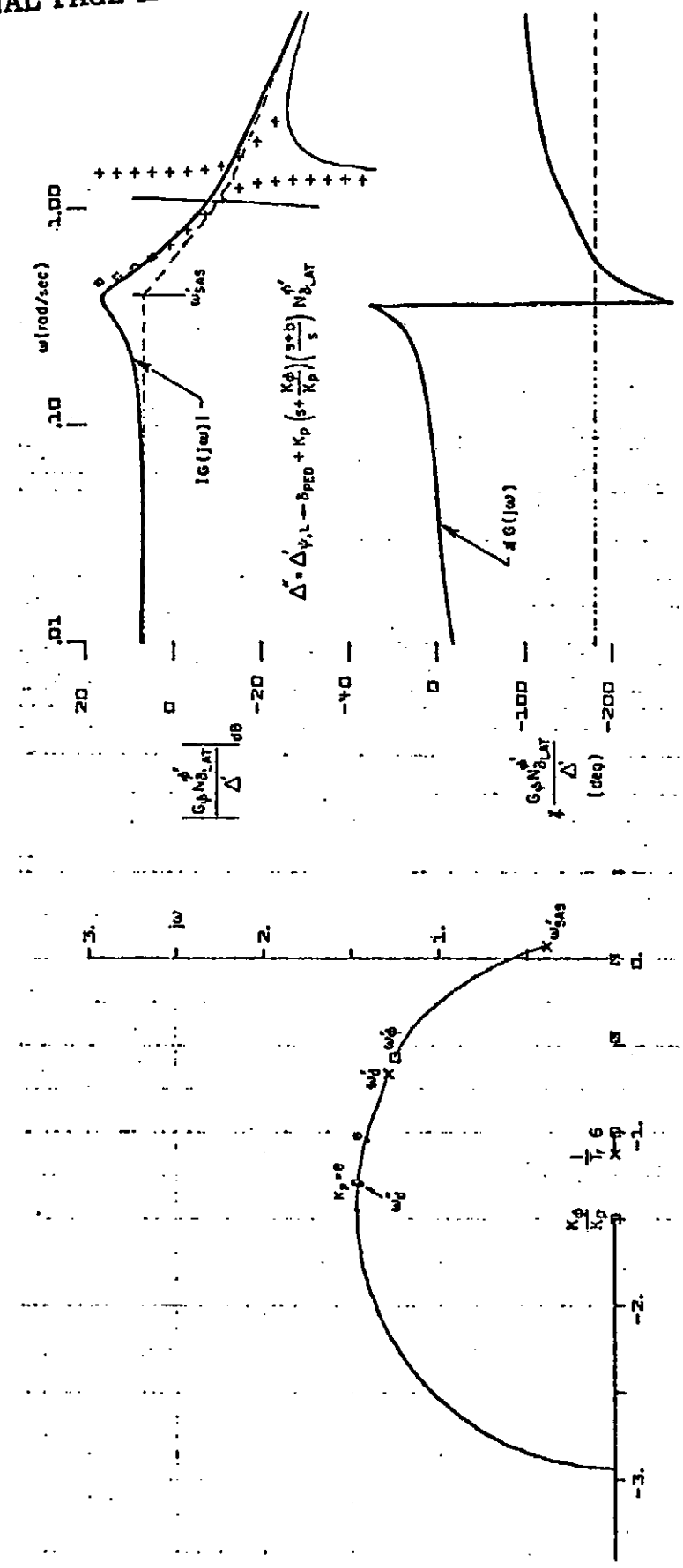

Figure 24. Effect of φ and p Feedback to Lateral Stick on the Lateral-Directional Characteristic Equation; V = 40 kt (21 m/s); Wing Low SCAS (LOC B)

while keeping K_φ low enough to minimize the possibility of lateral cyclic series servo saturation. For a series servo limit of 1 in. (0.025 m) and $K_\varphi/K_p = 1.5$, this implies limiting for a 4.8 deg (0.084 rad) roll excursion from the commanded value (output of the lateral stick shaping network).

Several performance metrics were utilized to evaluate the wing-low SCAS system before proceeding with the flight director and automatic flight control system design. These consisted of frequency response of bank angle to bank angle command, heading to pedal command and heading to lateral cyclic input.

The φ/φ_c frequency response bandwidth is primarily set by ω_d'' and is reasonably flat out to about 1.5 rad/sec for the 0, 20, 40 and 60 kt (0, 10, 21 and 31 m/s) flight conditions. These frequency responses are shown in Fig. 25 and indicate that the bandwidth of the bank angle response is 2 rad/sec at 60 and 40 kt (31 and 21 m/s) and improves to 2.4 rad/sec at 20 (10 m/s) and hover.

An attempt was made to relax the roll gain, K_p, from 8 to 6 and thereby increase the magnitude of roll excursion required to saturate the lateral cylic series servo. This gain change would allow an increase in bank angle error from 4.8 to 6.4 deg (0.08 to 0.11 rad) before saturation occurs. Time histories of the resulting φ/φ_c time responses indicate undesirable transient characteristics at the lower gain (see Fig. 26). This verifies that the design is tightly constrained by servo saturation on the one hand and unacceptable transient response characteristics on the other.

The directional SCAS is also a rate-command/attitude-hold system. Like the roll SCAS, the rate command feature is obtained via shaping of the pedal input. The frequency response characteristics of heading to pedal are shown in Fig. 27 for 0, 20 and 40 kt (0, 10 and 21 m/s). The responses are seen to be rate-like out to about 1.4 to 1.5 rad/sec at which point ω_{SAS}'' cuts off the rate-like response. Recall that ω_{SAS}'' is set by K_ψ and K_r which are both set to 13. Any further increases in these feedback gains would require an increase in the pedal series servo authority. It is felt that the bandwidth of the heading-to-pedal SCAS loop is adequate. The possibility of saturating the series servo is moderate in that only 4.4 deg or deg/sec of heading or yaw rate will result in 1 in. (0.025 m) of servo travel.

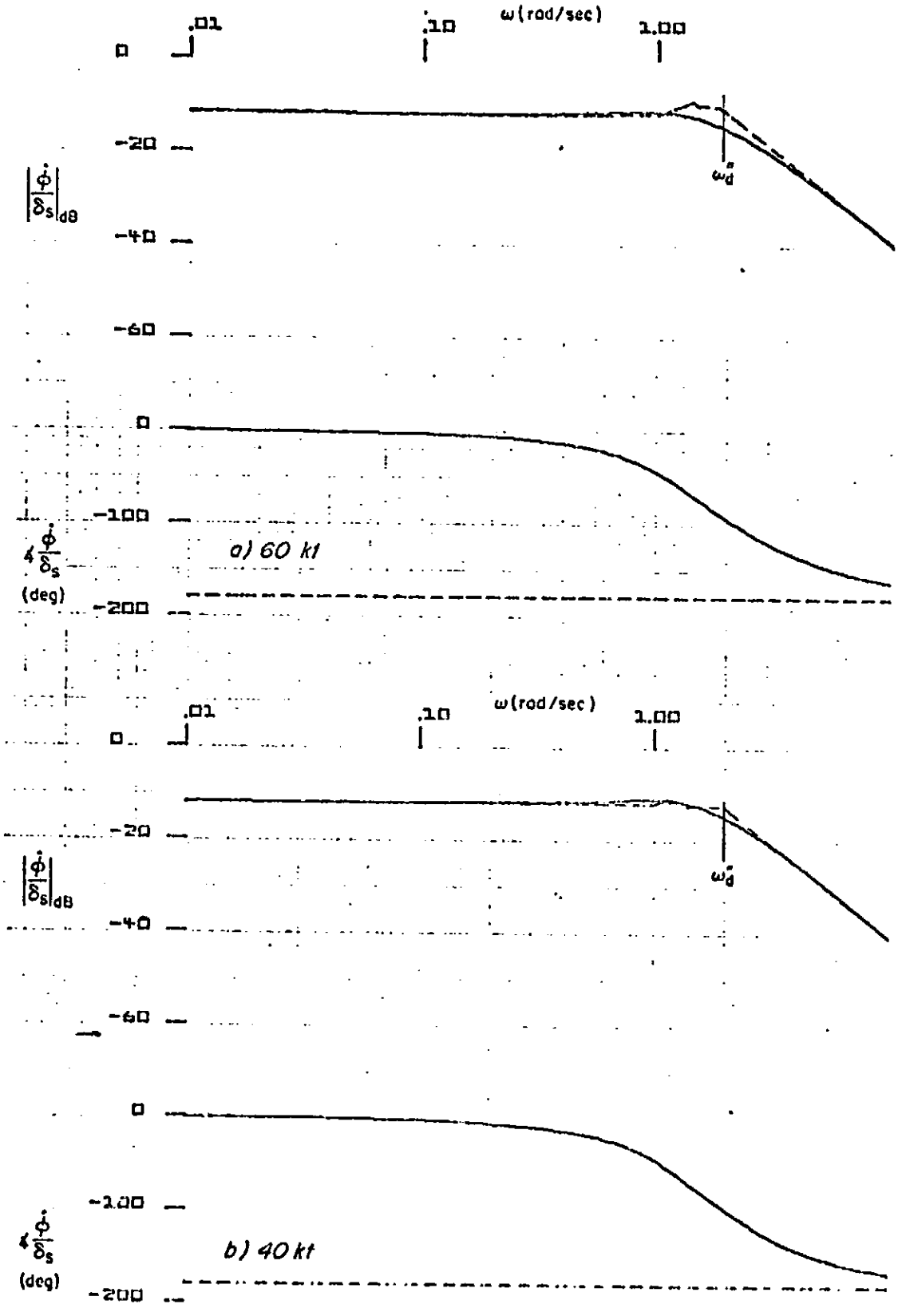

Figure 25. Frequency Response of Roll Rate to Lateral Cyclic Inputs; Wing Low SCAS (LOC B)

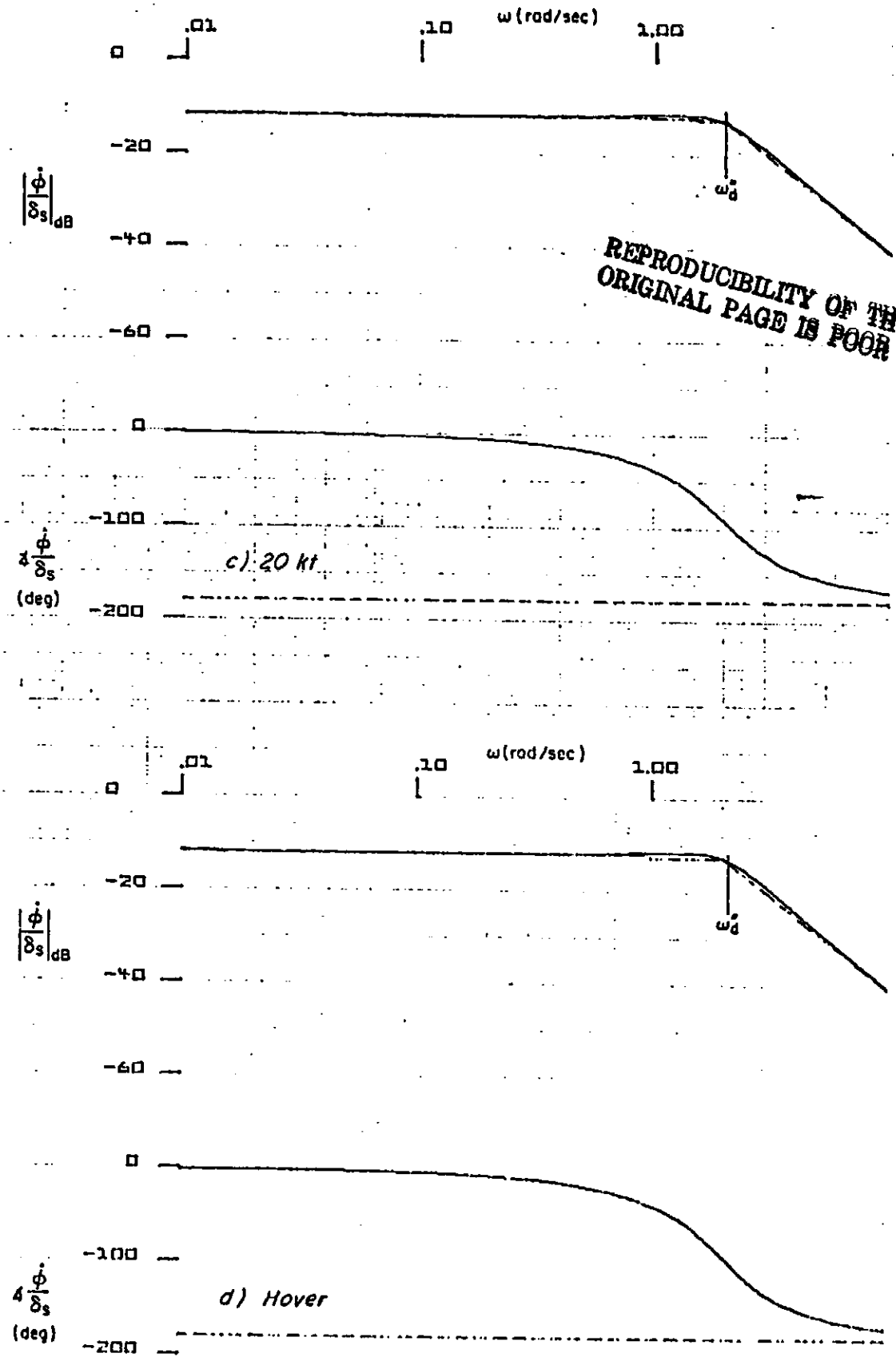

Figure 25 (Concluded)

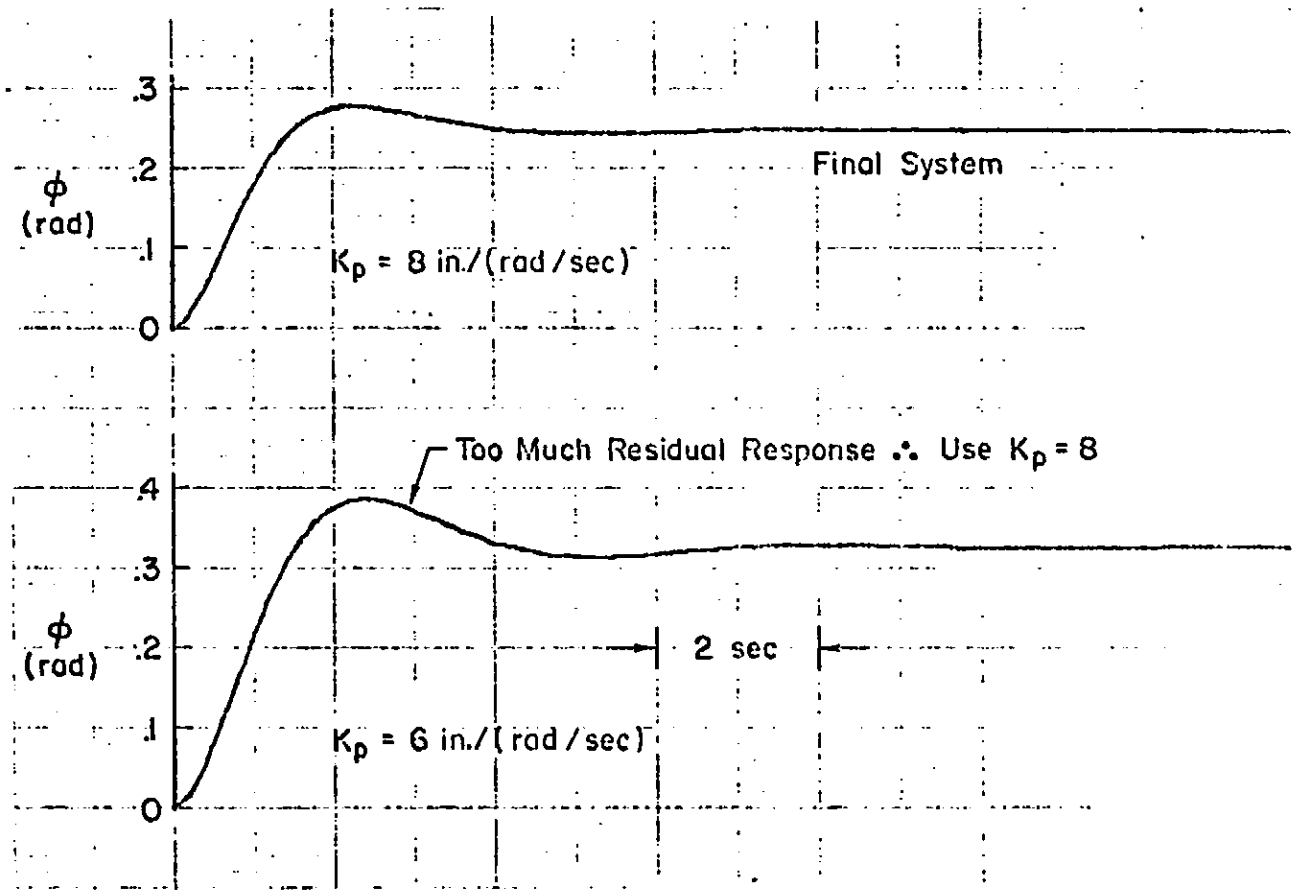

Figure 26. Bank Angle Response to φ_c = 1 in. (0.025 m) Step at Output of Stick Shaping Network; V = 40 kt (21 m/s); Wing Low SCAS (LOC B)

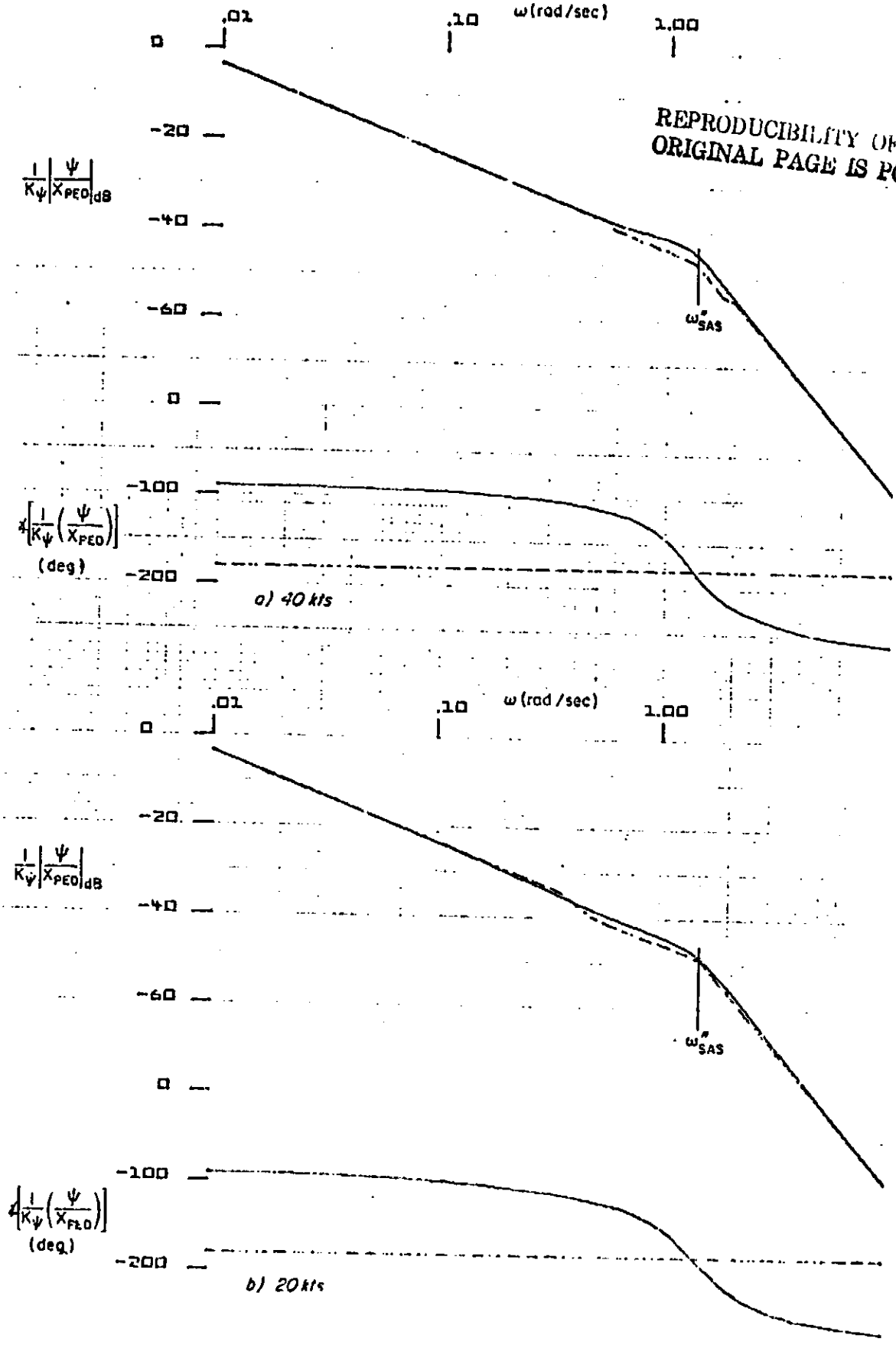

Figure 27. Heading to Pedal Frequency Response;
Wing Low SCAS (LOC B)

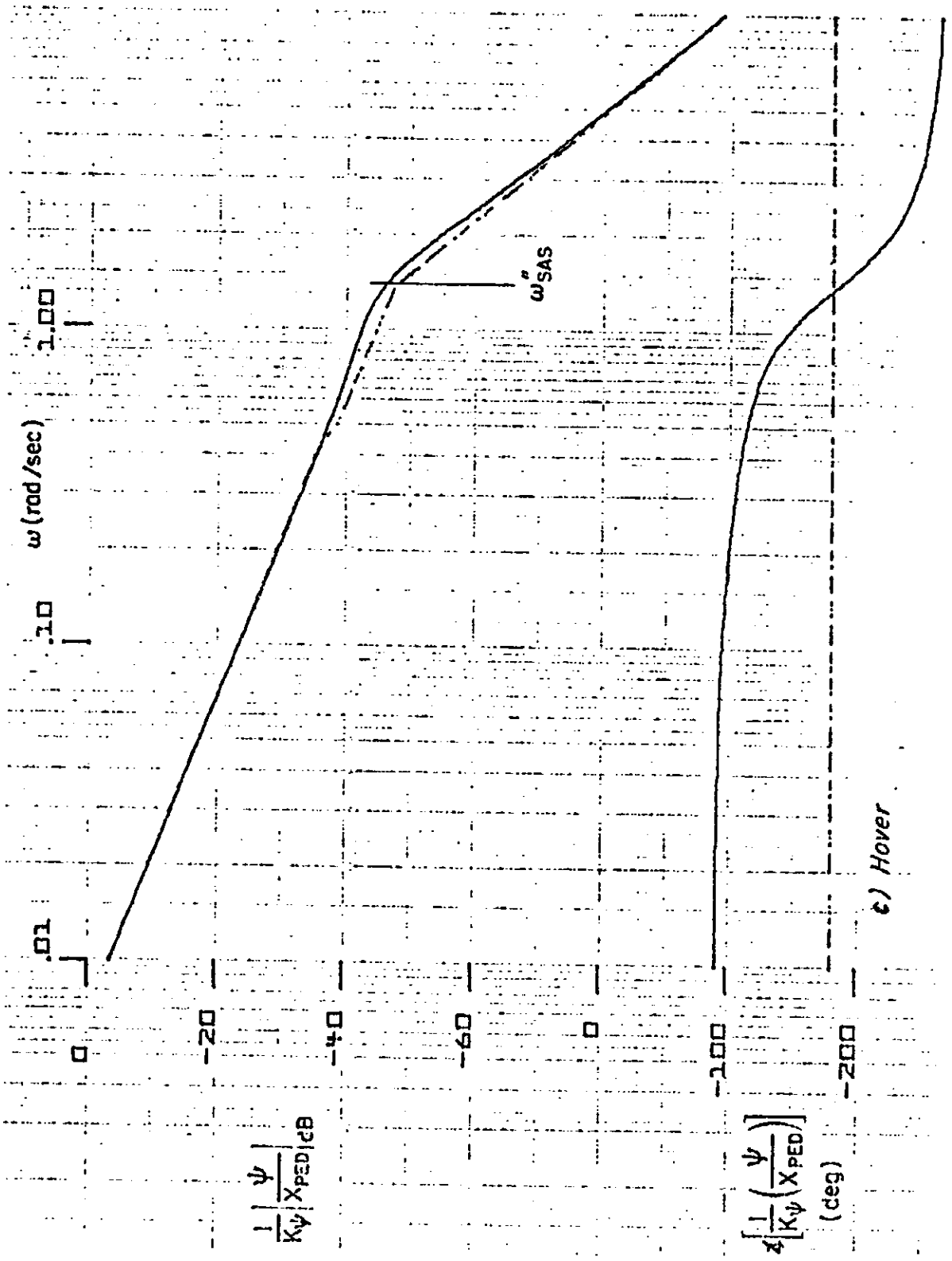

Figure 27 (Concluded)

Another metric chosen to evaluate the system was the heading response to a lateral cyclic input. For a wing-low approach we would like to minimize the heading response to lateral cyclic inputs at all frequencies. The heading to lateral cyclic frequency responses at 60, 40 and 20 kt (31, 21 and 10 m/s) and hover are shown in Fig. 28. These results indicate that moderate to large stick deflections will produce measurable heading excursions. For example, lateral cyclic excursions of 1 in. (0.025 m) at a frequency of 1.5 rad/sec will produce heading excursions which vary from a minimum of 1.1 deg (0.019 rad) at 60 kt (31 m/s) to a maximum of 3 deg (0.052 rad) at 0 kt (21 m/s). Recalling that the pedal series servo saturation occurs at heading excursions of 4.4 deg (0.076 rad), we can see again that the series servo authority could be marginal.

C. FLIGHT DIRECTOR FOR LOC A

LOC A is a conventional beam tracking mode where bank angle is used to develop a turn rate which results in heading changes. This mode is nominally used at speeds at and above 60 kt (31 m/s) for straight and curved localizer tracking. The analysis techniques used to select and shape the feedbacks were taken directly from Ref. 10. From Fig. 18 it can be seen that localizer error and derived error rate are fed back to the flight director to provide path following and path damping, respectively. Inner-loop stabilization is achieved via a bank angle feedback to the flight director. This feedback is washed out to avoid requiring a trajectory-dependent feedforward. Washout use allows tracking of arbitrary curved path without external inputs. Complementary filtering schemes using $a_y + g(\varphi - \varphi_c)$ to replace high frequency beam rate cannot satisfy the desired "no external inputs" design requirement. This is because the desired design must be capable of following any beam shape (within system limits) without prior knowledge of the beam geometry. Notice that $\varphi_c = \tan^{-1}(V_{GS}^2/gR)$ depends on beam geometry (R is the turn radius). Furthermore, the noise characteristics of the beam must be of low enough level and/or broad enough bandwidth to allow a sufficiently small value of T_y (beam rate filter time constant) so that unacceptable lags in following curved paths will not result. Normal values of T_y are about 2 sec in an ILS system, whereas a value of 0.25 sec or less are possible with an MLS system. This is so because

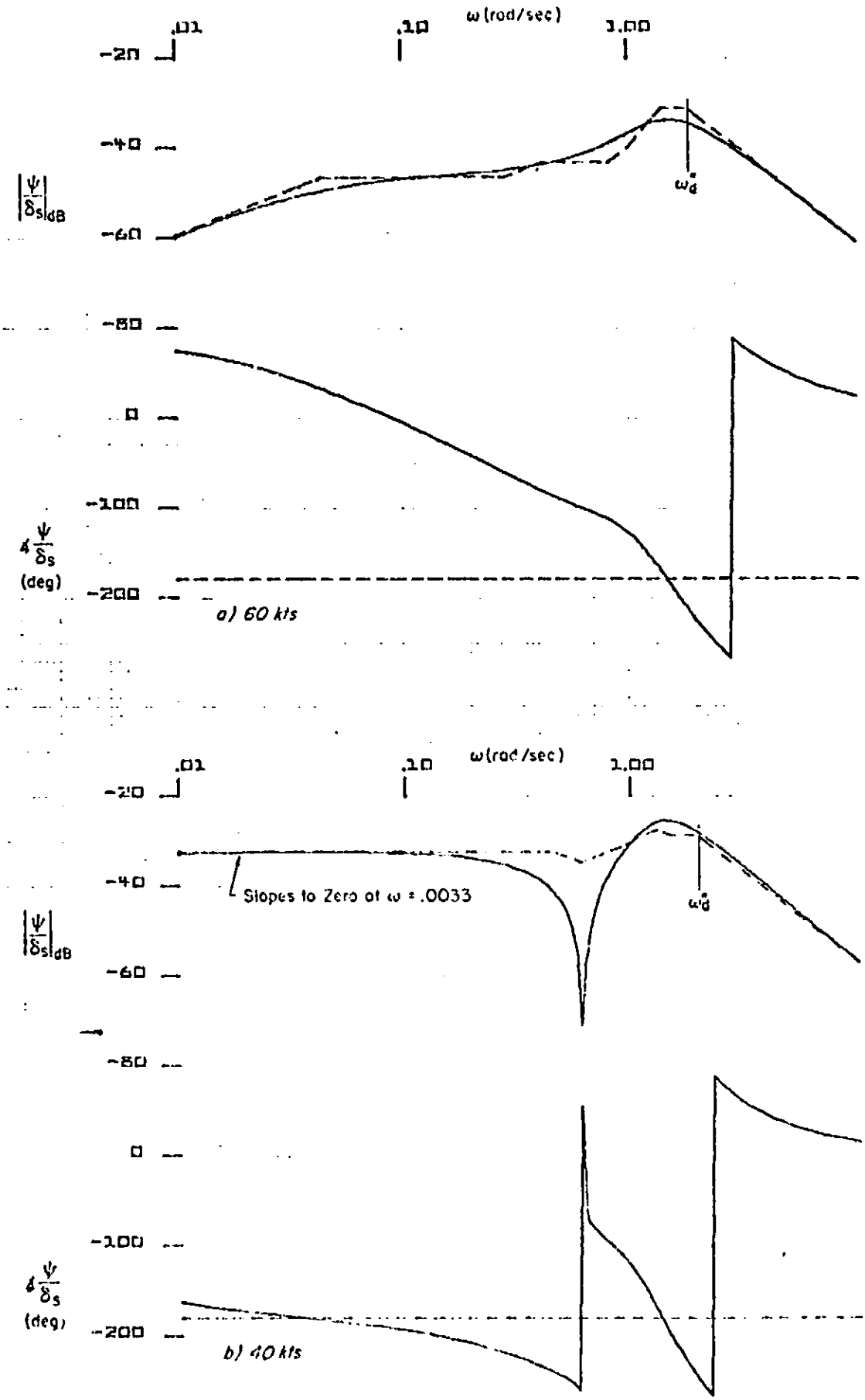

Figure 78. Frequency Response of Heading to Lateral Cyclic Inputs; Wing Low SCAS (10C B)

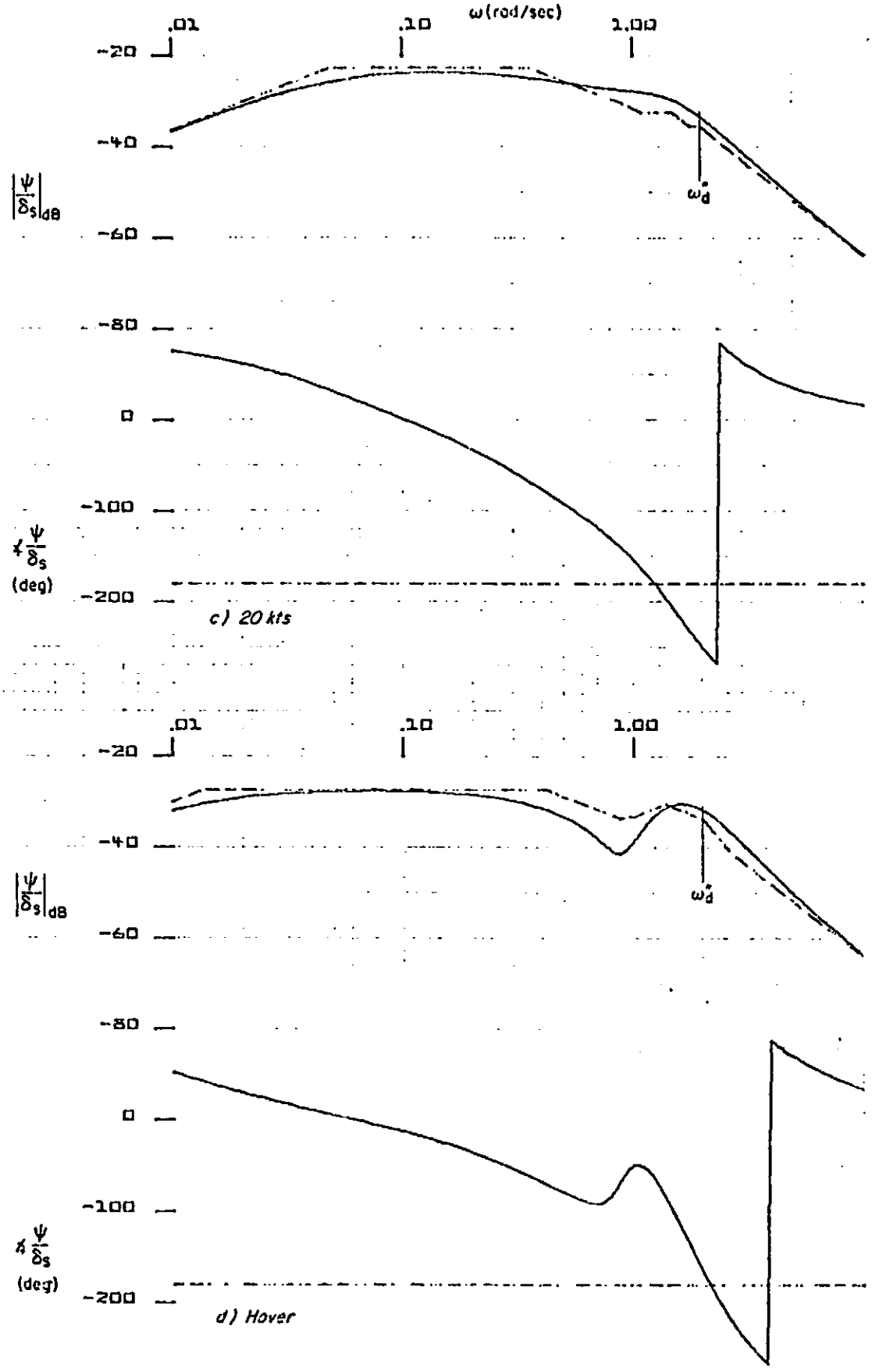

Figure 28 (Concluded)

the noise characteristics of microwave landing systems (MLS) are generally of much lower level and of broader bandwidth than for ILS.

1. Localizer Capture

The transition from heading hold (HH) to LOC A occurs automatically when $\epsilon_y = 0$ ($\epsilon_y = K_y y + K_{\dot{y}}\dot{y}$). Transition back to heading hold must be manually selected by the pilot. Transition to LOC B may be selected manually by the pilot or automatically based upon airspeed.

2. Parameter Adjustments

The feedback selection and shaping are as shown in Fig. 18 with the switches set to the LOC A position. The values of the time constants and gains were adjusted by the methods of Ref. 10 to obtain a K/s frequency response for the open-loop lateral flight director to lateral cyclic input in the region of the unit gain crossover frequency for manual flight director control. As shown in Fig. 29, the desired K/s-like characteristic is obtained with reasonable success in that the lateral flight director to lateral cyclic input is K/s in a frequency region from about 0.5 to 5 rad/sec.

The performance metrics used to evaluate the closed-loop system regulatory characteristics in the LOC A mode are the frequency responses of lateral beam error to lateral beam command (y_ϵ/y_c) and lateral beam offset to side gust inputs (y/v_g) and the time response to an initial condition offset. These closed-loop performance measures were obtained using an assumed unit gain crossover frequency under pilot control of 1.5 rad/sec and a neuromuscular lag of 0.17 sec. The resulting pilot model is:

$$G_{FFS}(0)Y_{p_y} = 3.7e^{-.17j\omega} \tag{31}$$

The ability of the closed-loop pilot/vehicle system to regulate against side gust disturbances is shown in terms of the lateral beam deviation to side gust frequency response in Fig. 30. The system is seen to regulate the errors to zero at frequencies below 0.3 rad/sec. This performance is considered to be acceptable.

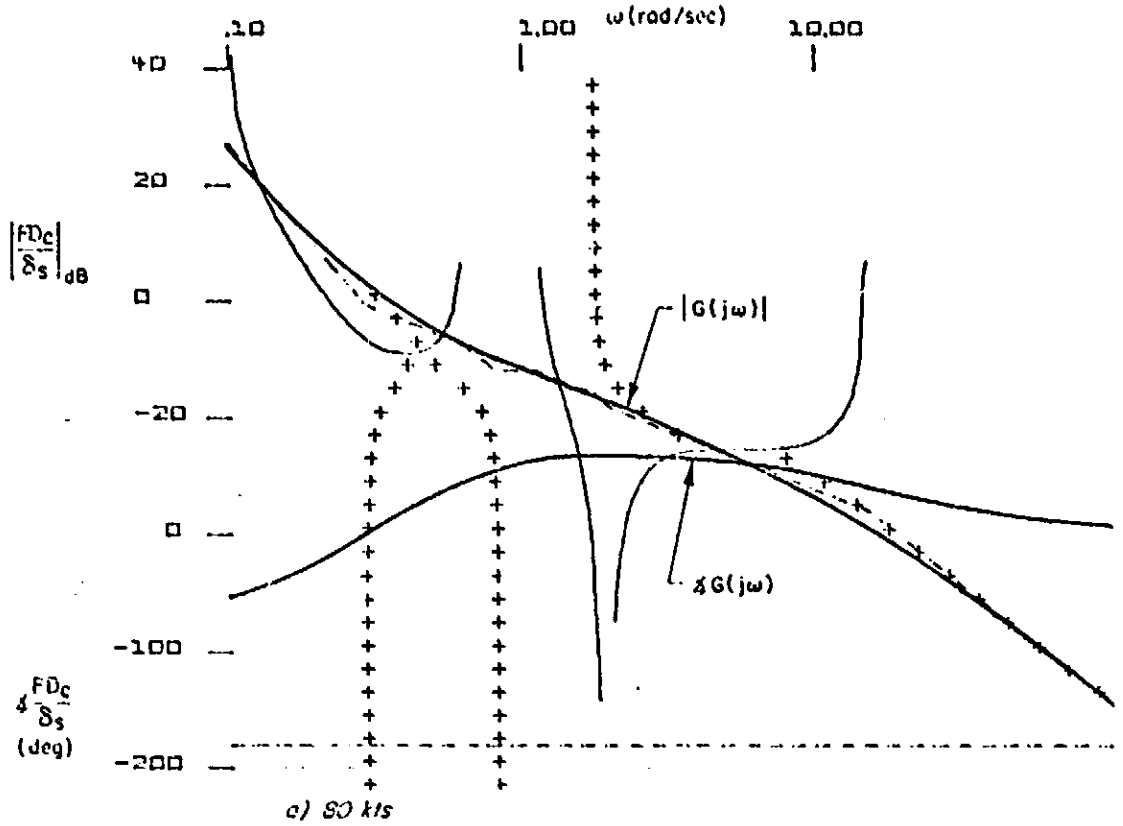

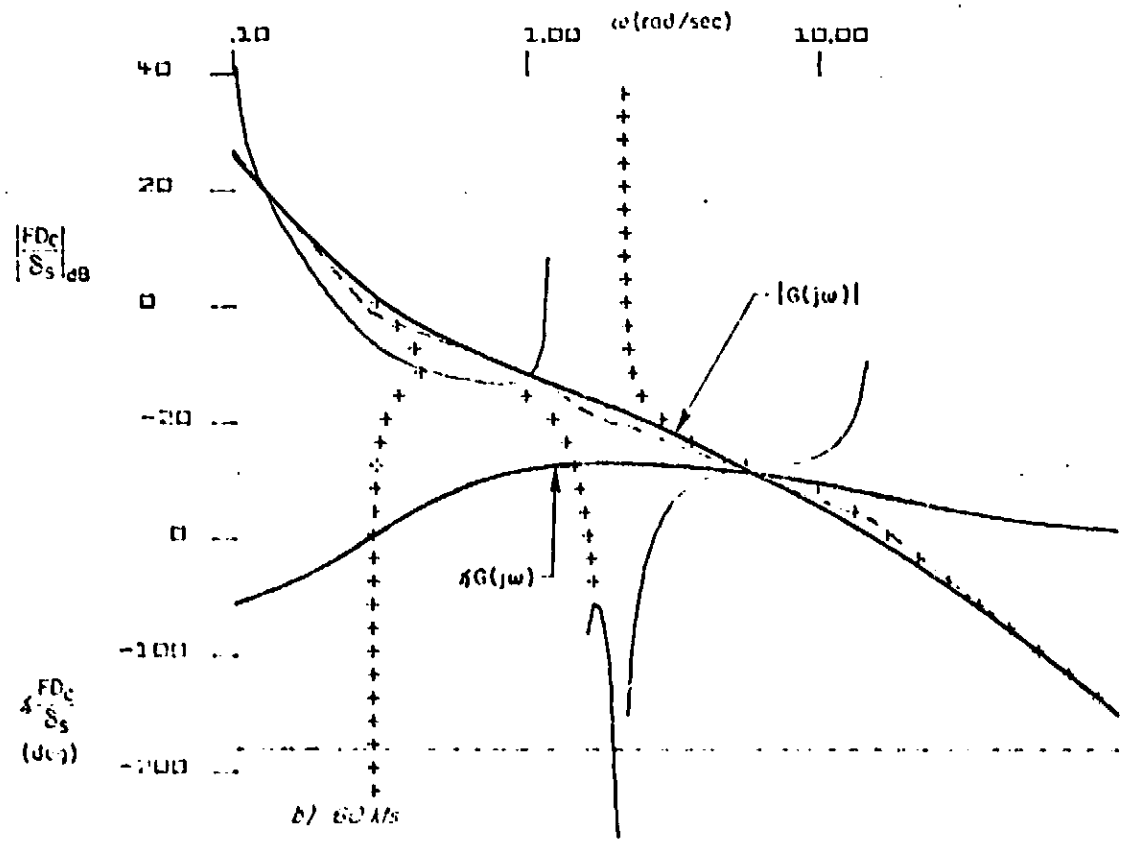

Figure 30. Open-Loop Lateral Flight Director to Lateral Cyclic Input Frequency Response; Turn Following SCAS (10C A)

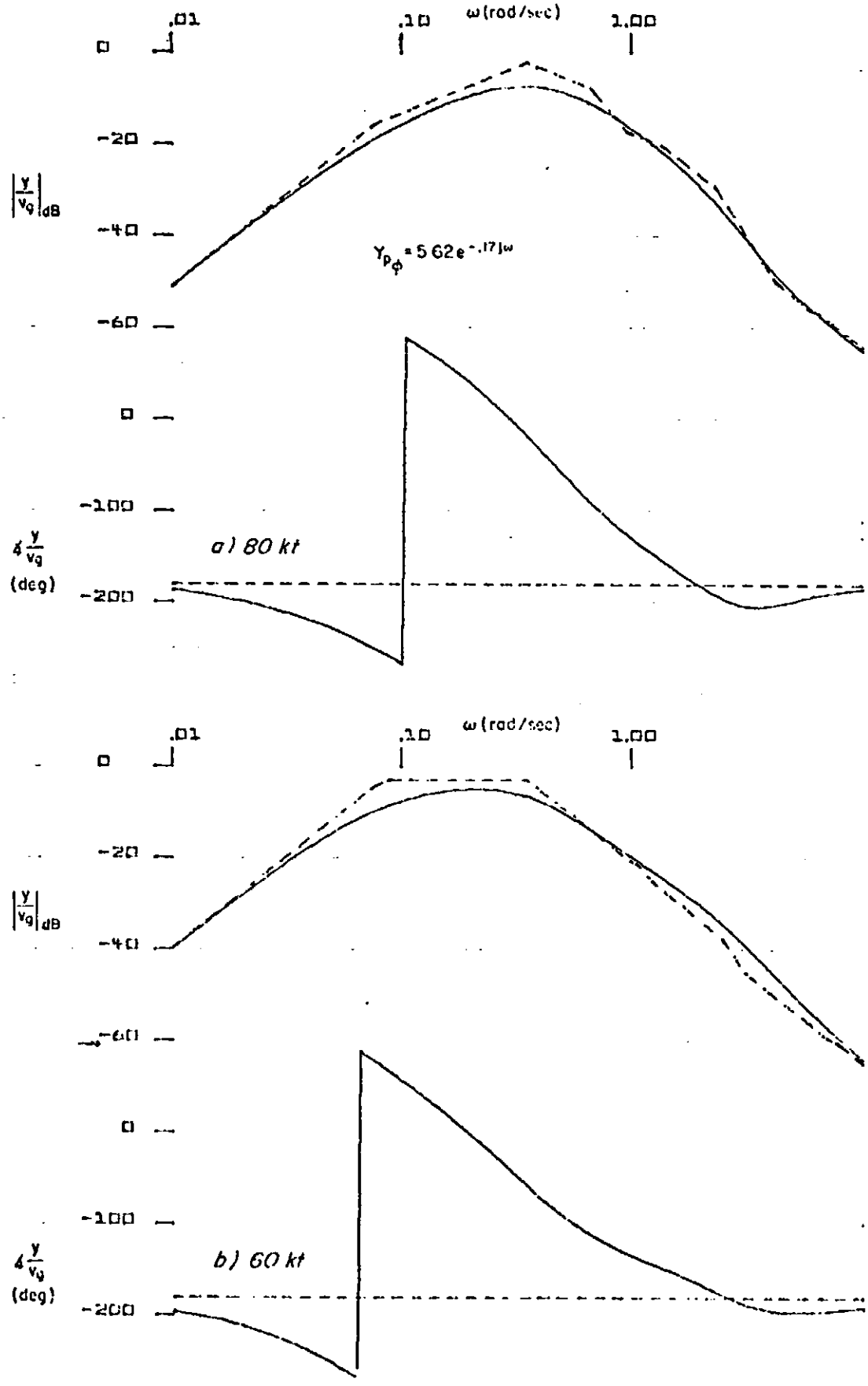

Figure 50. Closed-Loop Frequency Response in Lateral Beam Deviation to Side Gust Inputs; Turn-Following SCAS (LOC Λ)

The ability of the closed-loop pilot/vehicle system to follow external beam commands is shown in Fig. 51 in terms of the y_c/y_c frequency response. The closed-loop bandwidth for error regulation is seen to be 0.3 rad/sec at 60 and 80 kt (31 and 41 m/s). This is consistent with the performance achieved with the flight director developed in Ref. 10. That director received very good pilot ratings.

A time response of the closed loop pilot/airplane system to a 100 ft (30 m) initial condition offset is shown in Fig. 52. A similar time response obtained from the Ref. 10 system is shown superimposed on the XV-15 response and indicates that the two responses are nearly identical. The pilot ratings for the Ref. 10 flight director were very good (order of 2) indicating that the long tail (due to the washout of the bank angle feedback) is of little or no consequence in practice.

5. Flight Director for IMC B

The analysis techniques developed in Ref. 10 to select and shape the flight director feedbacks are for a turn-following SCAS. However, they also apply for a wing-low SCAS if the relationship between lateral deviation and bank angle can be shown to be the same for the two systems. Comparing the lateral deviation to bank angle characteristics of each system reveals the following:

- Turn-following: $y \cdot \frac{\phi}{s^2}$
- Wing-low: $y \cdot \frac{\phi}{s(s - Y_v)^2}$

Since $(-Y_v)$ is orders of magnitude below the path mode response frequency, the y/ϕ response is essentially identical for wing-low and turn-following stability and command augmentation systems. Therefore the Ref. 10 methods apply directly for synthesis of both the IMC B and IMC A modes. The resultant feedback selection and shaping are as shown in Fig. 18 with the switches in the IMC B position. The gains and time constants in Table 8 yield the open-loop lateral flight director to lateral stick frequency responses shown in Fig. 53 for 60, 80, 120 kt (31, 41 and 62 m/s), and hover. As in the case of the turn-following system, the wing-low system (IMC B) exhibits an

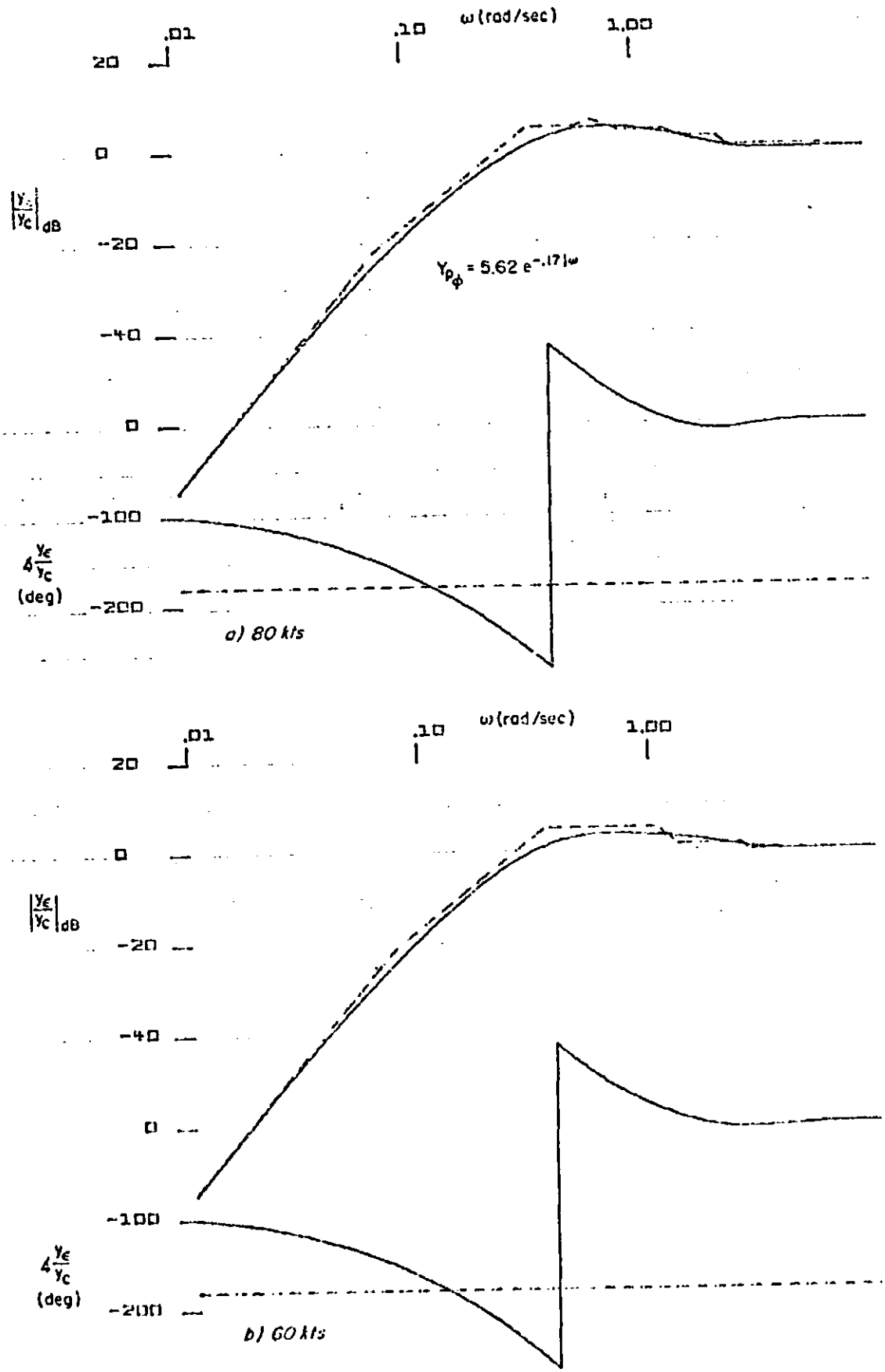

Figure 31. Closed-Loop Frequency Response in Beam Error to Beam Command; Turn-Following SCAS (LOC A)

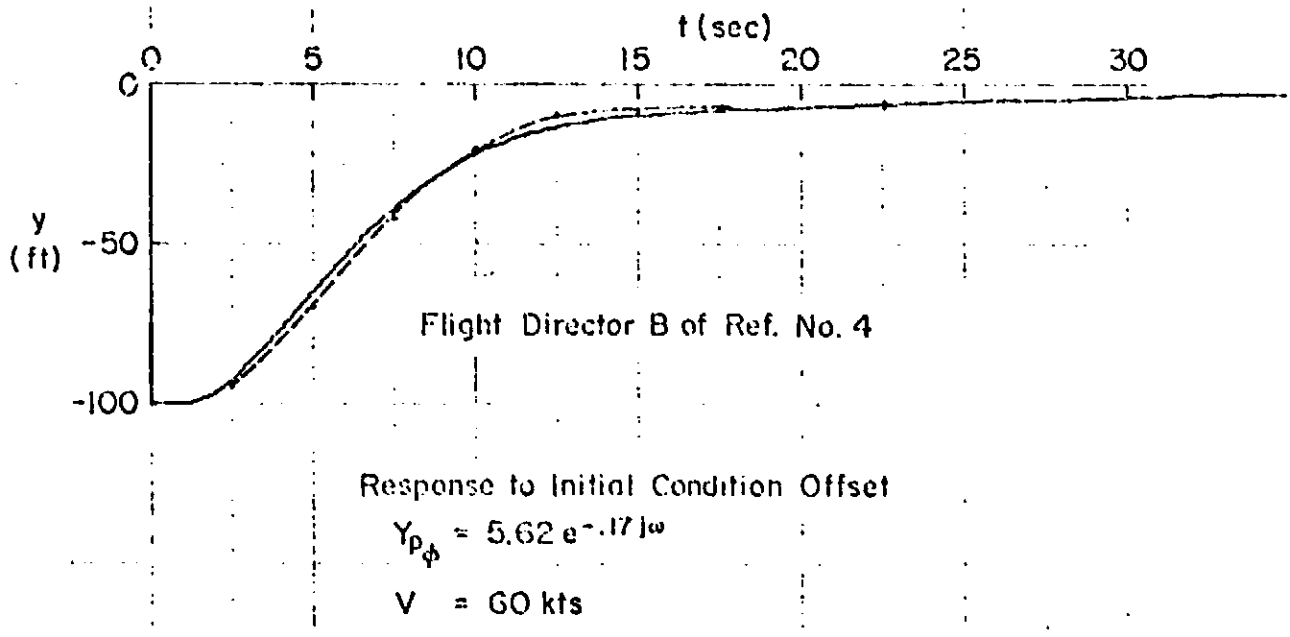

Figure 57. Comparison Between Initial Condition Responses of XV-15 and Flight Director B of Ref. 10 Turn-Following SCAS (LOC A)

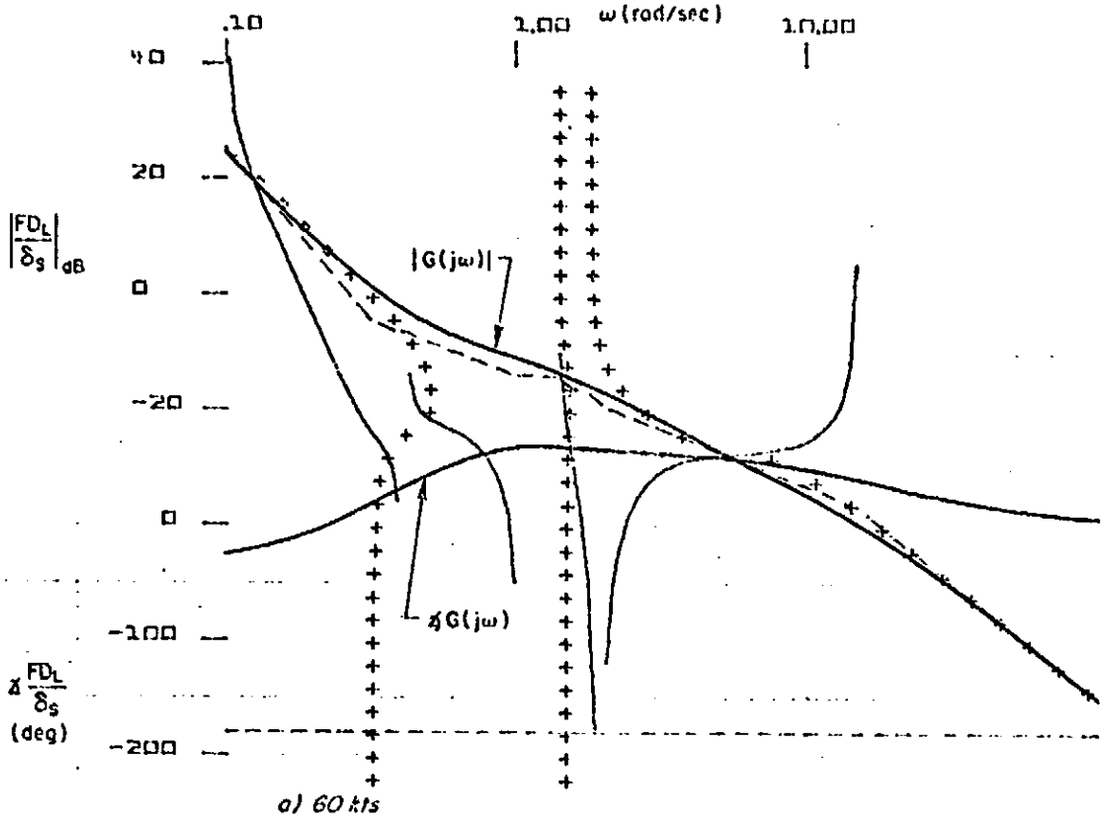

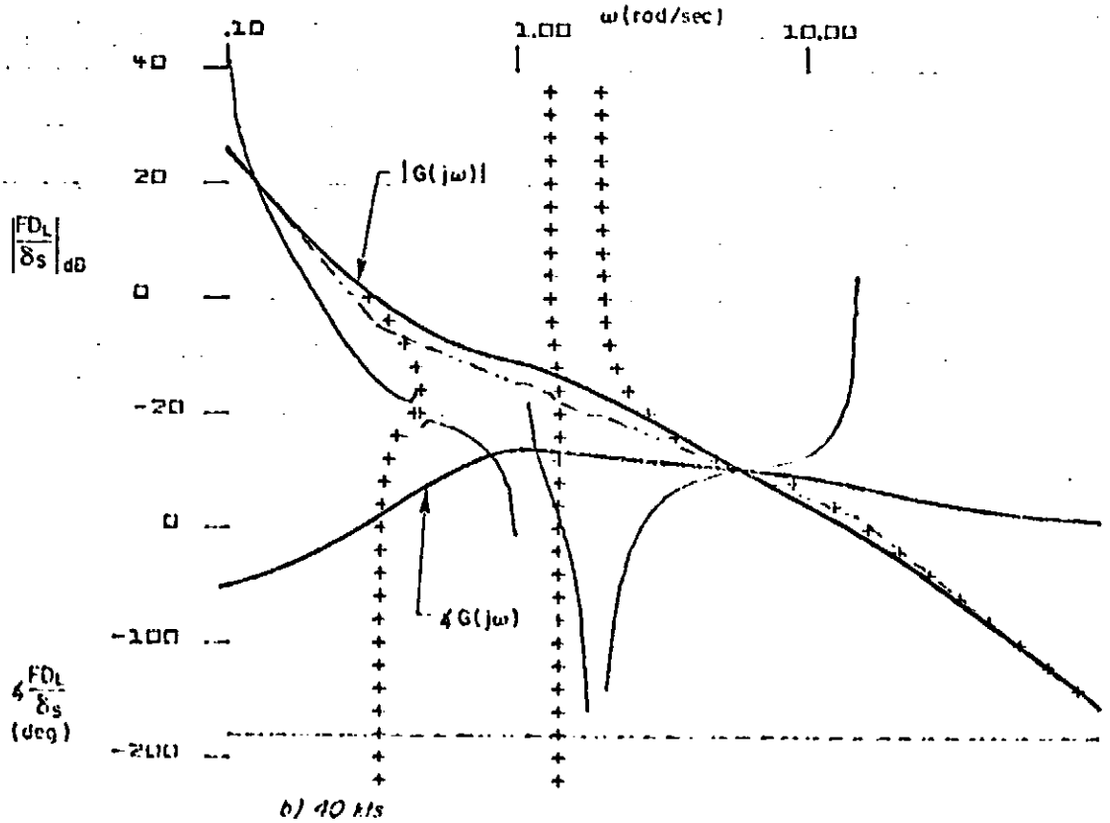

Figure 33. Open-Loop Frequency Response of Lateral Flight Director to Lateral Cyclic Inputs; Wing Low SCAS (LOC B) Mode

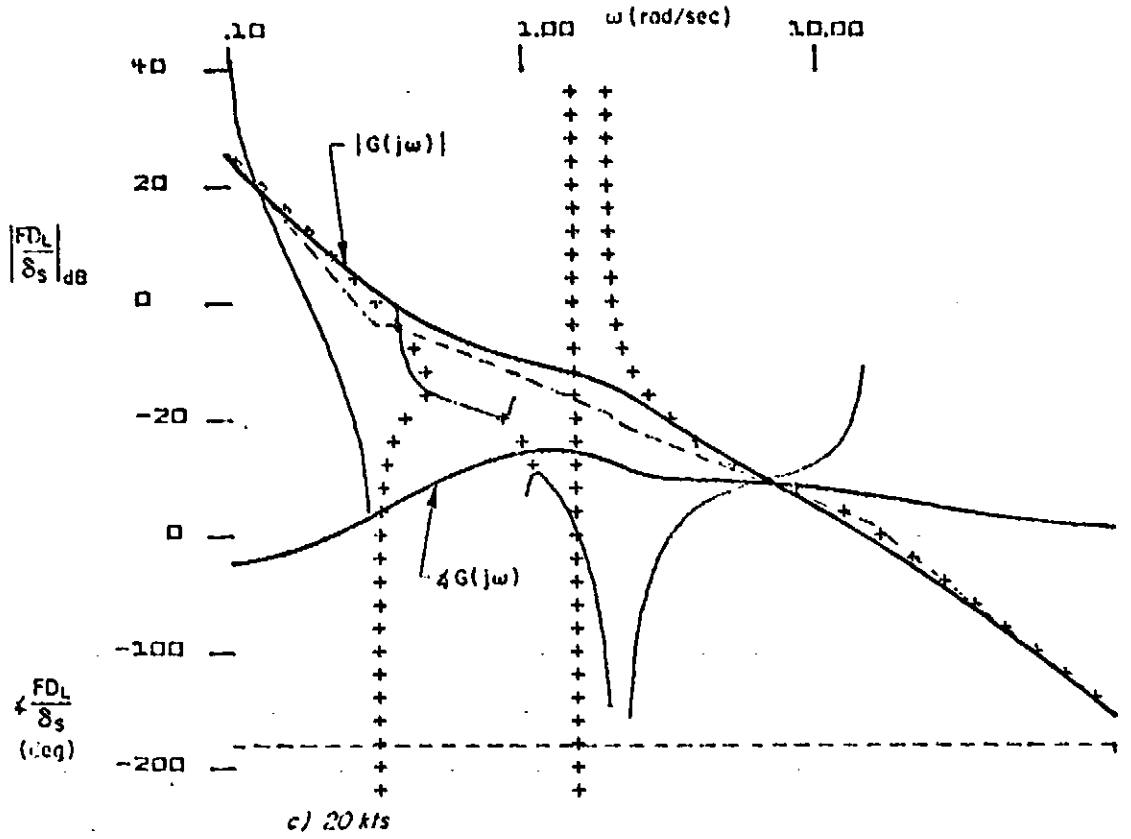

c) 20 kts

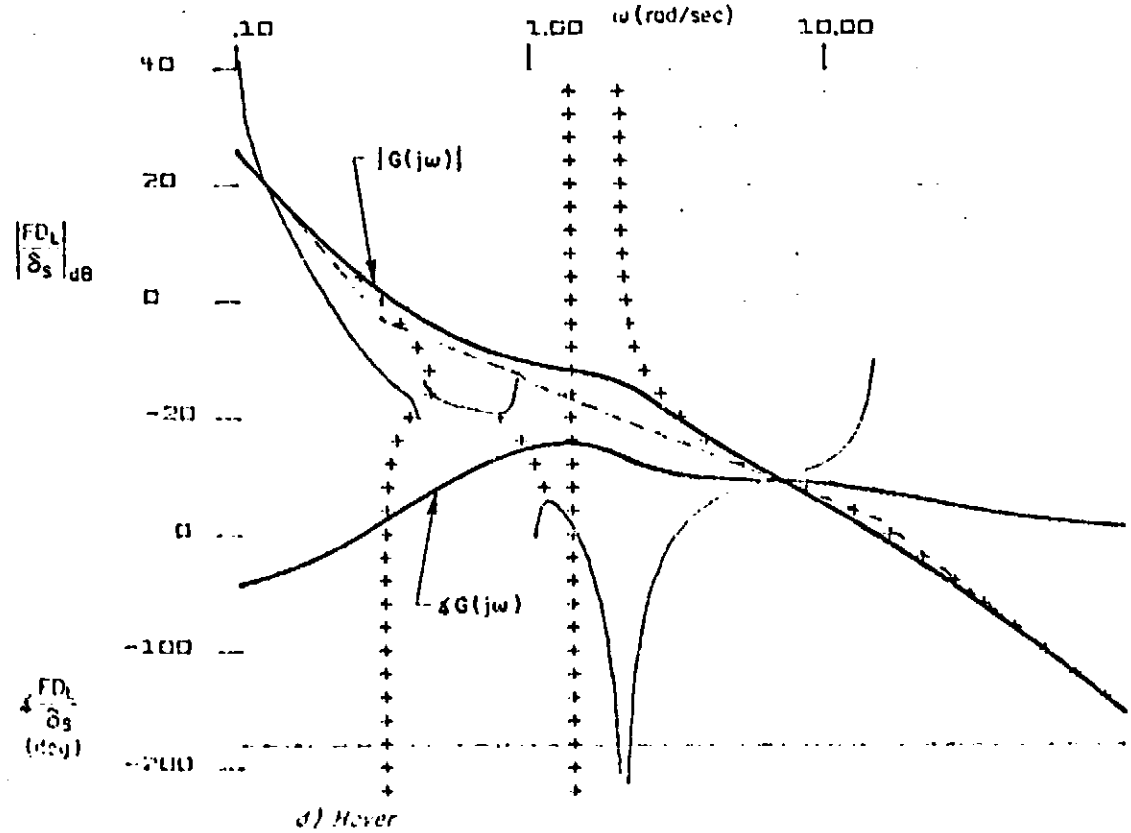

d) Hover

Figure 44. (Concluded)

open-loop lateral flight director-to-lateral cyclic input characteristic which is essentially K/s between 0.5 and 5 rad/sec. However, at 20 kt (10 m/s) and hover the frequency response exhibits a bulge at about 2 rad/sec. This is a direct result of a decreased closed-loop dutch roll damping ratio (ζ_d'') at lower airspeeds in the wing-low SCAS. The origin of this may be better understood by examining an equivalent system transfer function which is a close approximation for the wing-low SCAS system:

$$\frac{p}{\delta_s} = \frac{.25\omega_d''}{s(s^2 + 2\zeta_d''\omega_d''s + \omega_d''^2)} \tag{52}$$

where ζ_d'' and ω_d'' vary with speed as follows:

Airspeed (kt)*	ζ_d''	ω_d'' (rad/sec)
0	.50	2.02
20	.53	1.97
40	.66	1.95
60	.79	1.81

As shown in Fig. 24, an increase in ζ_d'' would require increased feedback gains which is not possible because of the SCAS feedback gain limitations imposed by the limited authority series servo.

It is also evident in Fig. 24 that the SAS mode has an even lower damping ratio than the dutch roll mode. However, the SAS mode poles are nearly canceled by the ω_ψ'' zeros with the result that there is virtually no net effect upon the open-loop flight director frequency response.

*1 kt = 5.144 x 10^{-1} m/s.

The K/s shape of the lateral flight director to lateral cyclic input transfer function is obtained by adjusting the first-order zeros arising from $1/T_1$ and K_{D_φ}/K_{D_p} to have the magnitude of ω_d''. Hence, the residues for the ω_d'' poles increase with decreasing ζ_d'' from 1.0. When the residues are large because of low damping of the closed-loop dutch roll mode, the result is a bulge in the open-loop amplitude ratio even though the transfer function asymptotes are K/s-like. This effect is significant at damping ratios as high as 0.7, and becomes very pronounced at damping ratios less than 0.5.

It is felt that the average slope of the amplitude ratio is close enough to K/s so that the pilot opinion will not suffer excessively at 20 kt (10 m/s) and hover. However, it must be recognized as a marginal situation which should receive attention during the piloted simulator evaluations. It will, of course, have little or no effect on the automatic system operation.

The performance of the closed-loop pilot/vehicle system was evaluated assuming a unit gain crossover frequency under pilot control of 1.5 rad/sec in the lateral flight director loop. This resulting pilot model is:

$$G_{FFS}(0)Y_{p_\varphi} = 3.1e^{-.17j\omega} \tag{33}$$

The same performance metrics are used as for the LOC A system. These are the frequency responses of lateral beam offset to lateral gusts (y/v_g), lateral beam error to lateral beam command (y_ϵ/y_c), and time histories of the path response to lateral initial condition offsets.

Figure 34 indicates that the lateral gust sensitivity of the closed-loop pilot/vehicle system varies widely with flight condition. The 60 and 20 kt (31 and 10 m/s) flight conditions exhibit the highest overall gust sensitivity, followed by the hover flight condition. The 40 kt (21 m/s) case exhibited the best regulation against side gusts. The gust sensitivity turns out to be more a function of basic aerodynamic characteristics than of variation in closed-loop regulation characteristics with speed. This can be seen from the following table of Y_v as a function of speed.

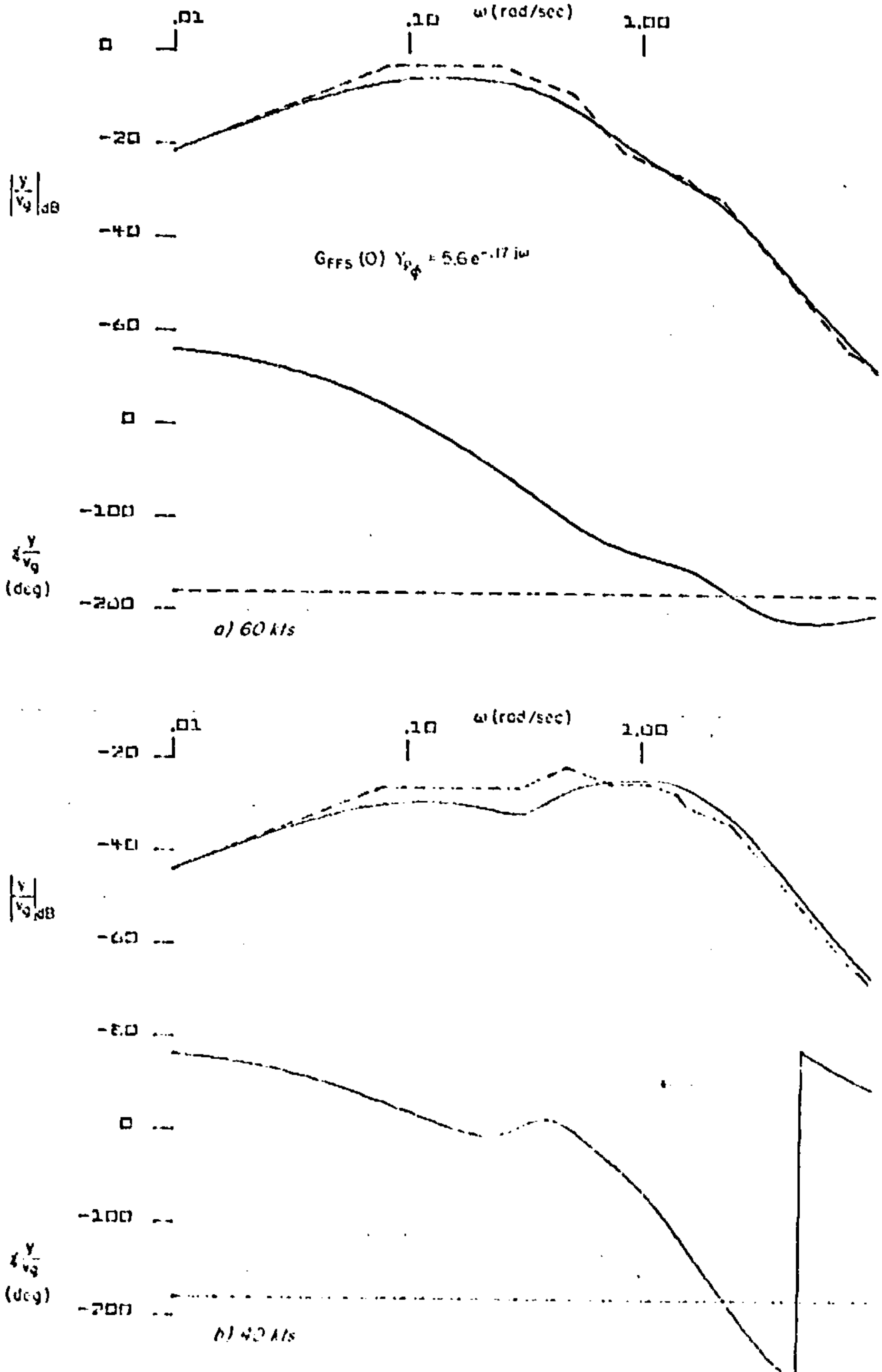

Figure [illegible]. Closed-Loop Frequency Response of Lateral Beam Deviation to Side Gust Input; [illegible]

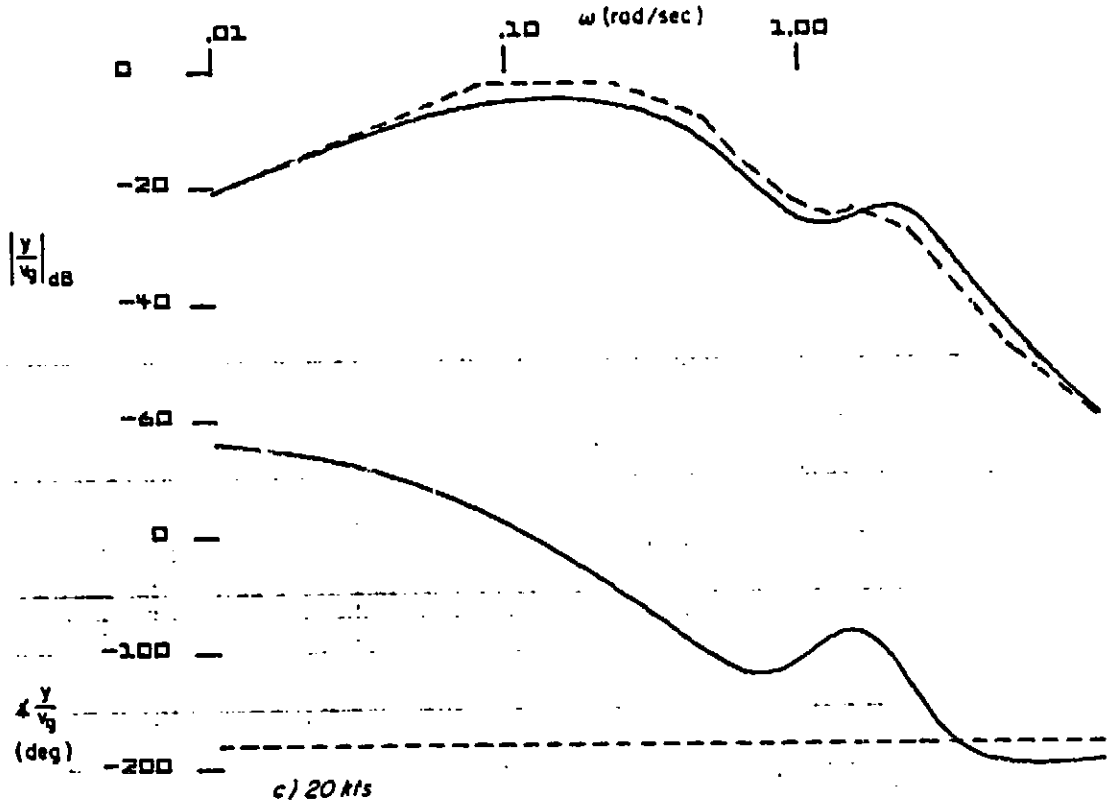

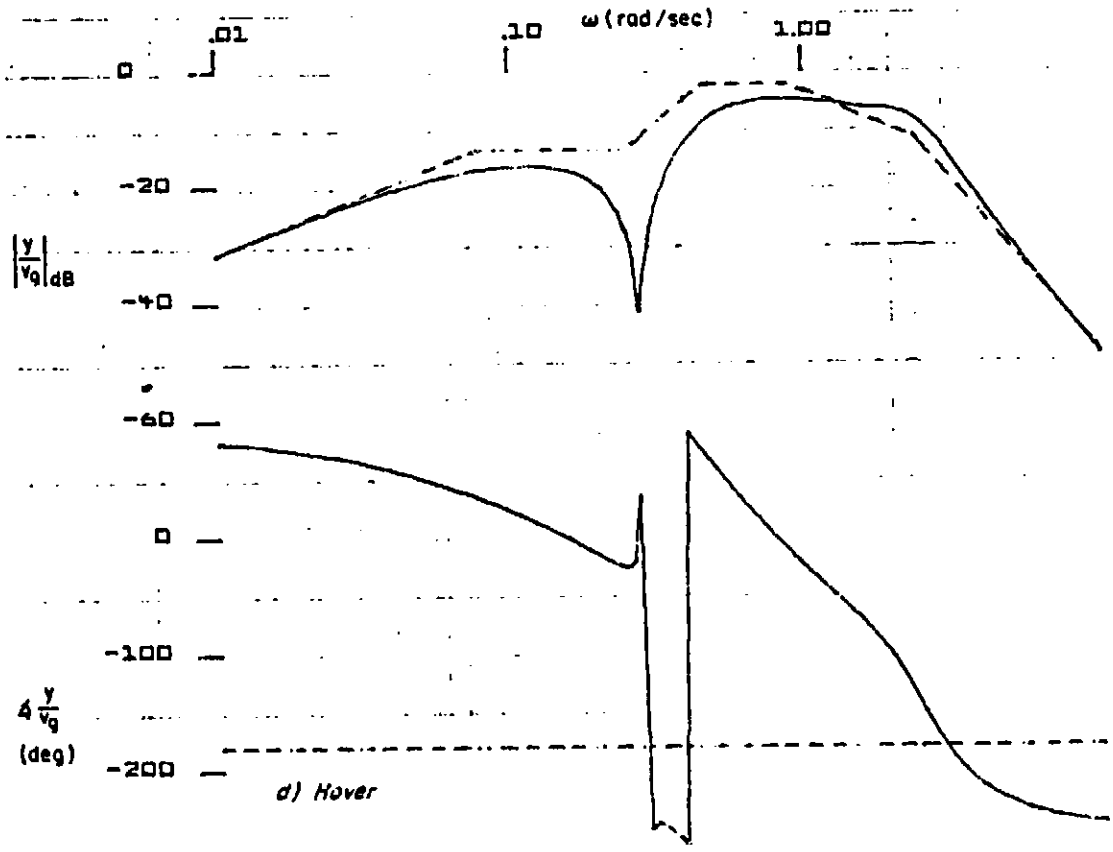

Figure 34 (Concluded)

Airspeed (kt)*	Y_v (sec^{-1})
0	-.007
20	-.038
40	-.0034
60	-.046

The values of Y_v correlate directly with the closed-loop y/v_g responses in Fig. 34. The lateral beam deviations at all flight conditions are seen to be decreasing to zero at frequencies less than 0.1 rad/sec.

The beam error to beam command frequency responses (Fig. 35) indicate that the bandwidth for reducing errors to zero is about 0.25 rad/sec for all flight conditions. This is well within the acceptable range.

The time responses to a lateral initial condition offset of 100 ft (30 m) are shown in Fig. 36 for the 40 kt (21 m/s) and hover flight conditions. Comparison with Fig. 32 shows the responses are essentially identical to the 60 kt (31 m/s) LOC A flight condition, which in turn was nearly the same as the Ref. 10 response. Hence, the objective of augmenting the airplane so that its performance is nearly invariant with flight condition has been achieved. Furthermore, the system performance is consistent with a lateral flight director system which is known to have pilot acceptable performance.

D. INTERAXIS COUPLING

A preliminary investigation of the XV-15 aerodynamic crosscoupling revealed that the pitching moment due to sideslip [$M(\beta)$] can be quite large at sideslip angles greater than 1 deg (0.025 rad). This did not show up initially because the perturbation derviatives supplied to STI were obtained for very small sideslip angles. At small sideslip angle, $M_{|\beta|}$ is very small. A plot of pitching moment vs. side velocity at the 40 kt (21 m/s) flight

*1 kt = 5.144×10^{-1} m/s.

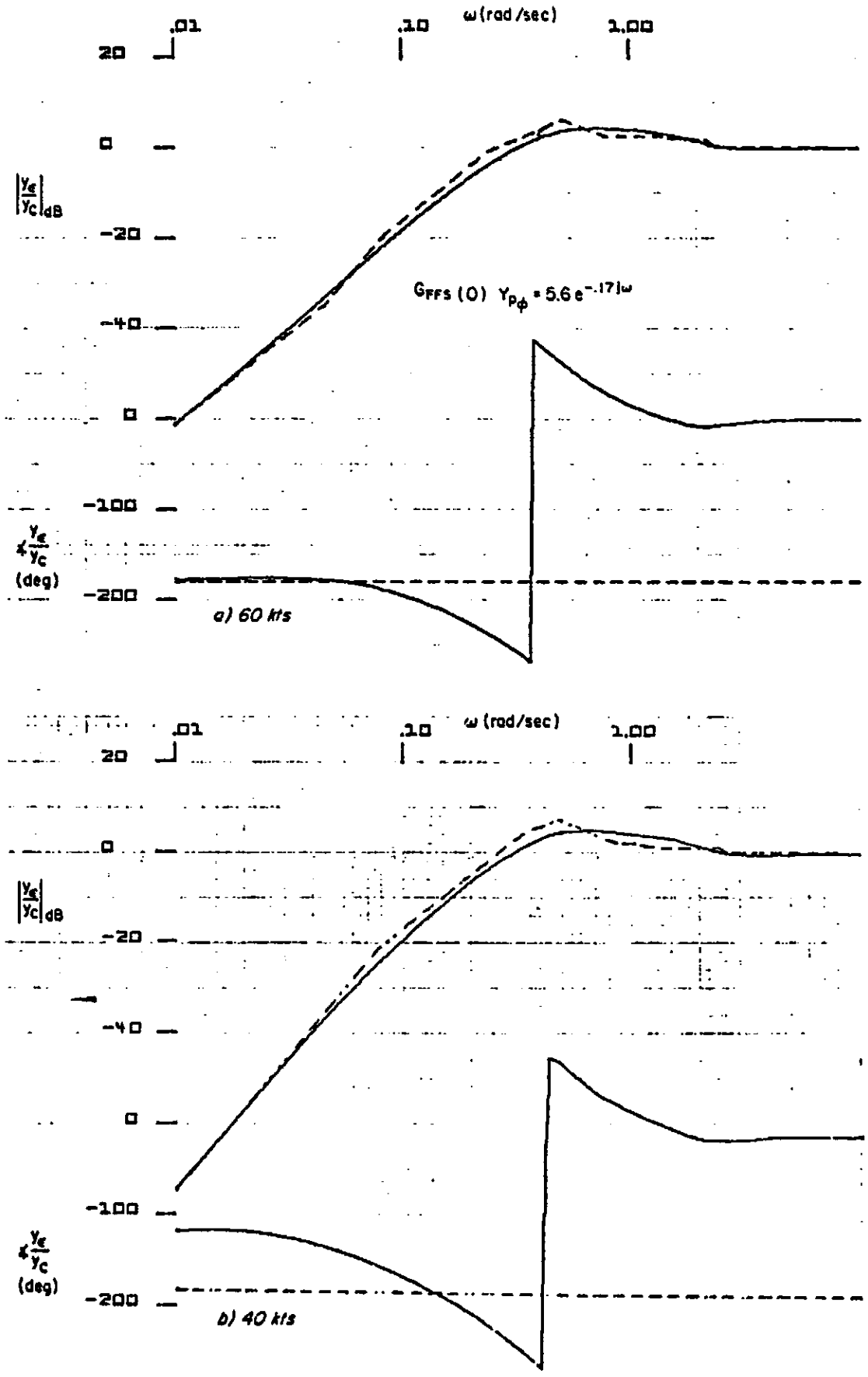

Figure 35. Closed-Loop Frequency Response in Beam Error to Beam Command

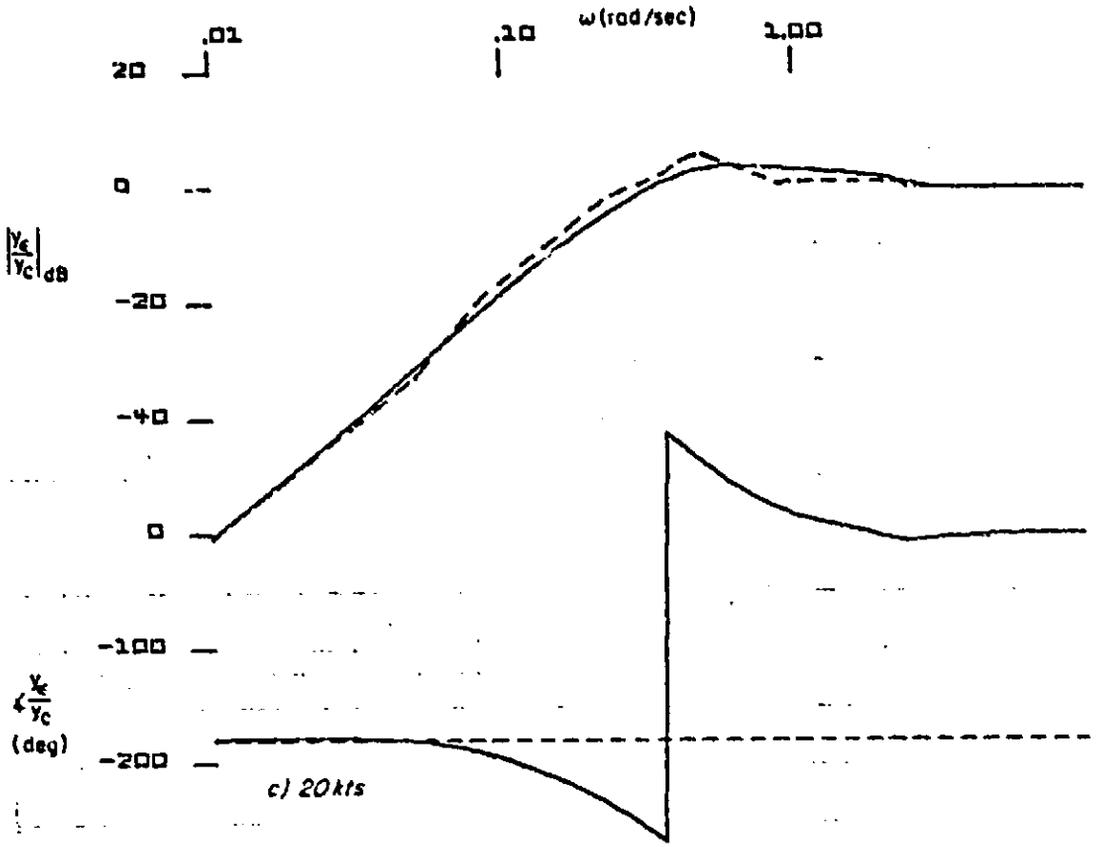

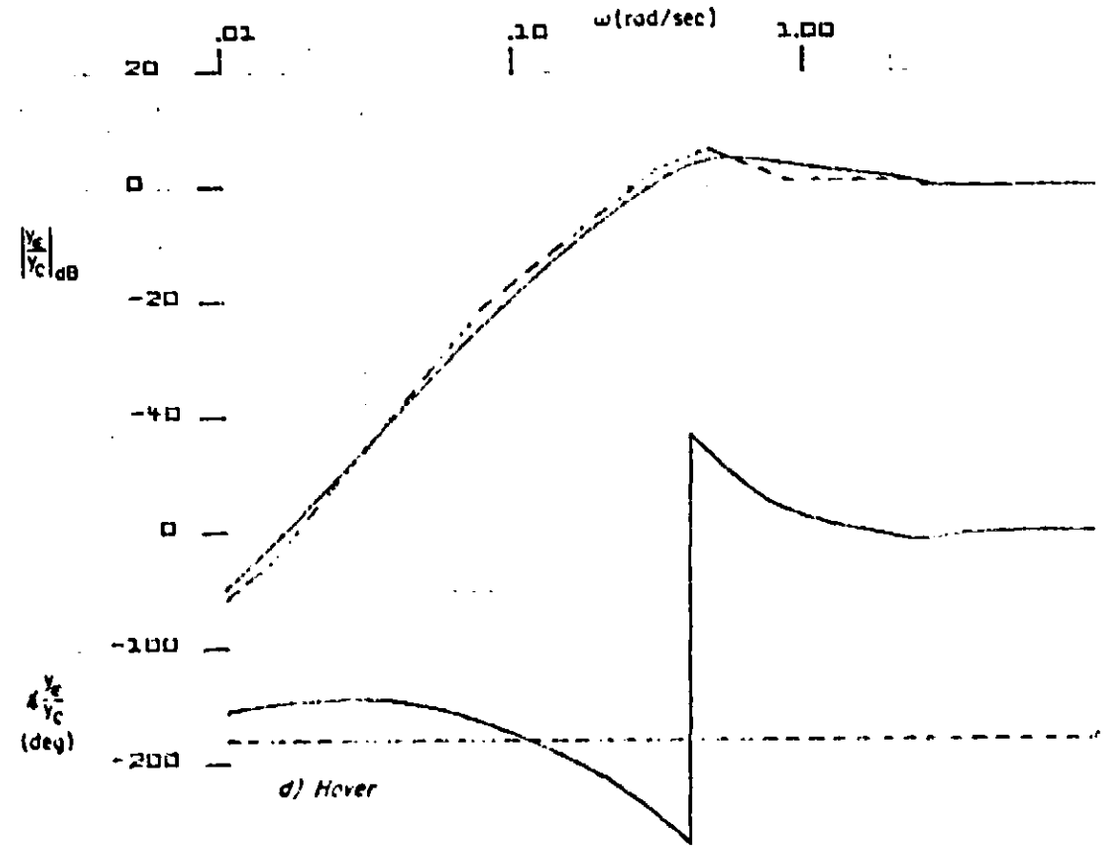

Figure 25. (Concluded)

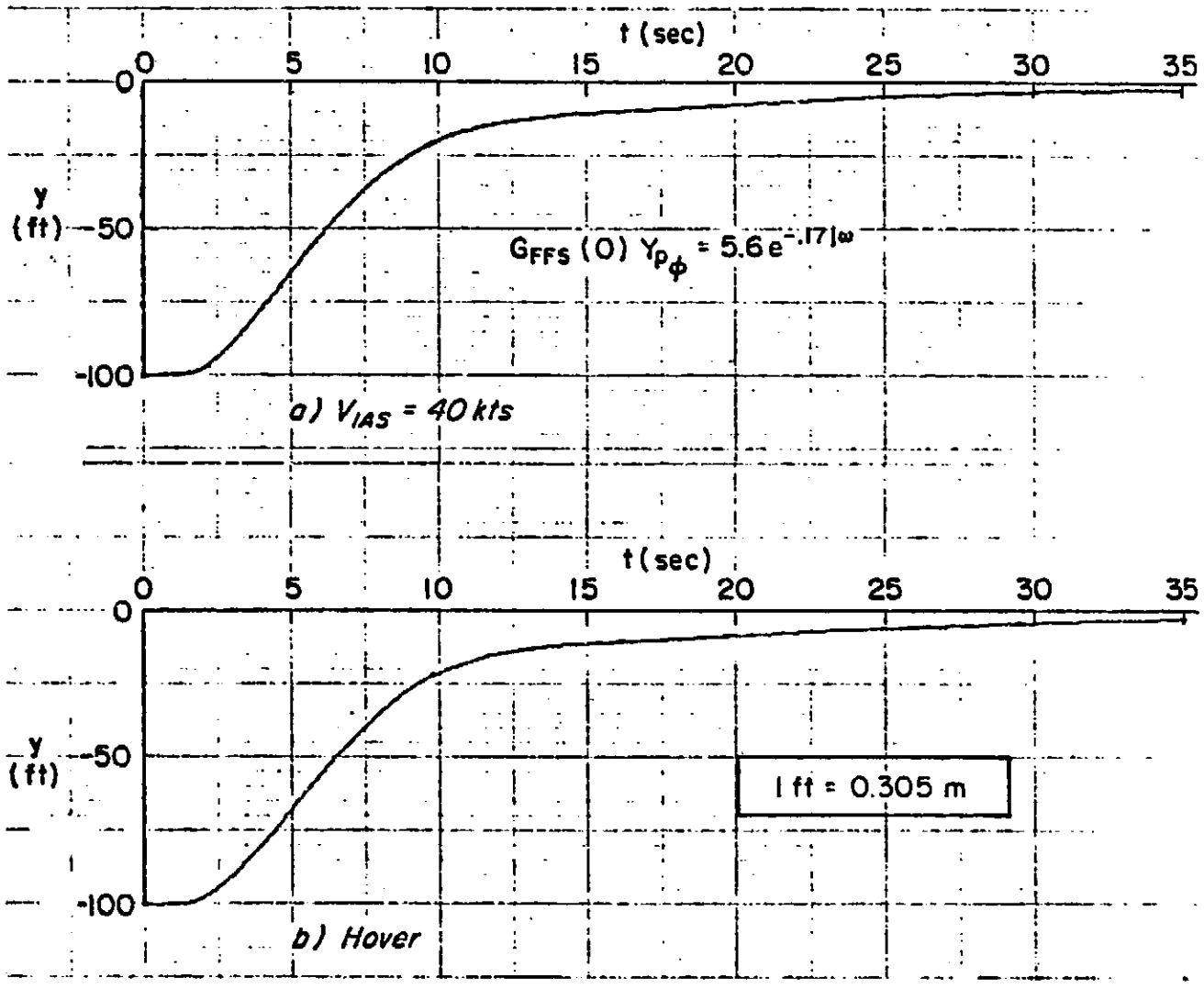

Figure 36. Lateral Beam Deviation Time Response for a 100 ft (30 m) Initial Condition Offset; Wing-Low SCAS (LOC B)

condition is given in Fig. 37a. The longitudinal cyclic required at 40 kt (21 m/s) to trim out the pitching moment due to steady sideslip (as occurs on a wing-low approach) is plotted in Fig. 37b. It is expected that these already large trim values will be still larger at hover.

The dynamic effects of $M_{|\beta|}$ were investigated briefly by examining the open-loop pitch attitude response to lateral cyclic inputs, and by examining the pitch flight director responses to lateral cyclic inputs with the pitch flight director loop closed by the pilot at 1.5 rad/sec. These results are shown in Figs. 38 and 39 respectively. Looking first at θ/δ_s it should be noted that with a rate command SCAS, the low frequency lateral cyclic activity will be extremely small. In fact we would expect that the majority of lateral cyclic activity will be concentrated in the region of crossover, say between 1 and 2 rad/sec. At $\omega = 1$ rad/sec the ratio of pitch to lateral cyclic is −32 dB or 1.4 deg (0.024 rad) of θ per inch (0.025 m) δ_s. Put another way, a roll rate command of 15 deg/sec (0.26 rad/s) will result in a 1.4 deg (0.024 rad) pitch attitude excursion in LOC B.

Assuming that the pilot is actively closing the longitudinal and lateral flight director loops at 1.5 rad/sec results in the FD_c/δ_s response shown in Fig. 39. This plot indicates that at 1 rad/sec the ratio of longitudinal cyclic flight director to lateral cyclic inputs is −14 dB, or 0.2 in. (0.005 m) of longitudinal cyclic flight director per inch (0.025 m) of lateral cyclic. This indicates that in spite of the pitch loop closure at 1.5 rad/sec the pilot will observe FD_c excursions which are 20 percent of full scale per inch (0.025 m) of lateral cyclic stick. The acceptability of these excursions can only be established in the simulator. Inasmuch as the pitch SCAS gains are already at a maximum, the only possible further refinement appears to be a crossfeed from lateral to longitudinal cyclic.

E. LIMITERS

The bank angle limit will be set to ±30 deg (±0.52 rad) until LOC B is selected. At that time it will be reduced to ±10 deg (±0.17 rad). Note that this involves setting the limits to $|\varphi_{lim}|/K_{\varphi_D}$.

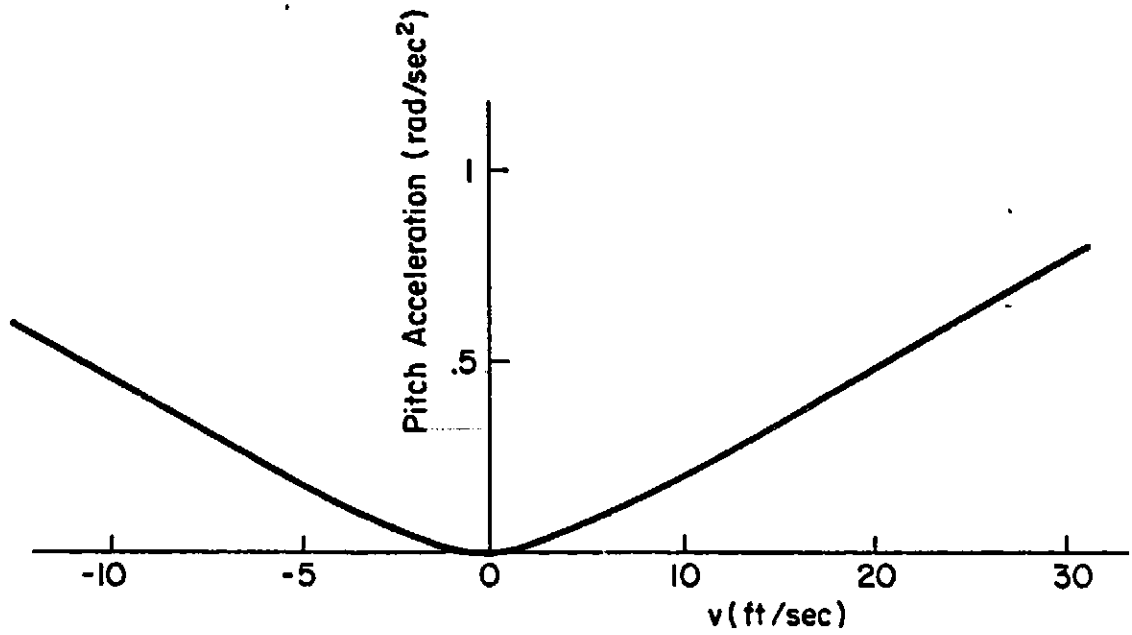

Figure 37a. Pitch Acceleration Due to Side Velocity at V = 40 kt (21 m/s)

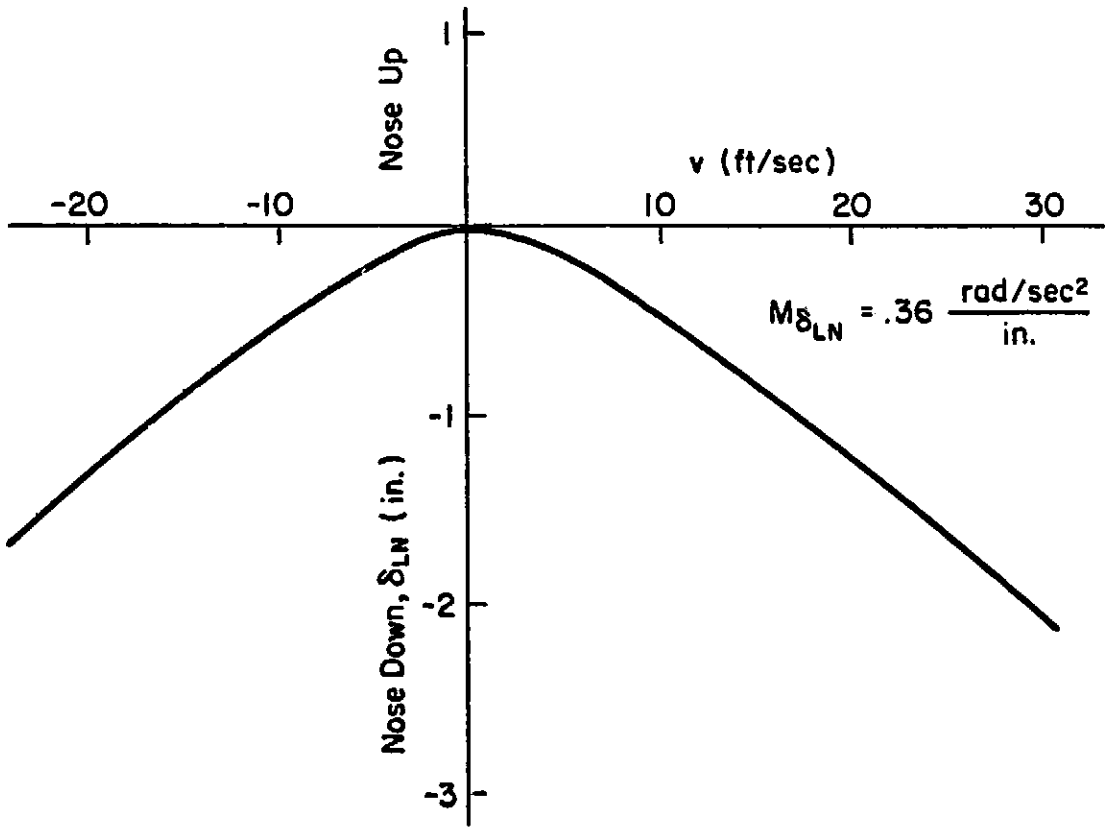

Figure 37b. Variation in Trim Longitudinal Cyclic Position with Side Velocity at V = 40 kt (21 m/s)

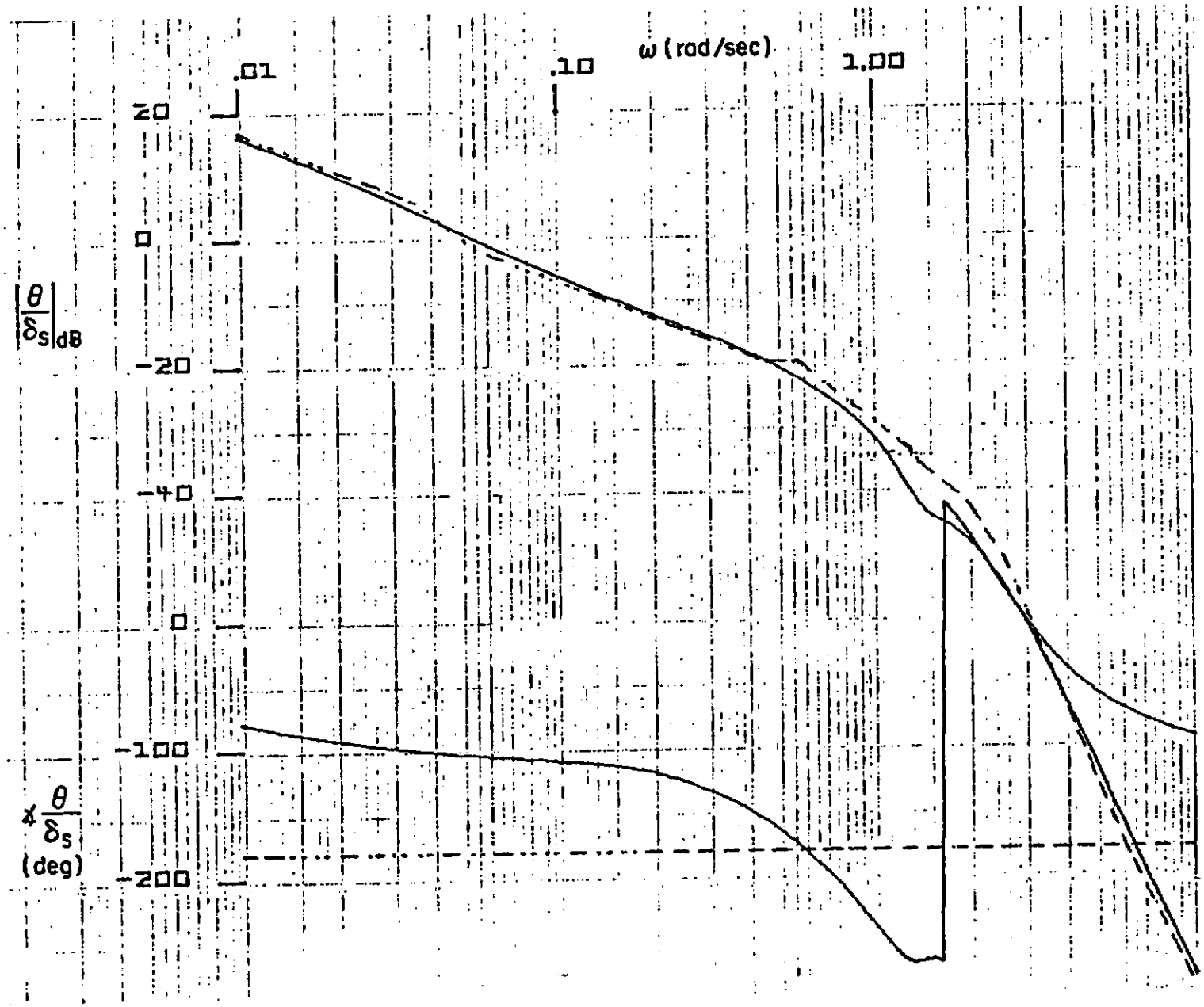

Figure 38. Frequency Response of Pitch Attitude to Lateral Cyclic Inputs; V_e = 40 kt (21 m/s)

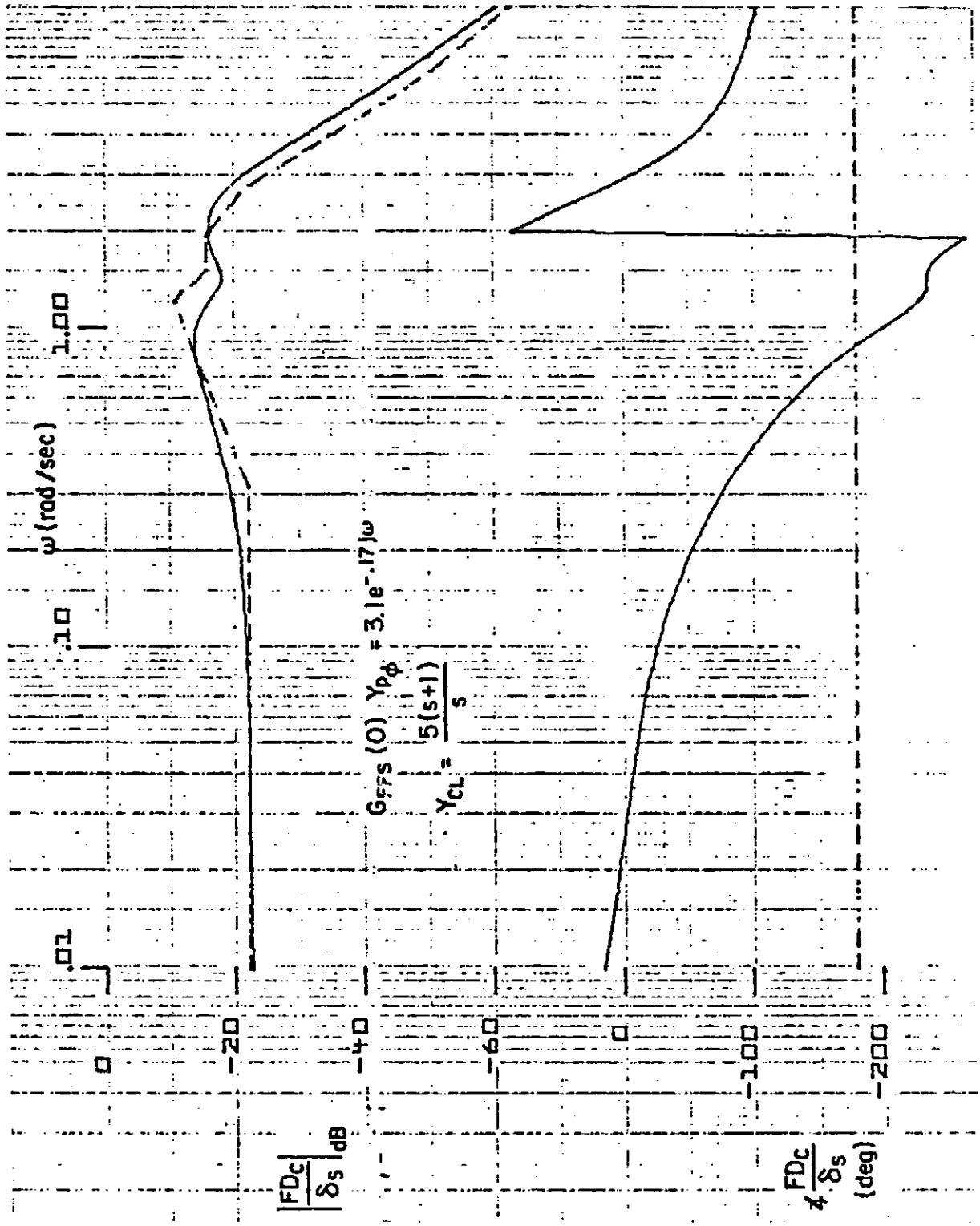

Figure 39. Closed-Loop Frequency Response of Longitudinal Cyclic Flight Director to Lateral Cyclic Inputs; V = 40 kt (21 m/s); LOC B Mode

The course rate limiter is set to preclude the possibility of commanding large bank angles rapidly. This would occur if the aircraft were significantly offset from course due to a combination of winds and pilot inattention. The limit level is set as a function of ground speed to achieve a 20 deg (0.35 rad) reintercept angle by the following method:

$$|y_{lim}| = \frac{K_{\dot{y}}}{K_y}\dot{y} = \frac{K_{\dot{y}}}{K_y} V_{GS} \sin 20^\circ \qquad \text{for } |y_{lim}| \geq 24 \text{ ft } (\geq 7.2 \text{ m}) \tag{34}$$

otherwise

$$|y_{lim}| = 24 \text{ ft } (= 7.2 \text{ m})$$

Note that initial course intercepts are made in the heading hold mode so that the $\dot{y}$ limiter will have no effect.

SECTION V

SYSTEM PERFORMANCE EVALUATION

The purpose of this section is to evaluate performance of guidance, autoland and flight director control laws described in Sections III and IV. These control laws are designed in a stationary (time invarient) system context to be suitable at several fixed speeds. The designs are also based upon perturbation equations in distinction to equations using the total quantities (perturbation + operating point) actually measured by sensors. Both approximations are removed in the system model used for performance evaluation. The remaining operative approximations then involve only assumptions of linearity and of separability of the longitudinal and lateral-directional performance evaluation problems.

Evaluation of the fully automatic and of the manually controlled flight director systems can be accomplished using the same math model. This is possible because the automatic mode control laws have been designed to automate the pilot's control function and use the same guidance and control computations as are used for the flight director. This means that the only difference between fully automatic and manual flight director operation is whether the gain constant relating flight director computer output to the force feel system input is supplied by the automatic system or by the pilot. Since this difference will not result in different performance for the fully automatic and manual flight director systems (assuming full pilot attention to the task), no distinction between these cases is necessary in evaluation. Care has been taken in generating performance data to include the variables for all flight director and status cockpit instruments indications and stick and lever positions required for complete performance evaluation.

Performance evaluation is based upon the control system block diagrams in Figs. 2 and 18 and the aircraft and disturbance models given in Appendix A. The equations and parameter values actually used are summarized in Appendix B.

A. APPROACH TO PERFORMANCE EVALUATION

The overall system model is the basis for performance evaluation. It includes parts representing

- Steady wind and wind shear
- Atmospheric turbulence
- MLS guidance geometry and structure

inputs, a dynamic model of aircraft response to the above atmospheric inputs and to control inputs obtained from dynamic models of

- Automatic system response to MLS inputs and aircraft motions or alternatively the pilot's manual control response to the flight directors
- Flight control system SCAS response to aircraft motions and inputs from the automatic system or pilot.

The overall model is such that it makes the mean value and the variance of every input and response variable available as a function of time. The model has two sections, namely:

- A deterministic section which produces the mean value of every input and response variable
- A stochastic section which produces the covariance matrix for the input and response variables. (The diagonal elements of the covariance matrix are the variances or mean square or σ^2 values of the input and response variables. σ is the standard deviation.)

Next consider these two sections of the complete model.

1. Deterministic Section of the Model

The deterministic section for the overall longitudinal system is described by the block diagram in Fig. 40. The block diagram for lateral system is similar. The mean values of variables are denoted by the bars over the variables in this figure. The block diagram indicates that the mean values of the aircraft, flight control system SCAS and coupler response are obtained as the result of forcing the model with the mean wind, $\bar{u}_w$, and the mean glide path,

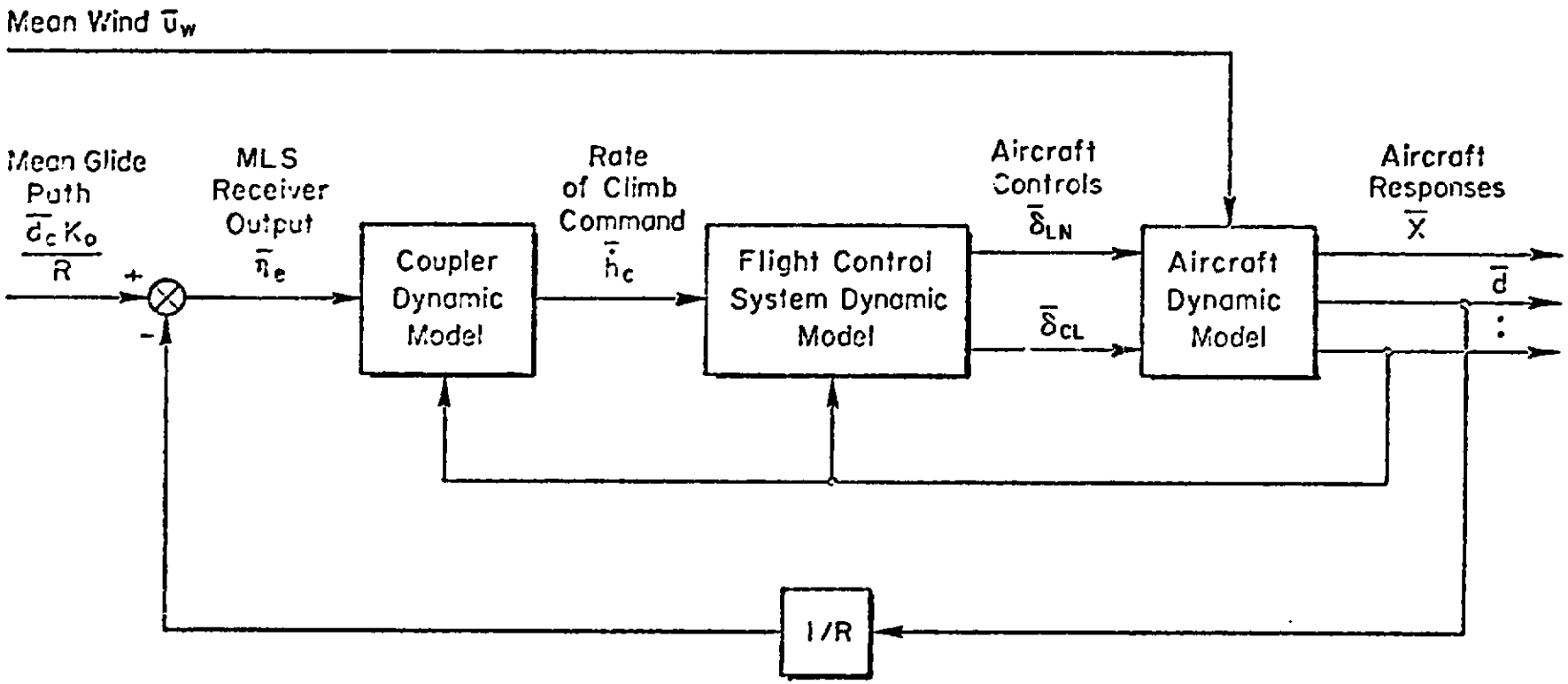

Figure 40. Block Diagram of the Deterministic Section of the Complete Longitudinal Model

$\bar{d}_c$. The level of the mean wind, $\bar{u}_w$, is the average headwind magnitude with respect to active runway landing direction.

The models in the blocks of Fig. 40 are the dynamic equations describing the particular subsystem. For example, the longitudinal aircraft equations of motion are the aircraft dynamic model, and so on, for the approach coupler, pilot's manual control and flight control system SCAS dynamic models. The complete details of the models actually used (for the MLS wind, wind shear and turbulence environment; the aircraft; approach couplers and flight control systems) are given in Appendices A and B.

The model shown in Fig. 40 will not be linear in general. However, between capture completion and touchdown an approximate linearized model of the complete system has been shown to be accurate (Ref. 15).

2. Stochastic Section of the Model

The stochastic section of the model for the overall longitudinal system is described by the block diagram in Fig. 41. The block diagram for lateral system is similar. Here the variances of the variables are denoted by $\sigma^2_{()}$ with the particular variable designated by the subscript. The dynamic models of the aircraft, flight control system, SCAS and approach coupler in Fig. 41 blocks are different from, but are closely related to the corresponding blocks of Fig. 40.

3. Mathematical Basis for System Performance Evaluation

Between capture completion and touchdown the dynamic models in the blocks of Fig. 40 can be described by linear differential equations. It can be shown that the time histories for the atmospheric and MLS inputs can also be described by linear differential equations (operating upon white noise). When this is the case, the entire system model can be written in the form of a first-order vector differential (state) equation and a vector algebraic equation. The specific equations are given in Appendix B for the longitudinal and lateral-directional systems. These are of the form

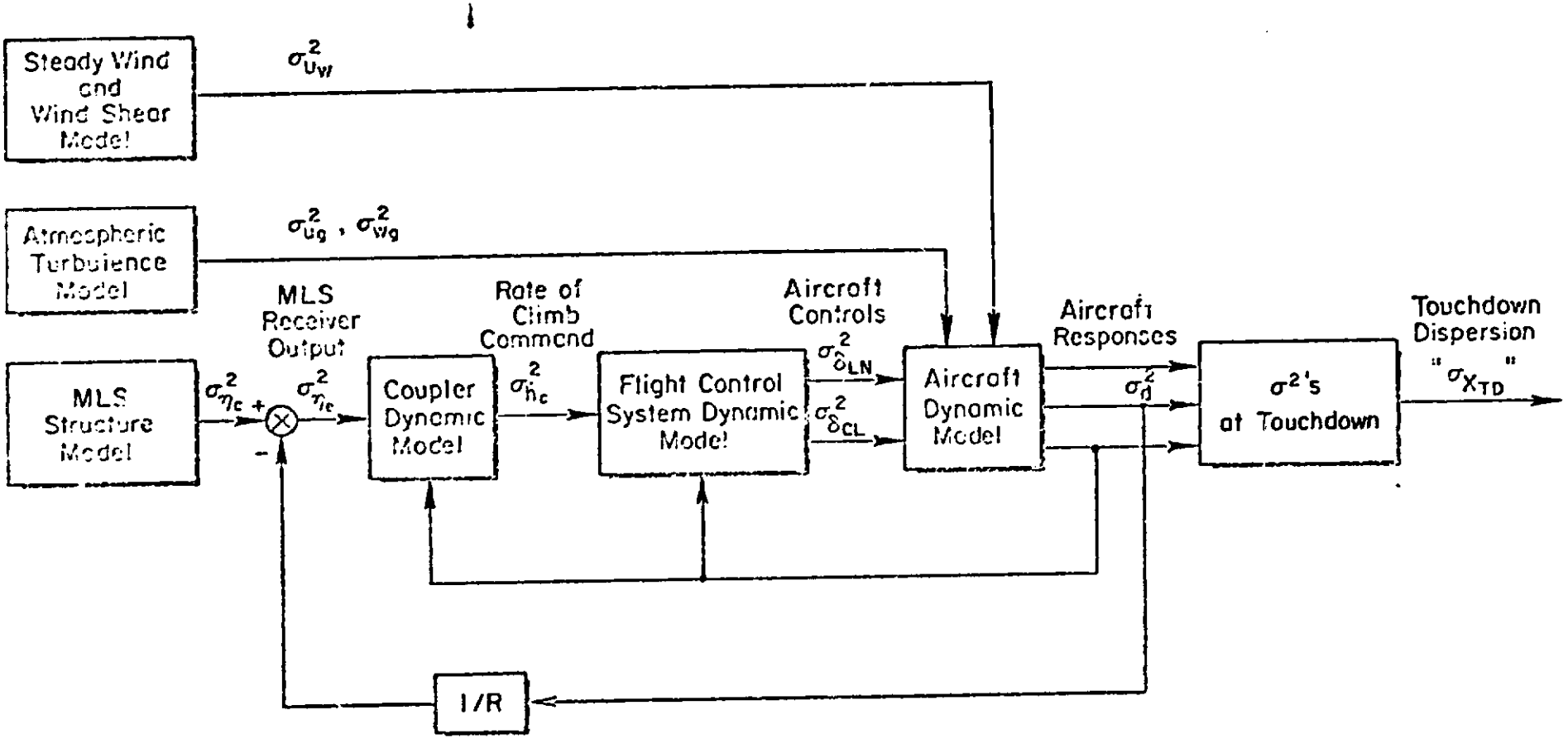

Figure 31. Block Diagram of the Stochastic Section of the Complete Longitudinal Model

$$\dot{x} = A(t)x + b(t) + w(t) \quad , \quad x(0) = x_o \tag{35}$$

$$y = H(t)x + g(t) \tag{36}$$

where $b(t)$ and $g(t)$ are deterministic input vectors, $w(t)$ is a vector of independent white noise processes with zero means. If we let $E[\cdot]$ denote the expected value of $[\cdot]$, then define the mean or expected value for x as $\bar{x}$, the differential and algebraic equations for the mean values are

$$\dot{\bar{x}} = A(t)\bar{x} + b(t) \quad , \quad \dot{\bar{x}}(0) = \bar{x}_o \tag{37}*$$

$$\bar{y} = H(t)\bar{x} + g(t) \tag{38}$$

given that $E[w] = 0$. The covariance matrix for x, $E[x(t)x'(t)]$, is C. The differential equations for the covariance matrix are (e.g., Ref. 16):

$$\dot{C} = A(t)C + CA'(t) + Q(t) \quad , \quad C(0) = C_o \tag{39}*$$

where $E[w(t)w'(t + \tau)] = Q(t)\delta(\tau)$. The covariance for the output, $E[y(t)y'(t)]$, is D.

$$D = H(t)CH'(t) \tag{40}$$

Now the importance of Eqs. 37 through 40 derives from the fact that $\bar{x}(t)$ and $C(t)$ completely determine the joint probability density function for $x(t)$ as a function of time. Namely:

*Discretized versions of Eqs. 37 and 39 are used in actual computation. The propagation interval used for the discretized equations is 2 sec.

$$\rho(x_1, \ldots x_n, t) = \frac{\exp[-(1/2)(x - \bar{x})' C^{-1}(x - \bar{x})]}{(2\pi)^{n/2}\sqrt{|C|}} \qquad (41)$$

where $\rho(x_1, \ldots x_n, t)$ denotes the n-dimensional joint Gaussian probability density function for x(t). $\bar{y}(t)$ and D(t) similarly define the joint probability density function for y(t). And, of course, x_1, x_2, ... and y_1, y_2, ... can be used to represent <u>all</u> system variables in the problem of interest. The above equation for $\dot{C}$ (Eq. 39) and the last equation for D (Eq. 40) constitute the stochastic section for the complete model shown in Fig. 41. This model is "closely related" to the one in Fig. 40 in that the same parameter matrices (which represent aircraft stability deriviatives, flight control system, SCAS and approach coupler gains, etc.) A(t), b(t), g(t) and H(t) characterize the equations for $\dot{x}$ and y as well as the equations for $\dot{C}$ and D.

Since the probability density function in Eq. 41 is Gaussian, the longitudinal touchdown dispersion $\sigma_{X_{TD}}$ is:

$$\sigma_{X_{TD}} = \left[\sigma_X \sqrt{1 - \rho_{XH}^2}\right]_{\bar{H}=0} \qquad (42)$$

ρ_{XH} is the correlation coefficient for ground range, X, and altitude, H, and σ_X is the standard deviation for X.

4. Results

Performance evaluation results and interpretations are presented in this subsection. Table 9 is a guide to these results. The system mode designations are given in terms of shorthand and code designations in Table 10. Results are in terms of time histories for the approach ensemble means and standard deviations of key variables. The noise and disturbance environment used to produce these results is summarized in Fig. 42. The disturbance environment includes a mean headwind profile (UW) which is a function of altitude to simulate wind shear. Also included are variable headwind (SUW) and crosswind (SVW) component

TABLE 9

GUIDE TO PERFORMANCE EVALUATION RESULTS

CASE	CONDITIONS		FIGURE NUMBER
Disturbance Environment	Mean and Standard Deviation	Deterministic and Stochastic Disturbances	42
Longitudinal	Mean	γ_o = −6 deg*	43
Longitudinal	Standard Deviation	γ_o = −6 deg	44
Longitudinal	Mean	γ_o = −10 deg	45
Longitudinal, Vertical Descent	Expanded Scale Mean and Standard Deviation	γ_o = −90 deg	46
Lateral-Directional	Standard Deviation	VTOL pad	47
Lateral-Directional	Standard Deviation	CTOL runway	48

*1 deg = 1.745×10^{-2} rad.

TABLE 10. CONTROL SYSTEM MODE CODE

LONGITUDINAL SYSTEM MODE	LSW CODE
Airspeed hold, Glide slope track (AS, GS)	1, 2
Deceleration initialization, Glide slope track (DECL I, GS)	3
Deceleration, Glide slope track (DECL, GS)	4
Point hover, Glide slope track (HOV, GS)	5
Point hover, Altitude hold (HOV, ALT)	6
Point hover, Vertical descent (HOV, VD)	7

LATERAL-DIRECTIONAL SYSTEM MODE	SA CODE
Localizer track, turn following (LOC A)	1
Localizer track, wing low (LOC B)	0

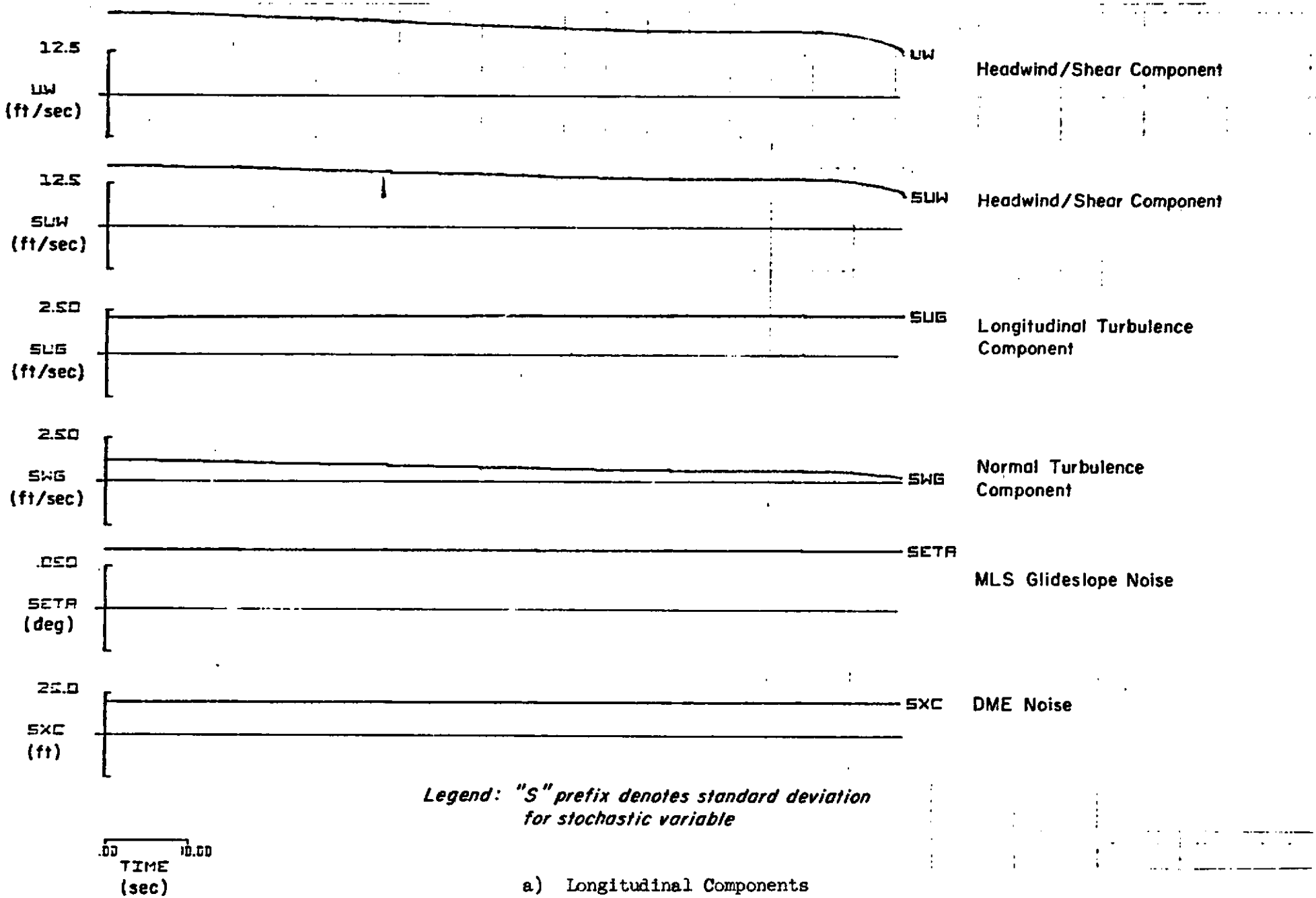

a) Longitudinal Components

Figure 42. Noise and Disturbance Environment Characteristics (γ_o = −6 deg)

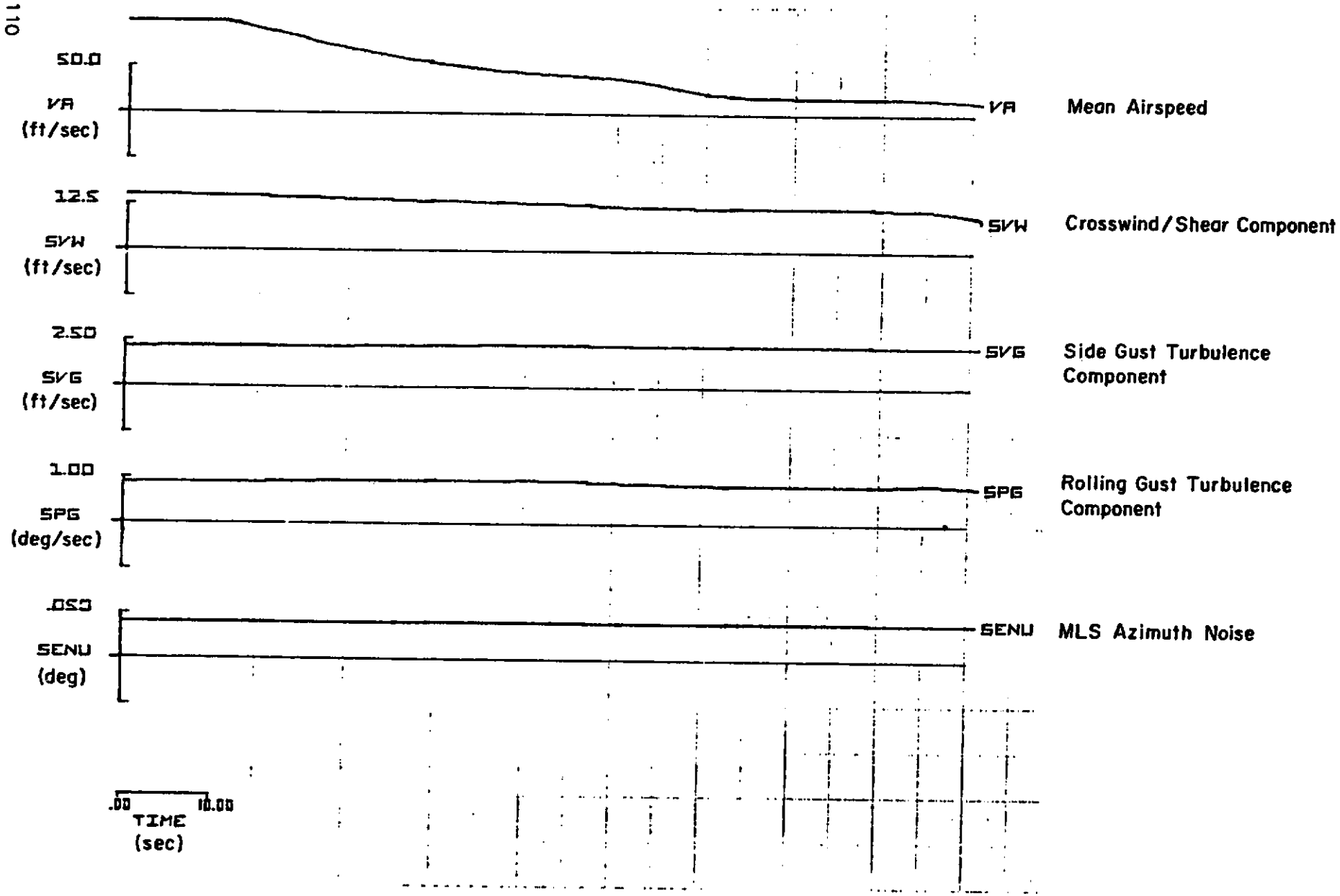

b) Lateral-Directional Components

Figure 42. (Concluded)

profiles. These components are also functions of altitude to simulate wind shear and have levels which are random variables from one approach to the next, but are constant during any one approach. Fifty percent-probability-of-exceedence turbulence is used. Selection of the 50 percent level was arbitrary, even though representing a typical level in operation. (Larger levels might result in significant series servo limiting.) Longitudinal (SUG), normal (SWG), side (SVG) and effective rolling (SPG) components are included. The levels and integral scale lengths are functions of altitude and airspeed in the manner of the Dryden turbulence model. MLS noise is modeled on the basis of the so-called path-following error budget described in Ref. 17. MLS glide slope (SETA), azimuth (SENU) and DME (SXC) components are included.

Longitudinal and lateral-directional response plots have been grouped by area of interest for Figs. 43-45, 47 and 48. These areas of interest are

Part a: Trajectory variables
- — Longitudinal: HD, ALTH, X, XD
- — Lateral-Directional: PHI, PSI, YD, Y

Part b: Cockpit indications
- — Longitudinal: LSW, VA, XD, XIND, ALTH, DE, HD, THET, DC, FDC, DCL, FDCL
- — Lateral-Directional: SA, YE, PSI, R, PHI, AYP, DS, FDL, FDP

Part c: Pilot acceptance variables
- — Longitudinal: Q, THEE, AZP, AX, VAE
- — Lateral-Directional: P, PHI, R, AYP

Part d: Limited variables
- — Longitudinal: THCD, FDC, DLN, DLNS, SR, DEH, FDCL, DCL
- — Lateral-Directional: PHDC, FDL, DLAT, DLTS, DPDS

The criteria for pilot acceptability are limits upon variability about the mean responses. These limits are listed in Table 11. These limits are generally accepted in the industry. Some have been stated in FAA Advisory Circulars or in ICAO Annex 10. In part c of the standard deviation response figures, these limits are shown by J-shaped brackets.

Variables which are limited by device constraints or by actual limiter functions have their limiting values listed in Table 12. These limiting values

TABLE 11. PILOT ACCEPTANCE LIMITS FOR FINAL APPROACH

Attitude Deviation

$\sigma_\theta, \sigma_\varphi \leq 2$ deg*

Attitude Rates

$\sigma_p, \sigma_q, \sigma_r \leq 2$ deg/sec

Linear Acceleration Deviation

$\sigma_{n_z} \leq 0.1$ g

$\sigma_{n_x}, \sigma_{n_y} \leq 0.05$ g

Airspeed Deviation (during airspeed hold)

$\sigma_{uAS} \leq 5$ kt†

TABLE 12. SUMMARY OF SYSTEM LIMIT LEVELS

VARIABLE	LIMIT LEVEL
Pitch Attitude Command Limit	±10 deg
Flight Director Longitudinal Cyclic Command Bar	±1 in.‡
Longitudinal Cyclic Pitch Deflection (Stick Units)	±4.8 in.
Longitudinal Cyclic Series Servo Deflection	±1 in.
Sink Rate Command	±8.33 ft /sec
Beam Rate Command	±44.1 ft/sec
Flight Director Collective Command Bar	±1 in.
Collective Pitch Deflection (Lever Units)	+1.78, +6.0 in.
Bank Angle Command	±30 deg (LOC A)
Flight Director Lateral Cyclic Command Bar	±1 in.
Lateral Cyclic Pitch Deflection (Stick Units)	±4.8 in.
Lateral Cyclic Series Servo Deflection	±1 in.
Rudder Series Servo Deflection	±1 in.

*1 deg = 1.745×10^{-2} rad.
†1 kt = 5.144×10^{-1} m/s.

‡1 in. = 2.54×10^{-2} m.
1 ft = 3.048×10^{-1} m.

are represented by C-shaped brackets on the part d mean response plots and by F-shaped brackets on the part d standard deviation response plots. The upper horizontal stroke of the "F" represents the limiting value; the middle stroke of the "F" represents the limiting value less the absolute value of the mean response. The interpretation to be made is as follows: If the standard deviation for a variable is less than one-half the distance between the base of the "F" and the middle horizontal stroke, then the probability of encountering the operative limit is less than 5 percent; if less than one-third the distance; less than 0.26 percent; if less than the distance itself, less than 32 percent; etc. In the case of the lateral-directional variables, the middle and upper horizontal strokes of the "F" coincide because the mean response for all lateral-directional variables is zero.

5. Interpretation of Results

a. Response Means for Longitudinal Variables

The response means may be interpreted either as the mean responses in the stochastic disturbance environment or as the deterministic responses in the absences of all disturbances except the mean headwind/shear (UW).

These responses (Figs. 43 and 45) show well-controlled glide slope tracking during the airspeed hold, constant attitude deceleration and point hover phases of the final approach for approach path angles of −6 and −10 deg (−0.10 and −0.17 rad). The aircraft continues to be well-controlled in the point hover mode through the transition from glide slope track to altitude hold at 50 ft (15 m) and during the exponential flare, vertical descent to touchdown. Figure 46 gives the key responses on expanded scales for the vertical descent maneuver.

Transient responses at initiation of the constant attitude deceleration and point hover phase are only very slightly different for the −6 and −10 deg (−0.10 and −0.17 rad) approach paths. This lack of sensitivity to approach path angle is desirable. It is the result of the particular switching logic used.

Initiation of the constant attitude deceleration maneuver results in modest "ballooning" above the glide path (refer to DE trace) because there

is no crossfeed of the pitch-up deceleration command to the cyclic pitch control. A crossfeed is deemed unnecessary because the peak glide slope deviation is only 5 ft (1.5 m) at a ground range (X) of 2000 ft (610 m) from the hover point.

Longitudinal (AX) and normal (AZP) accelerations encountered during deceleration and vertical descent phases are moderate. The longitudinal cyclic stick (DC) and collective pitch lever (DCL) deflections required are well within the available limits. The longitudinal series servo deflection (DLNS) required is well within the available authority.

b. Response Standard Deviations for Longitudinal Variables

Standard deviation responses are shown in Fig. 44 and on expanded scales for vertical descent in Fig. 46. The plots are for a −6 deg (−0.10 rad) approach path. Plots for other approach path angles are indistinguishable from the −6 deg (−0.10 rad) plots except for a slight stretching or shrinking of the time axis. There is virtually no dependence of the vertical descent results on approach path angle.

The standard deviation responses show low variability in all trajectory variables and cockpit indications with the exceptions discussed below. Variability in altitude (SALT) and ground range (SX) grow large during the constant airspeed and constant attitude deceleration phases of the approach. This is the (random walk) effect of the headwind (SUW) variability in producing along-path variations in aircraft position for a given time into the approach. This results because slant range is uncontrolled by this system. This along-path or slant-range component of variability is reduced to zero at t = 54.5 sec by a mathematical procedure. It must be emphasized that this procedure is actually part of the system model; it is not an arbitrary feature. Its purpose is to avoid introducing a fictitious slant-range dependency into the hover approach phase performance statistics. Airspeed (SVA) variability becomes large following the airspeed hold phase of the approach. This occurs because speed regulation ceases during the constant attitude deceleration phase and because ground speed is regulated during the subsequent hover phase. Pitch attitude (STHET) variability tends to increase transiently during initiation of the constant attitude deceleration and hover phases. The generally larger pitch attitude

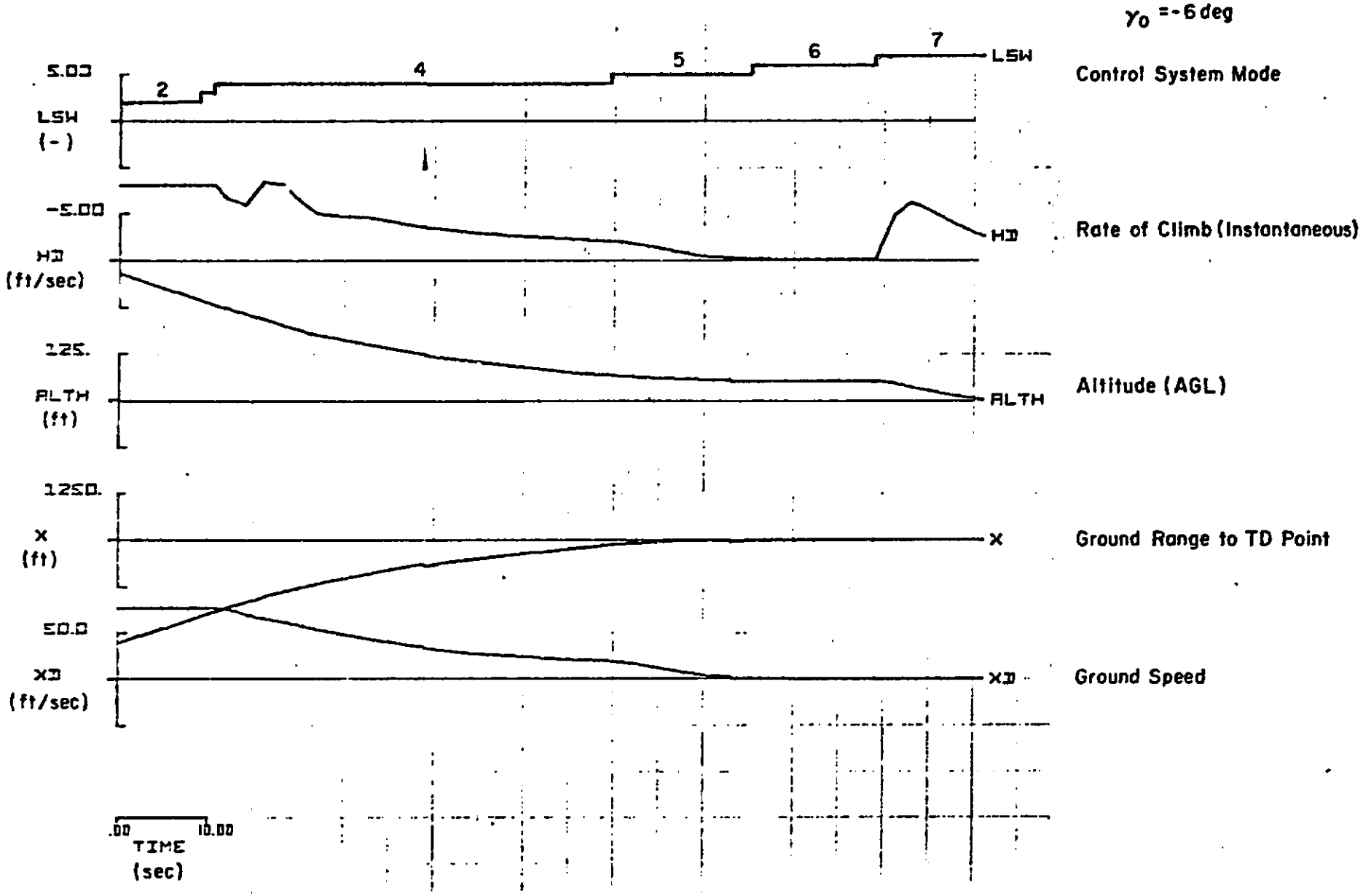

a) Longitudinal Trajectory

Figure 43. Mean Responses for Longitudinal System on -6° Approach from 340' Through Touchdown

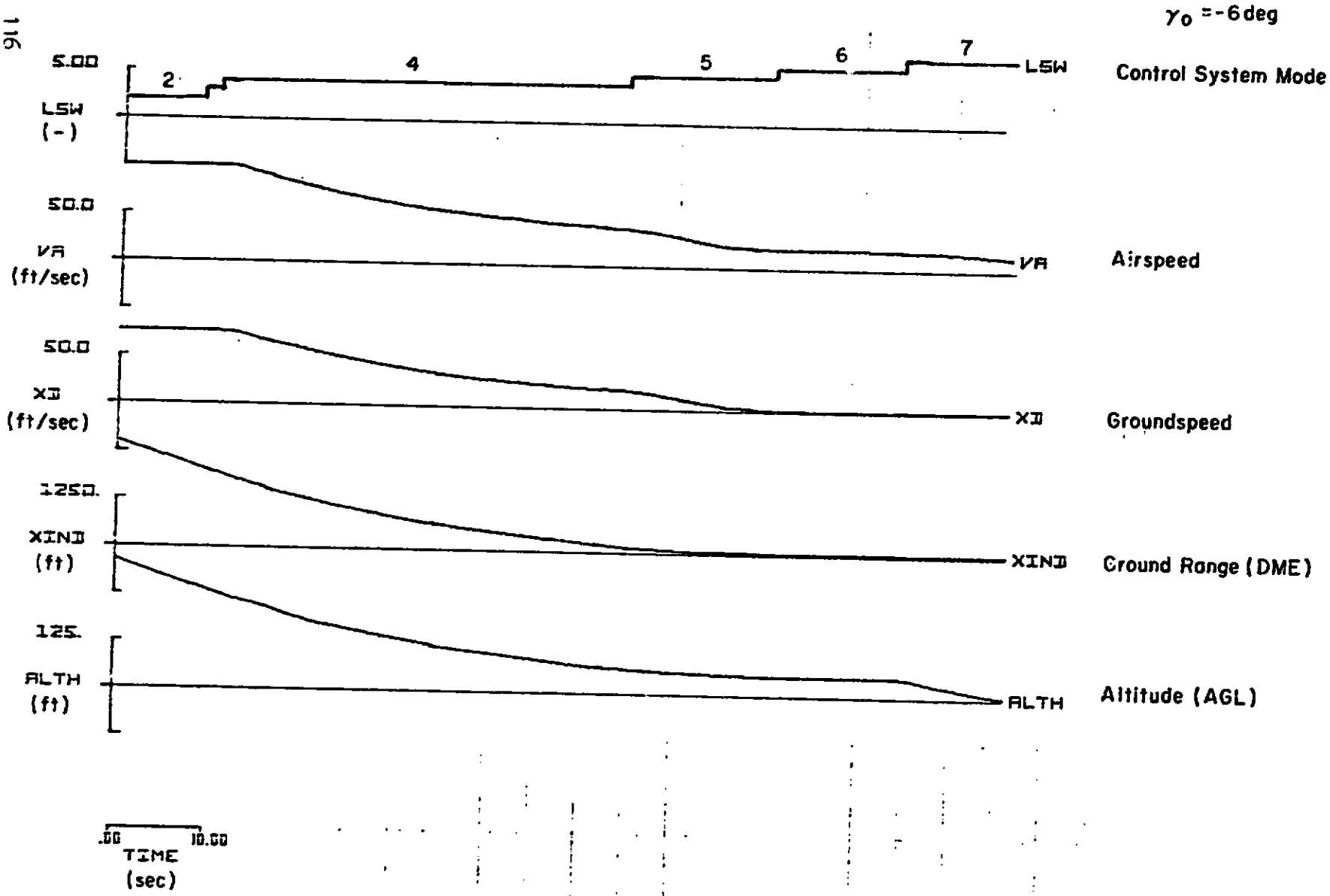

b) Longitudinal Cockpit Indications (i)

Figure 43. (Continued)

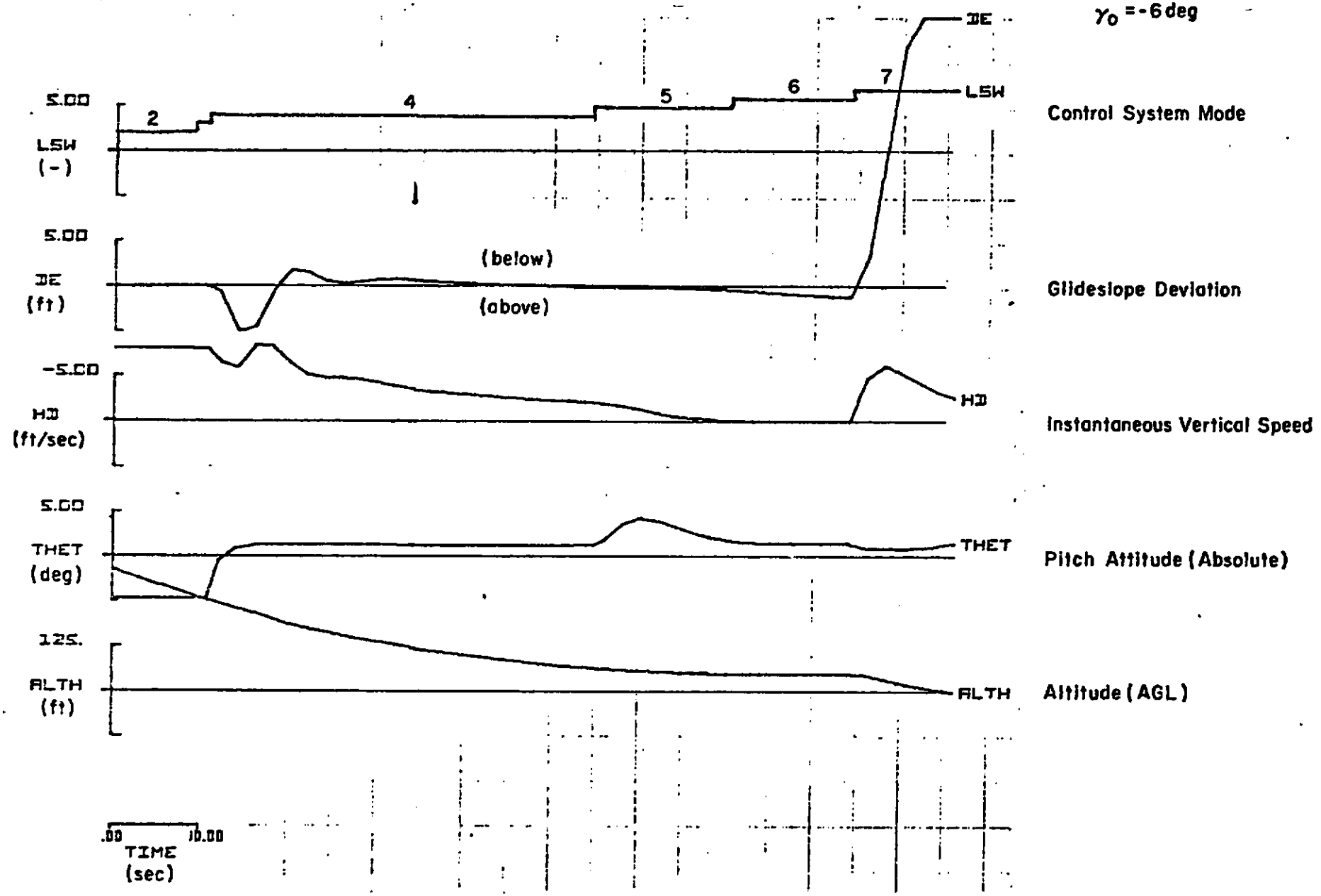

b) Longitudinal Cockpit Indications (ii)

Figure 43. (Continued)

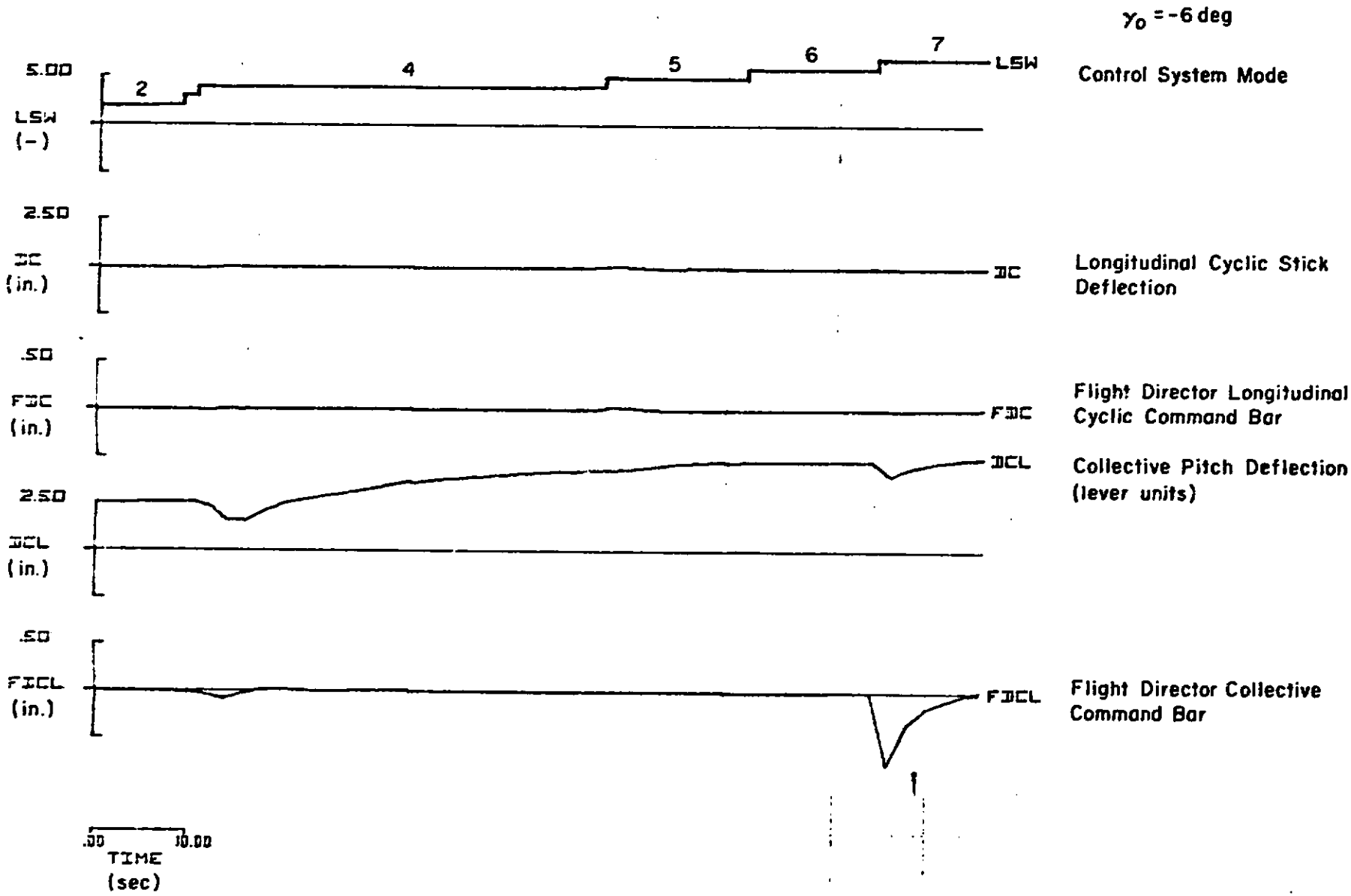

b) Longitudinal Cockpit Indications (iii)

Figure 43. (Continued)

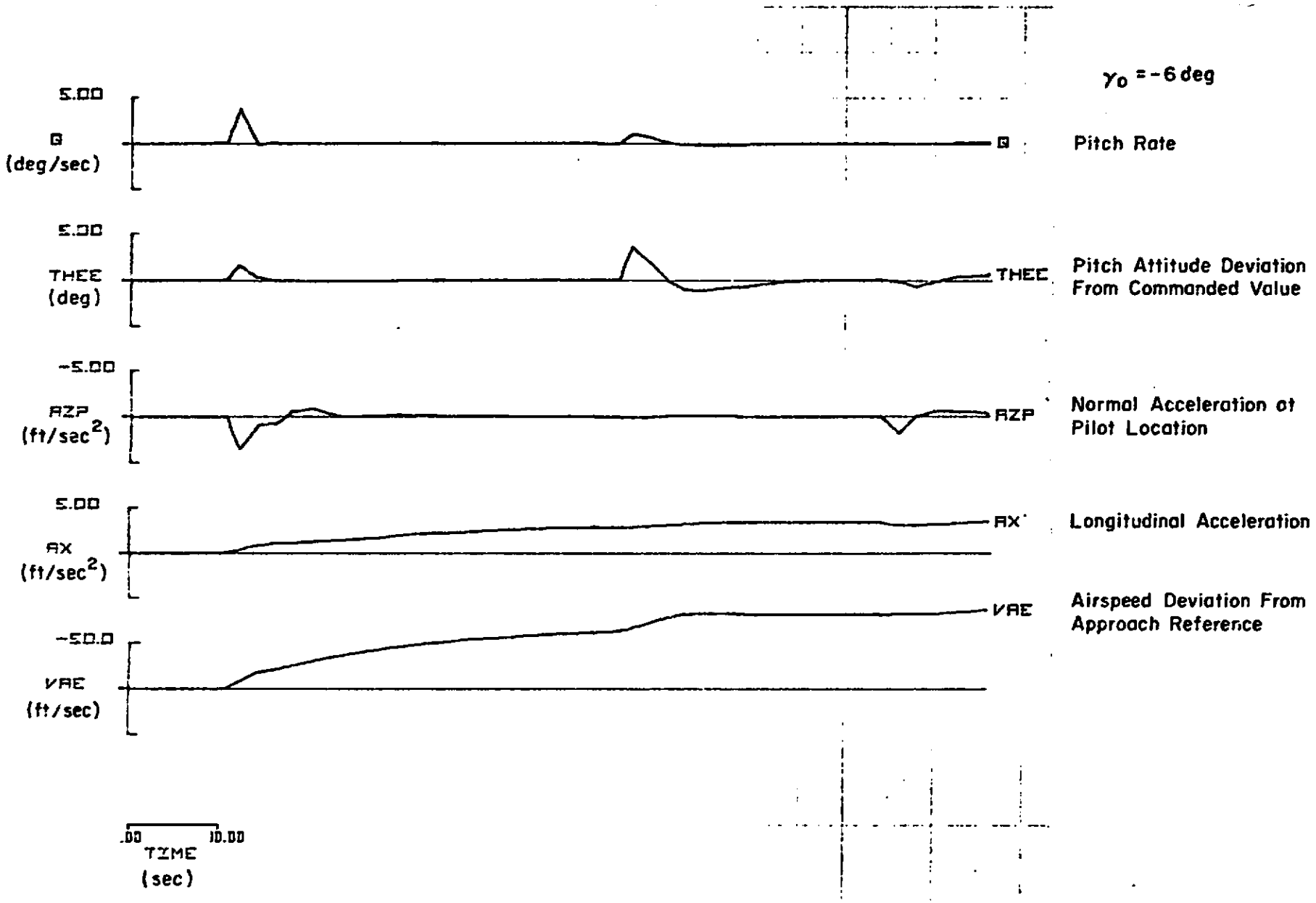

c) Longitudinal Pilot Acceptance Variables

Figure 43. (Continued)

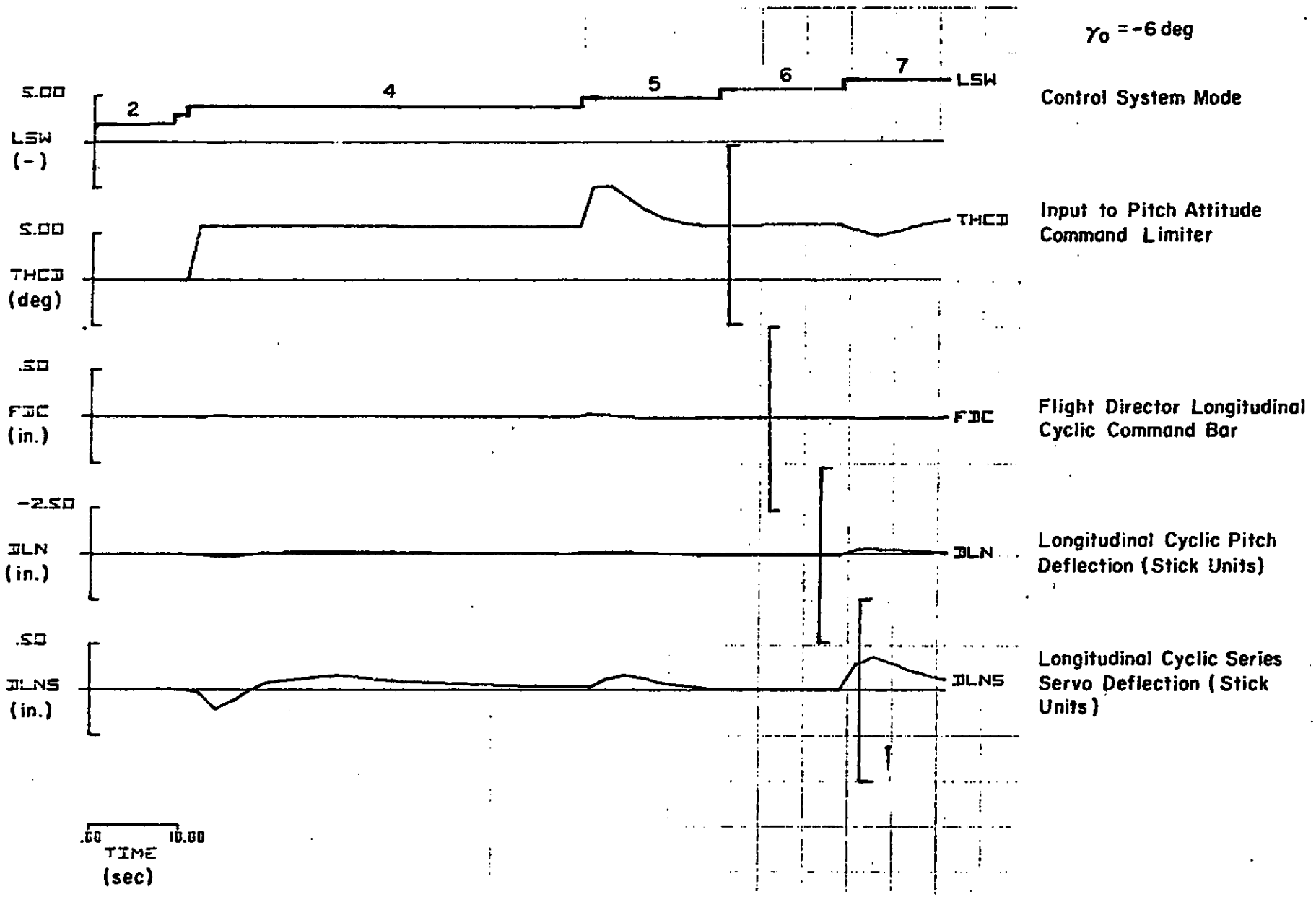

d) Longitudinal Limits (i)

Figure 43. (Continued)

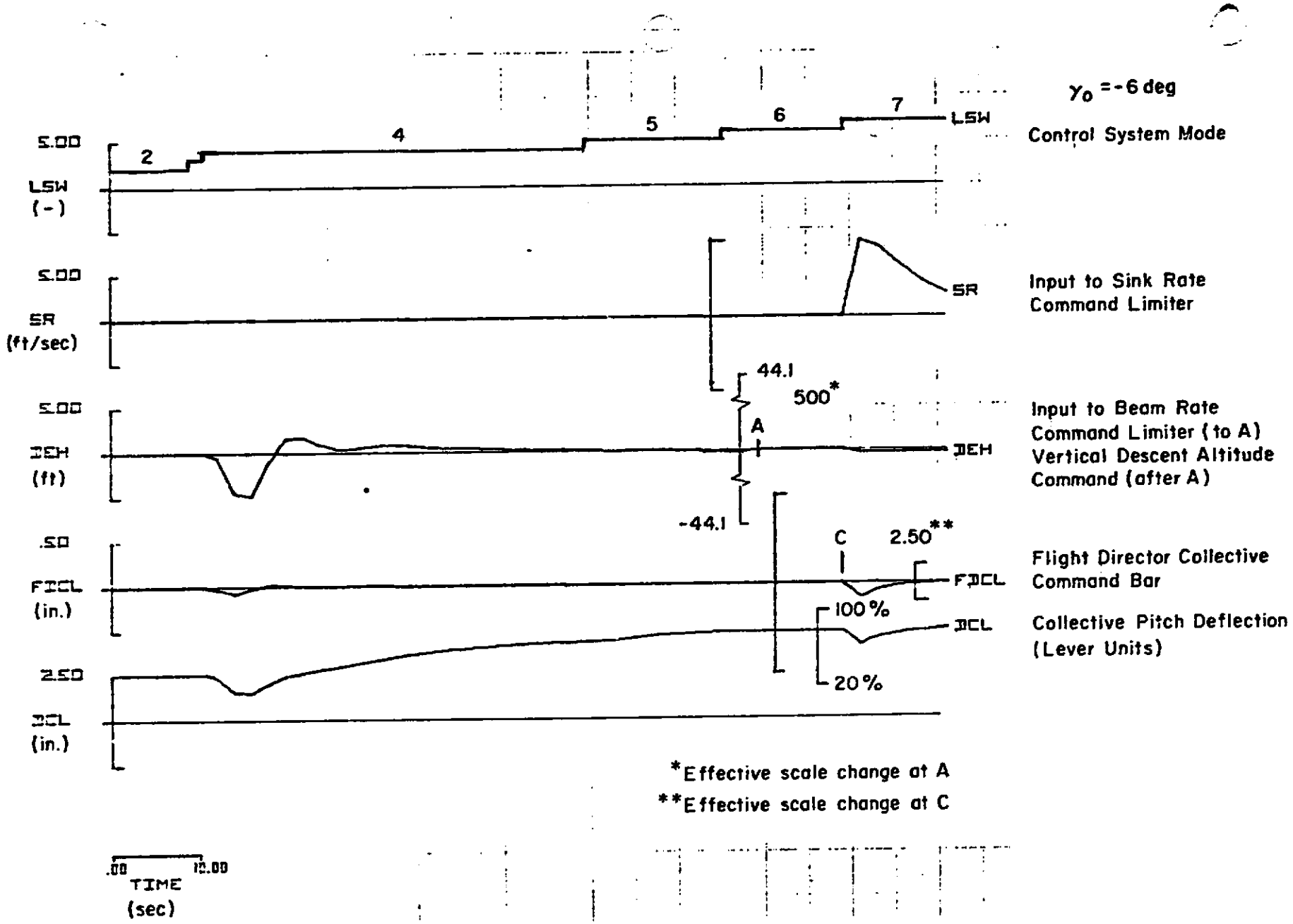

d) Longitudinal Limits (11)

Figure 43. (Concluded)

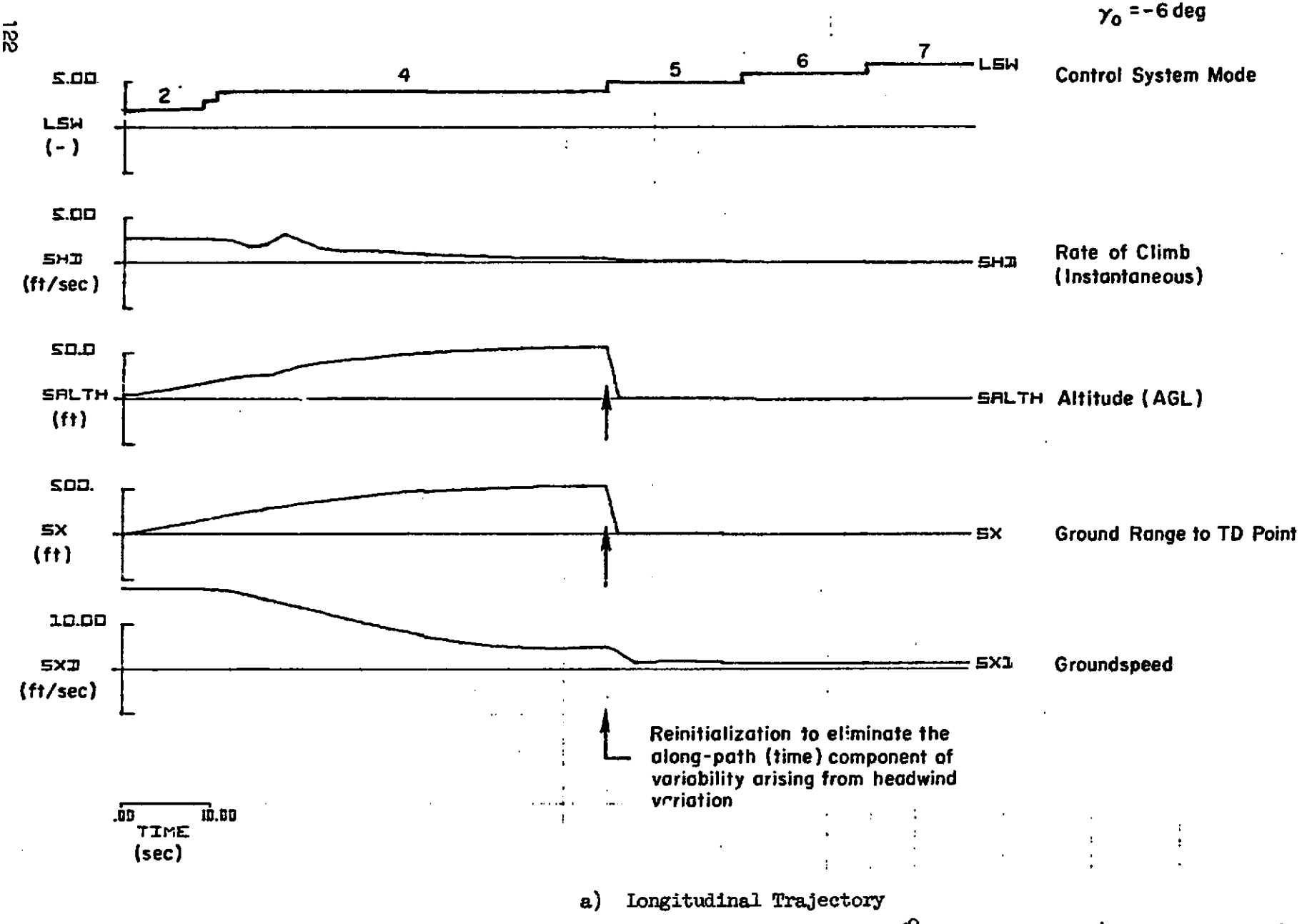

a) Longitudinal Trajectory

Figure 44. Standard Deviation Responses for Longitudinal System on -6° Approach from 340' Through Touchdown

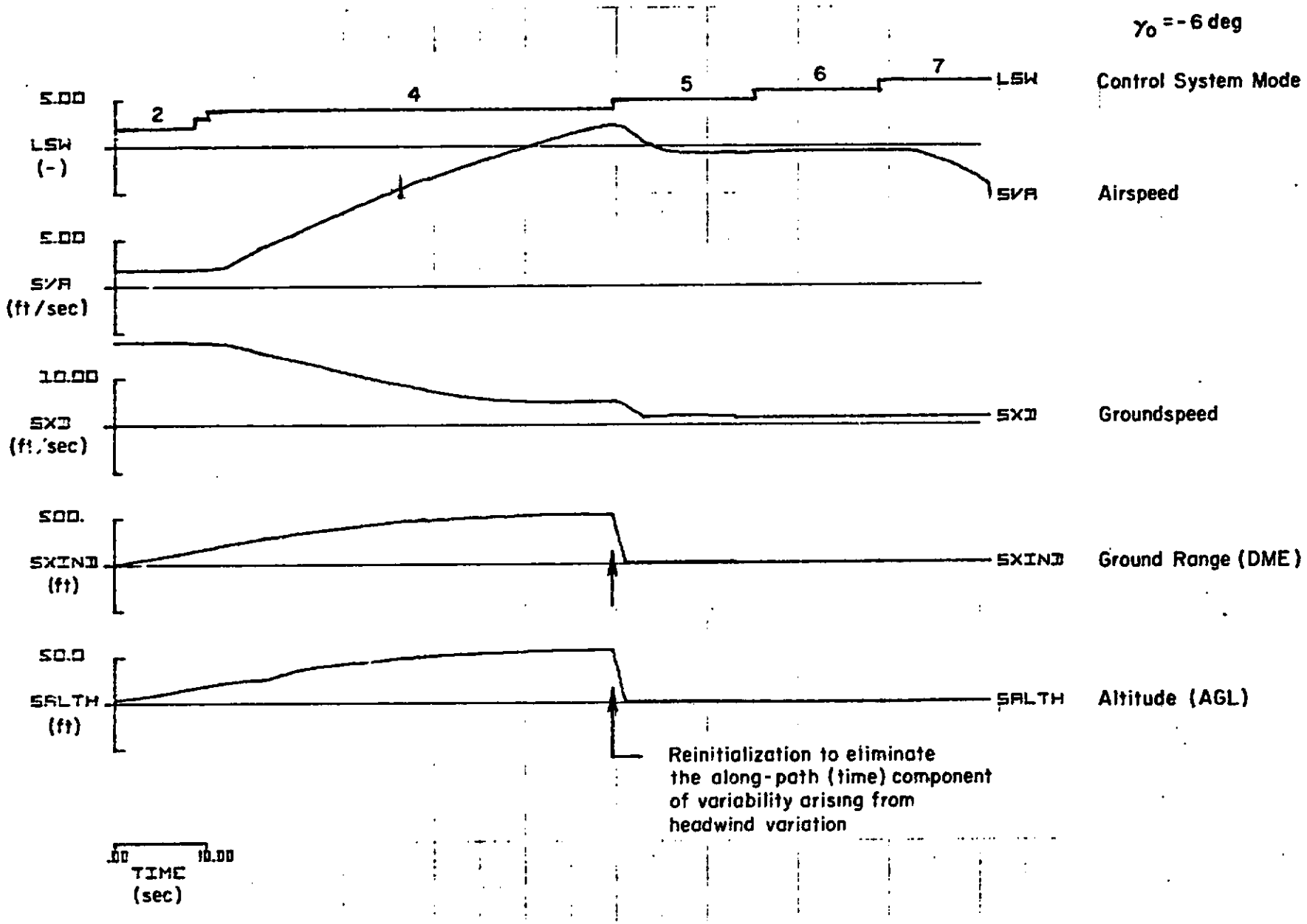

b) Longitudinal Cockpit Indications (i)

Figure 44. (Continued)

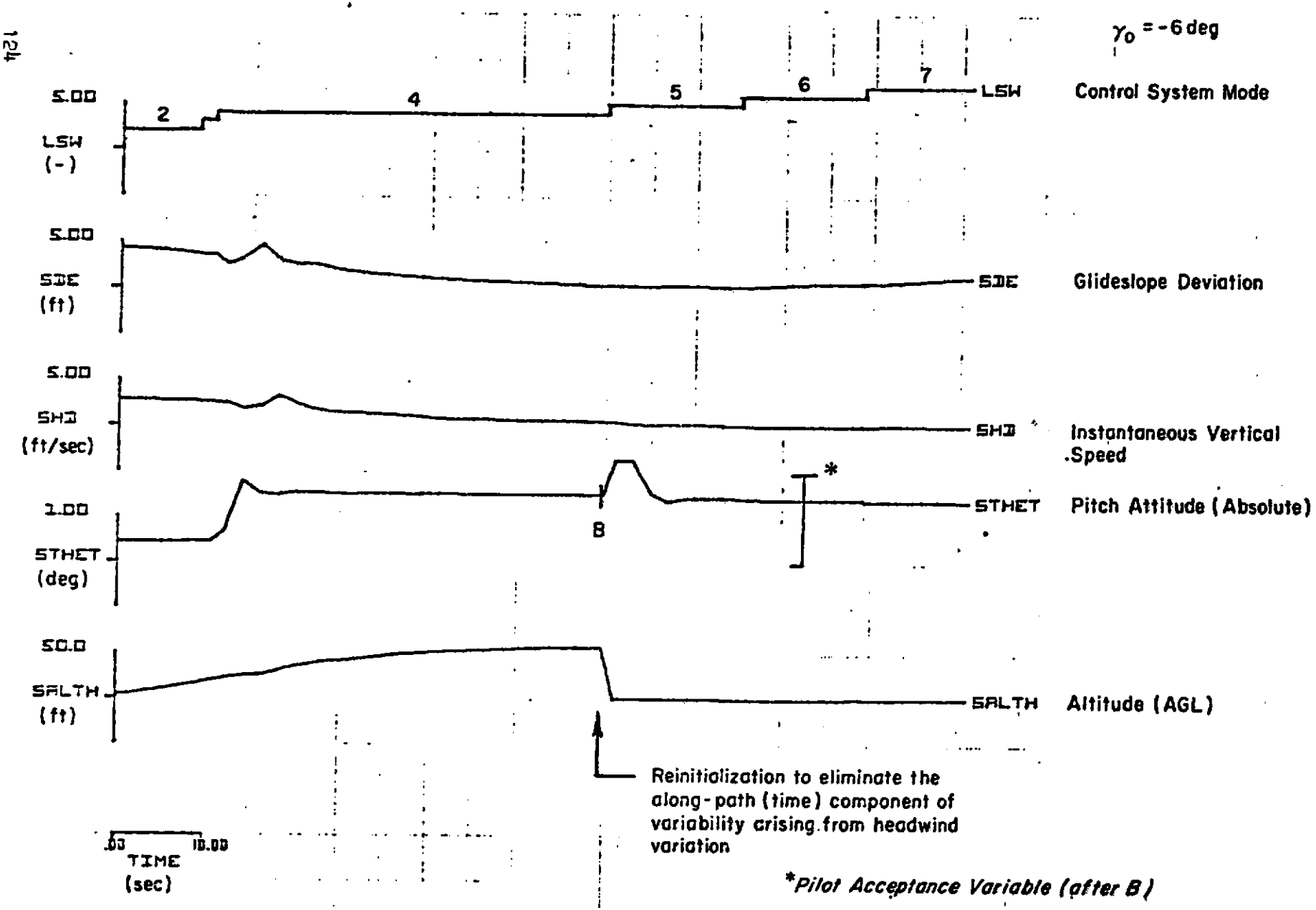

b) Longitudinal Cockpit Indications (ii)

Figure . (Continued)

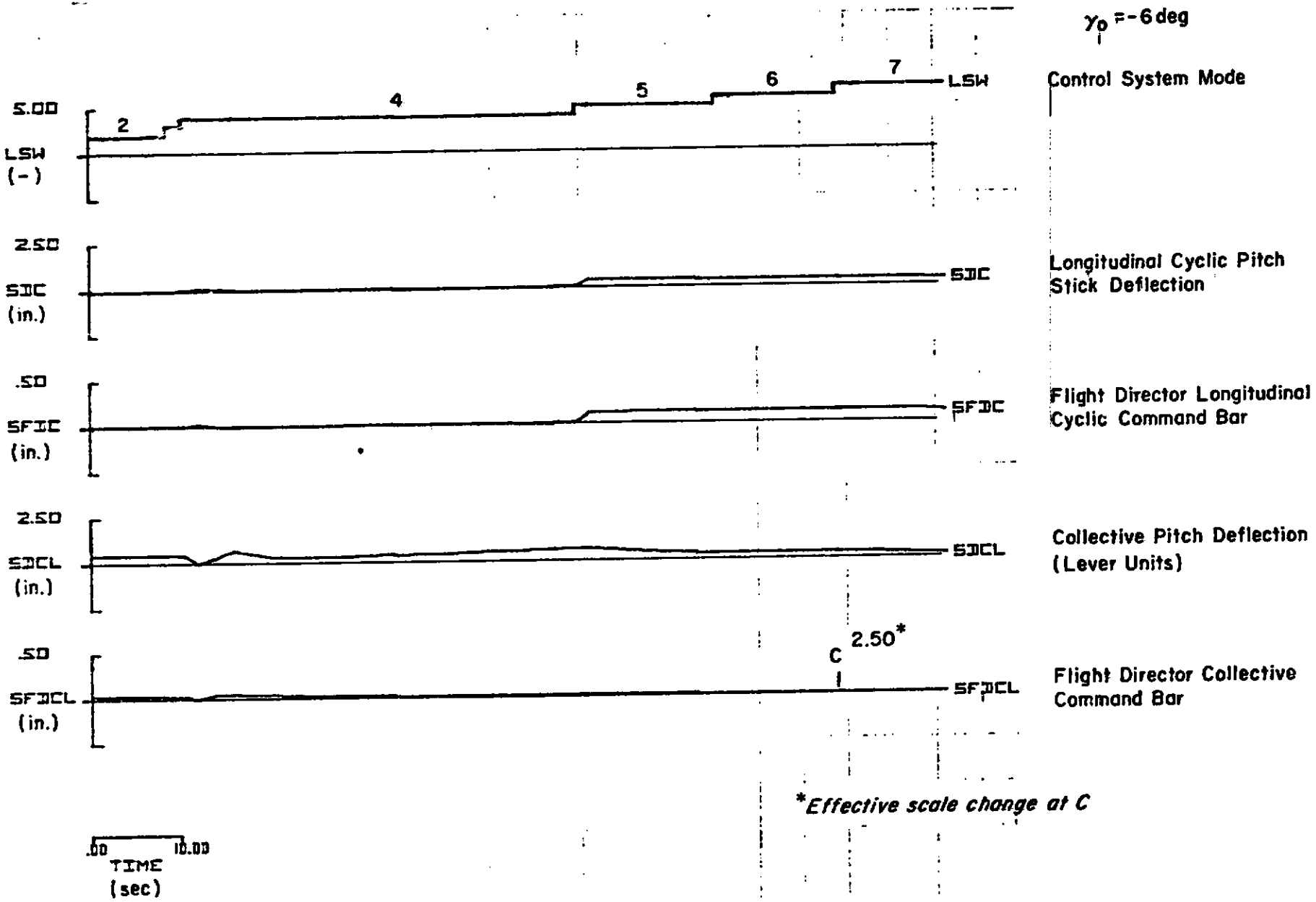

b) Longitudinal Cockpit Indications (iii)

Figure 44. (Continued)

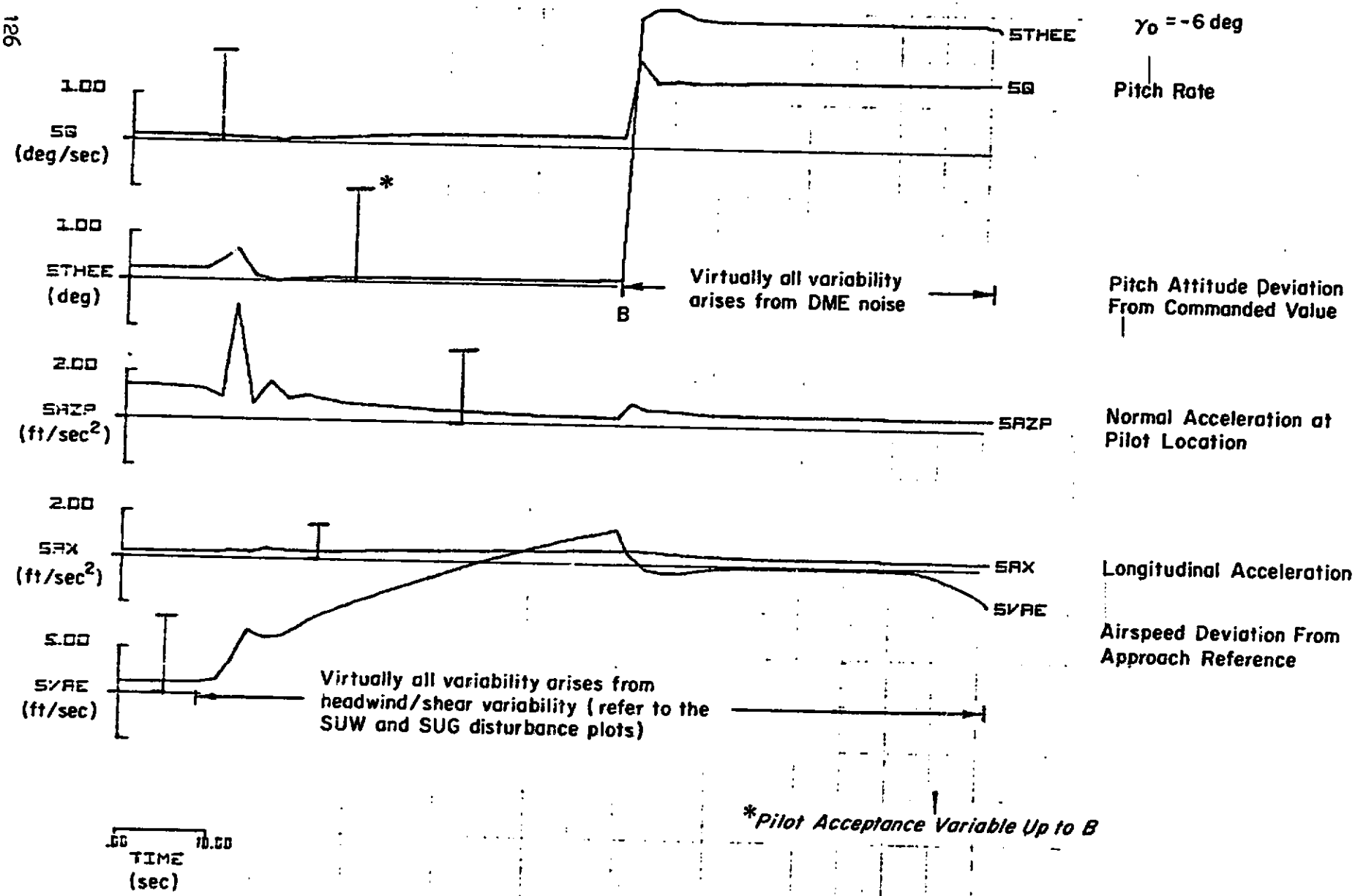

c) Longitudinal Pilot Acceptance Variables

Figure 44. (Continued)

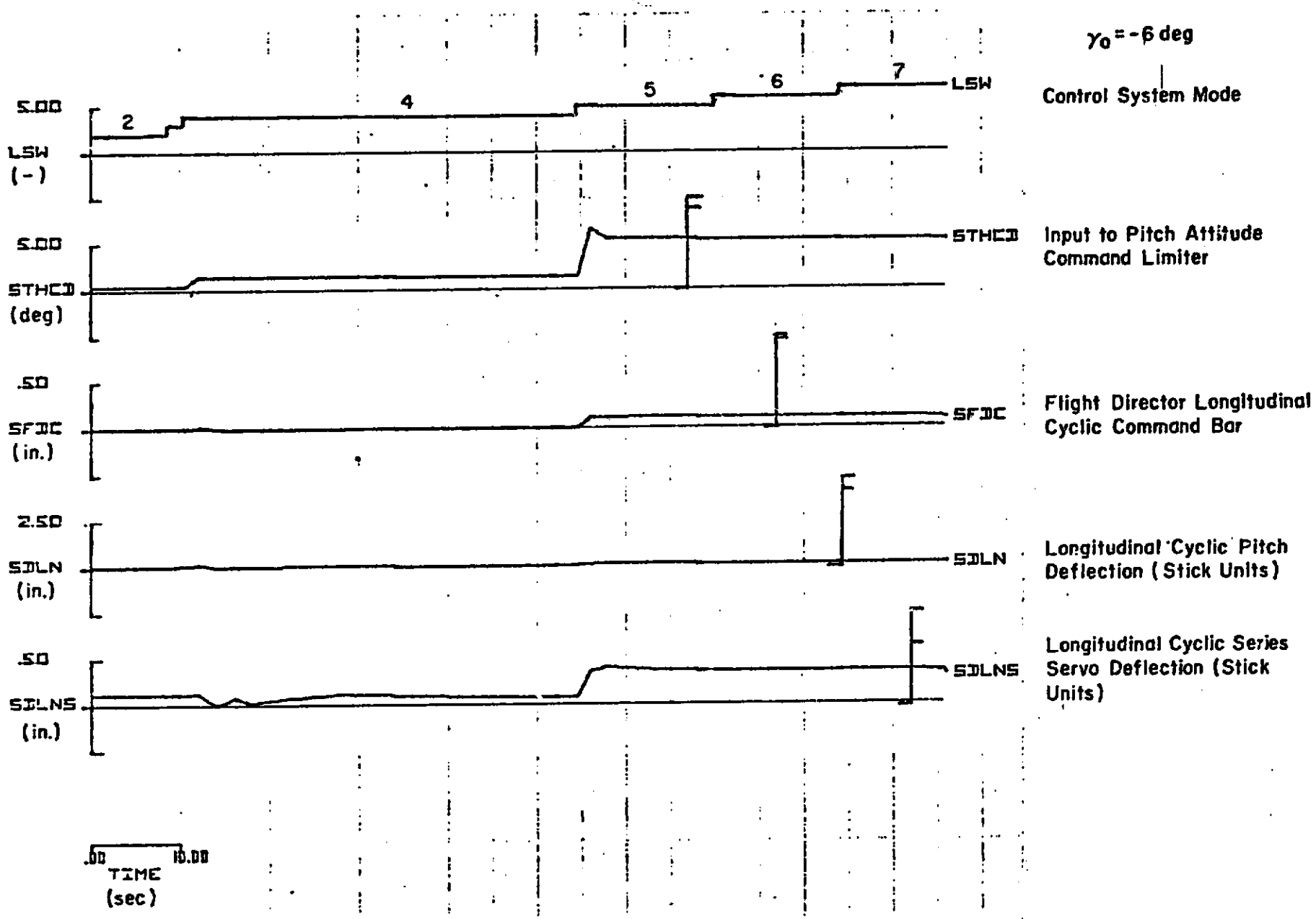

d) Longitudinal Limits (1)

Figure 44. (Continued)

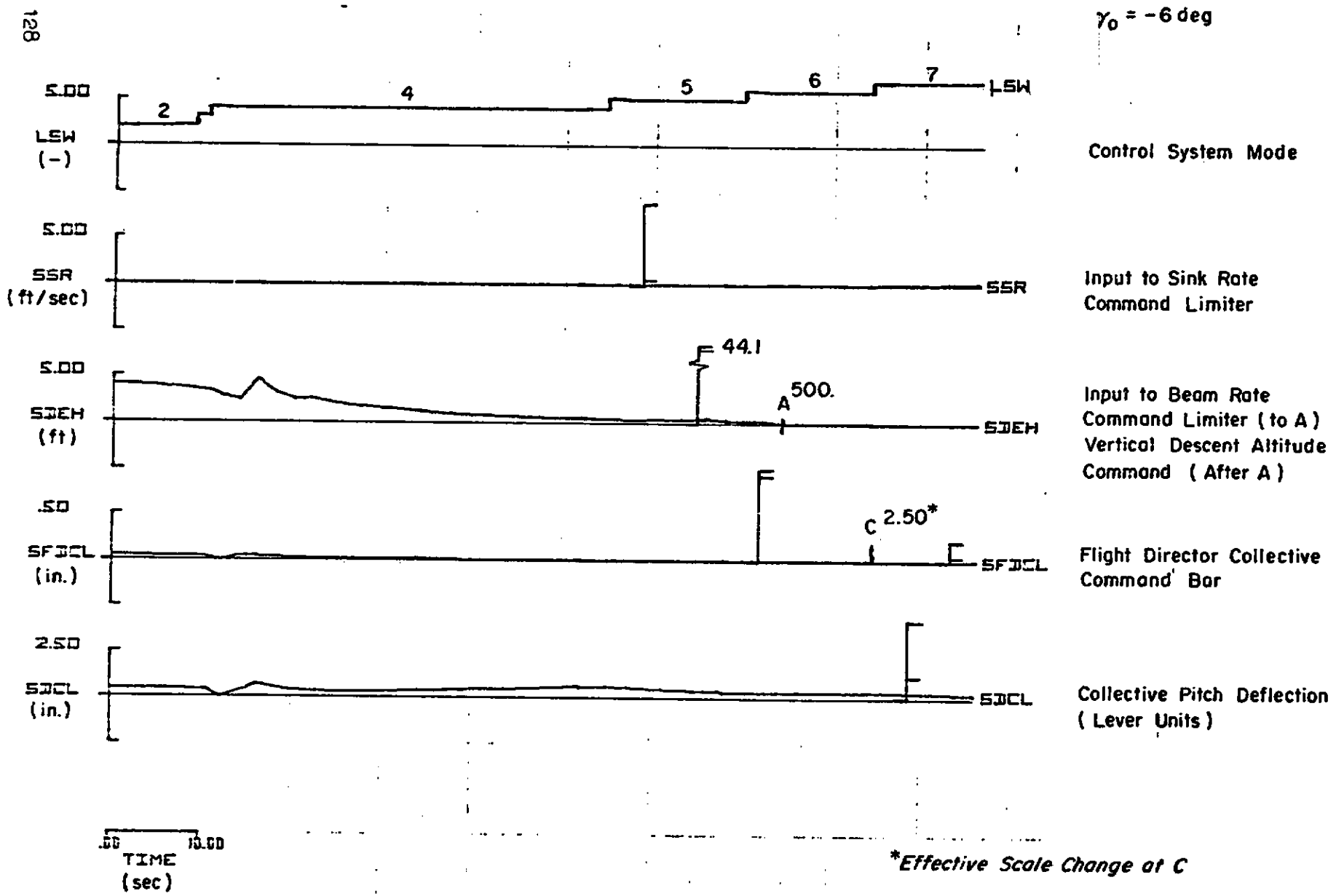

d) Longitudinal Limits (ii)

Figure b (Concluded)

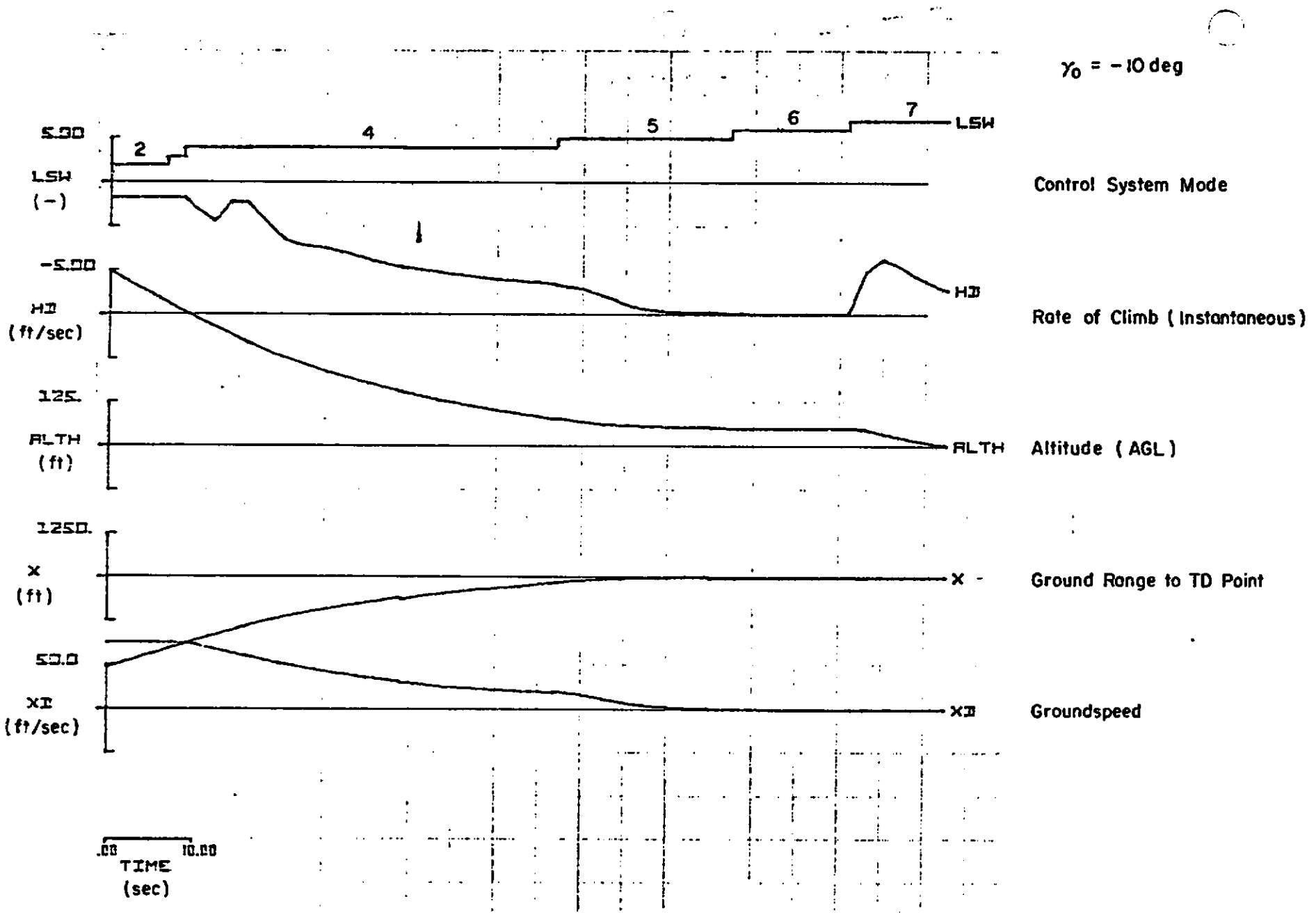

a) Longitudinal Trajectory

Figure 45. Mean Responses for Longitudinal System on -10° Approach from 500' through Touchdown

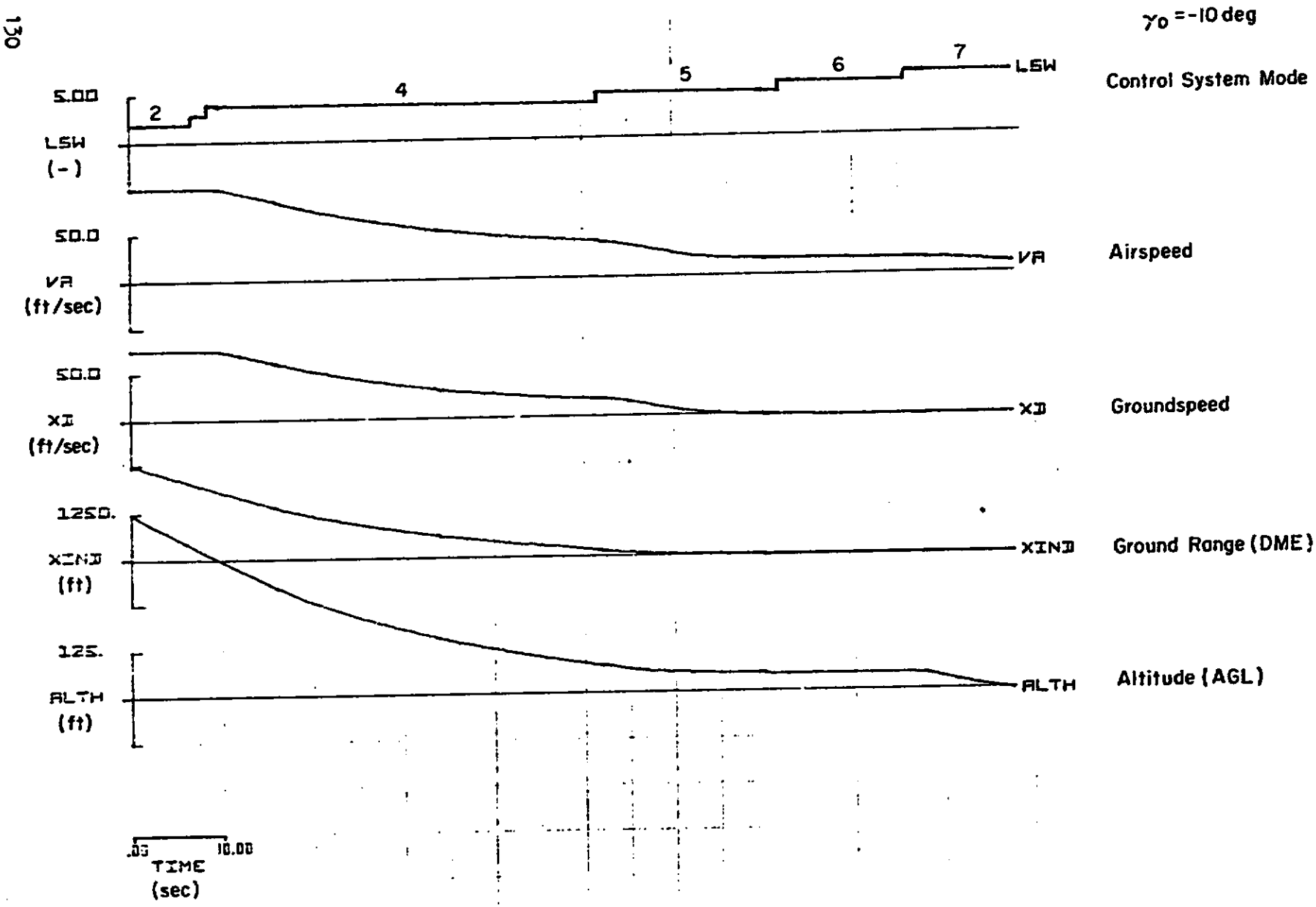

b) Longitudinal Cockpit Indications (i)

Figur 15. (Continued)

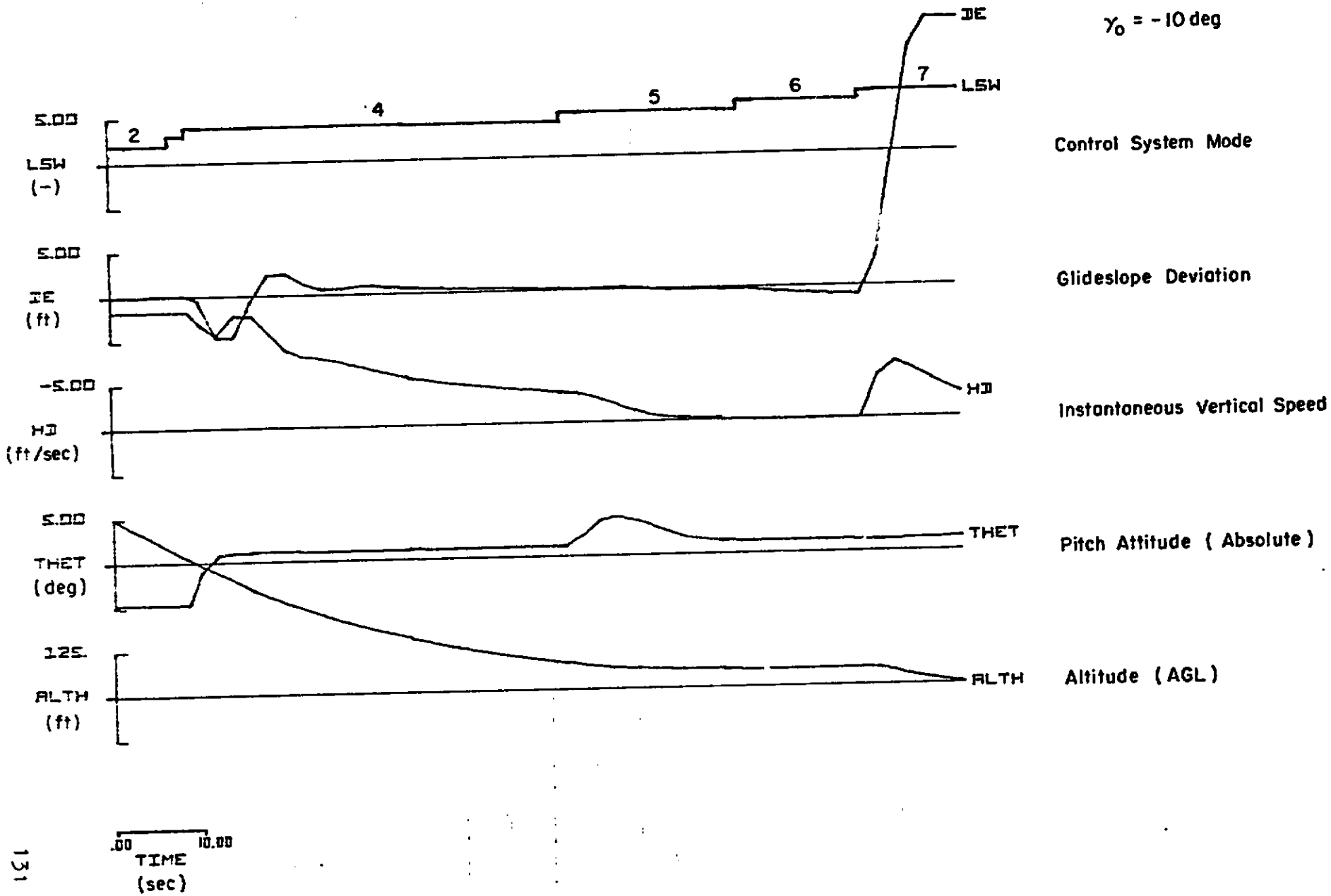

b) Longitudinal Cockpit Indications (ii)

Figure 45. (Continued)

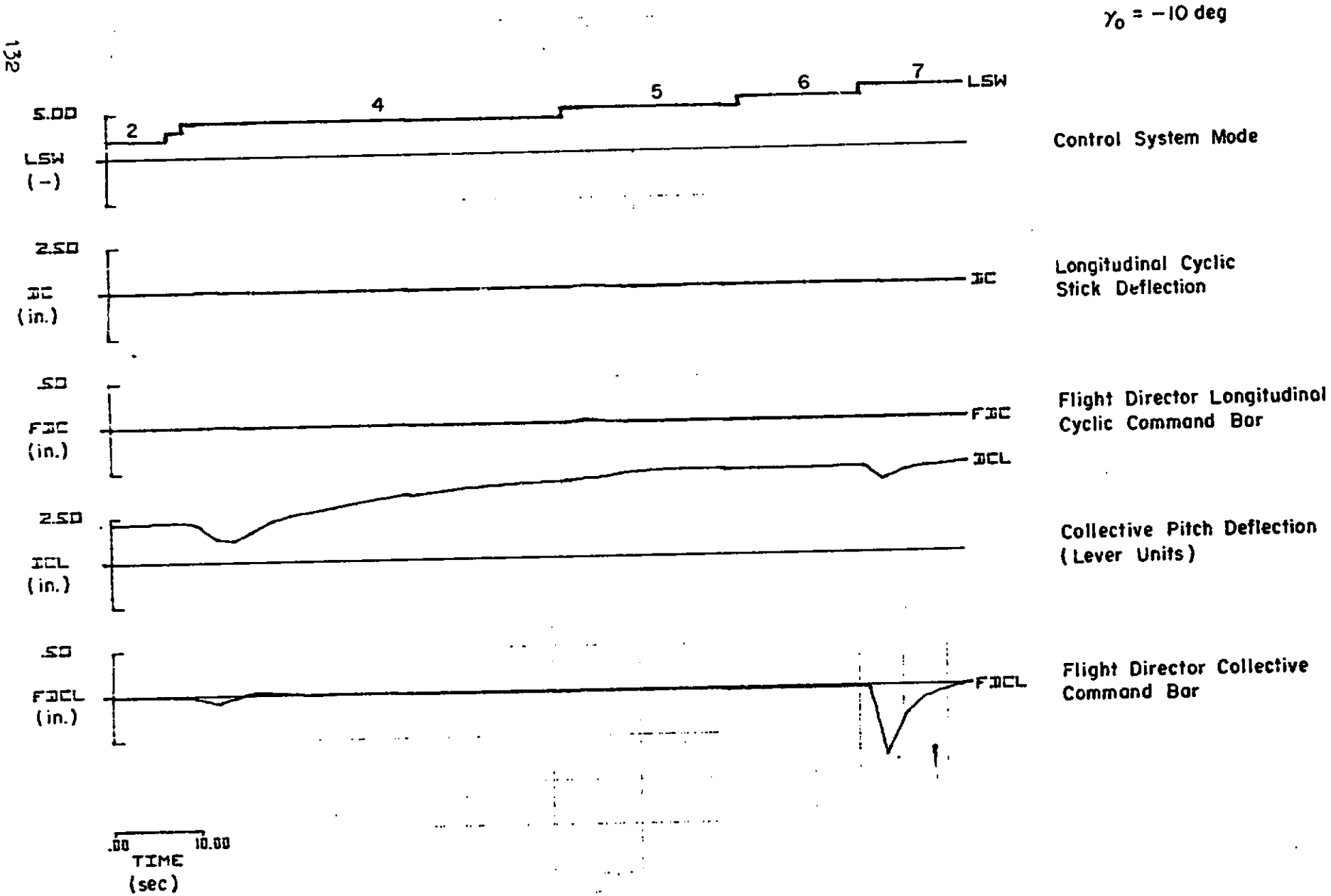

b) Longitudinal Cockpit Indications (iii)

Figure b- (Continued)

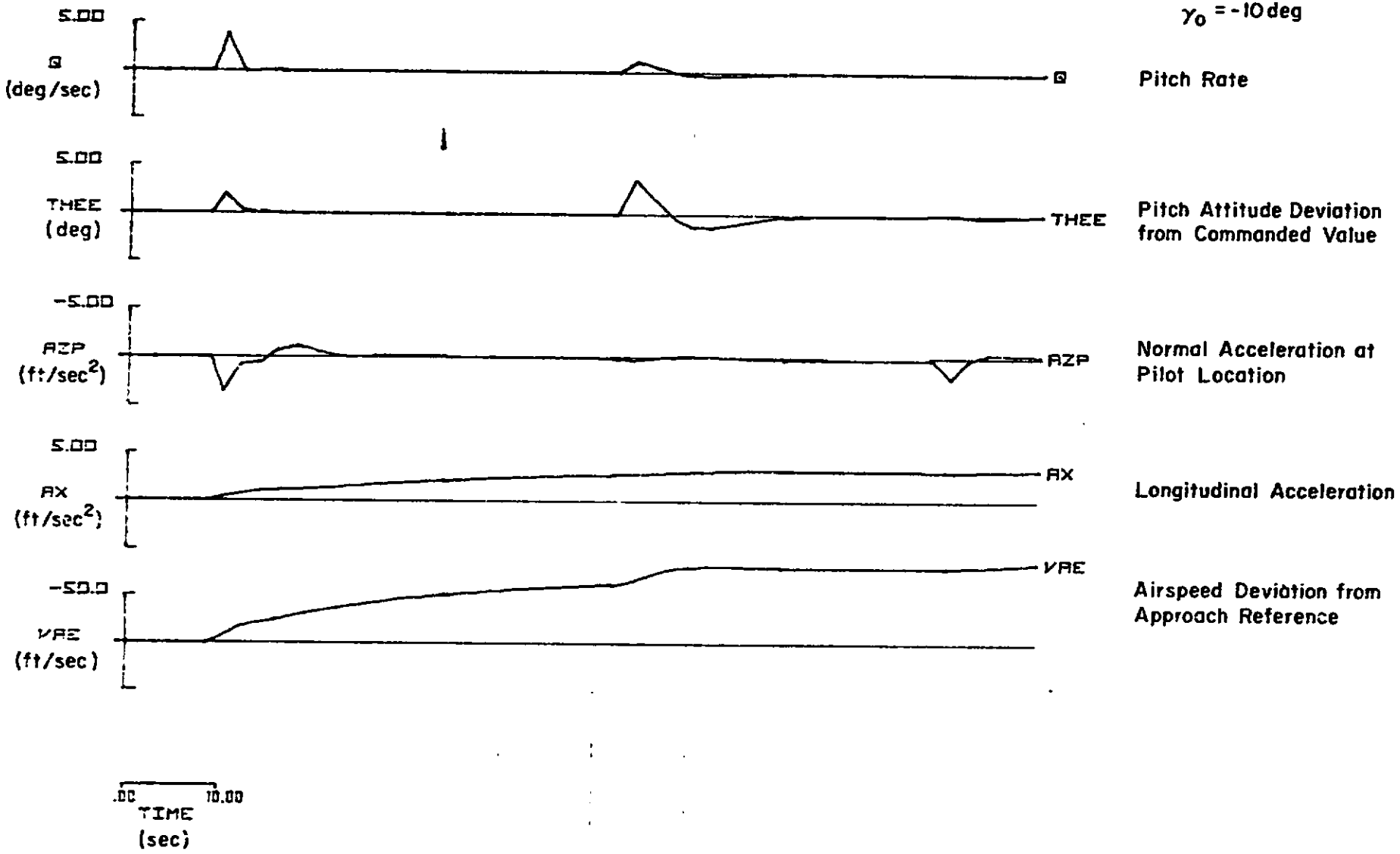

c) Longitudinal Pilot Acceptance Variables

Figure 45. (Continued)

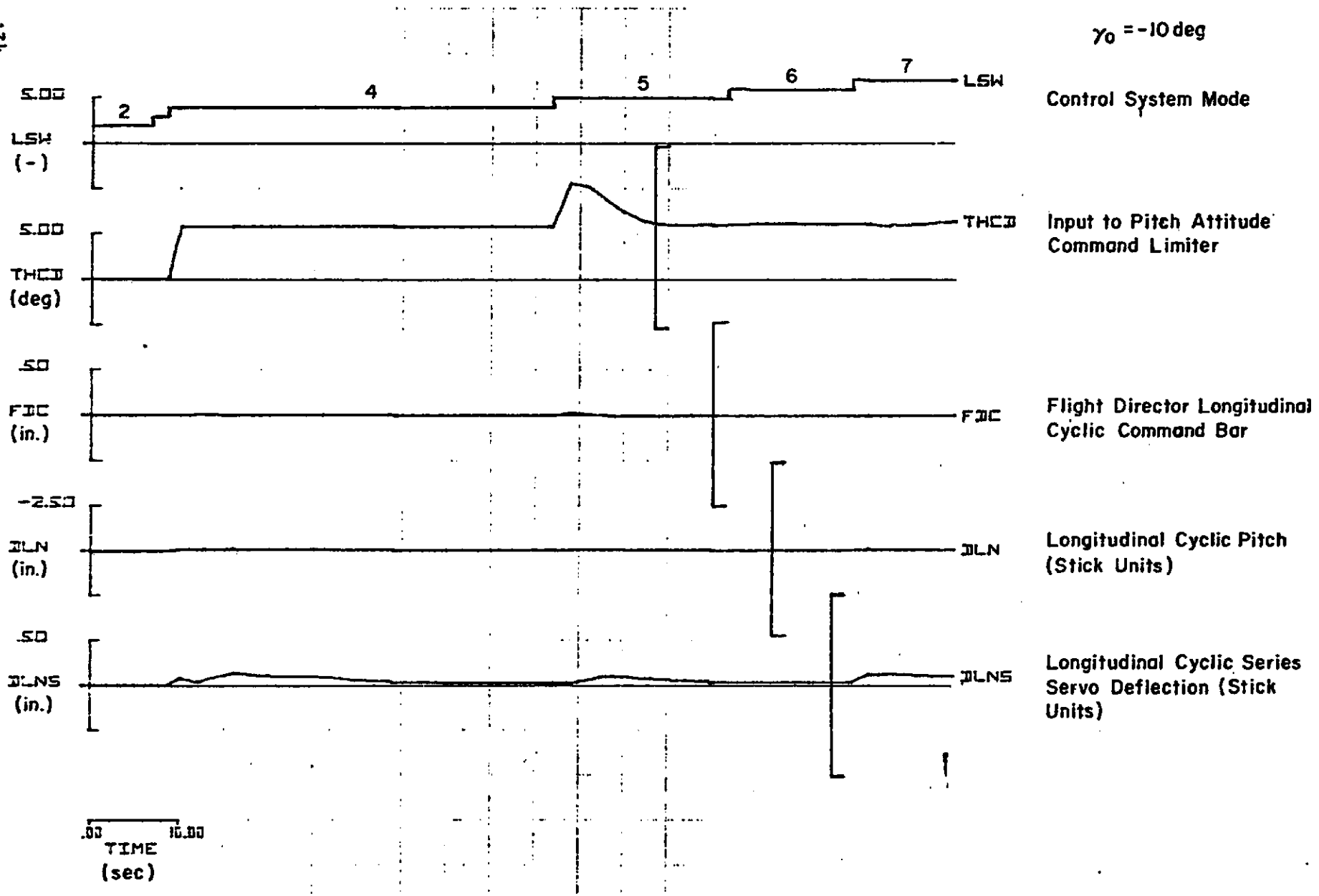

d) Longitudinal Limits (i)

Figure 45. (Continued)

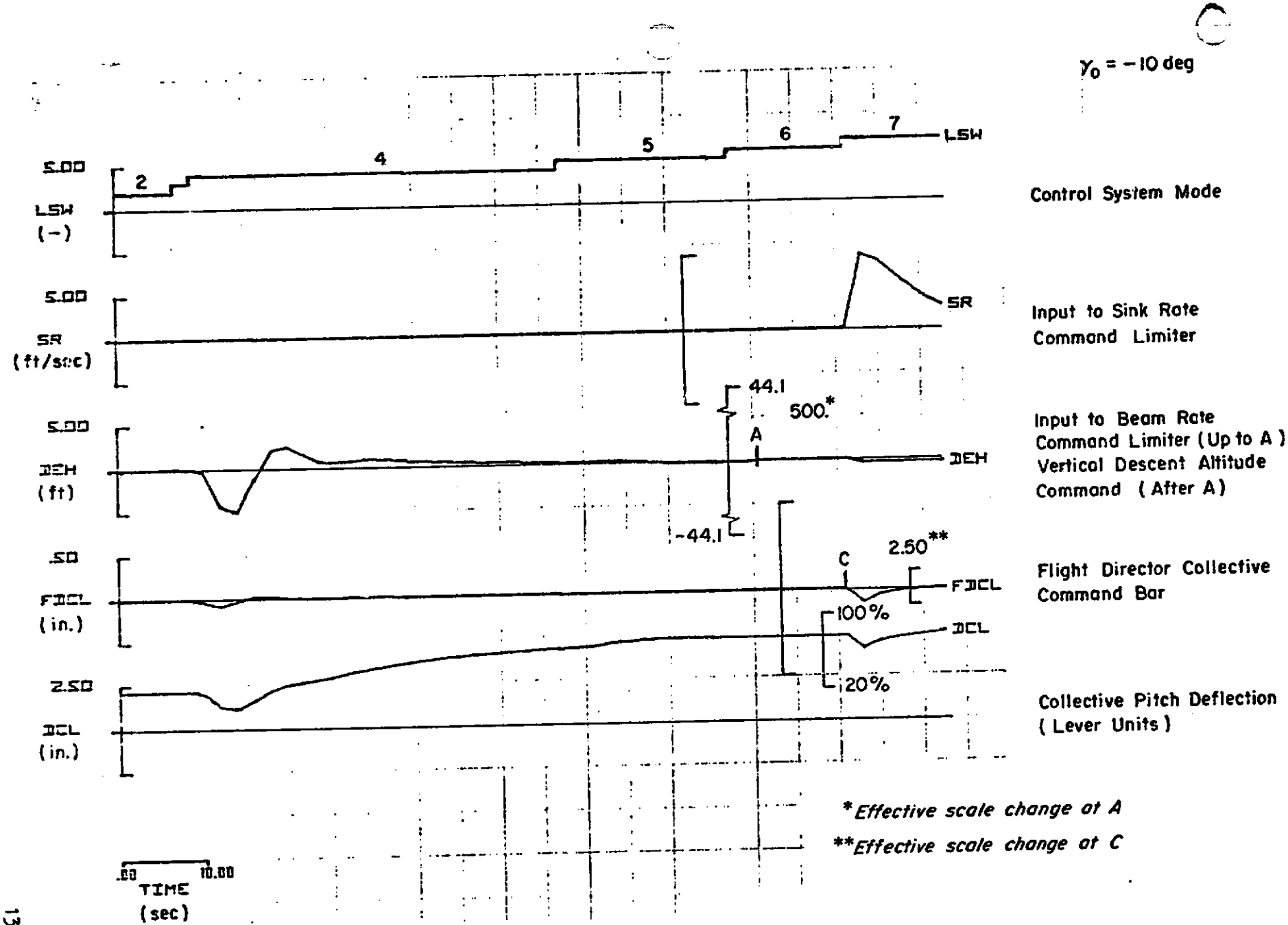

d) Longitudinal Limits (ii)

Figure 45. (Concluded)

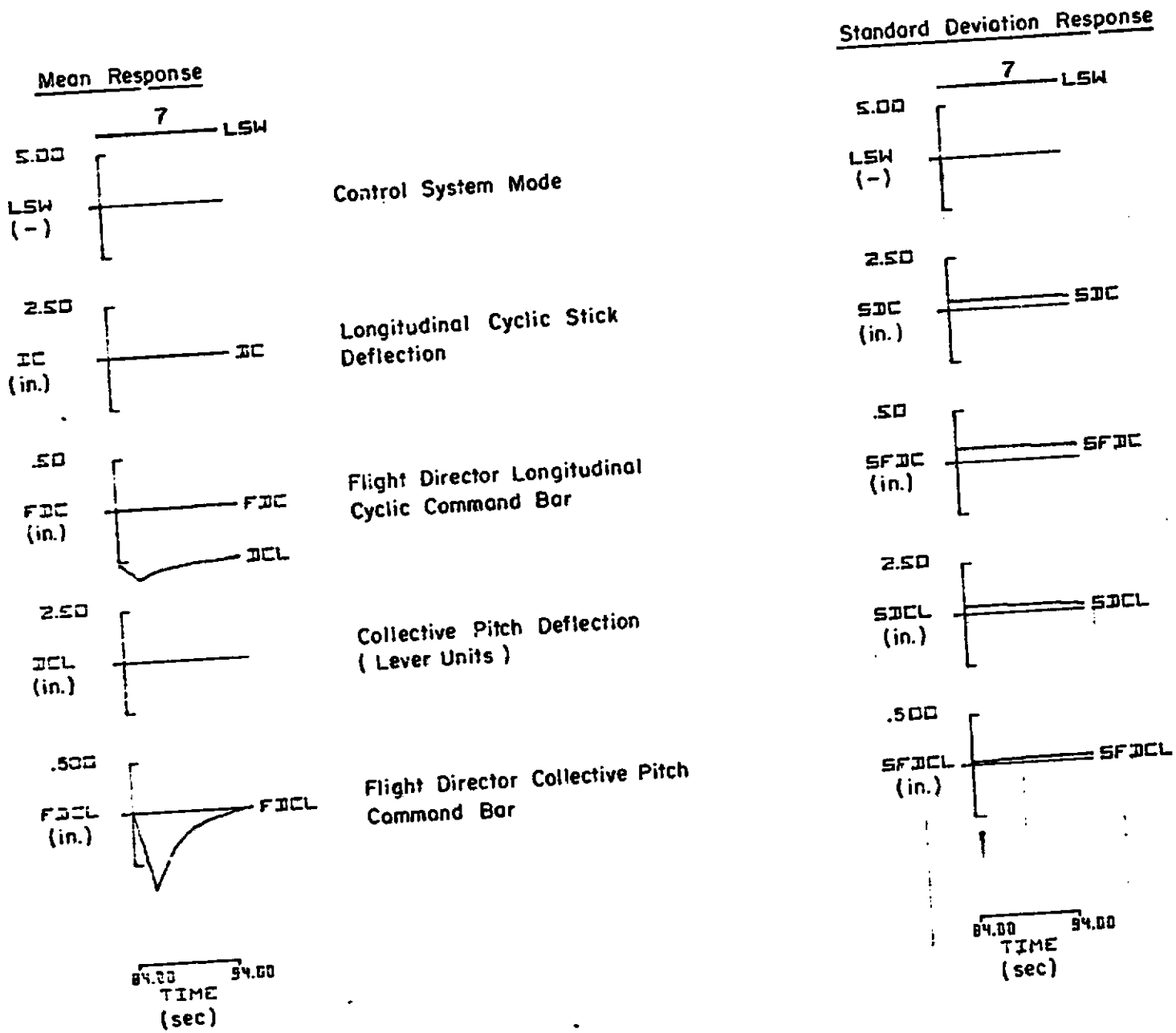

Figure 46a Expanded Scale Responses for Longitudinal System for Vertical Descent - om 50' to Touchdown

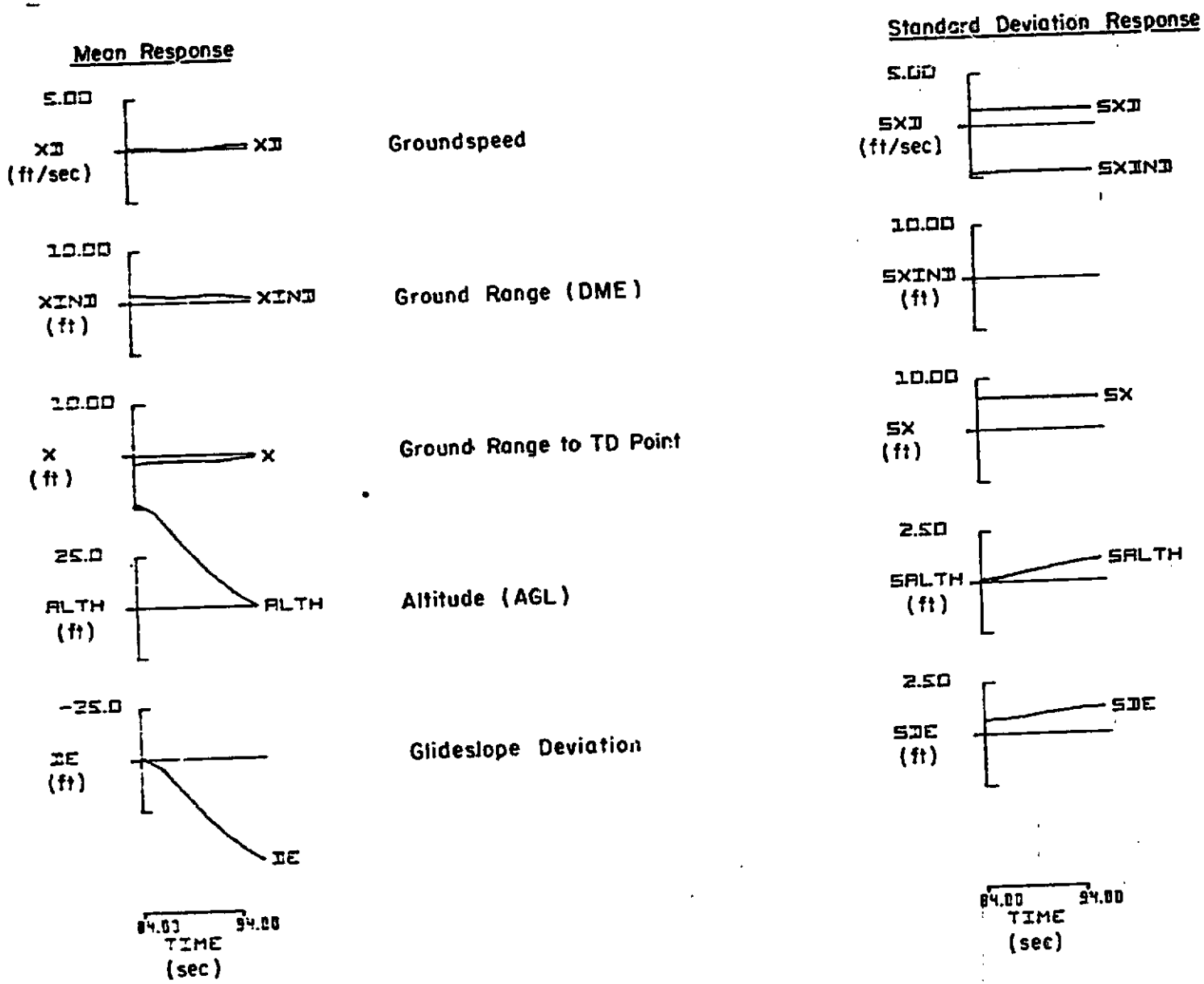

Figure 46b. Expanded Scale Responses for Longitudinal System for Vertical Descent from 50' to Touchdown

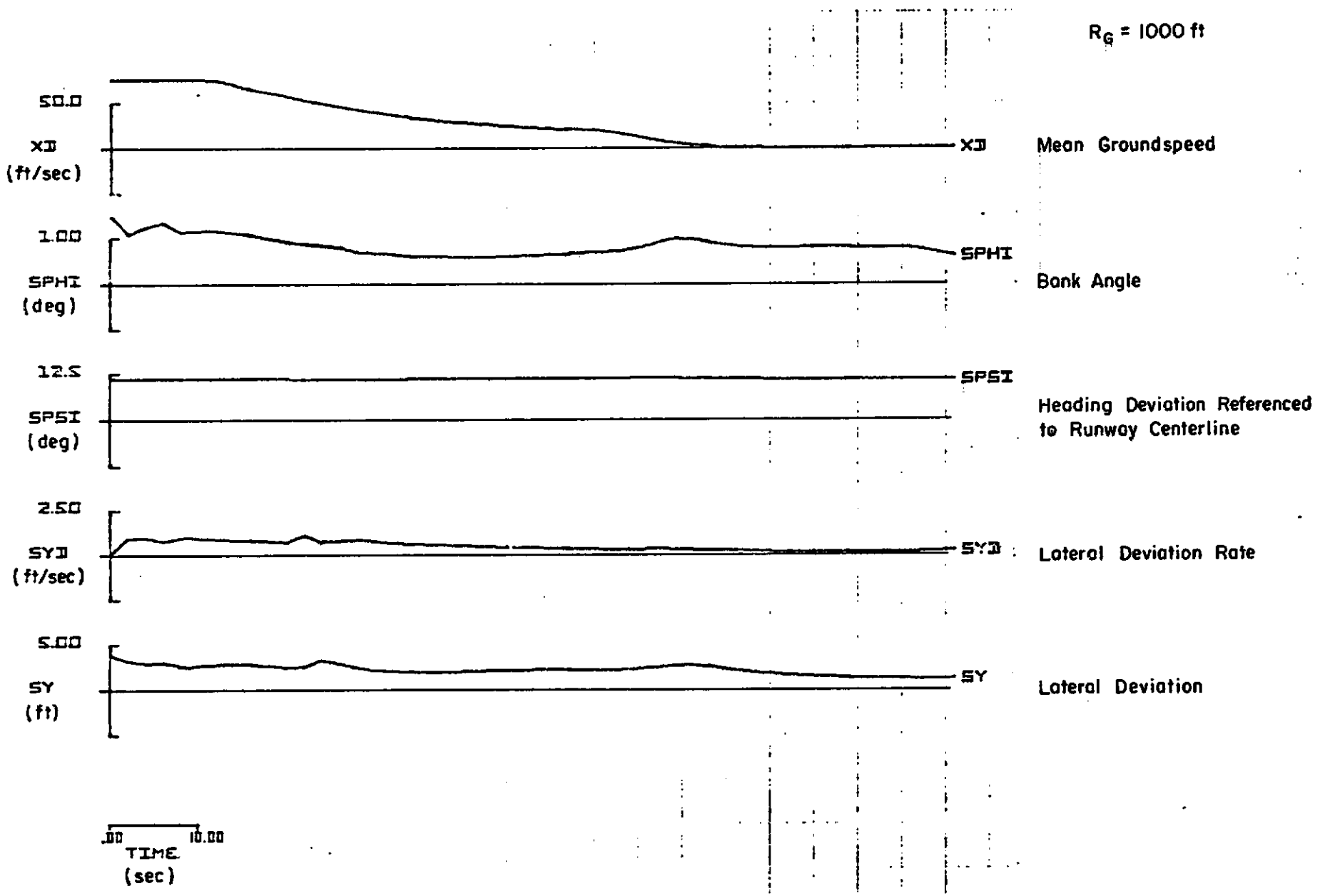

a) Lateral-Directional Trajectory

Figure 47. Standard Deviation Responses for Lateral-Directional System on -6° Approach from 340' through Touchdown on VTOL Pad

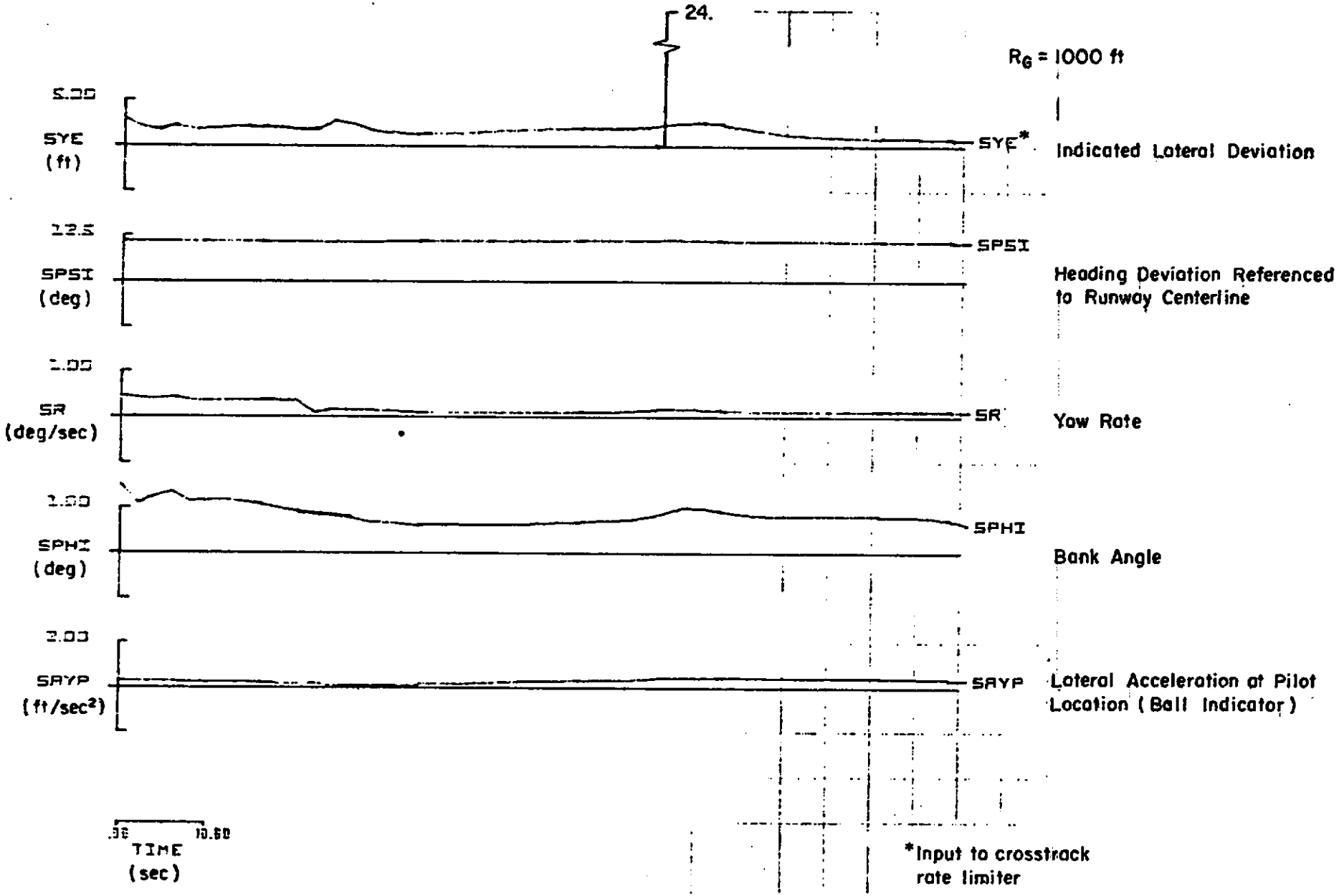

b) Lateral-Directional Cockpit Indications (1)

Figure 47. (Continued)

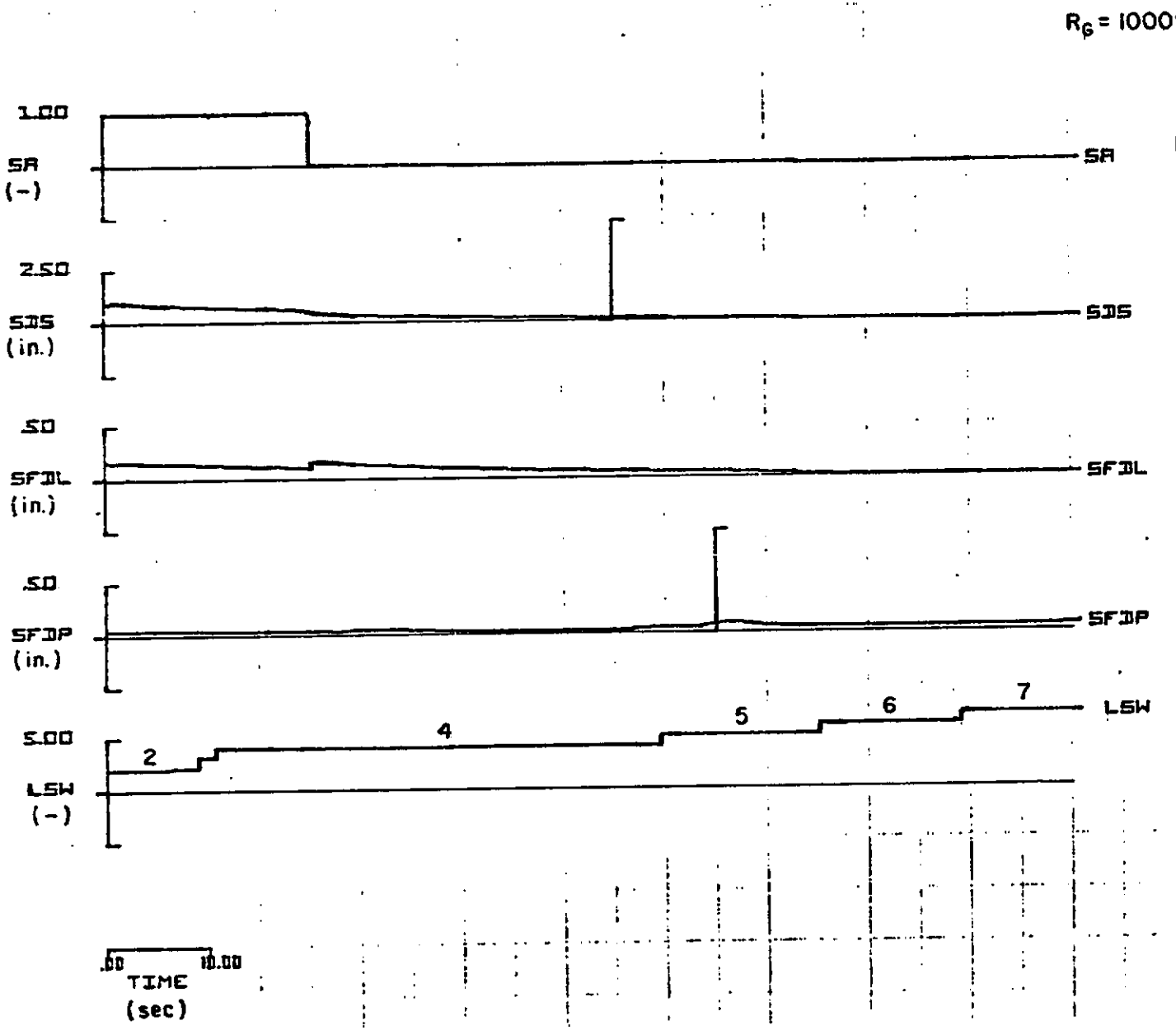

b) Lateral-Directional Cockpit Indications (ii)

Figure 47. (Continued)

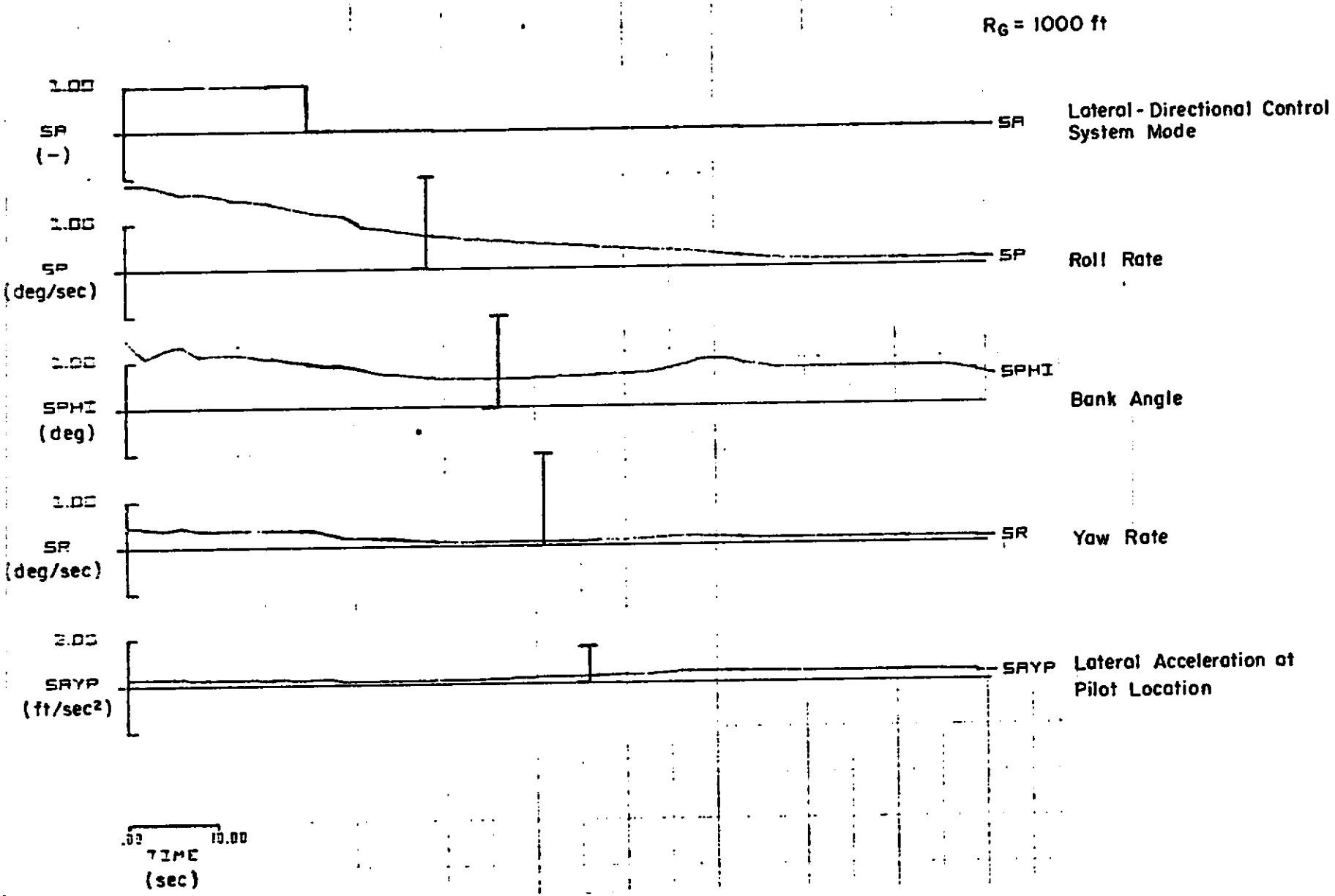

c) Lateral-Directional Pilot Acceptance Variables

Figure 47. (Continued)

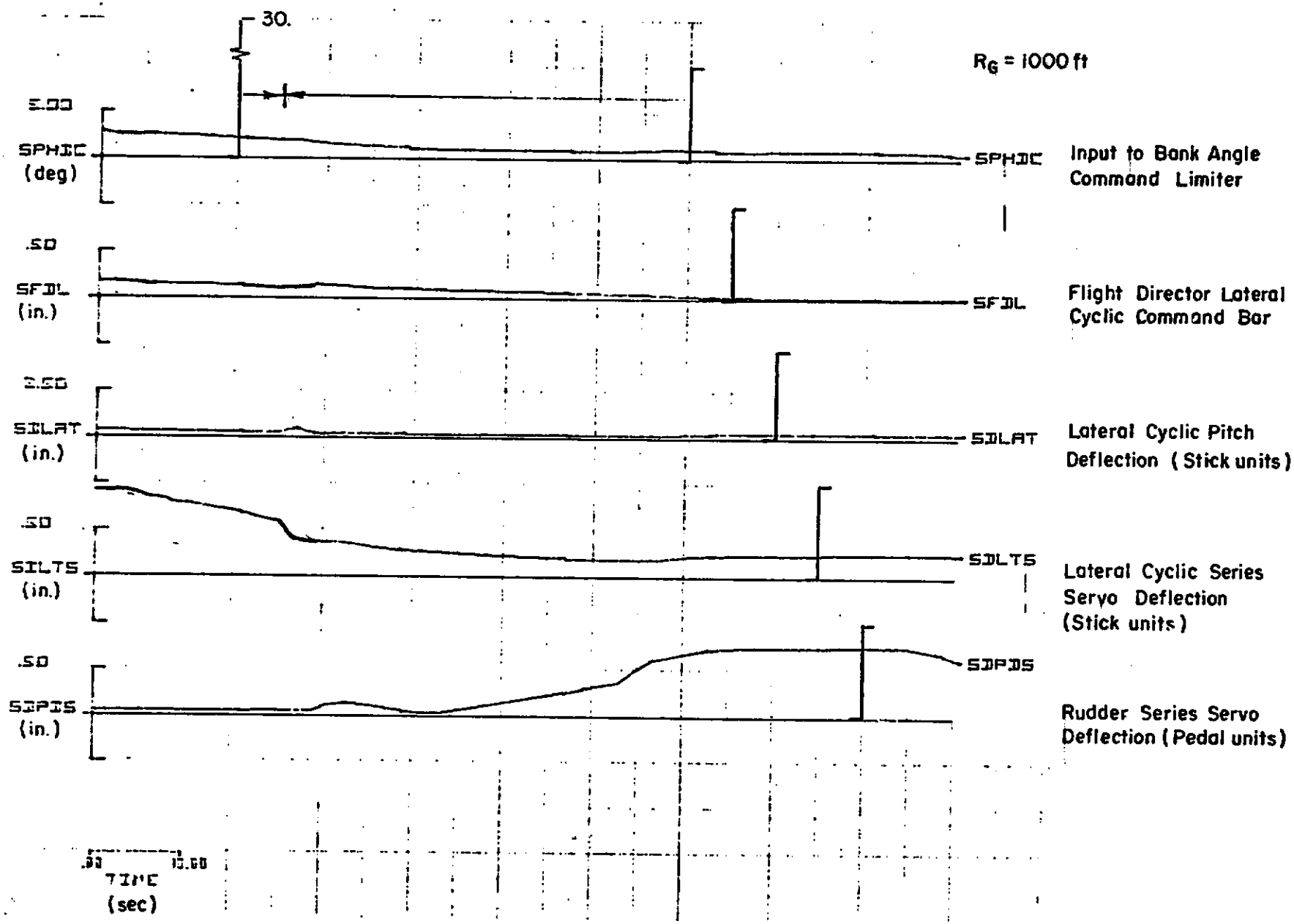

d) Lateral-Directional Limits

Figure 4-7. (Concluded)

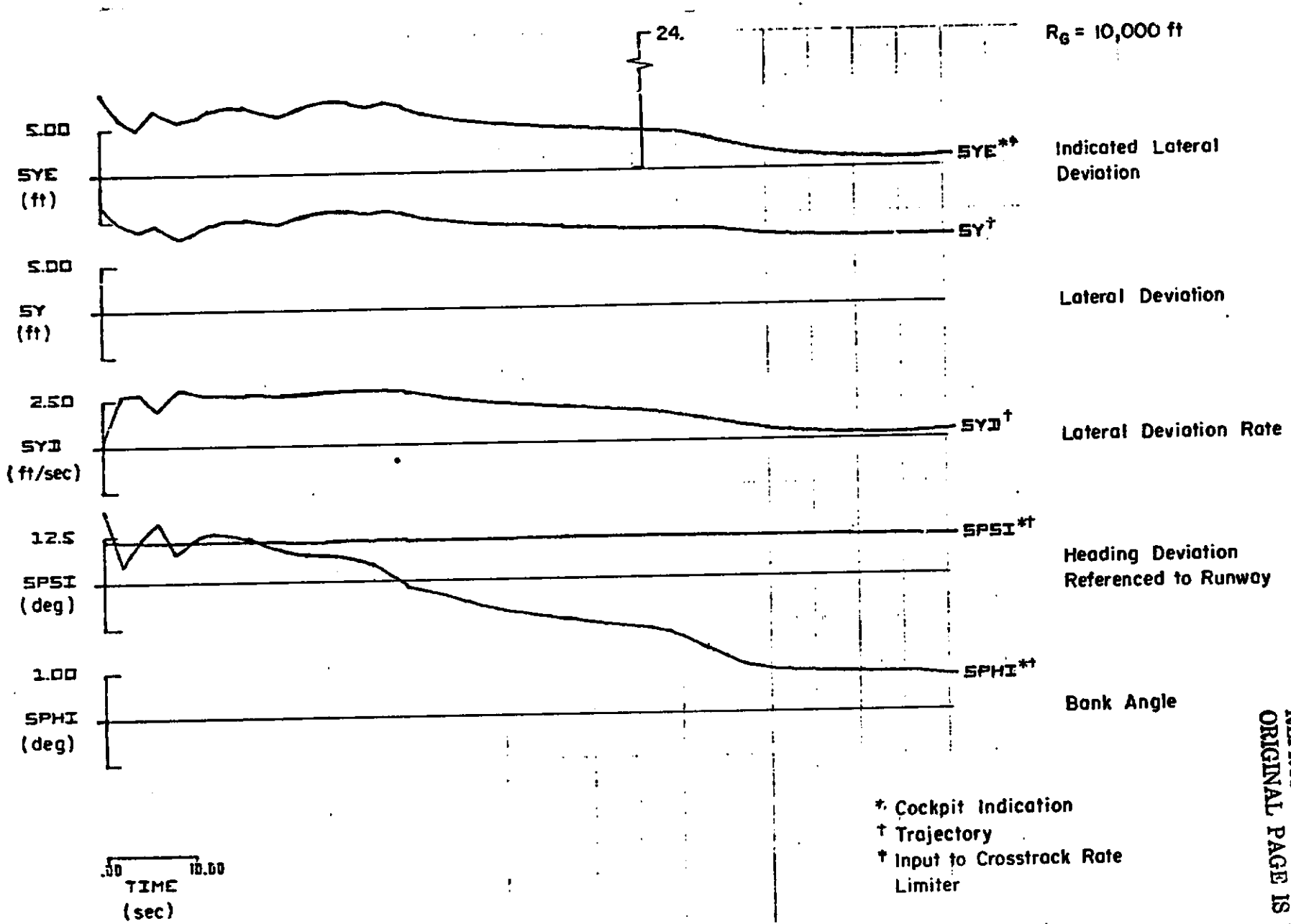

a) Lateral-Directional Trajectory and Cockpit Indications (1)

Figure 48. Standard Deviation Responses for Lateral-Directional System on −6° Approach from 340' through Touchdown on CTOL Runway

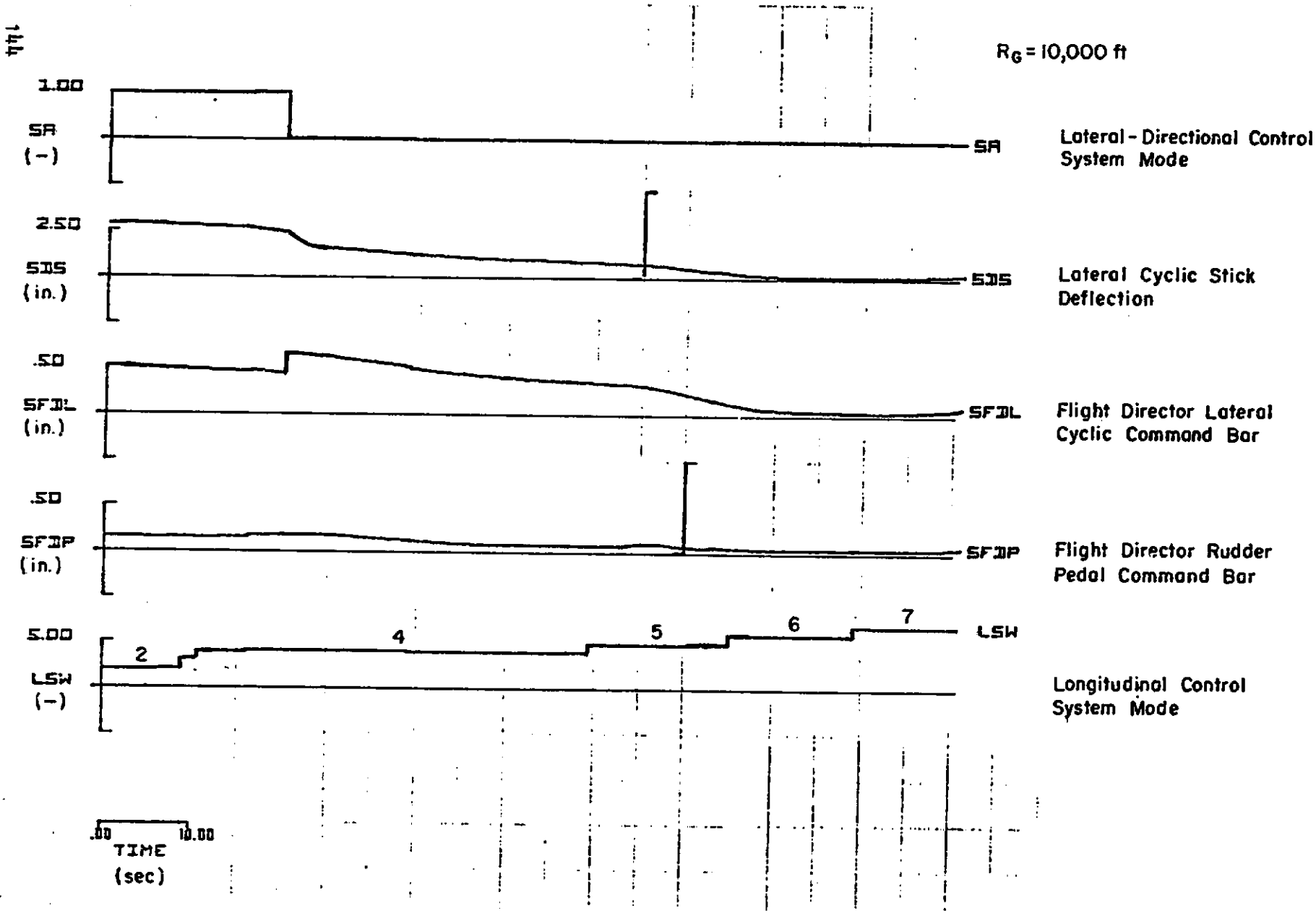

b) Lateral-Directional Cockpit Indications (ii)

Figure 42. (Continued)

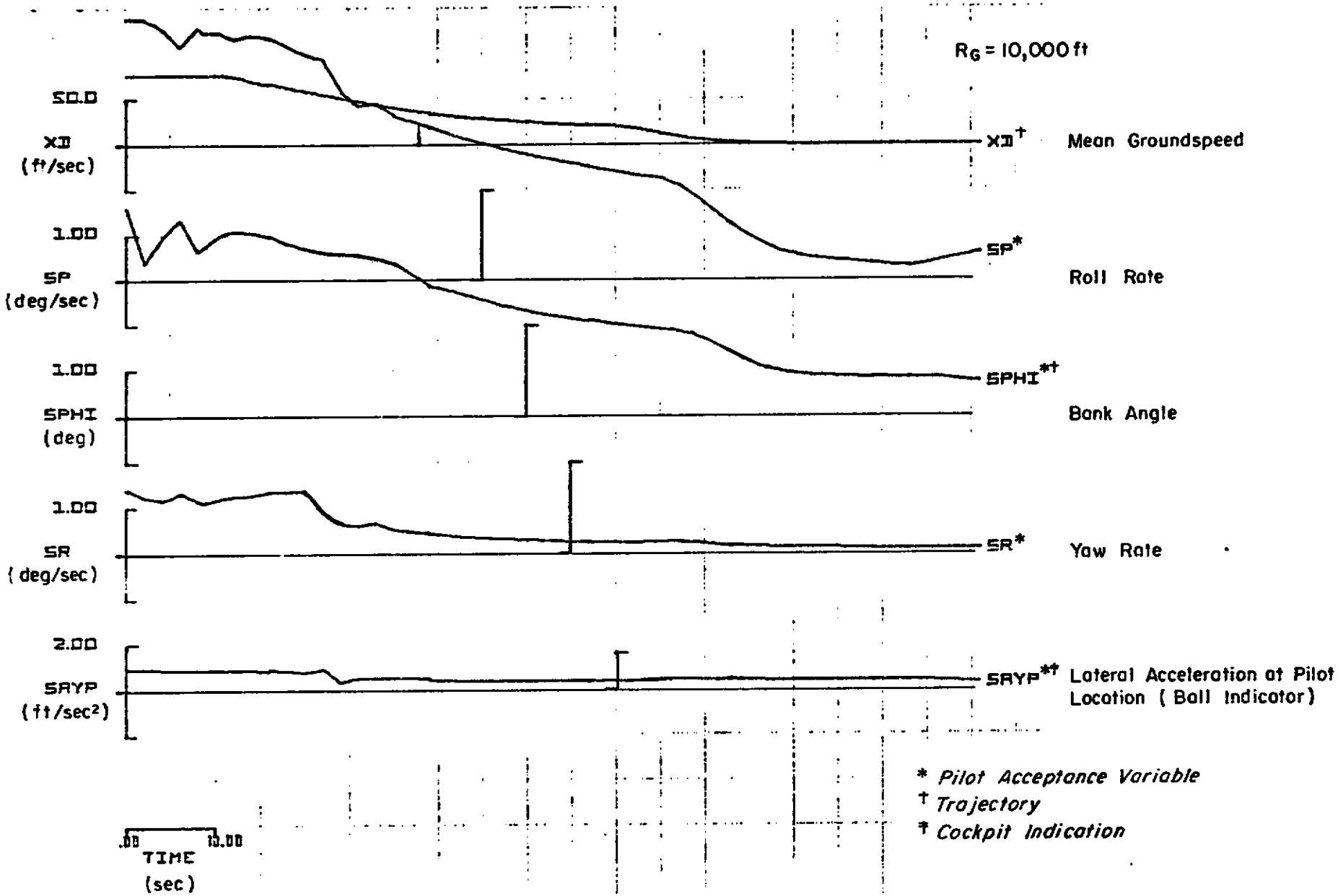

c) Lateral-Directional Pilot Acceptance Variables, Trajectory and Cockpit Indications (ii)

Figure 48. (Continued)

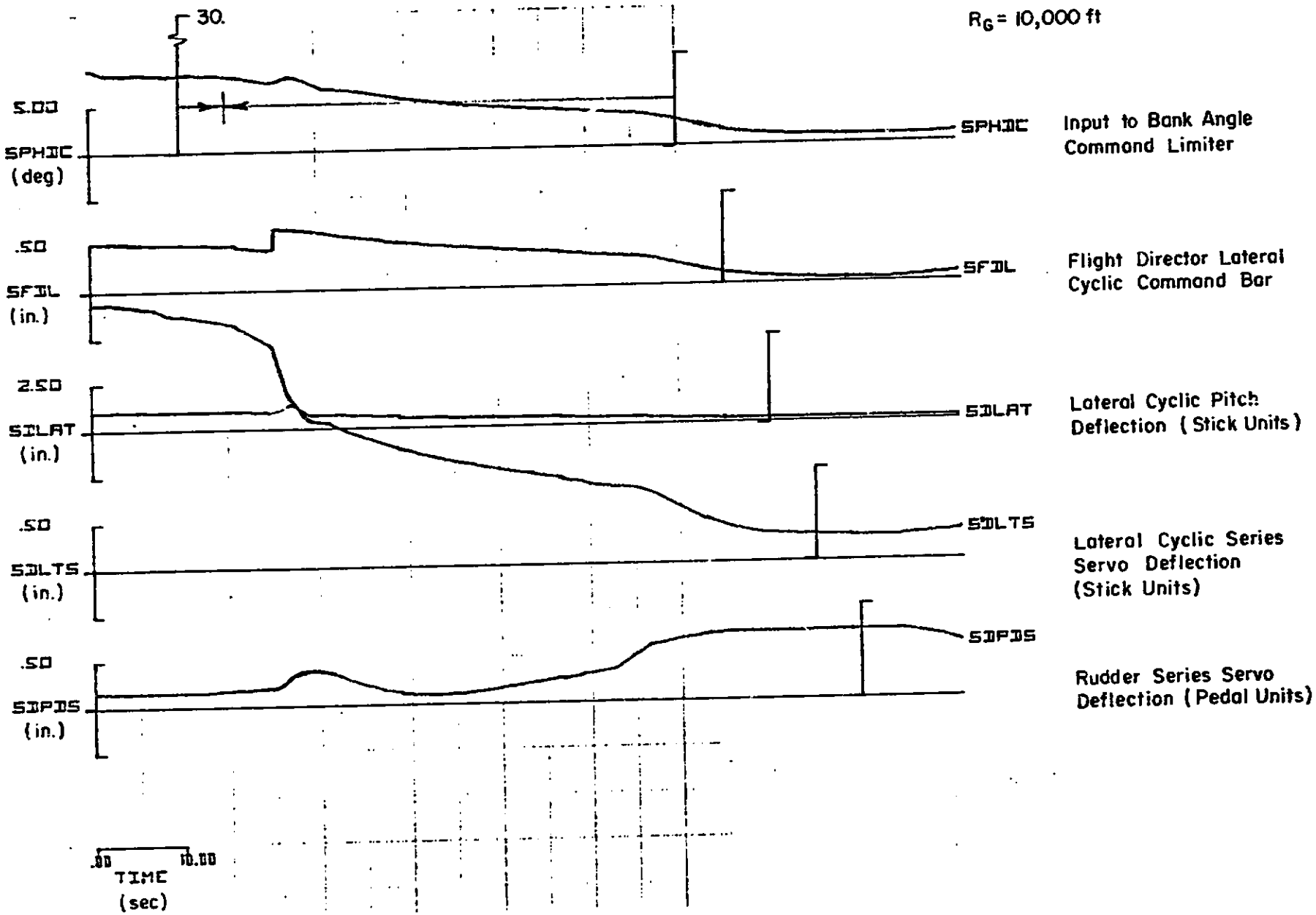

d) Lateral-Directional Limits

Figure 48. (Concluded)

variability during these two phases is basically the effect of the pitch attitude required to trim in the face of various headwind components.

Variability in rate of climb (SHD), the flight director command bars (SFDC and SFDCL) and the controls (SDC and SDCL) is very low throughout approach and landing. Figure 46 shows that ground speed (SXD) and longitudinal position (SX) variability is small throughout vertical descent.

Variability in the pilot acceptance variables is satisfactory, but the following interpretations are required. Pitch attitude deviations from the commanded value (STHEE) show low variability before the hover phase. During the hover phase the high additional variability encountered is the result of DME noise. The actual pitch attitude (STHET) variability during hover is in the acceptable range (±2 deg). Variability in normal acceleration (SAZP) is larger than the acceptability level only for a very brief interval during initiation of the constant attitude deceleration phase. The acceptability level for airspeed error variability (SVAE) applies only during the airspeed hold phase of the approach.

Inputs to all limiting functions except for pitch attitude command (STHCD) are such that the probability of limititing is less than 5 percent. The probability of pitch attitude limiting exceeds 5 percent only during the short hover initiation transient. This is nevertheless expected to result in acceptabile performance.

c. Response Standard Deviations for Lateral-Directional Variables

Recall that the mean response for all lateral-directional variables is zero. Response standard deviations are included for two landing site types, a VTOL pad in Fig. 47, and a CTOL runway in Fig. 48. The two sites have different separations between the azimuth and glide slope antennas. This separation is 1000 ft (305 m) for the VTOL pad and 10,000 ft (3,048 m) for the CTOL runway. The level of MLS noise disturbing the lateral-directional system is directly proportional to range from the azimuth antenna.

The standard deviation responses show low variability in all trajectory variables and cockpit indications except for bank angle (SPHI) in the CTOL runway case. The large bank angle variability is the result of coupling too

tightly to the localizer at large ranges from the aximuth antenna in the Section IV design. Reduced $K_{\dot{y}}$ and K_y gains or range-scheduled values for these gains will be required in the final system. In particular, lateral deviation (SY) and lateral deviation rate (SYD) standard deviations are small throughout the approach. The standard deviation in heading deviation (referenced to runway centerline) (SPSI) is almost entirely due to crab angle resulting from crosswind variability, one approach to the next.

All standard deviations for pilot acceptance variables are satisfactory for the VTOL pad case. For the CTOL runway case, the standard deviations for roll rate (SP) and bank angle (SPHI) exceed the acceptable level by a significant amount. This is for the reason explained in the preceding paragraph. This problem will be eliminated by the same fix in the final system.

Inputs to the crosstrack rate (SYE) and bank angle command (SPHDC) limiters, and to lateral cyclic pitch (SDLAT) and stick (SDS), flight director lateral cyclic command bar (SFDP) are all less than one-fourth of the limit level for the VTOL pad case. The rudder series servo deflection (SDPDS) is such the probability of limiting is 18 percent during very low speed flight. The effective reduction in yaw damping resulting from this may be tolerable in the final system. If it is not, low frequency inputs to the rudder series servo will have to be shifted to the rudder force feel system actuator. Early in the approach record the standard deviation of the lateral cyclic series servo deflection (SDLTS) approaches the limit level. This again is the result of overly tight coupling to the localizer.

The inputs to the limiting functions have similar characteristics for the CTOL runway case, but the limiting is more severe in the case of bank angle command (SPHCD) and lateral cyclic series servo deflection (SDLTS). Less tight coupling to the localizer in the final system will reduce these limiter inputs to acceptable levels.

d. Touchdown Statistics

Criteria for a successful touchdown are compared with the corresponding values resulting from performance evaluation in Table 13. It turns out that these performance evaluation values are unchanged to two significant figures

TABLE 13. COMPAIRSON OF KEY VARIABLES AT TOUCHDOWN WITH ACCEPTABLE LIMITS

PERFORMANCE			
VTOL Pad	CTOL Runway	REQUIREMENT	SOURCE
1.26	7.35 ft*	$\sigma_{Y_{TD}} \leq 0.1$ W (W = 150 ft, typical)	Touchdown point location
6.36 ft		$\sigma_{X_{TD}} \leq 0.1$ W (not critical for CTOL runway)	Touchdown point location
1.58 ft/sec		$\sigma_{\dot{X}_{TD}} \leq 5.0$ ft/sec (not critical for CTOL runway)	Roll off pad
−2.28 ft/sec		$\bar{\dot{h}}_{TD} + 3\sigma_{\dot{h}_{TD}} < 0$ ft/sec	Positiveness of touchdown
−2.98 ft/sec		$\bar{\dot{h}}_{TD} - 3\sigma_{\dot{h}_{TD}} \geq -12$ ft/sec	Landing gear strength
5.56 deg†		$\bar{\theta}_{TD} + 3\sigma_{\theta_{TD}} \leq 12.75$ deg	Airframe ground clearance
−2.65 deg		$\bar{\theta}_{TD} - 3\sigma_{\theta_{TD}} \geq -5.0$ deg	Nose gear-first touchdown limit
0.12	0.14 deg/sec	$\sigma_{r_{TD}} \leq 2.0$ deg/sec	Nose gear side load
0.23	0.43 ft/sec	$\sigma_{v_{TD}} \leq 2.0$ ft/sec	Landing side load
1.87	2.25 deg	$3\sigma_{\varphi_{TD}} \leq 15$ deg	Airframe ground clearance

*1 ft = 3.048×10^{-1} m. 1 deg = 1.745×10^{-2} rad.

when the missed approach decision rule is operative. In every case, the performance achieved is far better than the criterion specified in the "Requirement" column. This may be interpreted as permitting safe system operation in a more severe disturbance environment or as permitting operation with systems of lesser effectiveness than that developed herein.

The basic limitations upon touchdown accuracy for the current system arise from the significant noise levels on the DME and azimuth (CTOL runway only) guidance signals.

SECTION VI

APPROACH MONITORING CRITERIA

Development of approach monitoring criteria for both manually and automatically controlled approaches proceeds interactively with performance evaluation — These critieria are then implemented in the missed approach decision rule. In this section the important considerations involved are discussed first, then the technical results are presented.

The actual decision to break off an approach may of course be made at any point in the approach prior to the decision point. However, concepts based upon a single decision point are used since they are sufficient to protect against a landing accident arising from an out-of-tolerance approach. The development concepts are the same for both automatically and manually controlled approaches, and regardless of whether criterion evaluation is a computer or pilot task. However, it is possible that distinctly different criteria are appropriate for computer and pilot evaluation. This is so because of the pilot-centered requirements when conventional aircraft instruments (ADI, HSI, etc.) are used. Requirements are for acceptable workload level when aircraft is manually controlled via the flight director, ability to discern the criterion levels accurately using the given instrument scales, etc. These pilot-centered requirements are not operative when criterion evaluation is implemented in the computer.

A. BASIC CONCEPTS

Approach monitoring criteria tend to derive from three basic considerations:

- Airframe operational performance, e.g., control power envelope limits defining the safe operation corridor
- Limits upon dynamic excursions for reasons of pilot acceptance.
- Limits upon dynamic excursions for reasons of achieving landing on the pad/runway with precision adequate for safety

Operational characteristics tend to establish the "location" of the latest point in the approach at which a missed approach may be elected, that is, it establishes a selected altitude and/or distance as a "decision point." The XV-15 decision point location is selected to occur during the stabilized point hover while in the altitude hold mode, just prior to committing to vertical descent. This decision point is at the latest possible time in the approach because missed approach execution from the vertical descent maneuver appears unwise in the extreme. This is the case because later execution of a missed approach would require arrest of the established sink rate using the modest amount of remaining collective pitch control power. On the other hand, an earlier decision point is undesirable because the missed approach decision rule is then less effective in eliminating unsafe touchdown conditions. This is the case because of increased exposure to subsequent disturbances which can produce unsafe conditions. These are the key operational performance considerations.

Limits imposed by virtue of pilot acceptance of dynamic excursions in attitude, speed, etc., throughout the approach have already been evaluated in the previous section. Dynamic excursions in attitude, attitude rate, linear acceleration, and speed are found to remain generally within limits which inspire pilot confidence in the integrity of system performance throughout the approach.

The class of limits which arise from landing precision requirements is more difficult to determine. It requires that limits on acceptable touchdown dispersion and sink rate (as well as the other quantities listed in Table 13) be projected back up the approach path to establish limits upon the available approach status data at the decision point. The limits on the approach status data at the decision point must assure a high probability of achieving touchdown conditions which are within the "safe landing" limits without being unduly conservative (i.e., causing an excessive missed approach rate). By this description it is clear that this aspect of determining approach monitoring criteria can have an iterative interaction with the landing performance evaluation. Fortunately, selection of the covariance propagation method of performance evaluation provides a key relationship between dispersion at the decision point and dispersion at touchdown. This relationship enables identification

of the essential variables for approach monitoring and critical decision levels for those variables. These variables and the corresponding decision levels define an approach "window." If an approach trajectory passes through this window, there is a high probability that the resulting landing will be acceptable and that approach is continued to touchdown. All other approaches are converted to missed approaches as go-arounds are executed.

The method for developing approach monitoring criteria arising from touchdown dispersion must accommodate two facts:

- Acceptable landing must essentially be predicted on the basis of airborne sensor measurements existing at the time the decision point is reached.
- Acceptable values of the key variables characterizing touchdown conditions must be inferred from a different, only somewhat related, set of variables which are the airborne sensor measurements.

As a first step, define the key variables and limits characterizing acceptable touchdown. These are listed in the "Requirement" column of Table 13. A list of the available airborne measurements is in Table 14. (The fact that only some of these measurements are available to the crew via conventional instrumentation must be taken into account when approach monitoring is accomplished by the crew.)

The key step is to model the interaction between approach performance just prior to the decision point, just after the decision point, the missed approach rate, and touchdown dispersion. Define the following variables:

$\bar{x}$	Expected value (mean) of state vector
$\bar{y}$	Expected value (mean) of an alternate state vector including the key variables determining touchdown conditions (Table 13) and airborne measurements (Table 14), $\bar{y} = H\bar{x}$
D	Covariance matrix for an alternative state vector which includes the key variables determining touchdown conditions and airborne measurements
$(\cdot)_{DP}^{-}$	$(\cdot)$ evaluated just before the decision point
$(\cdot)_{DP}^{+}$	$(\cdot)$ evaluated just after the decision point
$(\cdot)_{TD}$	$(\cdot)$ evaluated at touchdown

TABLE 14

AIRBORNE MEASUREMENTS

d_e	Indicated MLS glide slope deviation*
y_e	Indicated MLS localizer deviation*
$\hat{d}$	MLS derived glide slope deviation rate
$\dot{h}$	Instantaneous vertical speed*
h	Barometric and radar altitude*
X_i	DME (distance)*
θ, φ, ψ	Pitch, roll, heading*
V_A	Airspeed*
$\dot{X}$	Ground speed (via DME)*
q, p, r	Pitch, roll, yaw rate gyros
a_x, a_x, a_y'	Normal, longitudinal, and lateral* acceleration
	Instrument flag signals*
	Rotor speed*
	Rotor cross-shaft torque*
	Differential collective pitch
	Flap position*
	Nacelle (pylon) angle*

} Require logical test for valid range

*Cockpit indications available.

Φ State transition matrix from the decision point to touchdown

Γ Covariance matrix component at touchdown arising from stochastic disturbance inputs acting during the interval from the decision point to touchdown

Θ Mean state vector component at touchdown arising from mean inputs during the interval from the decision point to touchdown

The following relationships (based on linear system theory) hold between quantities just after the decision point and quantities at touchdown:

$$\bar{y}_{TD} = \Phi \bar{y}^{+}_{DP} + \Theta \tag{43}$$

$$D_{TD} = \Phi D^{+}_{DP} \Phi' + \Gamma \tag{44}$$

(These equations may be thought of as the result of integrating Eqs. 37 and 39 between the decision point and touchdown, followed by application of Eqs. 38 and 40.)

It turns out that the imposition of a missed approach decision rule based on approach monitoring criteria has virtually no effect upon $\bar{y}^{+}_{DP}$ and $\bar{y}_{TD}$. Those characteristics are determined mainly by the selection of the nominal approach path, performance characteristics of the aircraft and the basic guidance and control law structure. D_{TD}, the dispersion in key touchdown variables, can be very sensitive to the approach monitoring criteria because D^{+}_{DP} is very sensitive to the approach monitoring criteria. (Recall that D^{-}_{DP} is converted to D^{+}_{DP} by imposing the missed approach decision rule based on the approach monitoring criteria.) The next step consists of identifying those measurement variables (or combinations of variables) in D^{+}_{DP} which affect the key touchdown variables in D_{TD} in a sensitive way. The covariance propagation method of performance evaluation makes numerical evaluations of Γ and Φ available so that this step is really less complex than it might appear. In the final step, the procedure described immediately below is used to convert quantities just prior to the decision point, $(\cdot)_{\bar{DP}}$, to quantities just after the decision point, $(\cdot)^{+}_{DP}$, for a trial set of approach monitoring criteria, and Eq. 44 is used to evaluate dispersion in key touchdown variables. This process is

continued iteratively until approach monitoring criteria satisfying all performance objectives are found. In this latter step, effects of electing missed approach execution or approach continuation on landing performance are evaluated and the missed approach rate is determined. The upper limit placed on the missed approach rate, P_{MA}, is $P_{MA} \leq 0.05$ in this iterative procedure.

Since out-of-tolerance approaches are converted to missed approaches at the decision height in our model, there must also be a correction of the joint probability density function (refer to Eq. 41) for all problem variables at the decision height so that only those approaches which are continued to touchdown are represented. For illustrative purposes only, consider example approach monitoring criteria for indicated distance (DME), X_i, and MLS glide slope deviation, d_e. Let the decision levels for these variables be ±60 ft (±18 m) and ±6 ft (±1.8 m), respectively. Just prior to the decision point the joint probability density function is:

$$[\rho(X_i, d_e, x_3, \ldots x_n, t)]_{\overline{H=50 \text{ ft } (15 \text{ m})}} \tag{45}$$

Just after the decision point it is

$$(1-P_{MA})^{-1} [\rho(X_i, d_e, x_3, \ldots x_n, t)]_{\overline{H=50 \text{ ft } (15 \text{ m})}} \tag{46}$$

for $-60 \leq X_i \leq 60$ and $-6 \leq d_e \leq 6$, and is zero elsewhere. $(1 - P_{MA})$ is the "volume" under the joint probability density function surface (Eq. 41) between the above limits on X_i and d_e. The joint probability density function just after the decision height is obviously non-Gaussian. This non-Gaussian joint probability density function for X_i and d_e is approximated by a Gaussian one having the same first and second moments. The influence of these first and second moments (i.e., the means and variances) upon the mean and covariance for other states is modeled in simulation as the expected outcome of a single discrete Kalman measurement update. The result of this update provides the initial conditions for continuing the solution of Eqs. 37 through 40 from the decision height to touchdown for IMC operations with the missed approach decision rule operative.

B. RESULTS

Recall that the standard deviations of the elements in the y_{TD} vector are square roots of the respective diagonal elements of D_{TD}. Referring to the right hand side of Eq. 44, two terms are apparent. The first term represents that component of D_{TD} which arises because variability in y_{TD} just after the decision point. This component may be modified by changing the approach monitoring criteria. The second term represents that component of D_{TD} which arises because of the stochastic components of turbulence and MLS noise acting between the decision point and touchdown. This component is not affected by the approach monitoring criteria. This component sets the lower bound on the reduction in standard deviations of y_{TD} obtainable via the approach monitoring criteria and the attendant missed approach decision rule.

Tables 15 through 17 summarize the standard deviation for y_{TD} vector in the absence of approach monitoring criteria, $\sqrt{(D_{TD})_{ii}}$, and the lower bound achievable with approach monitoring criteria, $\sqrt{(\Gamma)_{ii}}$. These tables together with Table 13 lead to the following conclusions.

- Dispersion in key variables at touchdown is well within acceptable safe limits in the absence of an approach monitoring criterion and attendant missed approach decision rule (Table 13).
- Potential for reduction in key variable dispersions at touchdown with use of an approach monitoring criterion and attendant missed approach decision rule is slight (Tables 15 through 17).

Regardless of the negative indication of necessity given above, approach monitoring criteria are imposed based on estimates of likely conditions resulting from pilot abuse of the approach and landing system operating procedures. These are given in Table 18. The resulting probability of missed approach assuming normal system use is $P_{MA} = 0.0082$ or a rate of about one in 122 IMC approaches. The significant contributions to P_{MA} are from the second and third items in Table 18 in approximately equal amounts.

In the earlier stages of the final approach missed approach decision levels given in Table 19 are recommended. The resulting probability of missed

TABLE 15

COMPONENTS OF LONGITUDINAL TOUCHDOWN DISPERSION REDUCIBLE BY MISSED APPROACH DECISION RULE AT 50 FT*

VARIABLE	UNITS	KEY AT TOUCHDOWN	STANDARD DEVIATION Total, $\sqrt{(D_{TD})_{ii}}$	STANDARD DEVIATION Minimum, $\sqrt{(\Gamma)_{ii}}$
$\dot{X}$	ft/sec	√	1.58	1.52
$\dot{H}$	ft/sec	√	0.116	0.083
q	deg†/sec		1.49	1.48
θ	deg	√	1.37	1.34
H	ft		1.14	0.396
X	ft	√	6.35	6.25
x_7	in‡		0.315	0.057
δ_{CL}	in.		0.214	0.051
x_9	ft/sec^2		0.663	0.384
x_{10}	in.		0.004	0.00+
$\hat{d}_e$	ft		0.00+	0.00
δ_s	in.		0.320	0.319
θ_c/K_θ	deg		2.45	2.43
x_{14}	in.		0.105	0.105
FD_c	in.		0.115	0.115
θ_{cd}	deg		5.39	5.39
x_{17}	ft/sec		11.0	3.49
d_e	ft		1.33	0.769
~~x_1~~	ft		20.9	20.9

*1 ft = 3.048×10^{-1} m.

†1 deg = 1.745×10^{-2} rad.

‡1 in. = 2.54×10^{-2} m.

TABLE 16

COMPONENTS OF LATERAL TOUCHDOWN DISPERSION REDUCIBLE BY MISSED APPROACH DECISION RULE AT 50 FT*
(VTOL PAD CASE)

VARIABLE	UNITS	KEY AT TOUCHDOWN	STANDARD DEVIATION Total, $\sqrt{(D_{TD})_{ii}}$	STANDARD DEVIATION Minimum, $\sqrt{(\Gamma)_{ii}}$
$\dot{y}$	ft/sec	√	0.227	0.108
p	deg†/sec		0.130	0.125
r	deg/sec	√	0.116	0.111
φ	deg	√	0.625	0.160
ψ	deg		10.9	0.146
y	ft	√	1.26	0.522
δ_{FDS}	in‡		0.606	0.109
$\psi - \psi_s$	deg		0.239	0.146
δ_{LTS}	in.		0.235	0.063
φ_c/K_φ	deg		0.618	0.252
x_{11}	in.		0.007	0.006
FD_L	in.		0.014	0.014
ϵ_y	deg		0.297	0.190
φ_{DC}	deg		0.611	0.208
y_e	ft		0.740	0.502

*1 ft = 3.048×10^{-1} m.

†1 deg = 1.745×10^{-2} rad.

‡1 in. = 2.54×10^{-2} m.

TABLE 17

COMPONENTS OF LATERAL TOUCHDOWN DISPERSION REDUCIBLE BY MISSED APPROACH DECISION RULE AT 50 FT*
(CTOL RUNWAY CASE)

VARIABLE	UNITS	KEY AT TOUCHDOWN	STANDARD DEVIATION Total, $\sqrt{(D_{TD})_{ii}}$	STANDARD DEVIATION Minimum, $\sqrt{(\Gamma)_{ii}}$
$\dot{y}$	ft/sec	√	0.435	0.386
p	deg†/sec		0.594	0.592
r	deg/sec	√	0.129	0.124
φ	deg	√	0.751	0.449
ψ	deg		10.8	0.155
y	ft	√	7.35	1.53
δ_{FDS}	in‡		0.606	0.119
$\psi - \psi_s$	deg		0.244	0.155
δ_{LTS}	in.		0.338	0.251
φ_c/K_φ	deg		1.47	1.36
x_{11}	in.		0.033	0.033
FD_L	in.		0.100	0.100
ϵ_y	deg		1.07	1.05
φ_{DC}	deg		1.19	1.04
y_e	ft		1.15	1.03

*1 ft = 3.048×10^{-1} m.

†1 deg = 1.745×10^{-2} rad.

‡1 in. = 2.54×10^{-2} m.

TABLE 18 .

MISSED APPROACH DECISION LEVELS
(JUST PRIOR TO VERTICAL DESCENT COMMITTMENT)

COCKPIT INDICATION	DECISION LEVEL	MOTIVATION
H	±6 ft* of hover reference altitude	Strong effect on touchdown sink rate
θ	+5.5, −2.5 deg†	Indicative of excessive turbulence and/or wind effects upon airframe ground clearance at touchdown
X_i	±60 ft	Indicative of gross system error
y_e	±15 ft	Indicative of gross system error

TABLE 19

MISSED APPROACH DECISION LEVELS
(FINAL APPROACH)

COCKPIT INDICATION	DECISION LEVEL	MOTIVATION
d_e	±12 ft	Indicative of gross system error
y_e	±24 ft	Indicative of gross system error
$\dot{X}_i$	> 20 kt (33.8 ft/sec)	At hover mode engage

*1 ft = 3.048×10^{-1} m.

†1 deg = 1.745×10^{-2} rad.

approach assuming normal system use is zero during the earlier stages of the final approach.

The data presented above lead to the conclusion that no intricately computed approach monitoring criteria would be beneficial for significantly reducing either the probability of missed approach or touchdown dispersion. Therefore, computer evaluated approach monitoring criteria selected are the same as the pilot evaluated criteria given in Tables 18 and 19.

SECTION VII

PILOTED FIXED BASE SIMULATION RESULTS

An abbreviated fixed base simulation was conducted using the VSTOLAND 1819B airborne computers for the system equations and an EAI 8400 for the equations of motion. The objectives of the simulation were as follows:

- Exercise system in an actual pilot-vehicle environment.
- Identify deficiencies not obvious from analysis and make required system modifications.
- Obtain preliminary evaluation of final system.
- Generate computer program tape of final system to allow direct use in XV-15 version of VSTOLAND.

All of the above objectives were achieved. One qualification is that the complementary filtered position and derived rate information from the VSTOLAND could not be used. This was due to the fact that the derivative relationships between the estimated positions and estimated velocities are not preserved when the values of the states (X, Y and Z) are small. This defect manifested itself as a loss of phase lead in the estimated velocities, and granularity in the estimated positions at low amplitudes. This in turn resulted in continuous low to moderate amplitude oscillations in path. In order to complete the program, the aircraft positions and velocities were taken directly from the equations of motion calculations (bypassing the VSTOLAND navigation equations). For this reason curved paths could not be flown.

Because of time and cost limitations, only the STI project pilot flew the simulation. Certain modifications were made to the system described in Section III. These modifications are discussed in the following subsection. The results of an abbreviated evaluation of the final system are given in Subsection B.

A. SYSTEM MODIFICATIONS

Manned simulation identified necessary refinements for the system described in Section III. These are discussed below.

1. Constant Speed Column Director

Unacceptably large airspeed errors (order of 7 percent) tended to persist even though the pitch flight director bar was kept reasonably centered. The problem turned out to be inadequate resolution on the display [e.g., 4 kt (2 m/s) was only 0.05 in. (0.0013 m) of flight director error]. Increasing the flight director gain (K_{FD_c}) by a factor of 2 resolved the airspeed error problem but resulted in a "twitchy" flight director. This further confirmed the basic requirement that the overall open-loop sensitivity for a K/s pitch flight director should be about 0.4 in./sec (0.0102 m/s) of flight director per inch of stick. (See Section III.) Hence the problem reduces to a fundamental tradeoff between SCAS sensitivity ($K_{\dot{\theta}_c}$) and allowable airspeed errors. Based on limited simulation, it appeared that $K_{\dot{\theta}_c}$ could be reduced by a factor of 2 in order to allow doubling of K_{FD_c}.

> In the final configuration, $K_{\dot{\theta}_c}$ was reduced from 10 deg/sec/in. to 5 deg/sec/in. and K_{FD_c} was increased to 2.86 in./rad (0.073 m/rad).

2. Revised Deceleration Strategy

The constant attitude open-loop deceleration was found to be somewhat unsatisfactory because of flight director display resolution problems and sensitivity to pilot abuses (delay in initiating deceleration, etc.). Fig. 49 shows the effect of holding the flight director bar high or low on the center dot. Both cases result in undesirable transients at transition to the hover mode.

Based on these results it was decided to reinterpret the equation for constant attitude deceleration (derived in Subsection III-H)

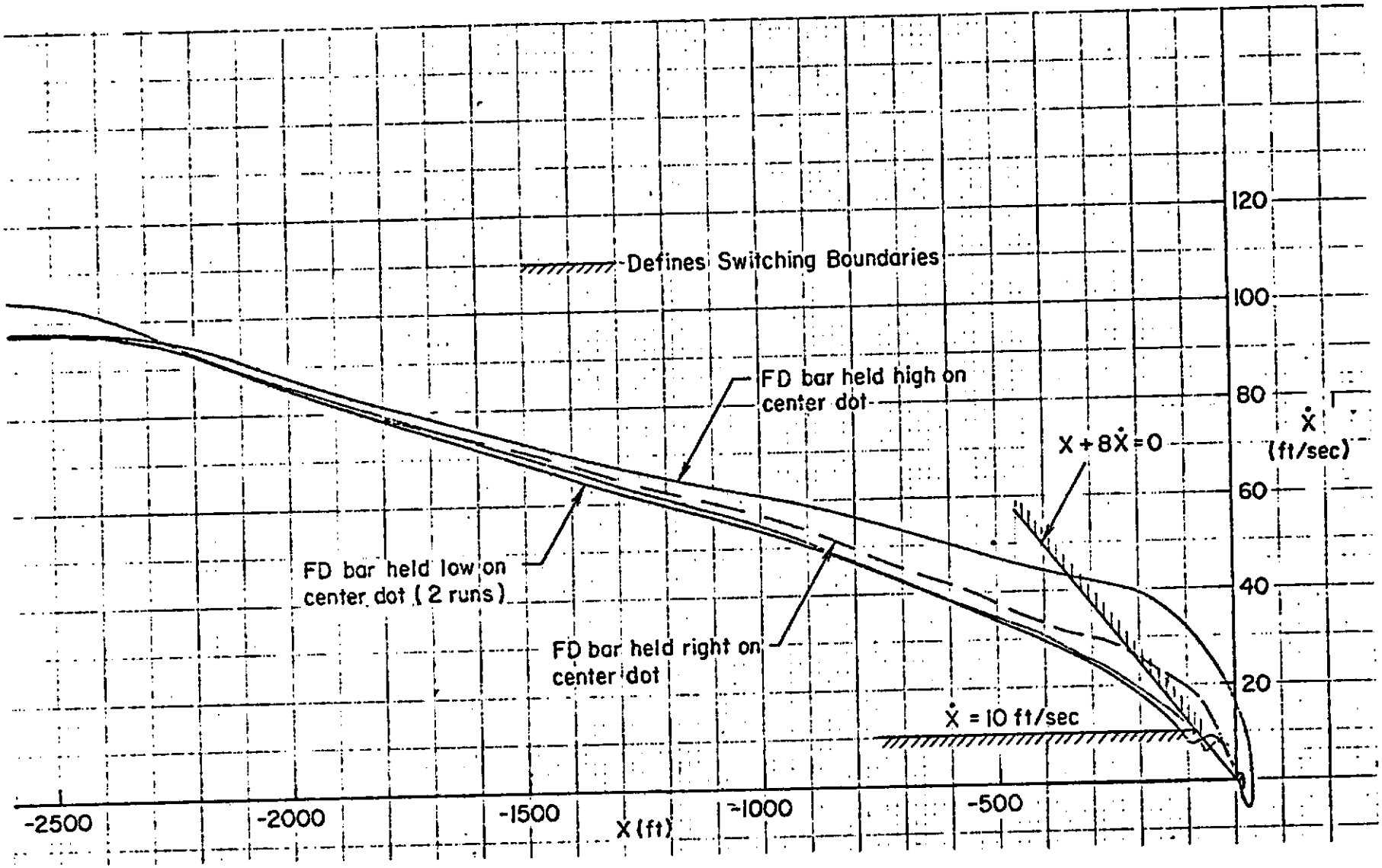

Figure 49. Piloted Simulation Runs Showing Effect of Flight Director Resolution on Deceleration Trajectory — Open Loop Deceleration

$$e_\theta = -x + \frac{57.3}{g\dfrac{d\theta_T}{dV_A}}\left\{\dot{X} + \frac{\theta_{INC}}{\dfrac{d\theta_T}{dV_A}} \ln\left[1 - \frac{\left(\dfrac{d\theta_T}{dV_A}\right)\dot{X}}{\theta_{INC}}\right]\right\} \qquad (47)$$

where $\theta_{INC} = \theta_D - \theta_H$ and $d\theta_T/dV_A$ is the change in trim pitch attitude with air-speed (assumed to be a constant, $K_{\theta VA}$). When $e_\theta \equiv 0$, the aircraft is on a trajectory which corresponds to deceleration at a constant attitude, θ_D. Hence, e_θ is a logical choice for a feedback variable.

> A relatively low feedback gain on e_θ ($K_{e_\theta} = -0.0275$ rad/ft) (−.09 rad/m) yields sufficiently good regulation of e_θ and does not alter the K/s characteristics of the flight director.

An attractive consequence of using e_θ feedback to the pitch flight director arises from the fact that pitch attitude feedback becomes an inner loop. As an inner loop, pitch attitude must be washed out to avoid standoffs. This washout requirement, in turn, results in the constant attitude deceleration mode pitch feedback being the same as for the other modes (airspeed hold and hover). The end result is considerable simplification of the original complex switching and synchronizing used to remove the washout during constant attitude deceleration. (See Fig. 2.)

The effect on the deceleration trajectory of varying the value of θ_{INC} in Eq. 47 is shown in Fig. 50. The trends are according to the analysis in Subsection III-H: increasing θ_{INC} ($\theta_{INC} = \theta_D - \theta_H$) delays the initiation of deceleration. The resulting trajectories are characterized by higher levels of deceleration and shorter deceleration times. An attractive feature of this guidance scheme could be provision of a pilot-selected deceleration level. For example, the pilot may select low θ_{INC}'s for IFR and larger θ_{INC}'s for VFR.

The degree to which constant attitude deceleration is achieved decreases as θ_{INC} increases as shown in the simulation time histories in Fig. 51. This is simply a result of the fact that delays in the initial pitch-up become more critical when the deceleration magnitude is greater and initiated later. Values of θ_{INC} between 1.0 and 1.5 were found to be desirable for IFR decelerations.

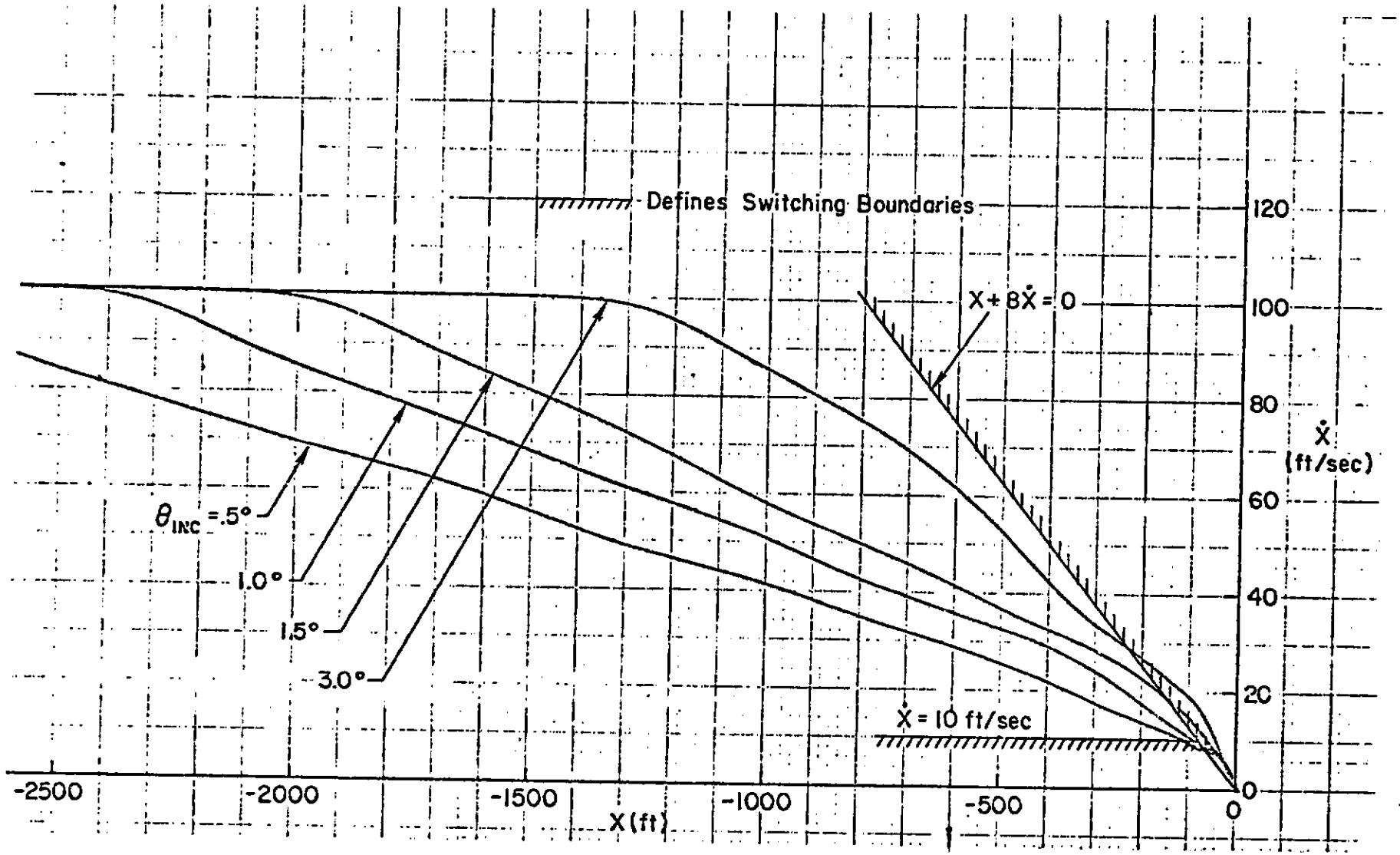

Figure 50. Effect of Deceleration Attitude on Trajectory (Closed-Loop Deceleration)

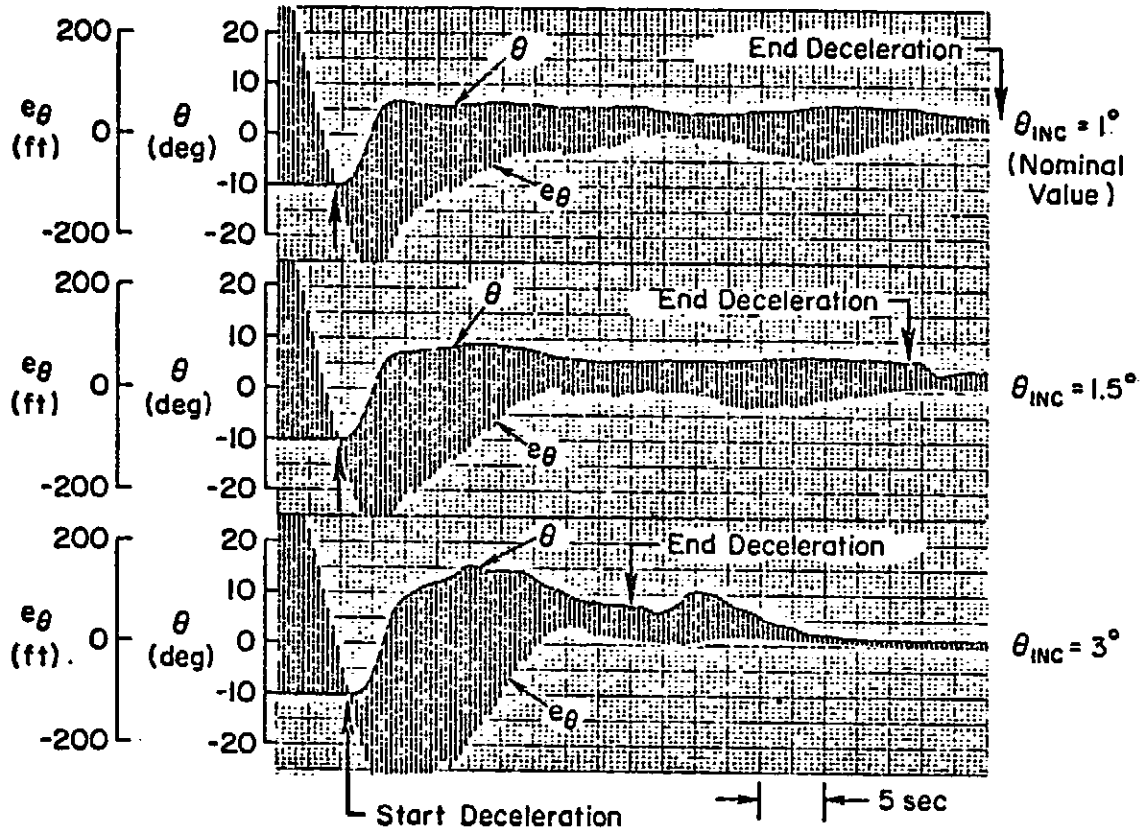

Figure 51. Effect of θ_{INC} on Pitch Attitude and e_θ

The use of e_θ feedback retains the basic philosophy of the open-loop, constant attitude deceleration scheme derived in Subsection III-H. That is, once a value of θ_{INC} is chosen, the deceleration trajectory is invariant with steady winds. (In the case of e_θ feedback the deceleration reference pitch attitude is automatically adjusted in the face of changing winds, whereas in the open-loop case it is calculated only once at initiation of deceleration.) Figure 52 demonstrates that similar trajectories are achieved for winds varying from a 10 kt (5 m/s) tailwind to a 40 kt (21 m/s) headwind.

A primary weakness of the original open-loop deceleration scheme was its inability to cope with wind shear. (See discussion on page 48.) As shown in Fig. 53, the e_θ feedback system does a reasonable job of regulating against a large [2 kt/sec (1 m/s)] decreasing headwind shear.

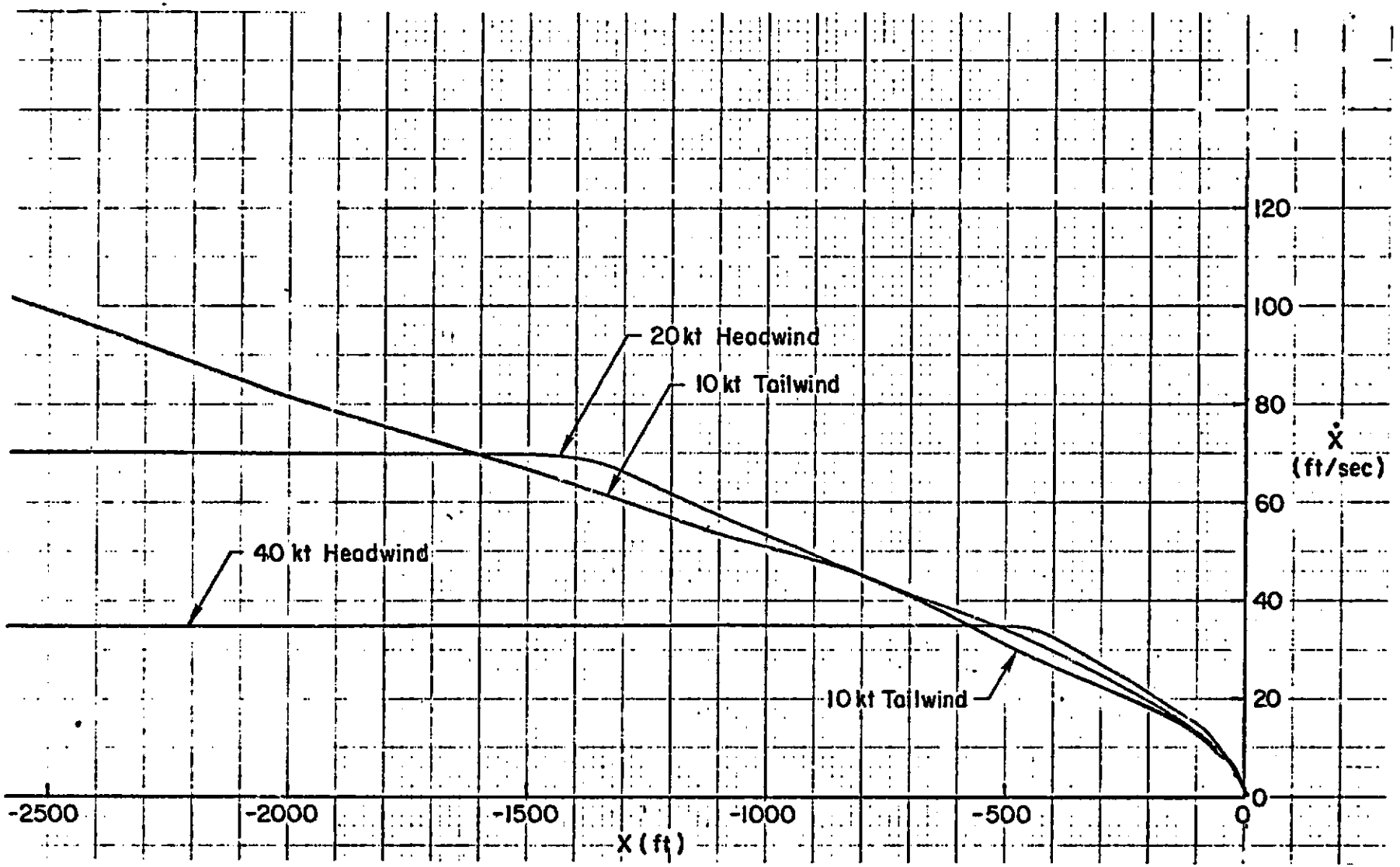

Figure 52. Effect of Steady Winds on Closed-Loop Deceleration Trajectories

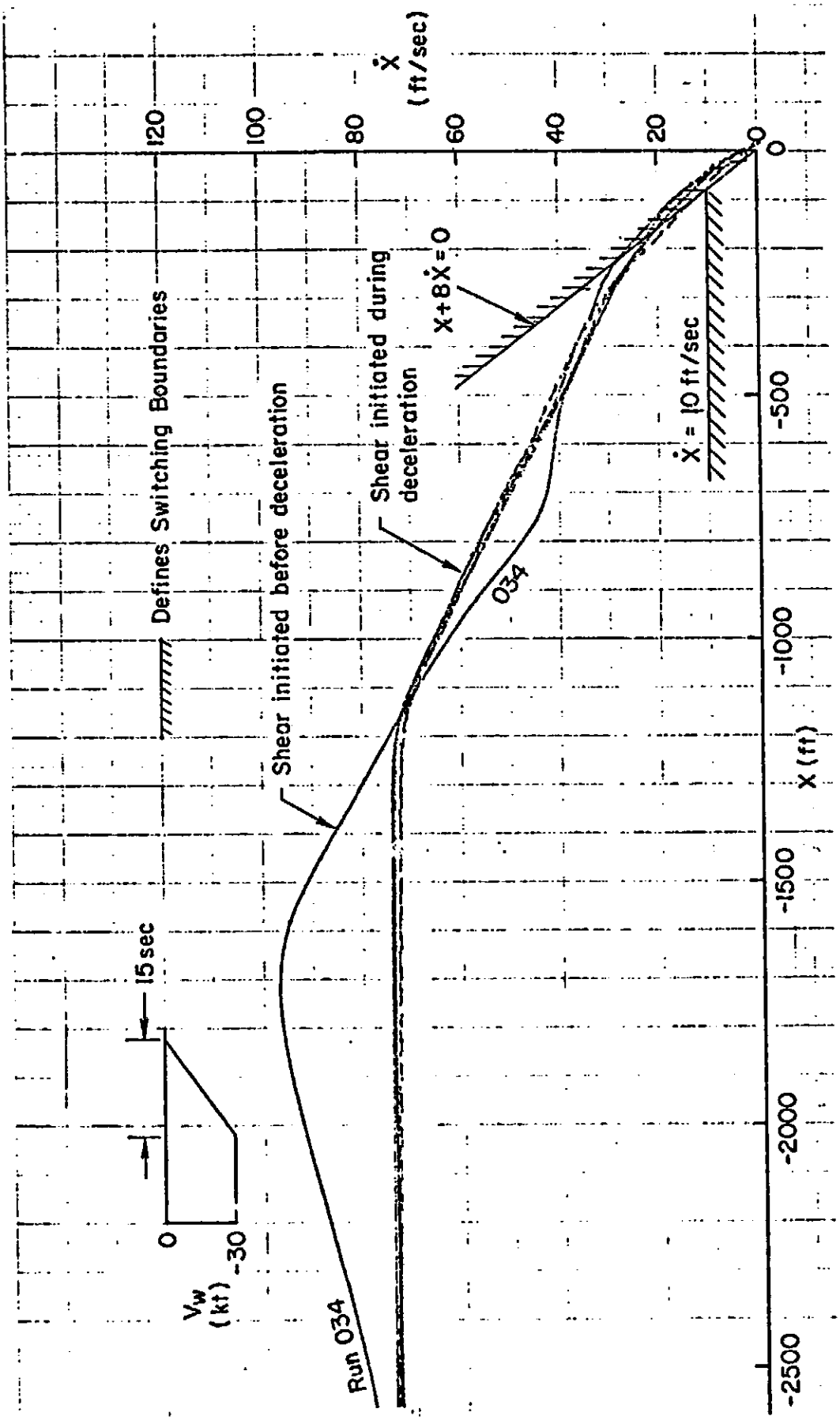

Figure 53. Effect of a Large Decreasing Headwind Shear (Closed-Loop Deceleration)

The value of $d\theta_T/dV_A$ (also called $K_{\theta VA}$) used in Figs. 50 through 53 was −0.0427 deg/(ft/sec) which is somewhat lower than the actual value measured from the XV-15 trim characteristics. To further complicate matters, the trim attitude vs. airspeed obtained from the perturbation simulation differs somewhat from those obtained from the full nonlinear FSAA simulation. These trim characteristics are summarized for a −6 deg (−0 10 rad) flight path angle in Fig. 54 below.

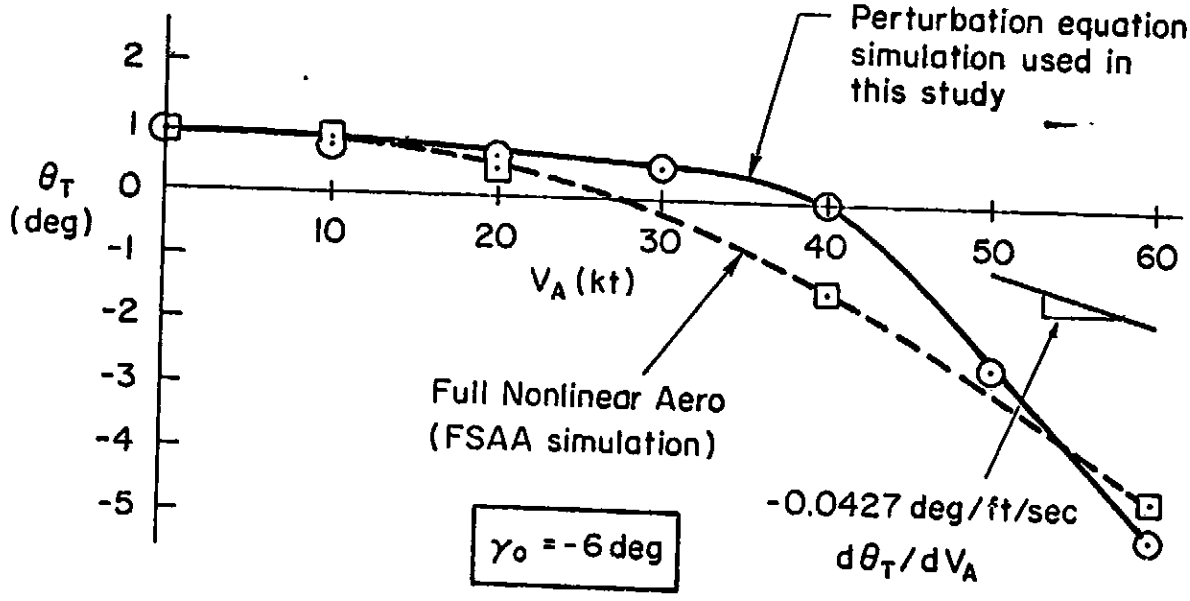

Figure 54. Comparison of Trim Characteristics

From Fig. 54 it can be seen that a value of −0.0427 for $K_{\theta VA}$ is somewhat less than the actual slope ($d\theta_T/dV_A$) in the deceleration region [between 60 and 20 kt (31 and 10 m/s)]. However, increasing $K_{\theta VA}$ tended to decrease the range at which deceleration was initiated. This has the same deleterious effect as increasing θ_{INC}, e.g., attitude is less constant during deceleration. It is believed that this effect is primarily due to delays between commanded and actual pitchup at deceleration initiation. Fortunately, the constant attitude feature of the deceleration guidance scheme is preserved as long as θ_{INC} is not made too large [less than 2 deg (0.035 rad)].

3. $\dot{X}$ Limiter

A limiter was added to prevent large velocity commands when the aircraft is displaced a large distance from the commanded hover position. The limiter is mechanized as shown in Fig. 55 below. The limiter is set so a maximum ground speed of ±20 ft/sec (6 m/s) could be commanded e.g., ±20 $K_{\dot{X}} = X_{LIM} = 160$ ft (48.8 m) .

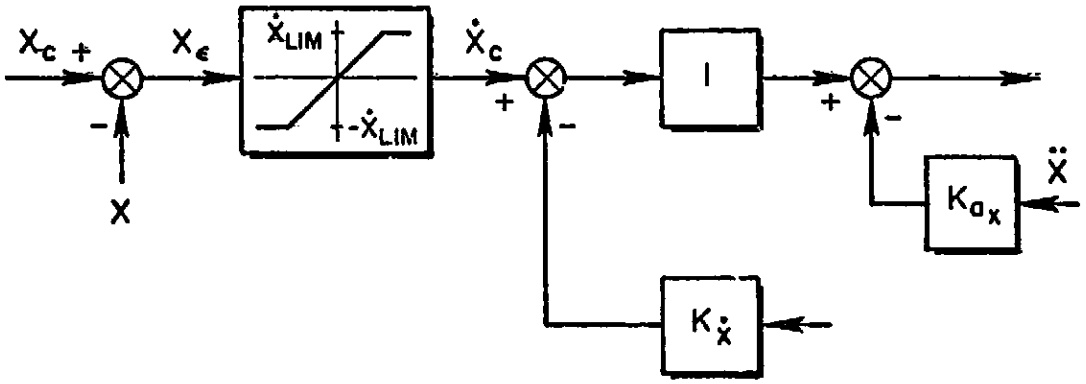

Figure 55. Addition of $\dot{X}$ Limiter

4. Vertical Descent Logic

The "P" blend in Fig. 2 was replaced with a simple switching function. This was necessitated by an undesirable transient output of the integrator (K_{ICL}/s) during the initial phase of vertical descent.

5. Summary Block Diagram

A summary of the status of the longitudinal system at the completion of the piloted simulation program is given in Fig. 56.

B. LIMITED EVALUATION

Some evaluation runs were made by the STI project pilot (Roger Hoh) to assess the performance of the final system. The pilot ratings given must be tempered by the fact that the project pilot played a major role in the system design.

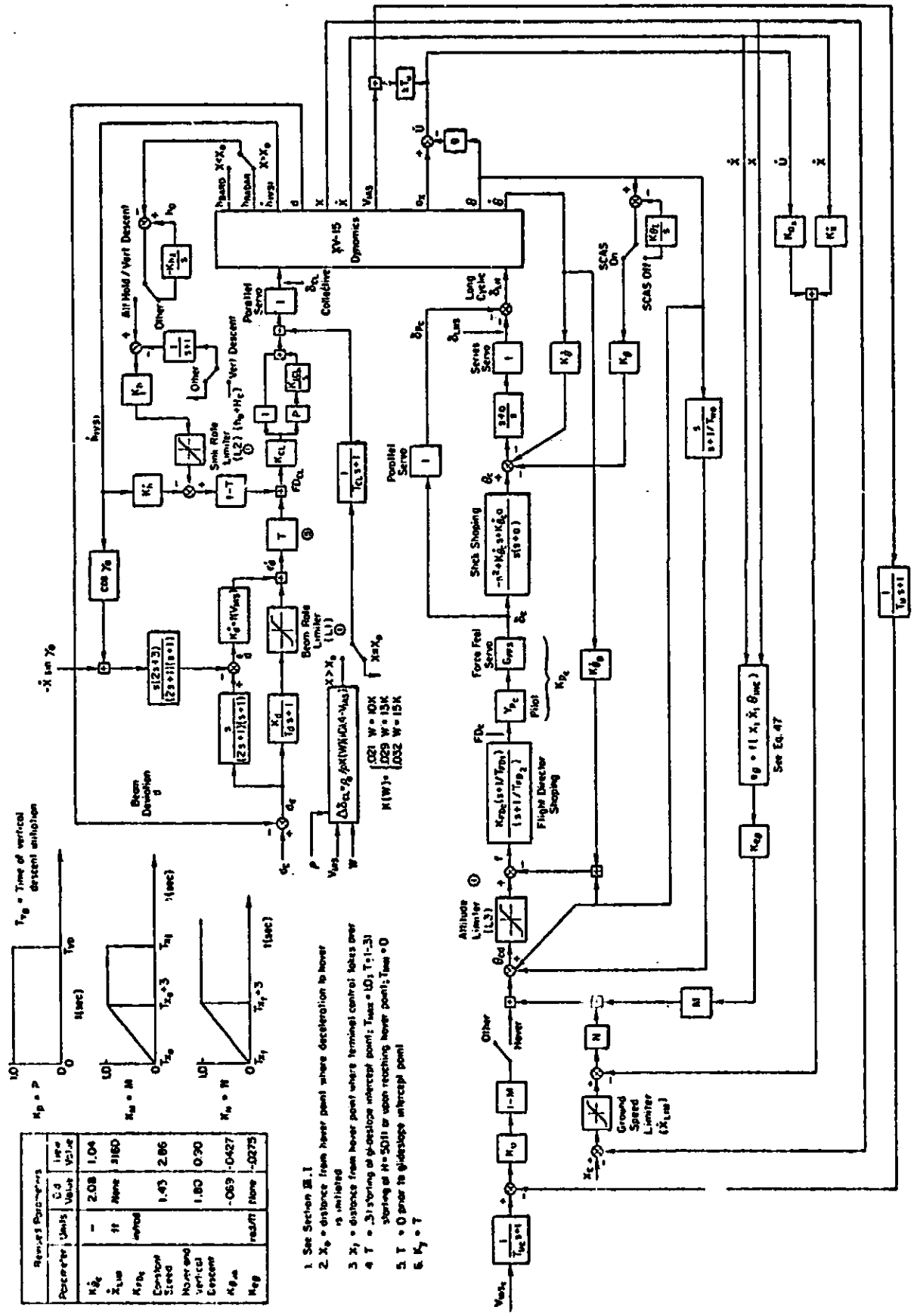

Parameters	Units	C-8 Value	New Value
$K_{\dot{\theta}_c}$	-	2.08	1.04
$\dot{X}_{Limit}$	ft/sec	None	3160
K_{FB_h} Constant Speed		1.45	2.86
Nominal vertical descent		1.80	0.90
$K_{\theta_{ss}}$		-.069	-.0427
K_{FB}	rad/ft	None	-.0275

K_p = P K_m = M K_n = N

Figure 56. Final Longitudinal System at Conclusion of Piloted Simulation

1. Longitudinal System

The longitudinal system performance was found to be excellent by any standard in that the tracking errors were negligible for the following inputs.

- Steady winds varying from a 10 kt (5 m/s) tailwind to a 40 kt (21 m/s) headwind.
- 30 kt (15 m/s) wind shears at a rate of 2 kt/sec (1 m/s/s) (both decreasing and increasing headwind shears). These shears were induced at each phase of the approach.
- 4.5 ft/sec (1.4 m/s) rms turbulence.*
- Large pilot abuses including a 5 sec delay from commanded deceleration to initiation of pitchup.

The measured performance was essentially identical for manual (flight director) and fully automatic approaches on glide slopes varying from 6 deg to 10 deg (0.10 rad to 0.17 rad).

As expected, the ratings and commentary for manual approaches reflect a very high workload situation. For a nominal approach with no disturbances, the Cooper Harper pilot ratings for deceleration and hover were 4-1/2. Addition of the major disturbances listed above had little effect on the ratings. The pilot's major complaints centered on the poor attitude precision during the large attitude maneuver required to decelerate, and the constant attention required on the director during hover. Neither of these deficiencies was unexpected (see Section III) and both are attributable to the design constraint imposed by the very limited authority of the series servos on the XV-15. Marginal attitude precision is attributable to the low attitude bandwidth (see Fig. 3) which must be used to prevent series servo saturation. Use of a rate command SCAS for hover was dictated solely by series

*Subsequent to completion of the manned simulation evaluation, the turbulence representation in the XV-15 simulator math model was found to be invalid. The exact nature of this discrepancy is not known to the authors.

servo saturation. It is well known that attitude command is significantly superior to rate command for hover. (For example, see Ref. 12.) Hence the ratings of 4-1/2 for hover are indicative of the best that can be done with a rate command system when hovering in instrument meteorological conditions (IMC). It is interesting that the ratings vary very little (maximum of 5) with the addition of very large disturbances.

2. Lateral System

The lateral system worked well in a no-disturbance environment. The LOC B mode was especially effective at low speeds [below 60 kt (31 m/s)]. Unfortunately, a problem in the XV-15 simulation math model did not allow evaluations in steady crosswinds. All the problems noted in hover for the longitudinal system also apply for the lateral system.

Time histories showing localizer recapture from a 50 ft (15 m) offset for LOC A and LOC B are shown in Fig. 57.

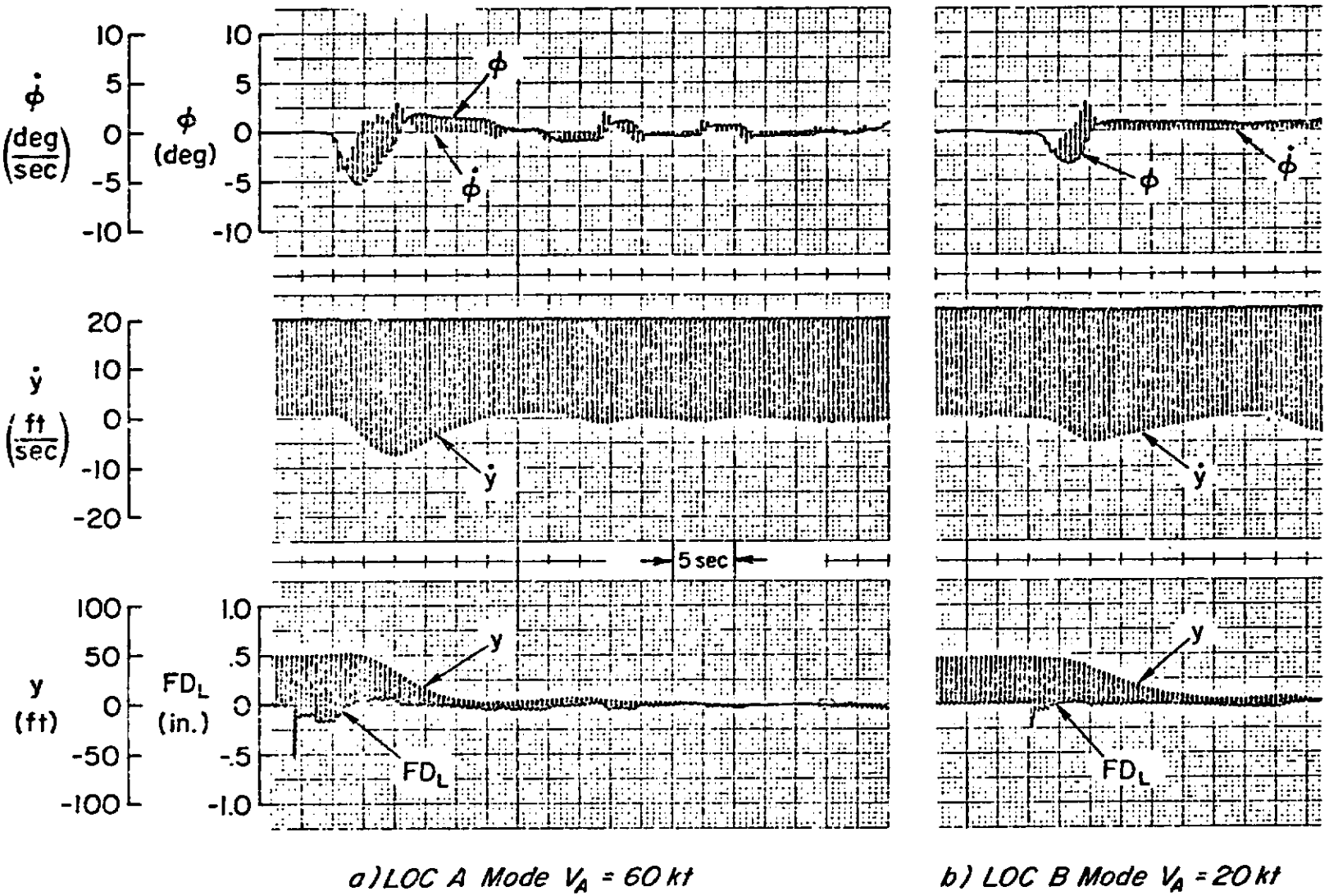

Figure 57. Response of Manual System to 50 ft Lateral Offset

SECTION VIII

CONCLUSIONS

A. BASIC OBSERVATIONS

XV-15 flight path angle on final approach in the helicopter mode is limited in the downward direction by −10 deg (−0.17 rad). Limitation arises from the minimum flight idle power setting which is the usual case for VSTOL aircraft. The −10 deg (−0.17 rad) limit is much more severe than the −30 deg (−0.52 rad) limit originally planned for however.

Significant force-feel system damping ratio increases with decreasing airspeed are undesirable.

The installed "rate command, attitude retention" SCAS is only approximately rate command. "Attitude retention" should not be confused with "attitude hold." The former is a part-time attitude feedback system, while the latter has full-time attitude feedback.

B. DESIGN CONSIDERATIONS

Pilot workload considerations in the flight director mode of operation dictate a maximum of two active director commands. Therefore the collective pitch and pedal control axes are made fully automatic for approach and landing.

Structuring the automatic modes of the approach and landing system in the manner of the manual flight director system is an effective design approach. This consists of replacing the pilot's control function by an automatic system gain coupling each flight director signal into the corresponding force-feel system actuator. All guidance and control and pilot-centered requirements are satisfied by both systems when this approach is used. Furthermore, automatic system operation is similar to the pilot's manual operation of the system. Still further, pilot monitoring of automatic system operation is facilitated by virtue of both systems satisfying the pilot-centered requirements.

Deceleration by means of a constant pitch attitude maneuver during final approach is an effective deceleration strategy which tends to have low workload contribution and acceptable duration (e.g., 45 sec). Required pitch attitudes (and longitudinal acceleration levels) are moderated by adjusting the range at which the constant attitude deceleration maneuver is initiated. Range is adjusted according to estimated wind speed and airspeed. The initiation point and reference pitch attitude are computed such that the range vs. range rate profile is not a function of steady wind speed. The latter two points are essential to viability of this scheme.

Combined lack of directional stability and an aerodynamic sideslip measurement for the XV-15 in the low speed regime requires minor loop heading regulation via the pedal series servo.

Pilot workload considerations indicate "rate command, attitude hold" as the minimum acceptable level of augmentation.

Limited authority of series actuation precludes use of higher levels of augmentation such as "attitude command" or "translational rate command."

Airspeed-to-collective crossfeeding is essential to precise glide path control below the speed for minimum power.

High turn rate sensitivity in a bank-to-turn lateral control mode at low speeds recommends transition to a bank-to-translate mode in this speed regime.

C. PERFORMANCE EVALUATION

Evaluation of landing system performance throughout a decelerating approach to touchdown can be accomplished economically and effectively using non-stationary covariance propagation techniques.

Approach monitoring criteria are required to protect against pilot abuse of normal system operating procedures (blunders). The precision of control attainable with the XV-15 + SCAS + MLS is such that reasonable disturbance levels do not result in violation of criteria for safe touchdown or for pilot acceptance in the case of normal system operation even in the absence of a missed approach decision rule. Therefore approach monitoring criteria are not

required for the usual primary purpose of protecting against unsafe levels of touchdown dispersion. Their usual purpose is to convert out-of-tolerance approaches to missed approaches by means of a missed approach decision rule.

High precision approach path and touchdown point control requires tight MLS guidance coupling. This in turn requires gain scheduling in coupling to the MLS guidance signals because of the range dependency of the guidance noise when expressed in linear units.

D. SIMULATOR EVALUATION

The system was able to regulate against very large disturbances with negligible errors in the longitudinal axis. The lateral axis worked very well but could not be tested against disturbances because of problems with the XV-15 simulation math model. Pilot ratings of 4-1/2 were obtained for hover and deceleration to hover with and without large disturbances. It is felt that these ratings would be improved with a higher bandwidth rate-command, attitude-hold SCAS during deceleration which would undergo conversion to an attitude or translational rate command SCAS in hover. Both of these options were disallowed in the present study due to a very limited series servo authority.

REFERENCES

1. V/STOL Tilt Rotor Research Aircraft, Vol. 1: Performance and Noise Analysis. Rept. No. 301-199-001, Rev. A, Bell Helicopter Co., Nov. 1974.

2. V/STOL Tilt Rotor Research Aircraft, Vol. 3: Structural Loads and Dynamics. Rept. No. 301-199-001, Rev. A, Bell Helicopter Co., Nov. 1974.

3. Bauer, Robert W.: "U.S. Army Experience in Low-Level Night Flight," The Guidance and Control of V/STOL Aircraft and Helicopters at Night and in Poor Visibility. AGARD CP-148, May 1975, pp. 6-1 to 6-6.

4. Barrett, J. N., and R. G. White: "The Flight Development of Electronic Displays for V/STOL Approach Guidance," The Guidance and Control of V/STOL Aircraft and Helicopters at Night and in Poor Visibility. AGARD CP-148, May 1975, pp. 16-1 to 16-16.

5. Radford, Robert C; Schelhorn, E. Arno; Siracuse, Ralph J.; Till, Robert D.; and Wasserman, Richard: Evaluation of XV-15 Tilt Rotor Aircraft for Flying Qualities Research Application. NASA CR-137828, Apr. 1976.

6. Hoh, Roger H.; Klein, Richard H.; and Johnson: Walter A.: Design of a Flight Director/Configuration Management System for Piloted STOL Approaches. NASA CR-114688, Sept. 1973.

7. Hoh, Roger H.; Craig, Samuel J.; and Ashkenas, Irving L.: Identification of Minimum Acceptable Characteristics for Manual STOL Flight Path Control, Vol. I: Summary Report. FAA-RD-75-123(I), June 1976.

8. Garren, John F., Jr.; Kelly, James R.; Sommer, Robert W.; and DiCarlo, Daniel J.: Flight Investigation of VTOL Control and Display Concepts for Performing Decelerating Approaches to an Instrument Hover. NASA TN D-6108, Feb. 1971.

9. Kelly, James R.; Niessen, Frank R.; Thibodeaux, Jerry J.; Yenni, Kenneth R.; and Garren, John F., Jr.: Flight Investigation of Manual and Automatic VTOL Decelerating Instrument Approaches to Landing. NASA TN D-7524, July 1974.

10. Hoh, Roger H.; Klein, Richard H.; and Johnson, Walter A.: Development of an Integrated Configuration Management/Flight Director System for Piloted STOL Approaches. NASA CR-2883, Aug. 1977.

11. Hoh, Roger H.; and Jewell, Wayne F.: Investigation of the Vulnerability of Powered Lift STOL's to Wind Shear. TR-1063-1, Systems Technology, Inc., June 1976.

12. Greif, Richard K.; Fry, Emmett B.; Gerdes, Ronald M.; and Gossett, Terrence D.: Effect of Stabilization on VTOL Aircraft in Hovering Flight. NASA TN D-6900, Aug. 1972.

13. Ringland, Robert F.; Craig, Samuel J.; and Clement, Warren F.: Survey of Piloting Factors in Fixed-Wing V/STOL Aircraft Design. TP 5941, Naval Weapons Center, Feb. 1977.

14. McRuer, D. T.; Ashkenas, I. L.; and D. Graham: Aircraft Dynamics and Automatic Control. Princeton University Press, 1974.

15. Johnson, Walter A.; and DiMarco, Richard J.: Application of an Approach and Landing System Model to the Space Shuttle Orbiter Vehicle. NASA CR-114465, Feb. 1972.

16. DeRusso, P. M.; Roy, R. J.; and Close, C. M.: State Variables for Engineers. Wiley, 1965.

17. Kelly, Robert J.: Guidance Accuracy Considerations for the Microwave Landing Systems. NAECON '76, Bendix Corporation Communications Div., May 18, 1976.

18. Kelly, R. J.: Time Reference Microwave Landing System Multipath Control Techniques. J. of The Institute of Navigation, Vol. 23, No. 1, Spring 1976, pp. 42-

19. Kelly, R. J.; System Design and Flight Test Results of the Bendix/Bell MLS Category II/III Elevation Approach Guidance Function. AIAA Paper 74-909, August 1974.

20. Wind Model for Space Shuttle Simulations. NASA Ames Research Center, circa 1970.

21. Automatic Landing Systems (ALS). FAA AC-20-57A, 12 Jan. 1971.

22. Flying Qualities of Piloted Airplanes. MIL-F-8785B(ASG), 7 Aug. 1969.

23. Chalk, Charles R.; DiFranco, Dante A.; Lebacqz, J. Victor; and Neal, Peter T.: Revisions to MIL-F-8785B(ASG) Proposed by Cornell Aeronautical Laboratory Under Contract F33615-71-C-1254. AFFDL-TR-72-41, Apr. 1973.

APPENDIX A

MODELS USED FOR MLS GUIDANCE; WIND, WIND SHEAR AND TURBULENCE; AND AIRCRAFT

The equations and numerical parameter values actually used in the overall system performance model are summarized in this appendix.

GLIDE SLOPE BEAM ALIGNMENT AND NOISE MODEL

This subsection documents the model of the MLS Glide Slope signal used in the system performance analysis. The model represents the received signal in the aircraft (in distinction to representing the MLS signal in space). Consequently, only the deterministic portion of the received signal model is a function of the receiving antenna location for a given range.

The model of the received signal consists of three components:

- The selected ideal straight path line at angle, Θ, with respect to horizontal in the vertical plane containing the runway centerline
- The deviation of the mean alignment by angle, $\Delta\Theta$, for the actual beam from the ideal above.
- The angular deviation, η, arising from actual beam structure with respect to the mean alignment of the beam.

The first of the above components is deterministic.

The forms for the second and third components of the model are based upon the actual MLS Glide Slope error budget (Table 2 of Ref. 18).

LOCALIZER ALIGNMENT AND NOISE MODEL

The model of the MLS localizer signal to be used in the system performance analysis represents the received signal in the aircraft. Consequently, only the deterministic portion of the received signal model is a function of the receiving antenna location for a given range.

The model of the received signal consists of three components:

- The selected ideal straight course line at angle Ψ with respect to the extended runway centerline as measured in a horizontal plane.
- The deviation of the mean alignment, $\Delta\Psi$, of the MLS localizer guidance reference in a horizontal plane with respect to the selected course line in azimuth.
- The angular deviation, ν, arising from irregularities in the localizer course structure with respect to the beam mean alignment.

The first of the above components is deterministic. The forms for the second and third components of the model are based upon the actual MLS Localizer error budget (Table 2 of Ref. 18).

Alignment Errors

The alignment errors represent biases or mean deviations which vary from facility-to-facility over a relatively narrow range. These errors can, in principle, be reduced to zero by adjusting the elevation or azimuth transmitting antenna pattern. However, from one approach and landing to the next the value of the mean deviation changes in the simulation model in order to represent a population of MLS facilities. The models for these components are given in Table A-1. Alignment error effects are negligible, therefore alignment errors are not included in the system performance analyses.

Noise Errors

The noise errors represent stochastic disturbances arising from in-beam multipath effects. It represents the variability about the mean deviation which causes a noisy deviation signal to be received. This component is represented in the model by a power spectral density consistent with the actual MLS error budget for multipath effects falling within the aircraft path response bandwidth. The models for these noise components are given in Table A-2.

TABLE A-1

MIS GUIDANCE ERROR MODEL FOR ALIGNMENT (BIAS)

Alignment (Bias) Error (2σ)

Elevation	0.06 deg*[1.4 ft† MGA at 1145 ft]
Azimuth	0.044 deg [9.0 ft MGA at 13000 ft]

Alignment Error Math Models

Elevation

State equation and mean initial value

$$\dot{\Delta\Theta} = 0 \quad , \quad \overline{\Delta\Theta}(0) = 0$$

Initial value for variance of $\Delta\Theta$

$$\sigma^2_{\Delta\Theta} = (0.022)^2 = 4.84 \times 10^{-4} \text{ deg}^2$$

Azimuth

State equation and mean initial value

$$\dot{\Delta\Psi} = 0 \quad , \quad \overline{\Delta\Psi}(0) = 0$$

Initial value for variance of $\Delta\Psi$

$$\sigma^2_{\Delta\Psi} = (0.03)^2 = 9.0 \times 10^{-4} \text{ deg}^2$$

*1 ft = 3.048×10^{-1} m.

†1 deg = 1.745×10^{-2} rad.

TABLE A-2

MLS GUIDANCE ERROR MODEL FOR NOISE
(IN-BEAM MULTIPATH)

"Path Following" (Low Frequency) Fluctuations

Passband: (Assumed constant power spectral density in interval cited, zero elsewhere)

Elevation Passband

0 to 1.0 rad/sec

Azimuth Passband

0 to 0.5 rad/sec

Assumed approach inertial speed is 200 ft†/sec

Level (2σ):

Elevation

0.07 deg‡ [1.4 ft MGA at 1145 ft]

Azimuth

0.04 deg [9.0 ft MGA at 13000 ft]

Fluctuation Math Models

Elevation

State equation and mean initial value

$$\dot{\eta} = -|V_T^*|/L_\eta \eta + \sigma_\eta \sqrt{2|V_T^*|/L_\eta}\, w_1 \quad , \quad \bar{\eta}(0) = 0$$

Inertial speed is V_T^*

Fluctuation scale length is L_η = 200 ft

Standard deviation is σ_η = 0.07 deg

Independent, zero mean, unit white noise is w_1

Azimuth

State equation and mean initial value

$$\dot{\nu} = -|V_T^*|/L_\nu \nu + \sigma_\nu \sqrt{2|V_T^*|/L_\nu}\, w_5 \quad , \quad \bar{\nu}(0) = 0$$

Inertial speed is V_T^*

Fluctuation scale length is L_ν = 400 ft

Standard deviation is σ_ν = 0.04 deg

Independent, zero mean, unit white noise is w_5

---

†1 ft = 3.048×10^{-1} m.
‡1 deg = 1.745×10^{-2} rad.

Distance Measuring Equipment (DME) Errors

The DME output is assumed to contain zero bias (Ref. 19). Fluctuations are budgeted to have a 2σ error of 40 ft (12 m) (Ref. 19) over a zero to 2 rad/sec rectangular passband (Ref. 17). The DME error, X_c, is modeled by the following differential equation and parameter values

$$\dot{X}_c = -\omega_c X_c + \sigma_{X_c}\sqrt{2\,\omega_c}\; w_4 \quad , \quad \bar{X}_c(0) = 0 \qquad \text{(A-1)}$$

where w_4 is an independent, zero mean, unit white noise. The standard deviation is σ_{X_c} = 20 ft (6 m). The half-power frequency is ω_c = 2. rad/sec.

WIND, WIND SHEAR, AND TURBULENCE MODELS

This subsection documents models for the atmospheric disturbance environment which forms part of the overall system performance model.

The atmospheric disturbance environment model represents disturbances of three types. These are the mean wind, wind shear and stochastic turbulence. All three types are characterized by parameters which are a function of altitude, and which themselves are possibly random variables.

The mean wind and wind shear are deterministic disturbances for any one approach and landing operation. However, from one approach and landing to the next, the level of the mean wind and wind shear is a random selection from a Gaussian distribution having a particular mean and standard deviation. These disturbances are therefore properly applied to the stochastic portion of the system performance model. The turbulence is a stochastic disturbance. The turbulence is therefore applied to the stochastic portion of the system performance model.

Mean Wind and Wind Shear (Ref. 15 and 20)

Headwind Component

The headwind component, u_w, of the steady headwind profile of Ref. 20 is used. This results in a profile whose magnitude is determined by a random

selection from Gaussian distribution. Thus, for any given approach and landing, the profile is fixed, but from one approach to the next the profile changes. A sample profile is shown in Fig. A-1. To obtain any other profile, it is only necessary to scale up (or scale down) the wind magnitude. Conveniently, any particular profile can be completely determined by specifying the magnitude at a given reference altitude. For the purpose of discussion, a wind reference altitude of 10 ft (3 m) will be selected. This corresponds to the approximate altitude of the center of gravity for a typical aircraft at the instant of touchdown. At this altitude the wind magnitude varies from a 10 kt (5 m/s) tailwind to a 26 kt (13 m/s) headwind ($\pm 3\sigma$) and has mean value of 8 kt (4 m/s). These values are consistent with the design values specified by the FAA in Ref. 21.

The probability density function for the mean wind, u_W, is a Gaussian distribution with mean and standard deviation given by:

$$\overline{u_W} = F_W e^{-h^*/H_W}(D_W \log_{10} h^* + E_W)/(D_W + E_W) \qquad \text{(A-2)}$$

$$\sigma_{u_W} = 0.75\ \overline{u_W} \qquad \text{(A-3)}$$

where

$$F_W = 13.5 \text{ ft/sec (8 kt) (4.1 m/s)} \qquad \text{(A-4)}$$

$$D_W = 0.43$$

$$E_W = 0.35$$

$$H_W = 10{,}000 \text{ ft (3048 m)}$$

and

$$h^* = H + h_{ocg}$$

H is the altitude of the main landing gear wheels and h_{ocg} is the aircraft c.g. altitude at touchdown. The mean wind $\overline{u_W}$ has the following shear characteristics (Ref. 20).

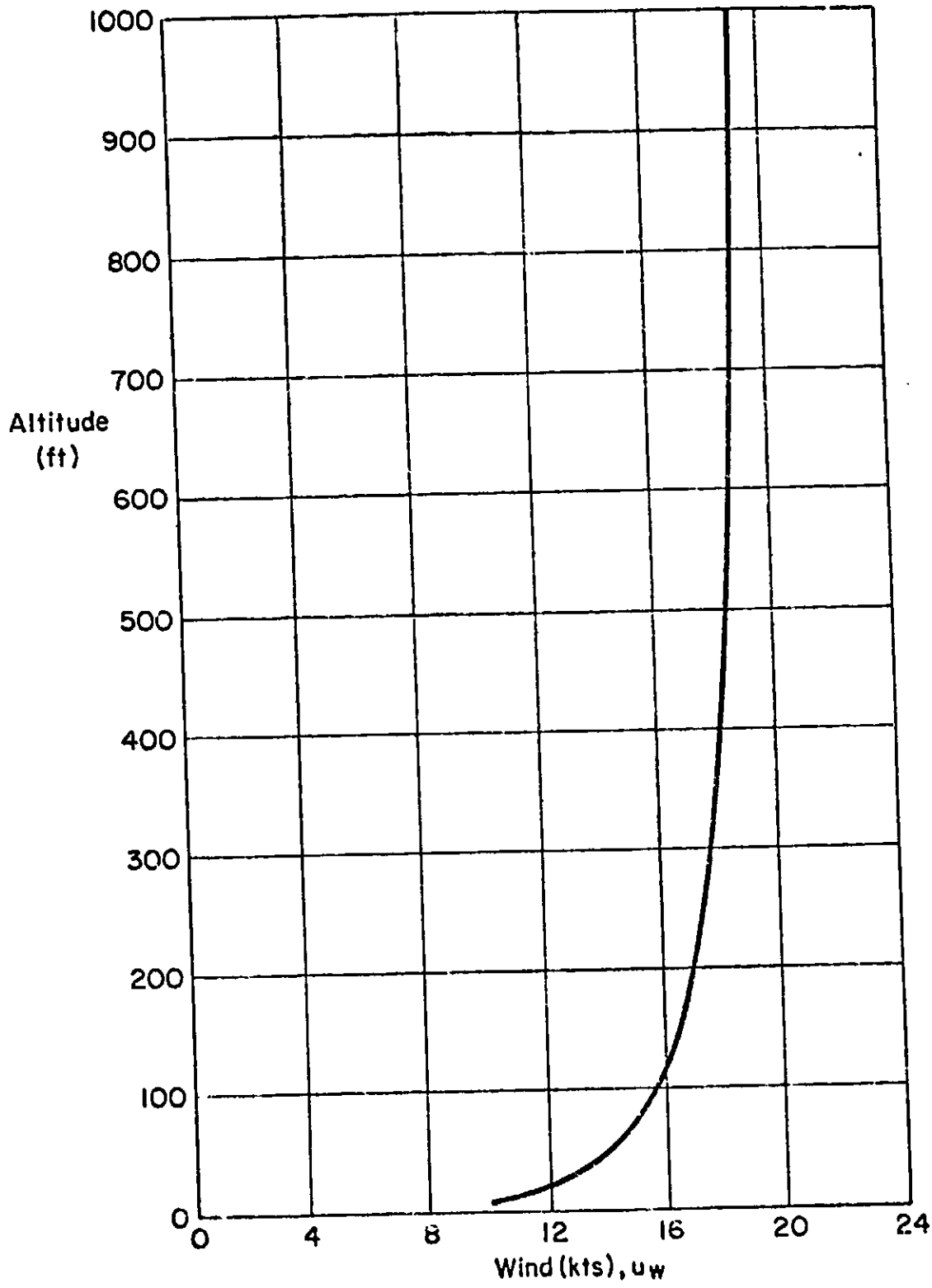

Figure A-1. Wind Profile Associated with 10 kt (5 m/s) Wind at 10 ft (3 m) Altitude (From Ref. 16)

TABLE A-3. SHEAR CHARACTERISTICS

h* (ft)	SHEAR	
	ft/sec/100 ft†	kt‡/100 ft
10	39.2	23.2
100	3.92	2.32
300	1.31	0.77

†1 ft = 3.048×10^{-1} m
‡1 kt = 5.14×10^{-1} m/s

These characteristics also tend to be consistent with 1/3 of the 8 kt/100 ft (30 m) specified by the FAA in Ref. 21 at an altitude of 100 ft (30 m). However, the increasing shear with decreasing altitude of the present model poses a more severe but perhaps more realistic environment than does the Ref. 21 model.

The state equation for modeling the reference value of the steady headwind and its mean initial condition are

$$\dot{u}_{wo} = 0 \; ; \; \overline{u_{wo}} = V_{HW_o} \text{ ft/sec} \tag{A-5}$$

where the initial value of the mean headwind V_{HW_o} is:

$$V_{HW_o} = \frac{F_w[D_w \log_{10} (H_o + h_{ocg}) + E_w]e^{-(H_o + h_{ocg})/H_w}}{D_w + E_w} \tag{A-6}$$

H_o is the initial altitude of the main landing gear wheels. The initial condition for the covariance equation is

$$E[u_{wo}^2] = \sigma_{\dot{u}_{wo}}^2 \tag{A-7}$$

where

$$\sigma_{u_{wo}} = \frac{0.75F_w(D_w \log_{10} [H_o + h_{ocg}] + E_w)e^{-[H_o + h_{ocg}]/H_w}}{D_w + E_w} \tag{A-8}$$

The headwind profile is then given by

$$u_w = K_w u_{wo}$$

where

$$K_w = K_w(H) = \frac{(D_w \log_{10} h^* + E_w)e^{-h^*/H_w}}{(D_w \log_{10} [H_o + h_{ocg}] + E_w)e^{-[H_o + h_{ocg}]/H_w}} \qquad \text{(A-9)}$$

Crosswind Component

The probability density function for the crosswind, v_w, is a Gaussian probability density function with a zero mean and standard deviation:

$$\bar{v}_w = 0 \qquad \text{(A-10)}$$

$$\sigma_{v_w} = J_w e^{-h^*/H_w}(D_w \log_{10} h^* + E_w)/(D_w + E_w) \qquad \text{(A-11)}$$

$$J_w = 8.455 \text{ ft/sec (5 kt) (2.574 m/s)} \qquad \text{(A-12)}$$

This model results in 3σ crosswind components of ±15 kt (7.7 m/s) at an altitude of 10 ft (3 m).

The state equation for modeling the reference value of the steady crosswind and its mean initial condition are

$$\dot{v}_{wo} = 0 \; ; \; \bar{v}_{wo} = 0 \qquad \text{(A-13)}$$

The initial condition for the covariance equation is

$$E[v_{wo}^2] = \sigma_{v_{wo}}^2 \qquad \text{(A-14)}$$

where

$$\sigma_{v_{wo}} = \frac{J_w(D_w \log_{10} [H_o + h_{ocg}] + E_w)e^{-[H_o + h_{ocg}]/H_w}}{D_w + E_w} \qquad \text{(A-15)}$$

The wind profile is then given by

$$v_w = K_w v_{wo} \tag{A-16}$$

where

$$K_w = K_w(H) = \frac{(D_w \log_{10} h^* + E_w)e^{-h^*/H_w}}{(D_w \log_{10} [H_o + h_{ocg}] + E_w)e^{-[H_o + h_{ocg}]/H_w}} \tag{A-17}$$

Random Turbulence Model (Ref. 22)

Longitudinal Components

The model for random turbulence is a simplified version of that given in Ref. 22. Gradient effects associated with the normal turbulence component are neglected. For any one approach the random turbulence components have Gaussian probability density functions with zero means. The standard deviation σ_{u_g} should be chosen for each approach from a Rayleigh probability density function* having a characteristic speed of $\sigma_{\sigma_{u_g}}$ ft/sec. However, for the sake of simplicity, the mean value of σ_{u_g}, which is $\sigma_{\sigma_{u_g}}$, is used for all approaches in the overall system performance model.

$$\sigma_{u_g} = \sigma_{\sigma_{u_g}} = 2.79 - 0.245 \log_{10} h^* \text{ ft/sec} \qquad h^* > 100 \text{ ft (30 m)}$$

$$= 2.3 \text{ ft/sec (0.7 m)} \qquad h^* \leq 100 \text{ ft (30 m)} \tag{A-18}$$

The standard deviation σ_{w_g} is a function of σ_{u_g}. The frequency content of the random turbulence and $\sigma_{\sigma_{u_g}}$ are functions of altitude.

*The Rayleigh probability density function is for u_g (rather than w_g as stated in Ref. 22. This reinterpretation is based on Ref. 23, paragraph 3.7.3, A, 1.

The power spectral densities for the longitudinal and normal random turbulence components at a given altitude are respectively:

$$\Phi_{u_g} = \frac{\sigma_{u_g}^2 2V_{A_o}/L_u}{\omega^2 + (V_{A_o}/L_u)^2} \tag{A-19}$$

$$\Phi_{w_g} = \frac{\sigma_{w_g}^2 2(1.594V_{A_o}/L_w)}{\omega^2 + (1.594V_{A_o}/L_w)^2} \tag{A-20}$$

where $$\sigma^2 = \frac{1}{2\pi}\int_{-\infty}^{\infty} \Phi \, d\omega \tag{A-21}$$

Φ_{w_g} is a lower order approximation to the power spectral density given in Ref. 23. The approximation is such that the mean-square level and half-power frequency are preserved.

The differential equations for unit-white-noise shaping filters producing output variables u_g and w_g having power spectral densities Φ_{u_g} and Φ_{w_g} respectively are:

$$\dot{u}_g = -|V_{A_o}^*|/L_u u_g + \sigma_{u_g}\sqrt{2|V_{A_o}^*|/L_u}\, w_2 \tag{A-22}$$

$$\dot{w}_g = -1.594|V_{A_o}^*|/L_w w_g + \sigma_{w_g}\sqrt{2(1.594)|V_{A_o}^*|/L_w}\, w_3 \tag{A-23}$$

where w_2 and w_3 are independent, zero-mean, unit white noises. V_{A_o} is the trim approach airspeed.

The integral scale lengths L_u and L_w are given as functions of altitude h^* by

$$L_u = 145[h^*]^{1/3} \qquad 100 \le h^* \le 1750 \text{ ft } (533 \text{ m})$$

$$= 145[100]^{1/3} = 673 \qquad h^* \le 100 \text{ ft } (30 \text{ m}) \qquad \text{(A-24)}$$

$$L_w = h^* \qquad h^* \le 1750 \text{ ft } (533 \text{ m}) \qquad \text{(A-25)}$$

The standard deviation for the normal turbulence component σ_{w_g} is related to the standard deviation for the longitudinal turbulence component σ_{u_g} through the integral scale lengths.

$$\sigma_{w_g} = \sqrt{L_w/L_u}\ \sigma_{u_g} \qquad \text{(A-26)}$$

The random turbulence model is used in the stochastic portion of the system performance model throughout the approach and landing.

Lateral Components

The model for random turbulence is a simplified version that given in Ref. 22. Gradient effects associated with the lateral turbulence component are neglected. For any one approach the random turbulence components have normal probability density functions with zero means. The standard deviation σ_{v_g} is chosen from a Rayleigh probability density function having a characteristic speed of $\sigma_{\sigma_{v_g}}$ ft/sec. The frequency content of the random turbulence and $\sigma_{\sigma_{v_g}}$ are functions of altitude.

The power spectral density for the lateral random turbulence components at a given altitude is:

$$\Phi_{v_g}(\omega) = \frac{\sigma_{v_g}^2\ 2(1.594)V_{A_o}/L_v}{\omega^2 + (1.594\ V_{A_o}/L_v)^2} \qquad \text{(A-27)}$$

$\Phi_{v_g}(\omega)$ is a lower order approximation to the power spectral density given in Ref. 22. The approximation preserves the half-power frequency and mean-square level.

The differential equation for a unit-white-noise shaping filter producing v_g having a power spectral density Φ_{v_g} is

$$\dot{v}_g = -1.594|V_A^*|/L_v v_g + \sigma_{v_g}\sqrt{2(1.594)|V_A^*|/L_v}\, w_6 \qquad \text{(A-28)}$$

where w_6 is an independent unit-white-noise. V_A^* is the approach airspeed.

The integral scale length $L_v = L_u$. The standard deviation σ_{v_g} is related to the standard deviation for the longitudinal turbulence component σ_{u_g} through the integral scale lenghts, viz.,

$$\sigma_{v_g} = \sqrt{L_v/L_u}\ \sigma_{u_g} \qquad \text{(A-29)}$$

which reduces to

$$\sigma_{v_g} = \sigma_{u_g} \qquad \text{(A-30)}$$

The Rayleigh probability density function for σ_{v_g} is <u>independent</u> of that for σ_{u_g}, but otherwise identical in formulation to that given by Eq. A-18.

This random turublence model is used in the stochastic portion of the system performance model throughout the approach and landing.

Spanwise gradient effects associated with the normal turbulence component will be represented by the simplified model of rolling gust velocity in Ref. 22. The power spectral density for this rolling turbulence component at a given altitude is

$$\Phi'_{p_g}(\Omega) = \frac{\sigma_w^2}{L_w}\,\beta\,\frac{0.8\left(\frac{\pi L_w}{4b}\right)^{1/3}}{1+\left(\frac{4b}{\pi}\,\Omega\right)^2} \tag{A-31}$$

where

$$\sigma^2 \triangleq \int_0^\infty \Phi'(\Omega)\,d\Omega \tag{A-32}$$

$$\Omega = \omega/V_A^* \tag{A-33}$$

$$\Phi'_{p_g}(\omega) = \frac{1}{V_A}\,\Phi'_{p_g}\left(\frac{\omega}{V_A^*}\right)$$

$$= \sigma_{w_g}^2\,\frac{0.8\,(\pi/4b)^{7/3}\,(V_A^*/L_w^{2/3})}{\left[\omega^2+(\pi\,V_A^*/4b)^2\right]} \tag{A-34}$$

If

$$\sigma^2 \triangleq \frac{1}{2\pi}\int_{-\infty}^{\infty}\Phi(\omega)\,d\omega \tag{A-35}$$

then $\Phi_{p_g}(\omega) = \pi\,\Phi'_{p_g}(\omega)$

$$= \sigma_{w_g}^2\,\frac{0.8\,\pi\,(\pi/4b)^{7/3}\,(V_A^*/L_w^{2/3})}{\left[\omega^2+(\pi\,V_A^*/4b)^2\right]} \tag{A-36}$$

The differential equation for a corresponding unit-white-noise p_g-filter is

$$\dot{p}_g = -(\pi|V_A^*|/4b)p_g + \sigma_{w_g}\sqrt{0.8\ \pi(\pi/4b)^{7/3}(|V_A^*|/L_w^{2/3})}\ \ w_7 \tag{A-37}$$

where w_7 is an independent unit-white-noise. b is the reference wing span. The effective value of σ_{p_g} is

$$\sigma_{p_g} = \sigma_{w_g}\frac{\sqrt{0.4\ \pi}\ (\pi/4b)^{2/3}}{L_w^{1/3}}\ \text{(rad/sec)} \tag{A-38}$$

so that the differential equation for the p_g shaping filter might be written in the alternative form

$$\dot{p}_g = -(\pi|V_A^*|/4b)p_g + \sigma_{p_g}\sqrt{2(\pi|V_A^*|/4b)}\ \ w_7 \tag{A-39}$$

AIRCRAFT LONGITUDINAL MOTION MODEL

The method used for system performance analysis requires that equations of motion for the aircraft be in state vector form, include the pertinent kinematic equations, and that appropriate measures be taken to incorporate steady wind effects. All of these considerations force some minor changes upon the customary equations-of-motion model.

The next three subsections cover in turn the kinematic equations, incorporation of deterministic wind effects and the final set of state equations for the aircraft and kinematics plus auxiliary equations for sensor inputs which are not states.

Kinematic Equations

The scenario for the system performance model is shown in Fig. A-2. A perfectly level runway is assumed. Figure A-3 defines the perturbed coordinates for the aircraft body axes with respect to the unperturbed (or nominal) coordinates. Kinematic equations locating the aircraft center of gravity with respect to the apparent source of the MLS Glide Slope and with respect to the runway are

$$\dot{X} = V_{T_o}^* \cos \gamma_o + u \cos \theta_o^* + w \sin \theta_o^* - (U_o^* \sin \theta_o^* - W_o^* \cos \theta_o^*)\theta \tag{A-40}$$

$$\dot{H} = V_{T_o}^* \sin \gamma_o + \theta(U_o^* \cos \theta_o^* + W_o^* \sin \theta_o^*) + u \sin \theta_o^* - w \cos \theta_o^* \tag{A-41}$$

$$U_o^* = V_{T_o}^* \cos (\theta_o^* - \gamma_o) \tag{A-42}$$

$$W_o^* = V_{T_o}^* \sin (\theta_o^* - \gamma_o) \tag{A-43}$$

Additional kinematic relationships of interest are

$$d = H \cos \gamma_o - X \sin \gamma_o - 50. \cos \gamma_o \tag{A-44}$$

$$R = \sqrt{H^2 + (X + 50/\tan \gamma_o)^2} \tag{A-45}$$

$$d_e = d_c - d = R\eta - d \tag{A-46}$$

R is the distance between the aircraft GPIP in Fig. A-3.

The steady wind* acts in the horizontal direction only. For a given airspeed, V_{A_o}, and flight path angle, γ_o, and steady headwind, V_{HW}, the

*The "steady wind" V_{HW} is here taken as the mean value of the wind u_w in the system performance model. See the second subsection of this appendix for a description of the mean wind.

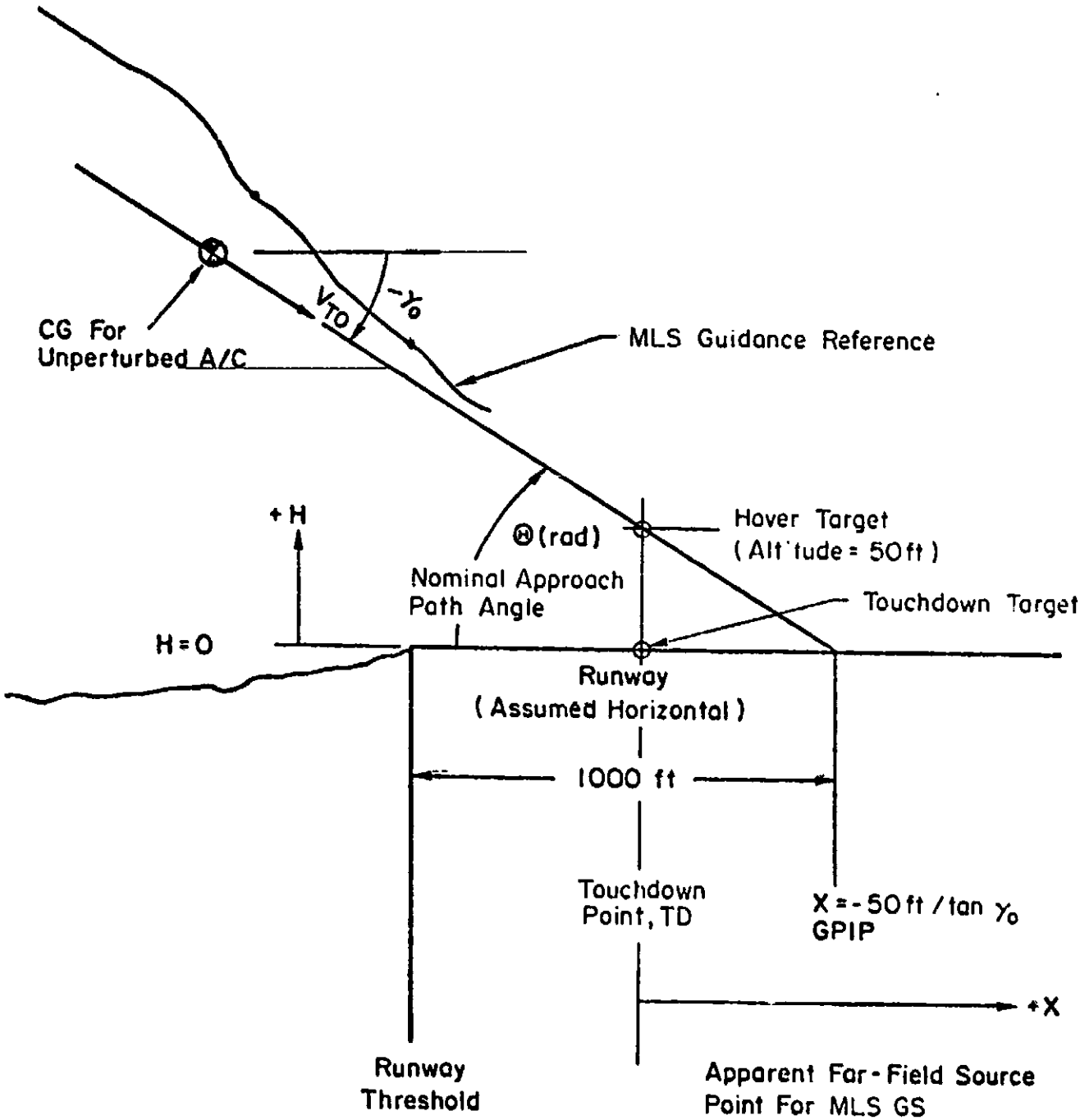

Figure A-2. Scenario for Approach and Landing for System Performance Analysis

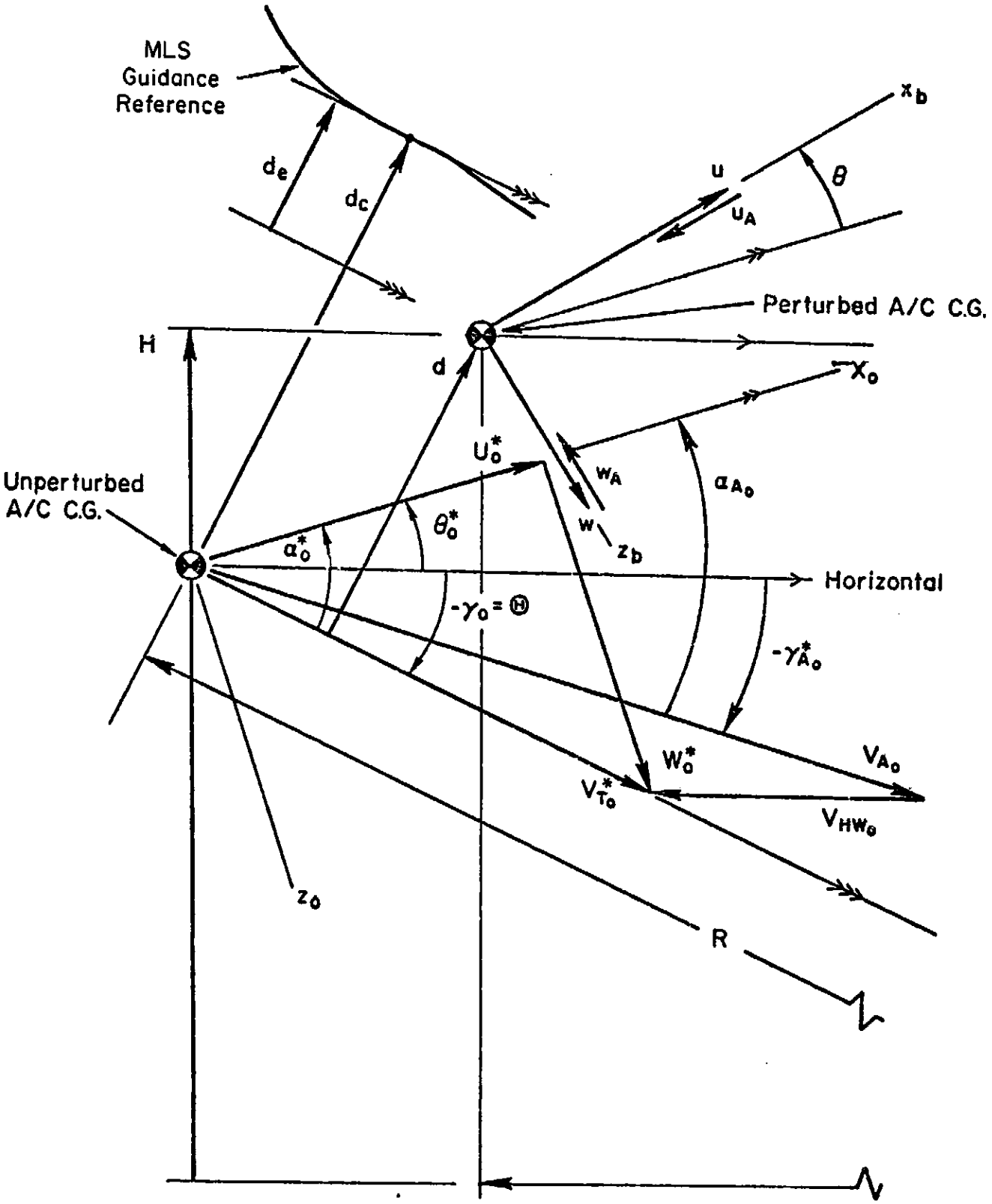

Figure A-3. Perturbed Coordinates Locating the Aircraft

corresponding steady inertial speed, $V^*_{T_o}$, and aerodynamic flight path angle, $\gamma^*_{A_o}$, are

$$V^*_{T_o} = \sqrt{V^2_{A_o} + V^2_{HW} \sin^2 \gamma_o} - V_{HW} \cos \gamma_o \tag{A-47}$$

$$\gamma^*_{A_o} = \sin^{-1} \frac{(\sqrt{V^2_{A_o} + V^2_{HW} \sin^2 \gamma_o} - V_{HW} \cos \gamma_o) \sin \gamma_o}{V_{A_o}} \tag{A-48}$$

When the steady headwind is zero, then $V_{A_o} = V^*_{T_o} = V_{T_o}$, $\theta^*_o = \theta_o$, $\gamma^*_{A_o} = \gamma_o$, $\alpha^*_o = \alpha_o$, $U^*_o = U_c$, and $W^*_o = W_o$ where the unstarred qualities have the customary definitions.

Deterministic Wind Effects

The mean wind and wind shear components of the atmospheric disturbance environment act in a horizontal direction and therefore must be resolved into aircraft body-fixed axis coordinates for proper application via the aircraft equations of motion. Let the longitudinal and normal components (with respect to body-fixed axes) of the deterministic atmospheric disturbance environment be designated u_A and w_A, respectively.

$$u_A = -u_w \cos (\theta^*_o + \theta) \doteq -u_w(\cos \theta^*_o - \theta \sin \theta^*_o) \tag{A-49}$$

$$w_A = -u_w \sin (\theta^*_o + \theta) \doteq -u_w(\sin \theta^*_o + \theta \cos \theta^*) \tag{A-50}$$

u_w represents the mean wind and wind shear component described in the second subsection of this appendix. The linearized approximate expressions for u_A and w_A are used in the system performance model. u_A and w_A enter the equations of motion in the manner of u_g and w_g.

State and Output Equations for the Aircraft

Aircraft perturbation equations of motion are customarily expressed in terms of states u, w, q and θ. Assuming $Z_{\dot{w}} = 0$ and neglecting normal gust gradient effects, the aircraft state equations are (Ref. 14)

$$\dot{u} = X_u u + X_w w - W_o^* q + (V_{HW_o} K_w X_w^{\square} - g \cos \theta_o^*)\theta + X_{\delta_{LN}}\delta_{LN} + X_{\delta_{CL}}\delta_{CL} - X_u u_g - X_w w_g + X_u^{\square} w u_{wo} - X_u^{\square} V_{HW_o} \quad ; \quad u(0) = 0 \tag{A-51}$$

$$\dot{w} = Z_u u + Z_w w + U_o^* q + (V_{HW_o} K_w Z_w^{\square} - g \sin \theta_o^*)\theta + Z_{\delta_{LN}}\delta_{LN} + Z_{\delta_{CL}}\delta_{CL} - Z_u u_g - Z_w w_g + Z_u^{\square} K_w u_{wo} - Z_u^{\square} V_{HW_o} \quad ; \quad w(0) = 0 \tag{A-52}$$

$$\dot{q} = (M_u + M_{\dot{w}} Z_u)u + (M_w + M_{\dot{w}} Z_w)w + (M_q + M_{\dot{w}} U_o^*)q + V_{HW_o} K_w (M_w^{\square} + M_{\dot{w}} Z_w^{\square})\theta + (M_{\delta_{LN}} + M_{\dot{w}} Z_{\delta_{LN}})\delta_{LN} + (M_{\delta_{CL}} + M_{\dot{w}} Z_{\delta_{CL}})\delta_{CL} - (M_u + M_{\dot{w}} Z_u)u_g - (M_w + M_{\dot{w}} Z_w)w_g + (M_u^{\square} + M_{\dot{w}} Z_u^{\square}) K_w u_{wo} - (M_u^{\square} + M_{\dot{w}} Z_u^{\square}) V_{HW_o} \quad ; \quad q(0) = 0 \tag{A-53}$$

$$\dot{\theta} = q \tag{A-54}$$

where

$$X_u^{\square} = X_u \cos \theta_o^* + X_w \sin \theta_o^* \qquad \text{(A-55)}$$

$$Z_u^{\square} = Z_u \cos \theta_o^* + Z_w \sin \theta_o^* \qquad \text{(A-56)}$$

$$M_u^{\square} = M_u \cos \theta_o^* + M_w \sin \theta_o^* \qquad \text{(A-57)}$$

and

$$X_w^{\square} = X_w \cos \theta_o^* - X_u \sin \theta_o^* \qquad \text{(A-58)}$$

$$Z_w^{\square} = Z_w \cos \theta_o^* - Z_u \sin \theta_o^* \qquad \text{(A-59)}$$

$$M_w^{\square} = M_w \cos \theta_o^* - M_u \sin \theta_o^* \qquad \text{(A-60)}$$

The airspeed equation is

$$V_A = V_{T_o}^* \cos (\gamma_{A_o}^* - \gamma_o) + u \cos (\theta_o^* - \gamma_{A_o}^*) - u_g \cos (\theta_o^* - \gamma_{A_o}^*)$$
$$+ w \sin (\theta_o^* - \gamma_{A_o}^*) - w_g \sin (\theta_o^* - \gamma_{A_o}^*) - \theta V_{HW_o} K_w \sin \gamma_{A_o}^*$$
$$+ u_{w_o} K_w \cos \gamma_{A_o} \qquad \text{(A-61)}$$

The output equation for $\dot{H}$ is given above with the kinematic equations.

Numerical Data for Example Aircraft and Kinematic Constants

Numerical stability and control data for the XV-15 aircraft (Fig. A-4) is given in Table A-4 for flight path angles of −6 and −10 deg (−0.10 and −0.17 rad) and airspeeds of 0, 20, 40, 60 and 80 kt (0, 10, 21, 31 and 41 m/s). Numerical trim map data is given in Table A-5. Linear interpolations between data points are used to compute $\theta_o^*(V_{A_o}^*, \gamma_{A_o}^*)$ and $\delta_{CL_o}^*(V_{A_o}^*, \gamma_{A_o}^*)$ trim values.

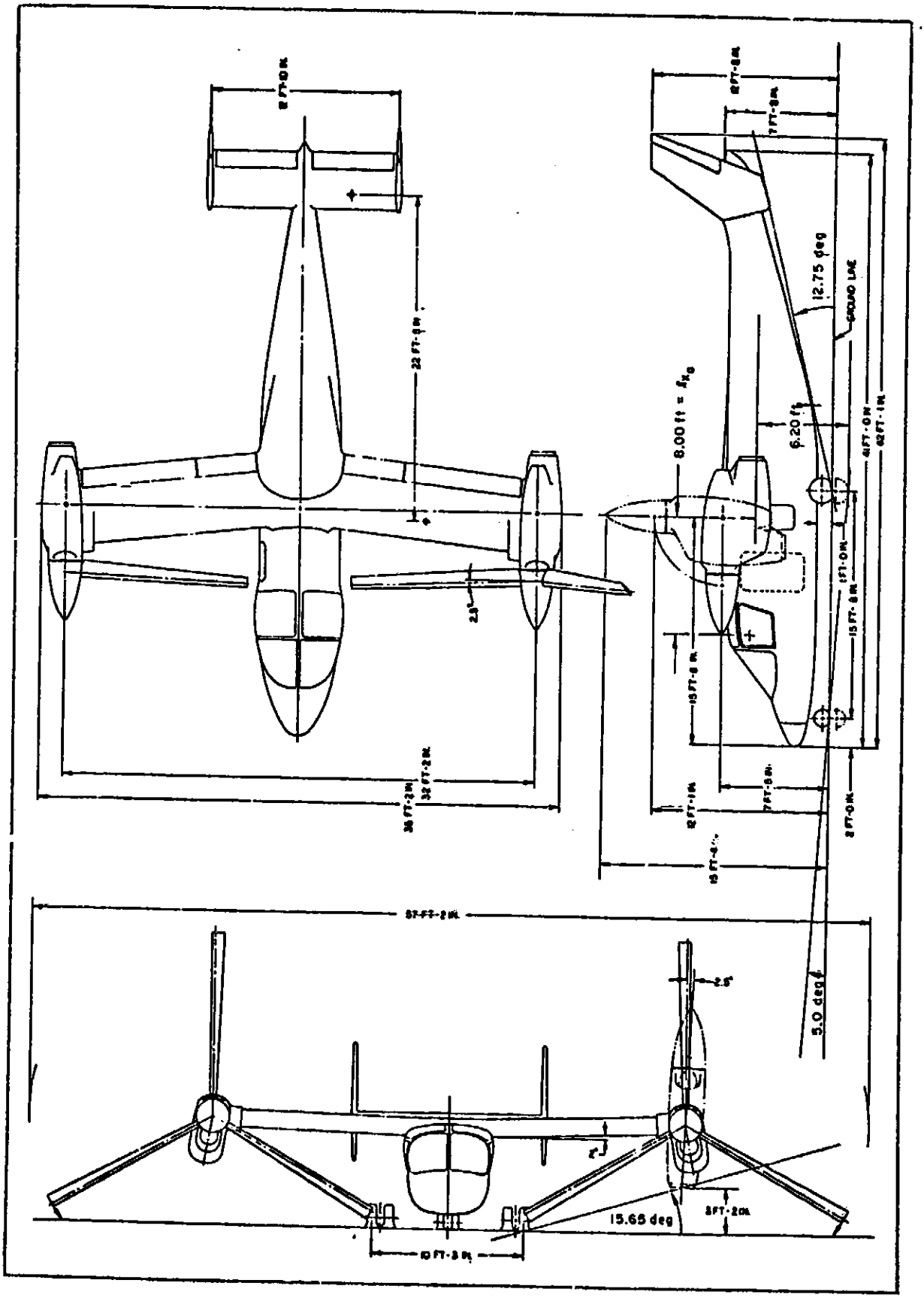

Figure A-4. XV-15 Three-View

TABLE A-4. XV-15 LONGITUDINAL DERIVATIVES (FULL HELICOPTER MODE)

UNITS										
ft*/sec	V_{A_o}	1.0	33.8	67.6	101.4	135.2	33.8	67.6	101.4	135.2
kt†	V_{A_o}	0	20	40	60	80	20	40	60	80
deg	α_o	2.2	6.5	4.5	1.6	−2.0	10.7	4.4	6.0	−1.8
deg	γ_o	0	−6.0	−6.0	−6.0	−6.0	−10.0	−10.0	−10.0	−10.0
1/sec	X_u	0.0	−.029	−.04	−.054	−.059	−.028	−.040	−.052	−.060
1/sec	Z_u	−.027	−.142	−.211	−.186	−.152	−.155	−.227	−.200	−.165
1/sec	M_u	.0014	+.00042	−.00473	+.0028	+.0071	.0028	−.0025	.0025	+.014
—	$Z_{\dot{w}}$	—	—	—	—	—	—	—	—	—
1/ft	$M_{\dot{w}}$	—	—	—	—	—	—	—	—	—
1/sec	X_w	+.0028	+.017	+.029	+.014	+.035	.015	+.035	.041	+.0016
1/sec	Z_w	−.203	−.300	−.466	−.547	−.680	−.260	−.455	−.580	−.681
1/sec-ft	M_w	0.0	−.029	−.022	+.0093	−.0076	−.0069	−.013	.003	−.0036
1/sec	M_q	−.429	−.879	−1.24	−1.43	−2.00	−.850	−1.18	−1.26	−1.39
ft/sec^2/in.	$X_{\delta_{LN}}$	+1.21	+1.20	+1.06	+.947	+.792	1.19	+1.23	.905	.705
ft/sec^2/in.	$Z_{\delta_{LN}}$	−.022	+.308	+.562	+.935	+1.29	.314	+.570	.950	1.34
1/sec^2/in.	$M_{\delta_{LN}}$	−.277	−.308	+.360	−.409	−.462	−.304	−.343	−.377	−.446
ft/sec^2/in.	$X_{\delta_{CL}}$	+.064	.035	−.04	−.199	+.152	.021	−.071	−.153	−.475
ft/sec^2/in.	$Z_{\delta_{CL}}$	−4.06	−4.03	−4.10	−4.51	−4.82	−4.00	−4.03	−4.41	−4.82
1/sec^2/in.	$M_{\delta_{CL}}$	+.0028	+.0094	0.0	−.033	−.032	.012	+.0044	.0051	+.0080
1/sec^2	$M_{\dot{\alpha}}$	0	−.98	−1.49	+.638	−1.02	−.23	−.879	+.304	−.487

*1 ft = 3.048×10^{-1} m.
†1 kt = 5.144×10^{-1} m/s.

TABLE A-5

TRIM DATA (W = 13000 lb)

V_{A_o} kt[a]	V_{A_o} ft[b]/sec	θ^*_o deg	$\gamma^*_{A_o}$ deg	$\delta^*_{CL_o}$ %	$\delta^*_{CL_o}$ in.	$\delta^*_{LN_o}$ in.
2	3.38	2	0	80	5.02	0.0
28	47.32	0	↓	62.5	4.08	↓
42	70.98	-2	↓	51	3.45	↓
57	96.33	-4	↓	45	3.13	↓
68	114.92	-6	↓	45	3.13	↓
79	133.51	-8	↓	48	3.29	↓
94	158.86	-10	0	56.5	3.75	0.0
1.75	2.96	2	-6	80	5.02	0.0
26	43.94	0	↓	61	3.99	↓
40	67.60	-2	↓	45	3.13	↓
55	92.95	-4	↓	33	2.48	↓
68.5	115.77	-6	↓	29	2.27	↓
80.5	136.05	-8	↓	29	2.27	↓
96	162.24	-10	-6	33	2.48	0.0
1.5	2.54	2	-12	80	5.02	0.0
24	40.56	0	↓	60	3.94	↓
37.5	63.38	-2	↓	40	2.86	↓
55	92.95	-4	↓	21	1.83	↓
71	119.99	-6	↓	11.5	1.32	↓
85	143.65	-8	↓	9	1.19	↓
101	170.69	-10	-12	9.5	1.21	0.0

[a] 1 kt = 5.144×10^{-1} m/s.

[b] 1 ft = 3.048×10^{-1} m.

The trim value for $\delta^*_{LN_o}$ was taken as zero for all conditions. The data for Table A-5 was obtained from Fig. 10 supplied by NASA.

The kinematic constants of interest are the initial unperturbed altitude of the wheels above the runway, H_o, and the pilot-selected Glide Slope angle, Θ, which is also equal to the negative of trimmed flight path angle, γ_o. Values for these are

$$H_o = 340 \text{ ft (104 m) for } \gamma_o = -6 \text{ deg}, \quad 500 \text{ ft (152 m) for } \gamma_o = -10 \text{ deg} \tag{A-62}$$

$$\gamma_o = -6.0, -10.0 \text{ deg } (-0.10, -0.17 \text{ rad}) \tag{A-63}$$

$$X_o = (H_o - 50)/\tan \gamma_o \text{ ft} \tag{A-64}$$

X_o is the initial location of the (unperturbed) aircraft, e.g., in the horizontal direction with respect to the touchdown point. The initial altitude of the aircraft c.g. above the touchdown point is $H_o + h_{ocg}$.

AIRCRAFT LATERAL-DIRECTIONAL MOTION MODEL

Kinematic Equations

The scenario for the system performance model is shown in Fig. A-5. A perfectly level runway is assumed. Figure A-6 defines the perturbed coordinates for the aircraft body axes with respect to the unperturbed (or nominal) coordinates. The longitudinal kinematic location of the aircraft center of gravity with respect to the touchdown point is obtained as a tabular function as the result of exercising the longitudinal model. The following mean value data is collected at 2 sec intervals and stored in a file: t, H, X, R, $(V_{A_o} + u_{AS}) = V_A$, $(\theta^*_o + \theta) = \theta^*$ and $(V^*_{T_o} + u) = V^*_T$.

Kinematic equations locating the aircraft center of gravity laterally with respect to the extended runway centerline are

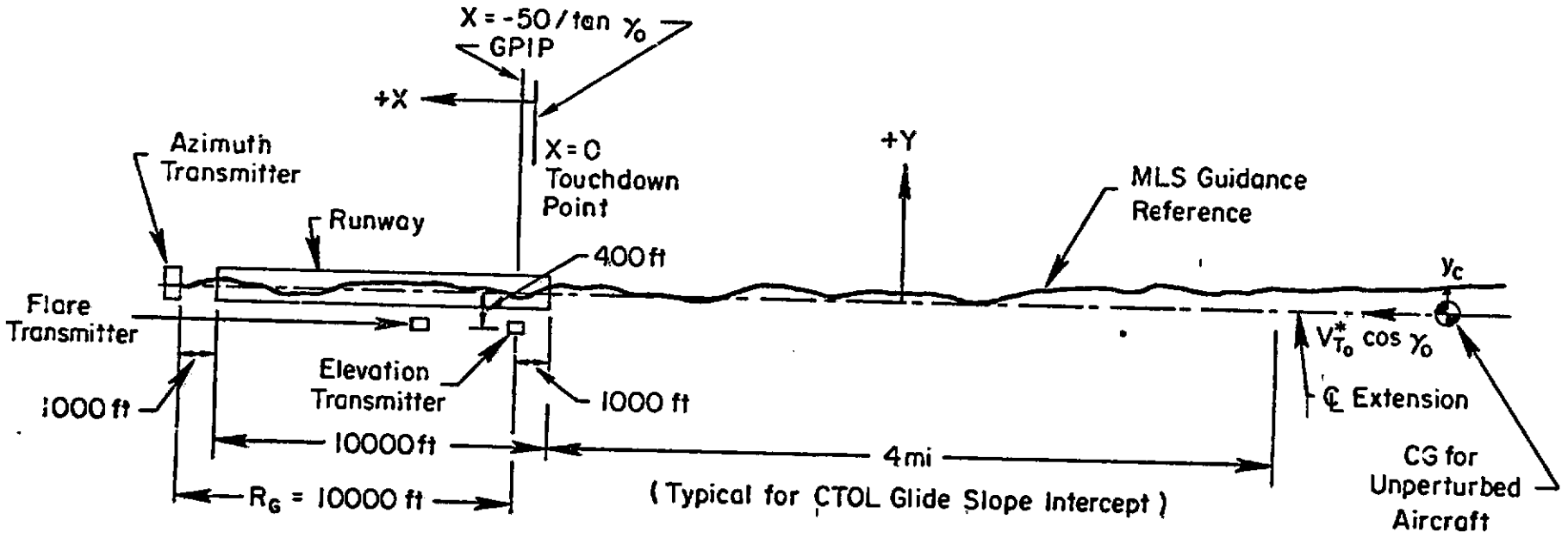

Figure A-5. Typical MLS Geometry for CTOL Runway

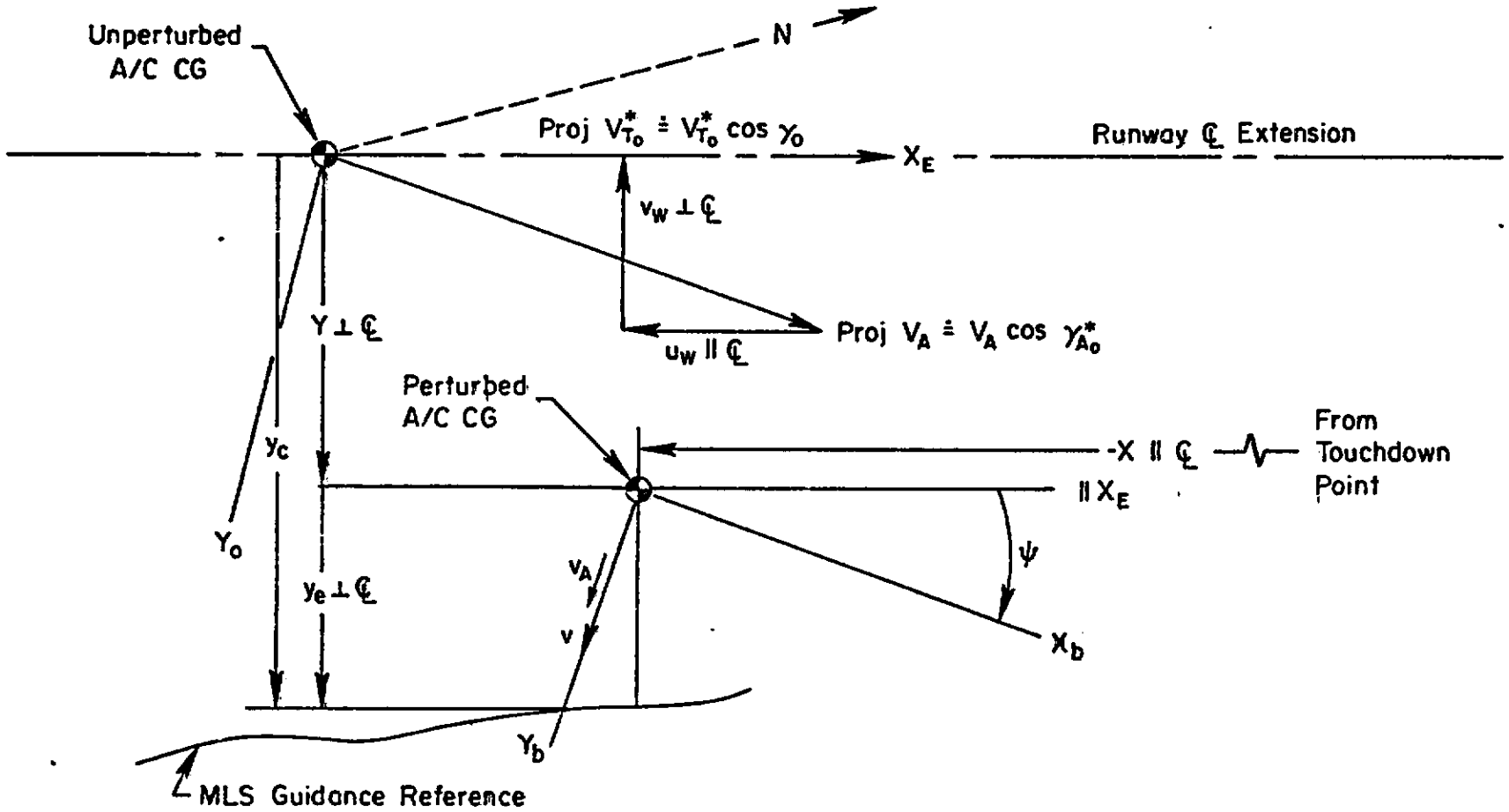

Figure A-6. Perturbed Coordinates Locating the Aircraft in a Horizontal Plane

$$\dot{y} = V_A\beta + \psi[U^* \cos\theta^* + W^* \sin\theta^*] - W^*\varphi \qquad \text{(A-65)}$$

$$\dot{\psi} = r/\cos\theta^* \qquad \text{(A-66)}$$

$$\dot{\varphi} = p + r\tan\theta^* \qquad \text{(A-67)}$$

$$a_y = V_A\dot{\beta} - W^*p \pm U^*r - g\cos\theta^*\varphi - \ell_{z_a}\dot{p} + \ell_{x_a}\dot{r} \qquad \text{(A-68)}$$

$$U^* = V_T^* \cos(\theta^* - \gamma_o) \qquad \text{(A-69)}$$

$$W^* = V_T^* \sin(\theta^* - \gamma_o) \qquad \text{(A-70)}$$

The crosswind and crosswind shear act horizontally and in a direction perpendicular to the runway. The positive sense of the crosswind is directed away from the runway centerline toward the left wingtip of an unperturbed landing aircraft. The crosswind, v_w, therefore must be resolved into aircraft body-fixed axis coordinates for proper application via the aircraft equations of motion. Let the longitudinal, side and normal components (with respect to body-fixed axes) of the deterministic crosswind disturbance be designated u_A, v_A and w_A, respectively.

$$u_A = -v_w \sin\psi \cos(\theta_o^* + \theta) \doteq -v_w\psi\cos\theta_o^* \doteq 0 \qquad \text{(A-71)}$$

$$v_A = -v_w[\sin\psi \sin(\theta_o^* + \theta)\sin\varphi + \cos\psi\cos\varphi] \doteq -v_w \qquad \text{(A-72)}$$

$$w_A = -v_w[\sin\psi \sin(\theta_o^* + \theta)\cos\varphi - \cos\psi\sin\varphi] \doteq -v_w[\psi\sin\theta_o^* - \varphi] \doteq 0 \qquad \text{(A-73)}$$

The linearized approximate expression for v_A is used in the system performance model. v_A enters the equations of motion in the manner of v_g.

The lateral displacement of the aircraft with respect to the MLS guidance reference is

$$y_e = y_c - y \tag{A-74}$$

y_c is obtained from a statistical description of the MLS guidance signal in terms of the received signal v_c (deg) as

$$y_c = \frac{v_c}{57.3} R_A \quad (\text{ft}) \tag{A-75}$$

where

$$R_A = \sqrt{[R_G - (X + 50/\tan \gamma_o)]^2 + H^2} \quad (\text{ft}) \tag{A-76}$$

State Equations for the Aircraft

The aircraft state variable equations are

$$\dot{\beta} = Y_v\beta + \frac{W^*}{V_A} p - \frac{U^*}{V_A} r + \frac{g \cos \theta^*}{V_A} \varphi + \frac{Y_{\delta_{LT}}}{V_A} \delta_{LT} + \frac{Y_{\delta_{PD}}}{V_A} \delta_{PD} - \frac{Y_v}{V_A} v_g + \frac{Y_v}{V_A} K_w v_{wo} \quad \left(\dot{\beta} \triangleq \frac{\dot{v}}{V_A} ; V_A = \text{const.}\right) \tag{A-77}$$

$$\dot{p} = L'_\beta\beta + L'_p p + L'_r r + L'_{\delta_{LT}}\delta_{LT} + L'_{\delta_{PD}}\delta_{PD} - L'_\beta/V_A \, v_g - L'_p p_g + L'_\beta/V_A \, K_w v_{wo} \tag{A-78}$$

$$\dot{r} = N'_{\beta}\beta + N'_{p}p + N'_{r}r + N'_{\delta_{LT}}\delta_{LT} + N'_{\delta_{PD}}\delta_{PD}$$

$$- N'_{\beta}/V_A \; v_g - N'_{p}p_g + N'_{\beta}/V_A \; K_w v_{wo} \qquad \text{(A-79)}$$

The coefficients for these equations and the kinematic equations given earlier for the lateral-directional model are time-varying by virtue of their dependdence upon kinematic variable values determined as a result of the longitudinal performance analysis calculations. The kinematic variables are t, H, X, R, V_A, θ^* and V_T^*. Numerical values for the stability derivatives in Eqs. A-77 through A-79 are given in Table A-6 as functions of airspeed and aerodynamic flight path angle.

TABLE A-6

XV-15 LATERAL-DIRECTIONAL DERVIATIVES

UNITS	VARIABLE					
ft*/sec	V_{A_o}	1.0	33.8	67.6	101.4	135.2
kt†	V_{A_o}	0	20	40	60	80
deg‡	α_o	θ_o = 2.2	6.5	4.5	1.6	−2.0
deg	γ_o	—	−6	−6	−6	−6
1/sec	Y_v	−.0071	−.038	−.0034	−.0460	−.073
1/sec^2	L'_β	−.0416	−.181	−.315	−.6859	−1.14
1/sec	L'_p	−.597	−.706	−1.04	−1.3292	−1.29
1/sec	L'_r	.0998	.393	.444	.3980	.276
1/sec^2	N'_β	.00447	.276	−.130	.11345	.502
1/sec	N'_p	.197	.187	.0636	.08425	.386
1/sec	N'_r	−.0212	−.129	.0646	−.10678	−.183
ft/sec^2/in.	$Y_{\delta_{LT}}$	.0066	−.108	−.045	−.019	.049

*1 ft = 3.048 x 10^{-1} m.
†1 kt = 5.144 x 10^{-1} m/s.
‡1 deg = 1.745 x 10^{-2} rad.
1 in. = 2.54 x 10^{-2} m.

TABLE A-6 (Concluded)

UNITS	VARIABLE					
$1/sec^2/in.$	$L'_{\delta_{LT}}$	.297	.290	.290	.3248	.362
$1/sec^2/in.$	$N'_{\delta_{LT}}$	−.0196	−.0207	−.0417	−.02637	−.0161
$ft/sec^2/in.$	$Y_{\delta_{PD}}$	.214	.166	.043	.10	−.324
$1/sec^2/in.$	$L'_{\delta_{PD}}$	.0201	−.0258	−.0707	−.13354	−.131
$1/sec^2/in.$	$N'_{\delta_{PD}}$	.121	.133	.143	.15492	.134

ℓ_{x_a} = 8.0 ft
ℓ_{z_a} = 0.0 ft

APPENDIX B

EQUATIONS AND DATA FOR SYSTEM PERFORMANCE EVALUATION

METHOD FOR USING PERTURBATION STABILITY DERIVATIVES

The XV-15 parametric data are in terms of small perturbation stability and control derivatives at specific static trim conditions in distinction to parametric data wherein the stability and control derivatives are expressed as functions of the trim variables. This and the fact that the performance evaluation required in this research program involves fairly rapid deceleration during final approach from 60-80 kt (31-41 m/s) to hover, in turn, has required development of a special procedure for using the available data. This has been necessary for three reasons:

- Validity of the (small) perturbation equations of motion requires that the perturbation variables indeed be kept reasonably small. This is particularly important for longitudinal perturbation velocity and airspeed which tend to grow large because of the wind shear and deceleration effects.

- Coefficients in the perturbation equations of motion for the aircraft are functions of trim airspeed, wind speed, pitch attitude, collective pitch, and longitudinal cyclic pitch, i.e., of the operating point.

- Trim data are for static, that is, unaccelerated conditions only. Valid application of the data requires that the operating point be a constant airspeed, wind speed, flight path angle and pitch attitude condition. Wind shear and deceleration to hover obviously make it impossible to select a single operating point for the landing approach which will cause all perturbation variables to be reasonably small.

The method developed for circumventing this difficulty without necessity for additional assumptions is given below.

Linear perturbation differential equations for the aircraft are in the form:

$$\dot{x} = Ax + b \quad , \quad x(0) = x_0 \qquad \text{(B-1)}$$

The actual response, X, consists of the perturbation response plus the operating point, X_o.

$$X = x + X_o \tag{B-2}$$

The elements of A and b are functions of the operating point, X_o.

Next consider how Eq. B-1 may be modified to allow for periodic adjustment of the operating point in the course of solution. This periodic adjustment is for two purposes:

- To select a new operating point for which the perturbation variables, x, are once again small (ideally, zero).
- To revise the coefficients, A and b, in the equations so their values correspond closely (ideally, exactly) to the coefficient values for the actual values of pitch attitude, wind speed, airspeed, flight path angle, collective and longitudinal cyclic pitch.

The ideal cannot be achieved for either of the above objectives if the system is not in static equilibrium (i.e., $\dot{x} \neq 0$). However, it is possible to approach the ideal closely for the decelerating conditions of interest. This is accomplished by using the actual values of airspeed, wind speed and flight path angle existing at the time of adjustment to partially define the revised operating point. The remaining parameters defining the revised operating point are determined by requiring static trim given those first several parameters. The difference between the static trim values for these latter operating point parameters and the actual values defines revised initial conditions for the perturbation variables. These are used in resuming solution of the differential equations. The specific procedures are given below.

Perturbation Equations

Let x_{o_n} be the constant, incremental revision to the operating point for the nth interval. Then the operating point for the nth time interval, X_{o_n}, is given by

$$X_{o_n} = x_{o_n} + X_{o_{n-1}} \quad , \quad n = 1, 2, \ldots \tag{B-3}$$

The perturbation differential equation for the nth time interval may be written:

$$\dot{x} = (\dot{x} + \dot{x}_{o_n}) = A(x + x_{o_n}) + b - Ax_{o_n} = Ax + b \tag{B-4}$$

The initial conditions are obtained by requiring that $(x + X_{o_n})$ at the beginning of the nth time interval be equal to $(x + X_{o_{n-1}})$ at the end of the $(n-1)$st time interval. The quantities $\dot{x}_{o_n}$ and Ax_{o_n} are zero by virture of the definition of trim for small increments of the operating point, x_{o_n}.

These differential equations must be discretized for use in the performance analysis program. Let the discretization interval be T. Then the transition from the beginning to the end of the nth time interval is given by

$$x_{n+1} = \varphi x_n + \theta b \tag{B-5}$$

where $\varphi = e^{AT}$ and $\theta = \int_o^T e^{A(T-\tau)}\, d\tau$. The quantities used previously may be used to obtain the recursion equations for x and X.

$$X_{o_n} = x_{o_n} + X_{o_{n-1}} \tag{B-6}$$

$$x_n = x_n + x_{o_n} \qquad \text{(value of x at } t^+\text{)} \tag{B-7a}$$

$$x_{n+1} = \varphi x_n + \theta b \qquad \text{(value of x at } t_{n+1}^-\text{)} \tag{B-7b}$$

$$X_{n+1} = x_{n+1} + X_{o_n} \qquad \text{(value of X at } t_{n+1}\text{)} \tag{B-7c}$$

Operating Point Revision

The operating point revision concept is to maintain the initial value of the airspeed perturbation variable zero for each time interval. Operating

point airspeed (V_{Ao_n}), flight path angle (γ_o), and wind speed (V_{HW_n}) are, in effect, given. Calculation of aerodynamic flight path angle (γ_{Ao_n}) enables us to calculate or look up values for all other trim quantities if equilibrium flight is assumed.

$$\gamma_{Ao_n} = \sin^{-1} \frac{\left(\sqrt{V_{Ao_n}^2 + V_{HW_n}^2 \sin^2 \gamma_o} - V_{HW_n} \cos \gamma_o\right) \sin \gamma_o}{V_{Ao_n}} \qquad \text{(B-8)}$$

Trim pitch attitude, collective pitch, and longitudinal cyclic pitch are obtained from trim maps as functions of V_{Ao_n} and γ_{Ao_n}. Trim values for inertial speed, longitudinal speed, normal speed are given by

$$V_{To_n} = \sqrt{V_{Ao_n}^2 + V_{HW_n}^2 \sin^2 \gamma_o} - V_{HW_n} \cos \gamma_o \qquad \text{(B-9)}$$

$$U_{o_n} = V_{To_n} \cos (\theta_{o_n} - \gamma_o)$$

$$W_{o_n} = V_{To_n} \sin (\theta_{o_n} - \gamma_o)$$

The aircraft stability and control derivatives are functions of V_{Ao_n} and γ_{Ao_n}.

Consideration of the above procedure for operating point revision reveals that assumption of static equilibrium results in different values for collective pitch, longitudinal cyclic pitch, and pitch attitude than exist in the actual, decelerating case. The differences tend to be small. The pitch attitude difference, in turn, affects the longitudinal and normal trim speeds, but also in a small way. These differences in each case are, of course, compensated by initial conditions on corresponding perturbation variables.

Equations and Data

Longitudinal equations used in performance evaluation are summarized in Table B-1. Numerical values for the control system parameters, switch settings and switching criteria for the longitudinal system modes are given in Tables B-2 through B-4. The lateral-directional equations used are summarized in Table B-5. Numerical values for the control system parameters are given in Table B-6. Switch settings and switching criteria for the lateral-directional control system modes are given in Table B-7.

TABLE B-1

LONGITUDINAL EQUATIONS FOR SYSTEM PERFORMANCE EVALUATION

STATE EQUATION: $\dot{x} = A_1 x + A_2 v + b_1$

$$\dot{x}$$

1) $\dot{u} = X_u u + X_w w - W_o^* q + (V_{HW_o} K_w X_w^{\square} - g \cos\theta_o^*)\theta + X_u^{\square} K_w u_{WO} - X_u u_g - X_w w_g + X_{\delta_{LN}}\delta_{LN} + X_{\delta_{CL}}\delta_{CL} - X_u^{\square} V_{HW_o} - X_{\delta_{LN}}\delta^*_{LN_o} - X_{\delta_{CL}}\delta^*_{CL_o}$

2) $\dot{w} = Z_u u + Z_w w + U_o^* q + (V_{HW_o} K_w Z_w^{\square} - g \sin\theta_o^*)\theta + Z_u^{\square} K_w u_{WO} - Z_u u_g - Z_w w_g + Z_{\delta_{LN}}\delta_{LN} + Z_{\delta_{CL}}\delta_{CL} - Z_u^{\square} V_{HW_o} - Z_{\delta_{LN}}\delta^*_{LN_o} - Z_{\delta_{CL}}\delta^*_{CL_o}$

3) $\dot{q} = M_u u + M_w w + M_q q + Y_{HW_o} K_w M_w^{\square}\theta + M_u^{\square} K_w u_{WO} - M_u u_g - M_w w_g + M_{\delta_{LN}}\delta_{LN} + M_{\delta_{CL}}\delta_{CL} - M_u^{\square} V_{HW_o} - M_{\delta_{LN}}\delta^*_{LN_o} - M_{\delta_{CL}}\delta^*_{CL_o}$

4) $\dot{\theta} = q$

5) $\dot{H} = \sin\theta_o^* u - \cos\theta_o^* w + [U_o^* \cos\theta_o^* + W_o^* \sin\theta_o^*]\theta + V_{T_o}^* \sin\gamma_o$

6) $\dot{X} = \cos\theta_o^* u + \sin\theta_o^* w + [-U_o^* \sin\theta_o^* + W_o^* \cos\theta_o^*]\theta + V_{T_o}^* \cos\gamma_o$

7) $\dot{x}_7 = -\omega_7 x_7 - \omega_7 K_{WT} V_A + \omega_7 K_{WP} V_{A_X}$

8) $\dot{x}_8 = K_{ICL} K_p K_{CL} F_{DCL}$

9) $\dot{x}_9 = -(\omega_{d_1} + \omega_{d_2})x_9 - \omega_{d_1}\omega_{d_2} x_{10} - \omega_{d_1}\omega_{d_2}(\omega_{d_1} + \omega_{d_2})(R/57.3)\eta + \omega_{d_1}\omega_{d_2} \cos\gamma_o \dot{H} - \omega_{d_1}\omega_{d_2} \sin\gamma_o \dot{X} + \omega_{d_1}\omega_{d_2}(\omega_{d_1} + \omega_{d_2})d$

10) $\dot{x}_{10} = x_9 + \omega_{d_1}\omega_{d_2}(R/57.3)\eta - \omega_{d_1}\omega_{d_2} d$

11) $\dot{\hat{d}}_e = -\omega_{11}\hat{d}_e + \omega_{11}(R/57.3)S_T\eta - \omega_{11}S_T d - \omega_{11}(1 - K_T)K_h S_{VD}(H_{VD} + H_c)$

TABLE B-1 (Continued)

12) $\dot{x}_{12} = -aK_\theta\theta - aK_{\dot\theta}q + a\theta_c + aK_\theta(\theta^*_{oo} - \theta^*_o)$

13) $\dot{x}_{13} = K_{\dot\theta_c}\delta_c$

14) $\dot{x}_{14} = -aX_{14} + a\delta_e$

15) $\dot{x}_{15} = -\omega_{FD_2}x_{15} + (\omega_{FD_1} - \omega_{FD_2})f$

16) $\dot{x}_{16} = \omega_{w\theta}\theta - \omega_{w\theta}x_{16} + \delta_{DEC}\omega_{w\theta}\Delta\theta_{DEC} - \omega_{w\theta}(\theta^*_{oo} - \theta^*_o)$

17) $\dot{x}_{17} = -kg\theta - \omega_u x_{17} + \omega_u V_A + ka_x - \omega_u V_{AR} - kg(\theta^*_o - \theta^*_{oo})$

18) $\dot{u}_{W_o} = 0$

19) $\dot{u}_g = -(|V^*_{A_o}|/L_u)u_g$

20) $\dot{w}_g = -(1.59k|V^*_{A_o}|/L_w)w_g$

21) $\dot{\eta} = -(|V^*_{T_o}|/L_\eta)\eta$

22) $\dot{x}_c = -\omega_{x_c}x_c$

TABLE B-1 (Continued)

AUXILIARY EQUATION: $\mathbf{v} = A_3\mathbf{v} + A_4\mathbf{x} + b_2$

$\mathbf{v}$

1) $\dot{X} = \cos\theta_o^* u + \sin\theta_o^* w + [-U_o^* \sin\theta_o^* + W_o^* \cos\theta_o^*]\theta + V_{T_o}^* \cos\gamma_o$

2) $\dot{H} = \sin\theta_o^* u - \cos\theta_o^* w + [U_o^* \cos\theta_o^* + W_o^* \sin\theta_o^*]\theta + V_{T_o}^* \sin\gamma_o$

3) $V_A = \cos(\theta_o^* - \gamma_{A_o}^*)u + \sin(\theta_o^* - \gamma_{A_o}^*)w - V_{HW_o}K_w \sin\gamma_{A_o}^*\theta + K_w \cos\gamma_{A_o}^* u_{W_o} - \cos(\theta_o^* - \gamma_{A_o}^*)u_g - \sin(\theta_o^* - \gamma_{A_o}^*)w_g + V_{T_o}^* \cos(\gamma_{A_o}^* - \gamma_o)$

4) $d = \cos\gamma_o H - \sin\gamma_o X - 50.\cos\gamma_o$

5) $FD_{CL} = -[(1 - K_T)K_{\dot{H}}^{\cdot} + K_T K_{\dot{d}}]\dot{H} + K_T K_{\dot{d}} x_{10} + [K_T K_d + (1 - S_T)]\hat{d}_e - (1 - K_T)K_h S_{AH} H + (1 - K_T)K_h S_{AH} H_{VD}$

6) $\delta_{CL} = K_{CL} FD_{CL} + x_7 + x_8$

7) $\Delta\theta_{DEC} = -(K_{\theta VA} K_{HUG}/57.3)\dot{X} + \theta_{INC}/57.3$

8) $\delta_{LN} = K_\theta\theta + K_{\dot{\theta}} q - x_{12} - x_{13} - x_{14} + K_\theta(\theta_o^* - \theta_{oo}^*)$

9) $a_x = X_{\delta_{LN}}\delta_{LN} + X_{\delta_{CL}}\delta_{CL} + X_u u + X_w w + (V_{HW_o}K_w X_w^{\alpha})\theta + X_u^{\alpha} K_w u_{W_o} - X_u u_g - X_w w_g - X_u^{\alpha} V_{HW_o} - X_{\delta_{LN}}\delta_{LN_o}^* - X_{\delta_{CL}}\delta_{CL_o}^* + g(\sin\theta_o^* - \sin\theta_{oo}^*)$

10) $\theta_{CD} = K_N K_X(-K_{\dot{X}}\dot{X} - K_{A_X} a_x) + K_N K_X(K_{a_x} g\theta + \dot{X}_c - X) + S_{DEC}(1 - S_{DECL})\theta + (1 - S_{DEC})x_{16} - S_u K_u x_{17} + K_N K_X K_{A_X} g(\theta_\delta^* - \theta_{\delta o}^*) + S_{DEC}(1 - S_{DECL})(\theta_o^* - \theta_{oo}^*)$

11) $f = \theta_{CD} - \theta - K_{\dot{\theta}_o} q + \theta_{\delta o}^* - \theta_\delta^*$

12) $FD_c = K_{FD_c} f + K_{FD_c} x_{15}$

13) $\delta_c = K_{p_c} FD_c$

14) $\theta_c = -\delta_c + x_{13} + x_{14}$

15) $\delta_s = \theta_c - K_\theta\theta - K_{\dot{\theta}} q + x_{12} + K_\theta(\theta_{oo}^* - \theta_o^*)$

TABLE B-1 (Continued)

ALTERNATE STATE EQUATION: $\dot{y} = A_5 v + A_6 x + B_3$

$\dot{y}$

1) $\dot{X} = v(1)$

2) $\dot{H} = v(2)$

3) $q = x(3)$

4) $\theta = x(4) + \theta_o^*$

5) $H = x(5)$

6) $X = x(6)$

7) $\Delta\delta_{CL_c} = x(7)$

8) $\delta_{CL} = v(6)$

9) $y_9 = x(11)$

10) $y_{10} = x(10)$

11) $y_{11} = x(11)$

12) $\delta_s = v(15)$

13) $\theta_c/K_\theta = v(14)/K_\theta$

14) $y_{14} = x(14)$

15) $FD_c = v(12)$

16) $\theta_{CD} = v(10)$

17) $y_{17} = x(17)$

18) $u_w = K_W U_{W_o}$

19) $u_g = x(19)$

20) $w_g = x(20)$

21) $d_e = -\cos\gamma_o \; H + \sin\gamma_o \; X + R\eta/57.3 + 50\cos\gamma_o$

22) $X_i = -X + X_c$

TABLE B-1 (Concluded)

OUTPUT EQUATION: $z = A_7 x + A_8 v + b_4$

z

1) $FD_{CL} = v(5)$

2) $A_z' = \dot{w} - \ell_{x_a}\dot{q} + (g \sin \theta_o^*)\theta$

3) $A_x = v(9)$

4) $\theta_e = \theta_{CD} - (1 - S_{DEC})(\theta + \theta_o^* - \theta_{oo}^*)$

5) $\delta_{LN} = v(8)$

6) $e_\theta = \frac{1.78}{K_{\theta VA}} \left\{\cos \theta_o^* u + \sin \theta_o^* w - \left[U_o^* \sin \theta_o^* - W_\theta^* \cos \theta_o^*\right]\theta\right\}$

$$- X - \frac{1.78}{K_{\theta VA}} \left\{V_{T_o} \cos \gamma_o + \frac{\theta_{NC}}{K_{\theta VA}} \ln \left[1 - \frac{K_{\theta VA}\dot{X}}{\theta_{INC}}\right]\right\} - (T_{D_3} + 2.0)\,\dot{X}$$

7) $e_x = -K_{\dot{X}}\dot{X} - K_{a_x}A_x + gK_{a_x}\theta - X + X_c + gK_{a_x}(\theta_o^* - \theta_{oo}^*) - K_{N_{DT_5}}\dot{X}/2.0$

$$= x(22) - x(6) - [K_{\dot{X}} + K_{N_{DT_5}}/2.0]y(1) - K_{a_x}z(3) + gK_{a_x}x(4) + gK_{a_x}(\theta_o^* - \theta_{oo}^*)$$

8) $V_A = v(3)$

TABLE B-2

LONGITUDINAL CONTROL SYSTEM PARAMETERS USED IN PERFORMANCE EVALUATION

ALL MODES

K_θ (in./rad)	$K_{\dot\theta}$ [in./(rad/sec)]	$K_{\dot\theta_c}$ (1/sec)	ω_a (rad/sec)	K_d (in./ft)
12.0	8.0	2.09	1.0	0.01
K_{CL} (-)	K_{ICL} (1/sec)	V_{AX} (ft/sec)	H_c (ft)	T_{D_3} (sec)
5.0	1.0	101.4	16.0	1.99
ω_{d_1} (rad/sec)	ω_{d_2} (rad/sec)	ω_{CL} (rad/sec)	K_u [rad/(ft/sec)]	k (-)
1.0	0.5	1.0	-0.005	7.5
K_X (rad/ft)	$K_{\dot X}$ (sec)	K_{a_X} (sec^2)	ω_u (rad/sec)	ω_{FD_2} (rad/sec)
-0.005	8.0	16.0	1.5	4.5
K_{p_c} (-)	$\dot X_{MIN}$ (ft/sec)	ω_7 (rad/sec)	$K_{N_{DT5}}$ (sec)	$K_{\theta VA}$ [deg/(ft/sec)]
3.2	10.0	1.0	0.01	-0.0427
θ_{INC} deg	K_{BUG} (-)			
1.0	1.5			

TABLE B-2 (Concluded)

CONTROL SYSTEM MODE			CONTROL SYSTEM PARAMETERS						
CYCLIC AXIS	COLLECTIVE AXIS	LSW CODE	K_h (in./ft)	$K_{\dot{h}}$ [in./(ft/sec)]	$K_{\dot{\theta}_D}$ (sec)	K_{FD_c} (in./rad)	ω_{FD_1} (rad/sec)	K_{WT} [in./(ft/sec)]	ω_{11} (rad/sec)
AS	GS	1, 2*	0.01	0.053	1.0	1.43	4.5	0	4.0
DECL I	GS	3*	0.01	0.053	0.5	2.52	4.5	0	4.0
DECL	GS	4*	0.01	0.053	0.5	2.52	4.5	0.029	4.0
HOV	GS	5†	0.01	0.053	1.33	1.8	2.0	0.029	4.0
HOV	ALT	6†	0.01	0.053	1.33	1.8	2.0	0.029	1.0
HOV	VD	7†	0.0064	0.04	1.33	1.8	2.0	0.029	1.0

*$K_{\dot{d}} = \dfrac{0.01}{0.19 + 0.00296V_A}$ [in./(ft/sec)] , V_A in ft/sec units.

†$K_{\dot{d}} = 0.053$ [in./(ft/sec)].

TABLE B-3. SWITCH SETTINGS FOR LONGITUDINAL PERFORMANCE EVALUATION

CONTROL SYSTEM MODE			SWITCH VARIABLE						
CYCLIC AXIS	COLLECTIVE AXIS	LSW CODE	$\omega_{w\theta}$ (rad/sec)	S_u	S_{DEC}	S_{DECL}	S_{AH}	S_T	S_{VD}
AS	GS	1, 2	0.2	1.0	0	0	0	1.0	0
DECL I	GS	3	4.0	0	1.0	0	0	1.0	0
DECL	GS	4	0	0	0	1.0	0	1.0	0
HOV	GS	5	0.25	0	0	0	0	1.0	0
HOV	ALT	6	0.25	0	0	0	1.0	0	0
HOV	VD	7	0.25	0	0	0	1.0	0	1.0

Legend for Control System Modes:

ALT	Altitude Hold
AS	Airspeed Hold
DECL	Constant Attitude Deceleration
DECL I	Fictitious mode introduced for performance evaluation to simulate pitch synchronizers without requiring additional model states
GS	Glide Slope Track
HOV	Longitudinal Point Hover
VD	Vertical Descent

TABLE B-4

LONGITUDINAL CONTROL SYSTEM MODE SWITCHING CRITERIA

CONTROL SYSTEM MODE			
CYCLIC AXIS	COLLECTIVE AXIS	LSW CODE	CRITERION
AS	GS	1	Problem Initialization: $e_\theta > 0$ ft,* $101.4 \leq V_A \leq 136.0$ ft/sec
AS	GS	2	$e_\theta > 0$ ft
DECL I	GS	3	$e_\theta \leq 0$ ft, $T_D^\dagger < 2.1$ sec
DECL	GS	4	$T_D \geq 2.1$ sec, $e_x \geq 0$ ft, $\dot{X} > \dot{X}_{MIN}$ ft/sec
HOV	GS	5	$e_x < 0$ ft or $\dot{X} \leq \dot{X}_{MIN}$ ft/sec and $H > 51.0$ ft
HOV	ALT	6	$H \leq 51.0$ ft, $T_H^\dagger < 15.0$ sec
HOV	VD	7	$T_H \geq 15.0$ sec, $H \geq 0$ ft

*1 ft = 3.048×10^{-1} m.

†Elapsed time from initiation of mode.

TABLE B-5

LATERAL-DIRECTIONAL EQUATIONS FOR SYSTEM
PERFORMANCE EVALUATION

STATE EQUATION: $\dot{x} = A_1 x + A_2 v + b_1$

$\dot{x}$

1) $\dot{\beta} = Y_v\beta + \frac{W^*}{V_A} p - \frac{U^*}{V_A} r + \frac{g \cos\theta^*}{V_A}\varphi + (Y_v/V_A)K_w v_{wo} - Y_v/V_A v_g + Y_{\delta_{LT}}/V_A \delta_{LAT} + Y_{\delta_{PD}}/V_A \delta_{PED}$

2) $\dot{p} = L'_\beta\beta + L'_p p + L'_r r + (L'_\beta/V_A)K_w v_{wo} - L'_\beta/V_A v_g - L'_p p_g + L'_{\delta_{LT}} \delta_{LAT} + L'_{\delta_{PD}} \delta_{PED}$

3) $\dot{r} = N'_\beta\beta + N'_p p + N'_r r + (N'_\beta/V_A)K_w v_{wo} - N'_\beta/V_A v_g - N'_p p_g + N'_{\delta_{LT}} \delta_{LAT} + N'_{\delta_{PD}} \delta_{PED}$

4) $\dot{\varphi} = p + \tan\theta^* r$

5) $\dot{\psi} = 1/\cos\theta^* r$

6) $\dot{Y} = V_A\beta - W^*\varphi + (U^* \cos\theta^* + W^* \sin\theta^*)\psi$

7) $\dot{x}_7 = -\omega_c\tilde{\psi}$

8) $\dot{\psi}_s = S_A K_\psi \psi - S_A K_\psi \psi_s$

9) $\dot{x}_9 = -\omega_b K_p p - \omega_b K_\varphi \varphi + \omega_b \varphi_c$

10) $\dot{x}_{10} = K\dot{\varphi}_c \zeta_s$

11) $\dot{x}_{11} = -\omega_b x_{11} + \omega_b \delta_s$

TABLE B-5 (Continued)

12) $\dot{x}_{12} = -\omega_{FD_2} x_{12} + (\omega_{FD_1} - \omega_{FL_2})r$

13) $\dot{x}_{13} = -\omega_y x_{13} - \omega_y y + (\omega_y R_A/57.3)v$

14) $\dot{x}_{14} = -\omega_{W_\varphi} x_{14} + \omega_{W_\varphi}\varphi$

15) $\dot{v}_{WO} =$

16) $\dot{v}_g = -1.594 V_A/L_v v_g$

17) $\dot{p}_g = -xV_A/(4b_{p_G})p_g$

18) $\dot{v} = (-V_T^*/L_v)v$

OUTPUT EQUATION: $z = A_7X + A_8v + b_4$

z

1) $A_y' = (V_A Y_v + \ell_{x_a} N_\beta')\beta + \ell_{x_a} L_p' p + \ell_{x_a} N_r' r + (Y_v + \ell_{x_a} N_\beta'/V_A)K_w v_{WO} - (Y_v + \ell_{x_a} N_\beta'/V_A)v_g - \ell_{x_a} N_p' p_g + (Y_{\delta_{IT}} + \ell_{x_a} N_{\delta_{IT}}')\delta_{LAT} + (Y_{\delta_{PD}} + \ell_{x_a} N_{\delta_{PD}}')\delta_{PED}$

2) $\delta_{LAT} = \delta_{LAT}$

3) $\delta_s = K_{p_\varphi} FD_L$

4) $S_A = S_A$

5) $-\tilde{\Psi} = -\Psi$

TABLE B-5 (Continued)

AUXILIARY EQUATION: $v = A_3 v + A_4 x + b_2$

$$
\begin{array}{lll}
 & v & \\
1)\ \epsilon_y = & -(K_y + \omega_y K_{\dot{y}})y - \omega_y K_{\dot{y}} x_{13} & + [K_y + \omega_y K_{\dot{y}}) R_A/57.3]v \\
2)\ \varphi_{DC} = & \epsilon_y + K_{D_\varphi} x_{14} & \\
3)\ q = & \varphi_{DC} - K_{DP} p - K_{D_\varphi} \varphi & \\
4)\ FD_L = & (K_{FD_L} \omega_{FD_2}/\omega_{FD_1}) f - (K_{FD_L} \omega_{FD_2}/\omega_{FD_1}) x_{12} & \\
5)\ \delta_s = & K_{P\varphi} FD_L & \\
6)\ \varphi_c = & -\delta_s & + x_{10} + x_{11} \\
7)\ \epsilon_{LAT} = & - K_p p - K_\varphi \varphi & + x_9 + x_{10} + x_{11} \\
8)\ \tilde{\psi} = & K_r r + S_A K_\beta + (1 - S_A) \cdot + S_A K_\beta (g/V_A)\varphi + K_\psi (1 - S_A)\psi - K_\psi (1 - S_A)\psi_s & \\
9)\ \delta_{PED} = & -\tilde{\psi} + x_7 &
\end{array}
$$

TABLE B-5 (Continued)

ALTERNATE STATE EQUATION: $\dot{y} = A_5 v + A_6 X + b_3$

	y						
1)	$\dot{y}$	=	$V_A\beta$		$-W^*\varphi$		$(U^* \cos\theta^* + W^* \sin\theta^*)\psi$
2)	p	=		p			
3)	r	=			r		
4)	φ	=				φ	
5)	ψ	=					ψ
6)	y	=					y
7)	δ_{FDS}	=	δ_{PED}				
8)	$(\psi - \psi_s)$	=					$\psi \quad -\psi_s$
9)	δ_{LTS}	=	$\delta_{LAT} - \delta_s$				
10)	φ_c/K_φ	=	$1/K_\varphi \varphi_c$				
11)	y_{11}	=					x_{11}

TABLE B-5 (Concluded)

12)	FD_L	=	FD_L						
13)	ϵ_y	=	ϵ_y						
14)	Φ_{DC}	=	Φ_{DC}						
15)	v_w	=		$K_w v_{WO}$					
16)	v_g	=			v_g				
17)	p_g	=				p_g			
18)	y_e	=					$-y$	$+(R_A/57.3)\nu$	

TABLE B-6

LATERAL-DIRECTIONAL CONTROL SYSTEM PARAMETERS
USED IN PERFORMANCE EVALUATION

LOC A AND LOC B

K_β [in.*/(rad/sec)]	K_r [in./(rad/sec)]	K_ψ (in./rad)	K_{SYN} (rad/sec)	K_y (rad/ft†)
10.0	13.0	13.0	10.0	0.002

$K_{\dot{y}}$ [rad/(ft/sec)]	$K_{D\varphi}$ (–)	K_{Dp} (sec)	$\omega_{W\varphi}$ (rad/sec)	ω_{FD_1} (rad/sec)
0.017	1.06	0.425	0.1	2.0

ω_{FD_2} (rad/sec)	ω_y (rad/sec)	R_G (ft)
14.9	4.0	1000‡

LOC A (S_A = 1.0)

K_p [in./(rad/sec)]	K_φ (in./rad)	$K_{\dot{\varphi}_c}$ (1/sec)	ω_b (rad/sec)	ω_c (rad/sec)
5.6	11.2	2.93	0	0

K_{FDL} (in./rad)	$K_{p\varphi}$ (–)
1.0	5.62

*1 in. = 2.54×10^{-2} m.

†1 ft = 3.048×10^{-1} m.

‡Number shown is for landing on VTOL pad. CTOL runway value is 10,000.

TABLE B-6 (Concluded)

LOC B (S_A = 0)

K_p [in./(rad/sec)]	K_φ (in./rad)	$K_{\dot{\varphi}_c}$ (1/sec)	ω_b (rad/sec)	ω_c (rad/sec)
8.0	12.0	3.14	1.0	0.5

K_{FDL} (in./rad)	$K_{p\varphi}$ (-)
1.6	2.5

TABLE B-7

LATERAL-DIRECTIONAL CONTROL SYSTEM MODE
SWITCHING CRITERIA AND SWITCH SETTINGS

CONTROL SYSTEM MODE	SA CODE/ VALUE	CRITERION
LOC A	1	$V_A > 84.5$ ft*/sec
LOC B	0	$V_A \leq 84.5$ ft/sec

*1 ft = 3.048×10^{-1} m.